REDUCTION OF TUNGSTEN OXIDES WITH CARBON AND HYDROGEN

Submitted in fulfilment of the requirements
for the degree of

Master of Science
of
Rhodes University

DEAN STUART VENABLES

February 1995

ABSTRACT

The reductions of WO_3 with hydrogen, with CO, and with carbon, as well as the reduction of WO_3/graphite mixtures with hydrogen, were studied using thermogravimetry, evolved gas analysis, X-ray powder diffraction, and scanning electron microscopy. The intermediate phases $W_{20}O_{58}$, $W_{18}O_{49}$, and WO_2 were observed in the reductions. The final product of the reductions with hydrogen and carbon was tungsten, and WC was formed in the reduction with CO. The reaction paths in the overall processes were determined.

The reactant/product gas ratio had a considerable influence on which reactions took place. The morphology of the sample was characterised at different stages of the reduction. The shape of the WO_3 particles was retained during the reduction. Particle growth was observed in the reduction with hydrogen and was attributed to the formation of $WO_2(OH)_{2(g)}$.

The kinetics of the reductions were investigated, and the reaction mechanisms determined. The reduction of WO_3 with CO was studied from 650 to 900°C, and occurred at a phase boundary with an activation energy of 40 kJ mol^{-1}. The reduction of WO_2 was studied under the same conditions. The reaction also occurred at a phase boundary and had an activation energy of 62 kJ mol^{-1}.

The reduction of WO_3 with carbon was studied from 935 to 1100°C and took place via CO and CO_2. Two stages were observed in the reduction. The first stage, which corresponded approximately to the formation of WO_2, had an activation energy of 66 kJ mol^{-1} and was limited by diffusion through the porous reacting particles. The second stage was first order and had an activation energy of 40 kJ mol^{-1}.

The reduction of WO_3 and WO_3/graphite mixtures with hydrogen were studied from 575 to 975°C. The reactions were controlled by mass-transfer under the conditions investigated. The addition of carbon increased the rate of the reduction process, but did not affect the phases formed in the system. CO_2 was evolved mainly at the start, and CO mainly at the end of the process.

The endless cycle of idea and action,
Endless invention, endless experiment,
Brings knowledge of motion, but not of stillness;
Knowledge of speech, but not of silence;
Knowledge of words, and ignorance of the Word.

from *The Rock*, T.S.Eliot

ACKNOWLEDGEMENTS

Many people have helped, guided, and encouraged me throughout this project, and have made this work and this time an enriching experience for me. I particularly wish to thank Professor Brown, my supervisor, for his open-door policy, his knowledge and advice which I have often needed, and for always expecting me to give of my best. I owe much of my training as a scientist to him.

My fellow chemistry students, especially Mike Tribelhorn, Steve Taylor, John Bacsa, and Annemarie de la Croix, often assisted me in my work, but more importantly, they provided the camaraderie of those who are all in the same boat. I have really appreciated their company over the last few years. Thank you to Ruth Whittaker, who helped immensely in the final production stages.

I am also grateful to the staff of the chemistry department who have gladly helped me with the problems which are inevitable in this type of work. I wish to single out Professor Eve, Margie Kent, and Johan Buys, who received more than their fair share of my problems. My thanks also go to Robin Cross and the Electron Microscopy Unit for aiding me in the use of the SEM.

AECI Ltd not only provided much of the financial backing for this project, for which I am grateful, but also carried out a number of experiments for me on their high temperature TG. Karol Cameron, Ian Porée, and Ian Sutherland have been especially helpful in this regard, sometimes at the expense of their own work. I thank them for the time and effort they have gone to, and hope that the interaction has been as fruitful for them as it has been for me. I also wish to acknowledge the FRD for generously supporting this work.

Finally, I wish to thank my family and friends for their love and support, for believing in me, and for showing me that in life chemistry is just one facet of a much greater whole.

CONTENTS

LIST OF FIGURES

Figure number

LIST OF TABLES

Table number

LIST OF SYMBOLS

A	frequency factor
A_p	pore surface area of pellet
b	stoichiometric coefficients
c	regression constant
C	concentration of gas
D_e	effective diffusivity
E_a	activation energy
ΔG°	standard Gibbs function
h_D	mass transfer coefficient
ΔH°	standard enthalpy
k	rate constant for the reaction
K	equilibrium constant for the reaction
$K_{A,C}$	Langmuir constant for gases A and C
n	order of reaction
N	flux of gas
P	partial pressure
R^2	correlation coefficient
r_p	original position of external surface
S°	standard entropy
t	time
T	absolute temperature
V_p	volume of pellet
X_{As}	mole fraction of gas A at surface
α	extent of reaction ("fractional reaction")
ρ	density
ρ_s	molar concentration of solid reactant

Subscripts

A,C	species A, C, and so forth
0	in the bulk of the gas phase
f	of formation
p	pellet (as opposed to a single particle)
r	of reaction
s	at surface

Chapter 1

INTRODUCTION

1.1 Tungsten and tungsten carbide

In recent history there has been an enormous expansion in the knowledge and control we have over our world. One aspect of this is that we have a much clearer understanding of the nature and properties of materials. This understanding, coupled with the discovery of many new materials, has resulted in a great diversity of products and technologies.

Two properties often sought in materials are those of strength and hardness. It is predominantly these properties which make tungsten a valuable element[1]. Tungsten metal is extremely refractory and can be used at very high temperatures, which makes it useful as a filament for incandescent lamps. Tungsten also imparts great strength and hardness to steels, making them suitable for heat-resistant and high-speed applications.

The most common use of tungsten is in the making of tungsten carbide (WC). Tungsten carbide is an exceptionally hard material and is used extensively in dies, tools, wear surfacing, and drill bits. It is usually used in the form of cemented carbides, in which the carbide is incorporated in the matrix of a metal, normally cobalt or nickel[1,2]. Binary and ternary solid solutions of tungsten carbide with other carbides are also important, especially WC-TiC and WC-TiC-TaC(NbC)[2], which are also used in cemented carbides.

The rigorous conditions under which tungsten carbide products are used demand stringent material requirements. For optimum mechanical properties, tungsten carbide powders should be chemically pure and consist of small particles with a narrow size distribution[3]. In particular, the size of the tungsten carbide particles has a large bearing on their strength and hardness, because large particles are more brittle than smaller ones. The demand for submicron (less than 1 μm diameter) and ultrafine (less than 0.5 μm diameter) tungsten carbide powders has increased considerably recently[3], and there is much interest in the manufacture of ultrafine tungsten carbide

powders.

Tungsten carbide is produced by carburising tungsten powder with either methane or carbon in the presence of hydrogen gas[1]:

$$W \xrightarrow[>1400^\circ C]{CH_4/C \text{ in } H_2} WC \qquad (1.1)$$

The properties of the resulting tungsten carbide powder are largely determined by the properties of the tungsten reactant. Consequently, a lot of work has concentrated on producing tungsten powder which is suitable for use in tungsten carbide production. The present study also focuses attention on the production of tungsten powder.

Tungsten is produced industrially by reducing a tungsten oxide with hydrogen. The usual starting material is ammonium paratungstate (APT), which is calcined either in air to form tungsten trioxide (WO_3, a yellow powder), or in an inert atmosphere to form tungsten blue oxide (a mixture of $W_{18}O_{49}$ and $W_{20}O_{58}$). These tungsten oxides are then reduced with hydrogen between 600 and 900°C[1].

Growth of tungsten particles occurs during reduction in hydrogen, thus decreasing the value of the resulting tungsten powder. Water vapour produced by the reduction is responsible for the increase in particle size, because it facilitates the transport of tungsten through the gas phase[3,4]. Conditions should thus be as dry as possible to minimise grain growth, and small samples, low temperatures and high hydrogen flowrates must be used. These conditions are costly to maintain and are not suited to large-scale industrial processing. Other methods of producing tungsten also have disadvantages. In particular, reduction using carbon is not usually employed because it introduces impurities and coarse tungsten particles are produced[1]. However, recent work by Asada *et al.*[5] has suggested that reduction with carbon may still be a viable process to form tungsten and tungsten carbide.

Because carbon is a reducing agent and is also used in the subsequent carburisation of tungsten, it would be useful to know how it affects the reduction of tungsten oxides with hydrogen. Recent work has indicated that solid carbon improves the conditions of the reduction of cobalt-tungsten oxides with hydrogen[6]. On thermodynamic grounds, carbon is likely to reduce the concentration of water vapour in the system, which could improve the properties of

the resulting tungsten and tungsten carbide powders. Furthermore, the carburisation of tungsten might be accomplished more conveniently, since carbon is already present in the system. This could improve the efficiency of the overall tungsten carbide manufacturing procedure.

1.2 Aims of the investigation

This project aims to study the influence of carbon on the reduction of tungsten oxides with hydrogen. This will involve studying the reduction of tungsten oxides with carbon and hydrogen separately, and then investigating the reduction using both reductants simultaneously. Because the structures of ultrafine hard metals are very sensitive to the conditions under which they are produced, an accurate knowledge of the reduction mechanism is necessary to determine the optimum processing conditions. Thus, a detailed mechanistic understanding of the reduction will be sought. This will involve a kinetic analysis of each system, as well as a study of the morphological changes which occur during reduction. The knowledge gained from this project is likely to be valuable for possible industrial implementation.

Chapter 2

LITERATURE REVIEW

2.1 An overview of kinetic analysis

2.1.1 Introduction

The kinetic analysis of a reaction is an important, and often the most convenient, technique for studying the reaction mechanism. A goal of the analysis is to fit the data describing the progress of the reaction to a kinetic model. Conformity of the experimental data to a particular kinetic model is then regarded as necessary, but not in itself sufficient, evidence for the occurrence of the mechanism on which the model is based. To prove that the proposed mechanism actually occurs requires additional supporting experimental evidence[7]. However, such evidence is often difficult to obtain.

An evaluation of the kinetic models starts with calculating the extent of reaction, α, from the experimental data. The kinetic models are then usually expressed as $f(\alpha) = kt$, and the linearity of $f(\alpha)$ for probable models is evaluated. The models which are the most linear generally describe the experimental data best. The rate coefficients can then be used in an Arrhenius plot to calculate the activation energy, E_a, and frequency factor, A, of the reaction.

2.1.2 Reactions in solids

Numerous kinetic equations have been proposed for reactions involving solids and are described in a number of texts.[7-9] Some of these equations are listed in Table 2.1, which has been taken from Brown *et al.*[7] Rate equations referred to in this study will follow the labelling convention used by those authors—i.e., R3, D4, and so forth. The rate equations based on geometric models and on diffusion-limited processes are particularly important in this study and will be

briefly described.

Table 2.1. Selected rate expressions for solid state reactions.

Label and title		Rate equation, $f(\alpha) = kt$
Acceleratory rate equations		
	Power law	$\alpha^{1/n}$
Sigmoid rate equations		
An	Avrami-Erofe'ev	$[- \ln (1 - \alpha)]^{1/n}$
B1	Prout-Tompkins	$\ln [\alpha / (1 - \alpha)]$
Deceleratory rate equations		
D1	One-dimensional diffusion	α^2
D2	Two-dimensional diffusion	$(1 - \alpha) \ln (1 - \alpha) + \alpha$
D3	Three-dimensional diffusion	$[1 - (1 - \alpha)^{1/3}]^2$
D4	Ginstling-Brounshtein	$1 - 2\alpha/3 - (1 - \alpha)^{2/3}$
R2	Contracting-area	$1 - (1 - \alpha)^{1/2}$
R3	Contracting-volume	$1 - (1 - \alpha)^{1/3}$
F1	First order reaction	$- \ln (1 - \alpha)$
F2	Second order reaction	$(1 - \alpha)^{-1}$
F3	Third order reaction	$(1 - \alpha)^{-2}$

The geometric models, which are also referred to as the contracting-volume and contracting-area models, or phase-boundary or topochemical models[10], are based on reaction occurring at a sharply-defined interface between two phases. The reaction rate is proportional to the area of the reaction interface, with the result that the interface advances into the solid at a constant velocity. The rate equations for these models are readily derived from geometric considerations.

On the other hand, the rate of the overall reaction may be limited by the diffusion of reactants to, or products from, the reaction interface. Various rate equations have been derived for diffusion-limited models in particles of various geometries; namely, plates (D1), cylinders (D2), and spheres (D3 and D4). The D3 or Jander equation has been criticised by a number of authors[8,11], who have demonstrated that it is theoretically flawed and only approaches a reasonable representation of diffusion in spheres at quite low conversions.

2.1.3 Reactions between gases and solids

Reactions of solids with gases form an integral part of this investigation, and such reactions may be limited by a number of factors. These include[9]:

(1) mass transfer of reactant gases to, or product gases from, the bulk of the gas phase to the surface of the solid;

(2) diffusion of the reactant and product gases through the pores of the solid;

(3) adsorption of reactant gases on, and desorption of product gases from, the solid surfaces;

(4) diffusion of reactants and products through the solid;

(5) chemical reaction.

As Szekely *et al.*[9] point out: "The objective of the experimental study is then to establish which of these steps, or what combination thereof, is rate controlling over the conditions of interest and then to develop a detailed understanding of this rate-controlling step(s)".

The macroscopic structure of the solid has a large influence on the transport of gases within the solid, and therefore must be taken into consideration. Moreover, the structure may change during the course of the reaction. Because the structure is so important in gas-solid

reactions, reactions between gases and solids will be categorised according to the structure of the solid, and how the structure changes during the reaction. A convenient division is according to whether the solids are initially porous or nonporous.

In many reactions between gases and solids, the rate of reaction is limited by the transfer of gases between the surface of the solid and the bulk of the gas phase. The rate at which mass is transferred from a solid surface into a moving gas stream may be described by the equation[9]:

$$N_A = h_D(C_{As} - C_{A0}) + X_{As}(N_A + N_C) \qquad (2.1)$$

where N_A and N_C are the fluxes of gases A and C, h_D is the mass transfer coefficient, C_{As} and C_{A0} are the concentrations of gas A at the solid surface and in the bulk of the gas phase, and X_{As} is the mole fraction of gas A at the solid surface. The second term on the right-hand side of eqn. (2.1) falls away in the case of equimolar counterdiffusion. The mass transfer coefficient, h_D may be calculated from empirical correlations.

For reactions in which the rate is limited by the rate of mass-transfer of the gases to or from the solid, the course of reaction may be described by[9]:

$$\alpha = \frac{bh_D(C_{A0} - (C_{C0}/K))}{(1 - \epsilon)\rho_s}\left(\frac{A_p}{V_p}\right)\frac{K}{1 + K}t \qquad (2.2)$$

where α is the extent of reaction, b is the stoichiometric coefficient of the reactant solid, K is the equilibrium constant for the reaction, ϵ is the porosity, ρ_s is the molar density of the pore-free solid reactant, and A_p and V_p are the surface area and volume of the solid pellet. Thus, in reactions controlled by mass-transfer, the extent of reaction varies linearly with time, the concentration of the reactant gas, and the ratio of the surface area to the volume of the pellet. Mass transfer becomes relatively more important with increasing temperature and decreasing pellet size.

When the solid is porous, or becomes porous during the course of the reaction, the rate of diffusion of the gases through the pores may become significant. Pore diffusion is inherently more complex than molecular diffusion, but its incorporation may be simplified by assuming that

the laws of molecular diffusion are obeyed and then working in terms of an effective diffusivity, D_e.

The interaction between the gaseous reactant and the surface of the solid proceeds via adsorption of the gas, and possibly also involves reaction of this adsorbed species on the surface, and then desorption of product gases. Again, one or more of these processes may be rate-limiting. When the adsorption of the reactant gas is rate-limiting, the rate is described by[9]:

$$Rate = k\frac{P_A - P_C/K}{1 + (K_A/K + K_C)P_C} \tag{2.3}$$

where K_A and K_C are the Langmuir constants for gases A and C, and P_A and P_C are the partial pressures of A and C. A similar expression is obtained for reactions limited by desorption. Reactions limited by the rate of surface reactions are described by Langmuir-Hinshelwood kinetics, according to which:

$$Rate = k\frac{K_A P_A}{(1 + K_A P_A + K_C P_C)} \tag{2.4}$$

For reaction between a nonporous solid and a gas, occurring at a sharply-defined interface, the reaction may or may not result in the formation of a solid product layer around the reactant. When the products of the reaction are gases, the reaction may be controlled by mass transport, chemical reaction, or by a combination of these. When chemical reaction is rate-limiting, the rate equation takes the form of the R2 and R3 models, described here by[9]:

$$\begin{aligned} g_{F_p}(\alpha) &= \left(\frac{bk}{\rho_S}\right)\left(\frac{A_p}{F_p V_p}\right)[C_{A0}^n - (C_{C0}^m/K)]t \\ &= 1 - (1 - \alpha)^{1/F_p} \end{aligned} \tag{2.5}$$

If a solid product layer forms around the reactant—the so-called "shrinking unreacted core" model—diffusion through the product layer may also be important. Here the applicable expression is

$$p_{F_p}(\alpha) = \left(\frac{2bD}{\rho_s r_p^2}\right)(C_{A0} - C_{C0}/K)\left(\frac{K}{1+K}\right)t$$

$$= 1 - 3(1-\alpha)^{\frac{2}{3}} + 2(1-\alpha) \qquad (2.6)$$

$$= \alpha^2 \qquad (2.7)$$

$$= \alpha + (1-\alpha)\ln(1-\alpha) \qquad (2.8)$$

(where r_p is the original position of the external surface) to describe reactions limited by diffusion through the pores. These equations clearly parallel the solid-state diffusion models. In the regime where both chemical reaction and pore diffusion contribute significantly to the overall reaction rate, the rate expression

$$t^* = g_{F_p}(\alpha) + \sigma_S^2 p_{F_p}(\alpha) \qquad (2.9)$$

should be used. Here

$$\sigma_s^2 = \left(\frac{k}{2D_e}\right)\left(\frac{V_p}{A_p}\right)\left(1 + \frac{1}{K}\right) \qquad (2.10)$$

is the shrinking-core reaction modulus, and indicates the relative importance of chemical reaction and diffusion. Care has to be taken in assessing the kinetics of these types of reactions because it is often difficult to distinguish between different reaction mechanisms. The rate-controlling mechanism can only be determined accurately by a careful investigation of other important variables.

When a porous solid reacts with a gas, the reaction may occur in a diffuse zone, as opposed to a sharply-defined interface. In gasification reactions, pore diffusion must also be considered for porous solids, in addition to the factors which influence the gasification of nonporous solids. If a product layer is formed around the pellet, the overall rate may be controlled by chemical reaction, pore diffusion, or by a combination of these. When chemical

reaction controls the overall rate, the reaction of the individual grains in the pellet may be described by eqn (2.9). For reactions controlled by pore diffusion, the analysis is identical to that of the diffusion-controlled shrinking unreacted-core model, given by eqns (2.6), (2.7), and (2.8). When both chemical reaction and pore diffusion contribute significantly to the rate of the overall process, the rate equation becomes complex and must be solved numerically.

2.1.4 Reactions between solids occurring via intermediate gases

In some reactions between solids, the direct reaction between the solid phases may be overshadowed by indirect reaction involving the formation and reaction of intermediate gases with the solid species. The process thus involves two gas-solid reactions:

$$A_{(g)} + bB_{(s)} \longleftrightarrow cC_{(g)} + eE_{(s)} \qquad (2.11)$$

and

$$C_{(g)} + dD_{(s)} \longleftrightarrow aA_{(g)} + fF_{(s)} \qquad (2.12)$$

Although the kinetics of reactions between solids and gases, and of other solid state reactions have been extensively studied, reactions of solids occurring via intermediate gases are considerably more complicated, and until quite recently the theory of these reactions had not received much attention.

Early kinetic studies were usually simplified by assuming that only one of the reactions was rate-limiting. In the reduction of hematite (Fe_2O_3) with carbon, Rao[12] assumed that reaction of CO_2 with carbon was the slow step in the process. Based on the first-order kinetics of this reaction, he derived a simple expression relating the extent of reaction to time:

$$\log\,(1.743 - \alpha) = \frac{-kt}{2.303} + \log\,1.743 \qquad (2.13)$$

In a later article[13], Rao extended this model to take account of mass transfer of gases out of the sample. The concentrations of CO and CO_2 were considered as a function of time and position within the sample, as well as of the CO/CO_2 equilibrium ratios between different iron oxide phases. The reaction of CO_2 with carbon was described by a Langmuir-Hinshelwood rate equation. He derived kinetic equations which had to be solved numerically.

Sohn and Szekely[14] proposed a more general kinetic analysis, by assuming that the rates of both reactions (2.11) and (2.12) were controlled by chemical kinetics, and that the concentration of gas species was uniform throughout the pellet. They used Langmuir-Hinshelwood rate expressions to describe both reactions, and obtained a rate expression which had to be solved numerically. In the case where the reactivity and relative molar quantity were much greater for one reactant than for the other, the kinetics became identical to the geometric models. Their model could predict the relative molar ratio at which both solids would be completely reacted. The effect of changing particle size and temperature could also be predicted. However, they pointed out that the intrinsic mechanism of the individual reactions should be determined separately.

2.2 Reduction of tungsten oxides with hydrogen

2.2.1 Introduction

Reduction with hydrogen is the primary means of obtaining tungsten for the cemented carbide and other industries and has been extensively studied. The effects of temperature, gas flowrate, powder layer height and the properties of the starting oxide on the reduction and the resulting tungsten powder are well known. However, different experimental conditions have sometimes produced contradictory results, and care must be taken when interpreting and comparing results in the literature.

2.2.2 Tungsten oxides occurring during the reduction

A number of stable, well-defined phases exist between WO_3 and tungsten metal. Pure WO_3 is yellow, but a slight loss of oxygen (between $W_{20}O_{58}$ and WO_3) results in a marked change in colour. It has a slightly distorted cubic ReO_3 structure, in which neighbouring WO_6 octahedra share corners[15] (see Fig. 2.1a). Depending on the amount of oxygen present, the colour may vary between yellow and blue. (So-called tungsten blue oxide falls in this composition range, but it does not have a precisely defined stoichiometry.)

The suboxide closest in oxidation state to WO_3 has a well-defined stoichiometry, $W_{20}O_{58}$, and arises from the formation of crystallographic shear planes in the WO_3 lattice[15]. These shear planes are composed of edge-sharing WO_6 octahedra and occur at regular intervals throughout the lattice (Fig. 2.1b). $W_{20}O_{58}$ is a deep blue colour. The next suboxide is $W_{18}O_{49}$, which has a reddish-violet colour and forms needle-like crystals. The unit cell contains both six and seven-coordinate tungsten atoms, and wide tunnels run straight through the structure[15], Fig. 2.1c.

Further reduction produces WO_2, a brown solid with a distorted rutile structure[15]. It contains WO_6 octahedra linked in chains by sharing edges. Tungsten itself is a silver-grey metal, usually existing as the stable phase, α-W, which has a body-centred cubic structure[16]. Another tungsten allotrope, β-W, has been proposed, but disagreement exists as to whether it is metallic tungsten, or is actually a suboxide, W_3O. It is a metastable phase, and has a cubic structure[16].

The extent to which these phases occur in a particular system is governed by the temperature and the H_2O/H_2 ratio, as is depicted in the phase diagram of Bousquet and Perachon[17-19], Fig. 2.2. In particular, the humidity found in the powder layer increases with increasing sample size and layer height, and with decreasing hydrogen flowrate. A concentration gradient of water vapour is formed across the powder layer, and thus different reactions may occur at different depths in the powder layer, as has often been observed[20-22]. The H_2O/H_2 ratio may also be affected by diluting the hydrogen with an inert gas, or by increasing the rate of formation of water vapour by increasing the temperature.

The reduction of tungsten oxides with hydrogen is distinct from the reductions of other metal oxides in that it involves the formation of a volatile ternary compound, $WO_2(OH)_2$. The existence of this compound was first inferred by Millner *et al.*[23], who observed that water vapour greatly increased the volatility of tungsten oxides. This increase in volatility facilitates growth of tungsten oxide and tungsten metal particles during reduction with hydrogen. The temperature dependence and the influence of the H_2O/H_2 ratio on the formation of $WO_2(OH)_{2(g)}$ are shown in Figs. 2.3[24] and 2.4[22]. As Fig. 2.5 shows, the partial pressure of $WO_2(OH)_{2(g)}$ is much higher than the partial pressures of gaseous tungsten oxides at 1000°C.

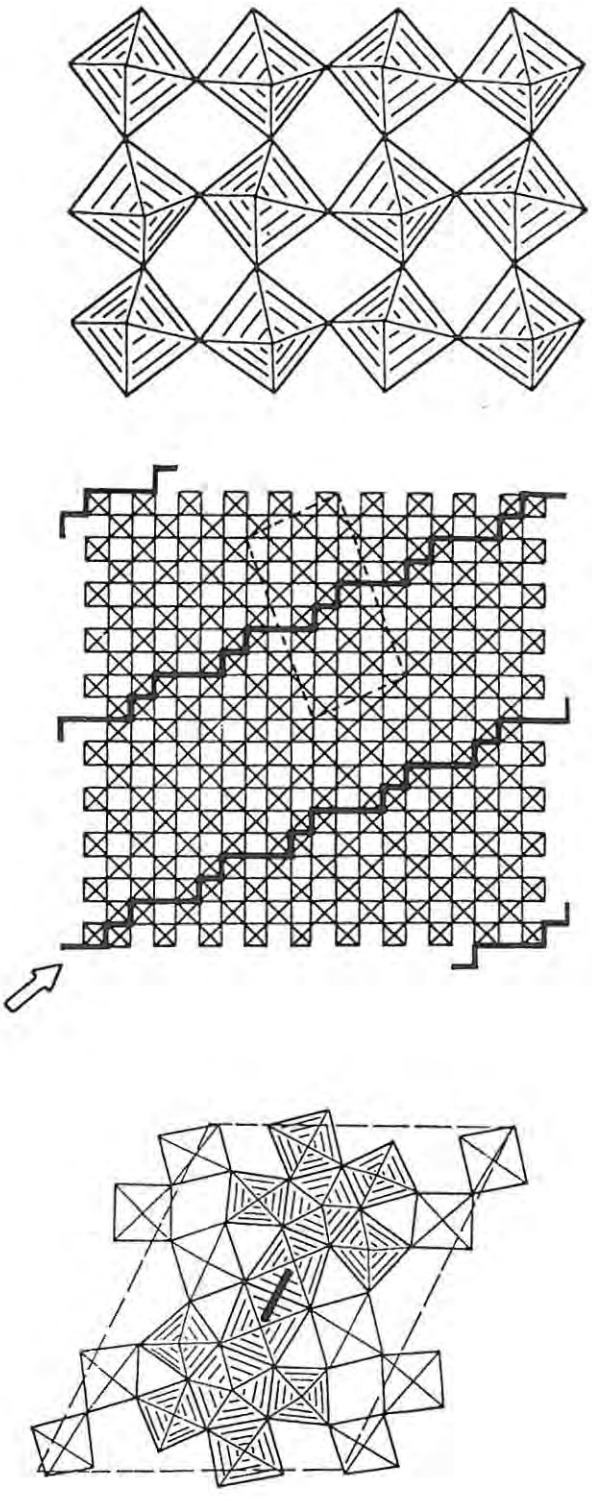

(a)

(b)

(c)

Fig. 2.1. The structures of (a) WO_3, (b) $W_{20}O_{58}$, and (c) $W_{18}O_{49}$.

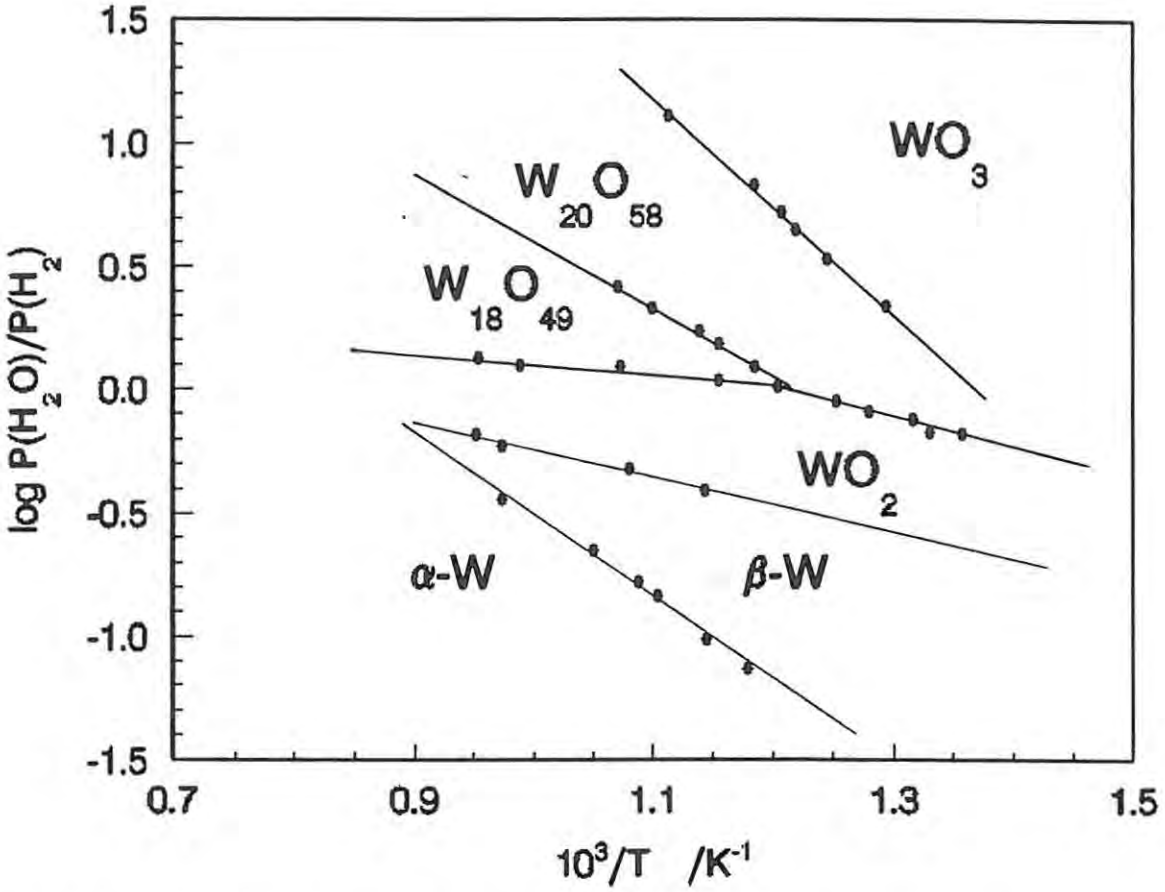

Fig. 2.2. The phase diagram of tungsten and tungsten oxides (from Bousquet and Perachon[17-19]).

2.2.3 Reaction paths in the reduction

The existence of different phases during the reduction depends on the particular system being studied. Changes in the temperature and humidity in the system may alter the phases and hence the reaction paths which occur. Wilken *et al.*[25] carried out a comprehensive study of the reaction paths which the reduction follows. In more recent work, Schubert[22] obtained a similar reaction scheme, which is shown in Fig. 2.6. Individual paths in the reaction will be discussed below.

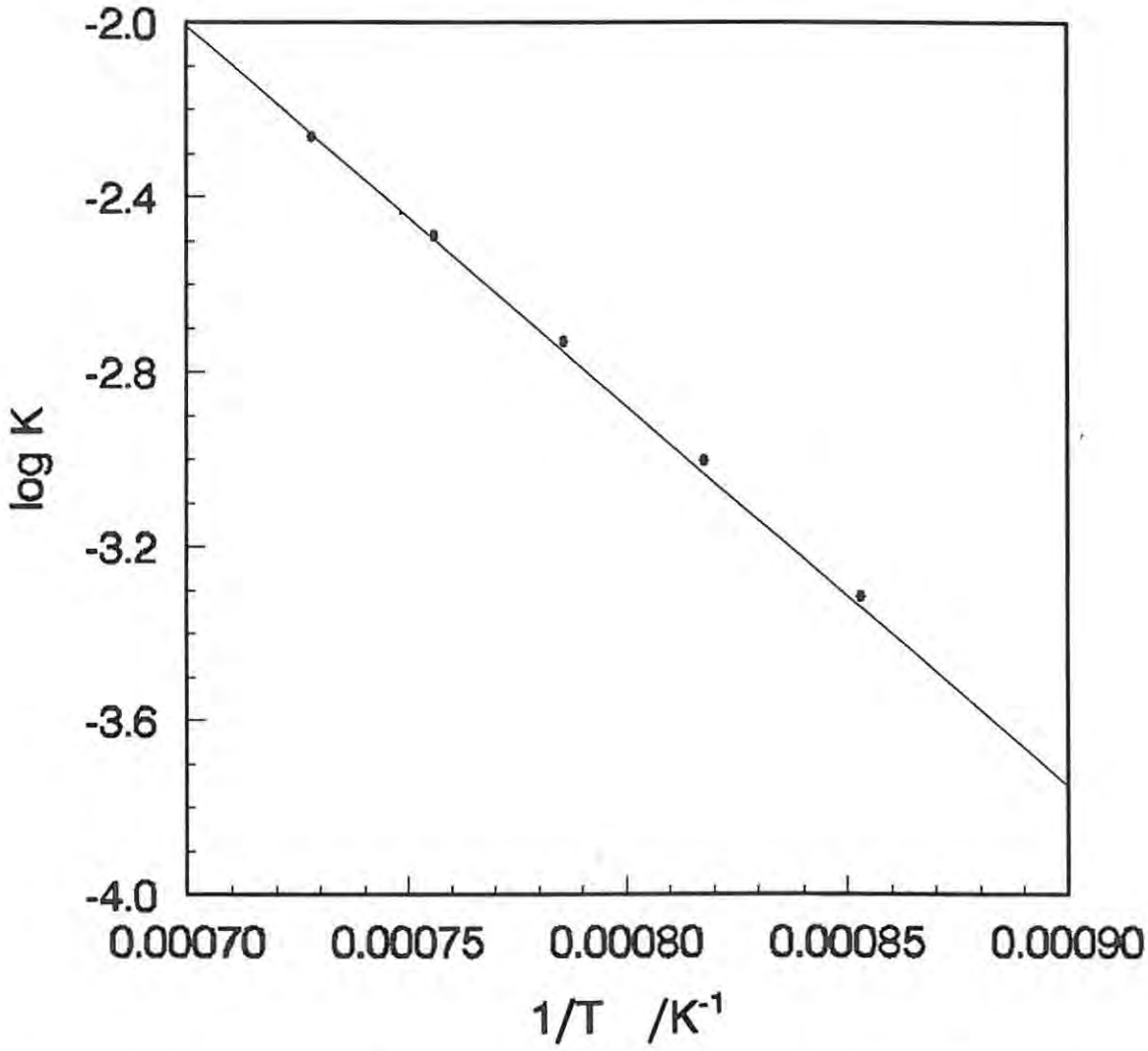

Fig. 2.3. The temperature dependence of the equilibrium $WO_{3(s)} + H_2O_{(g)} \leftrightarrows WO_2(OH)_{2(g)}$ (from Glemser and Haeseler[24]).

The first step in the reduction is the formation of $W_{20}O_{58}$, which occurs at all temperatures and humidities. (Whittingham and Dickens[26] have reported that WO_3 may be reduced directly to α-W if it is first heated at 900°C for 6 hours in a vacuum, but they did not explicitly rule out possible decomposition of WO_3 to $W_{20}O_{58}$.) In dry conditions and below about 600°C, $W_{20}O_{58}$ is reduced directly to β-W. Pure β-W (as indicated by X-ray diffraction) may be prepared in this way at about 500°C[27]. At this temperature, β-W is transformed very

slowly to α-W, although the transformation occurs much more rapidly at higher temperatures. Moisture increases the stability of β-W. Schubert[22] has reported that $W_{20}O_{58}$ is reduced directly to α-W between 550 to 620°C.

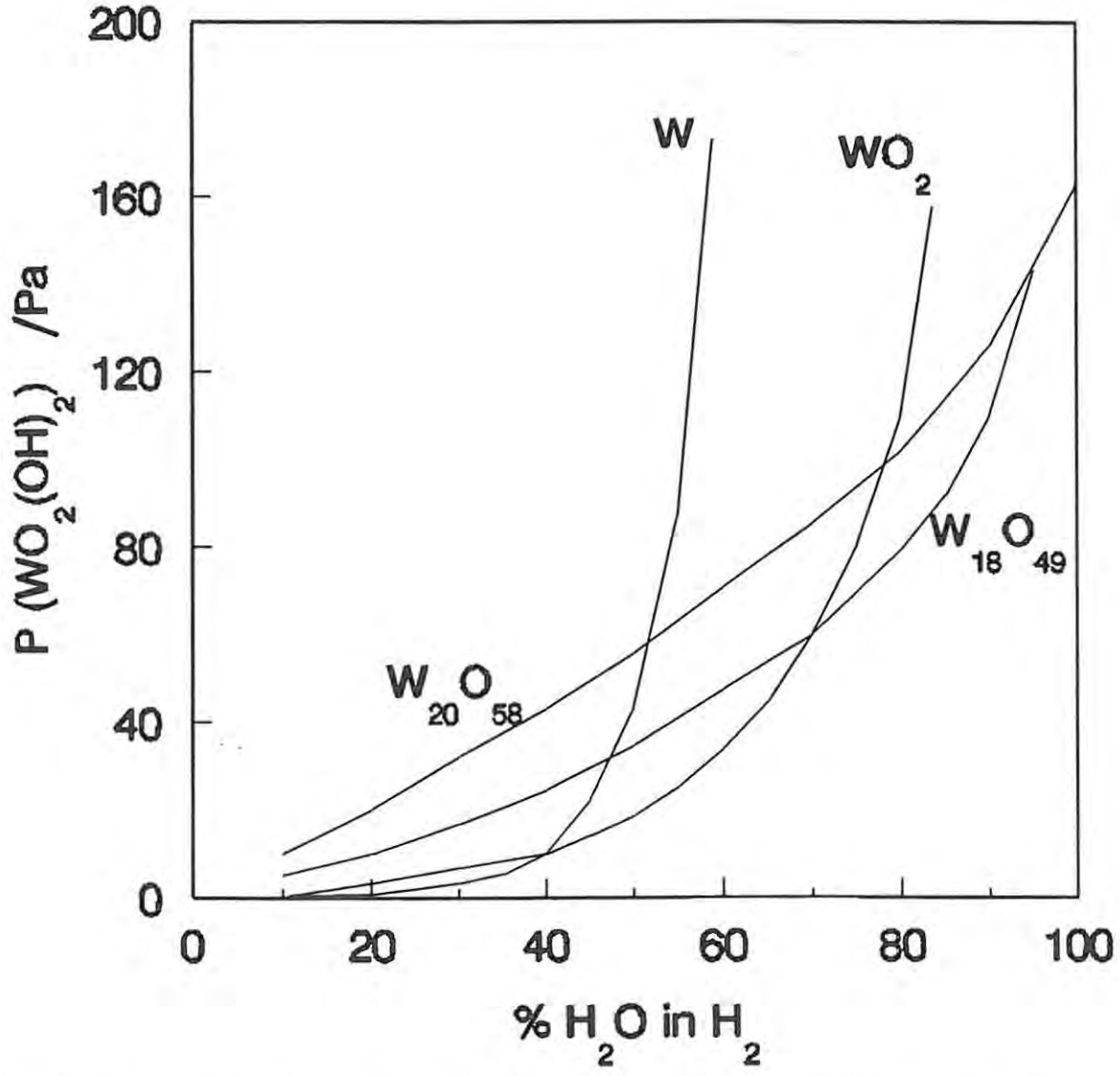

Fig. 2.4. The variation in the calculated partial pressures of $WO_2(OH)_{2(g)}$ at different H_2O/H_2 ratios at 1000°C[22].

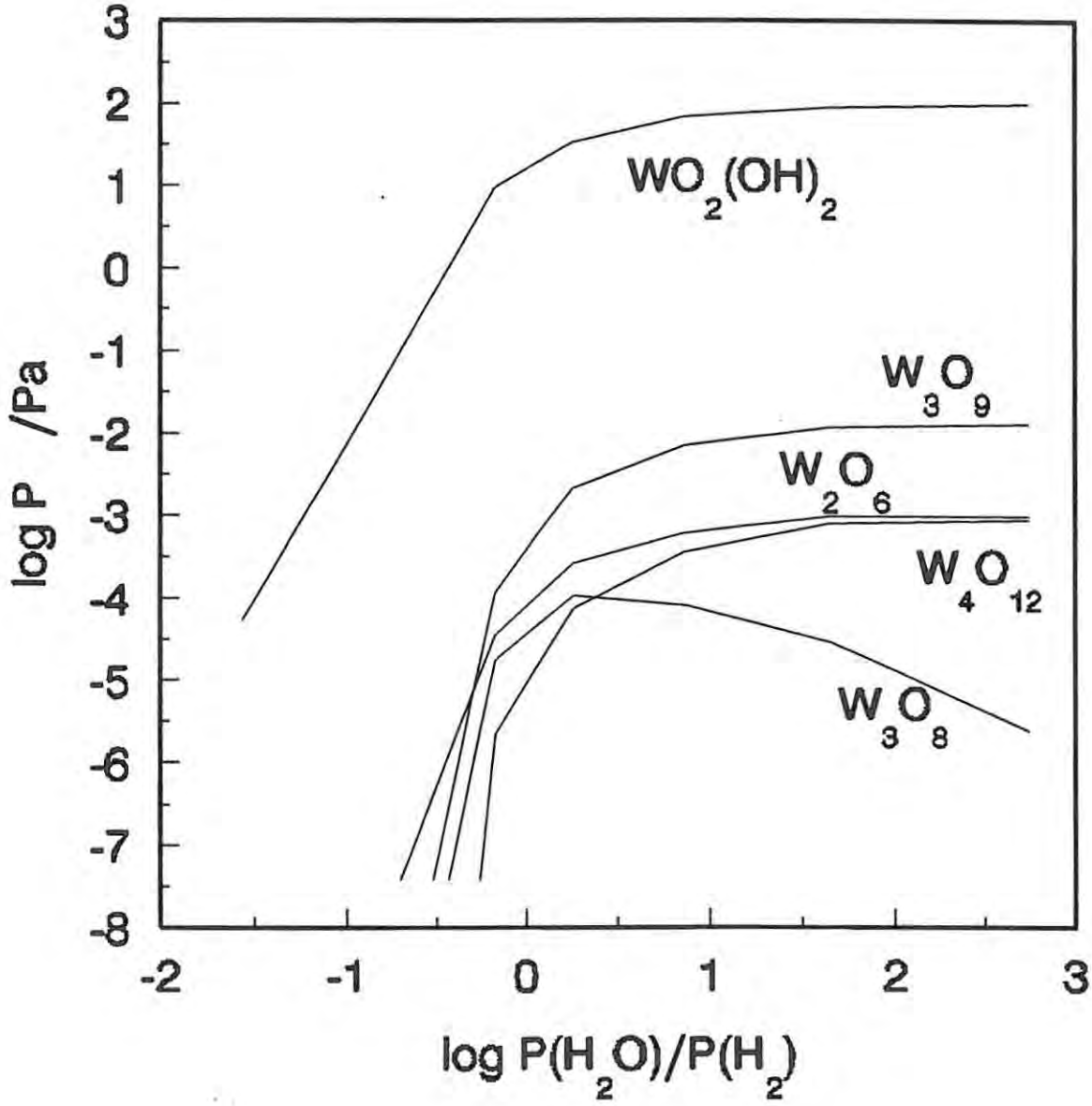

Fig. 2.5. The equilibrium partial pressures of various tungsten oxide and hydroxide species at 1000°C[35].

At higher temperatures and humidities, the reaction proceeds mainly by reduction of $W_{20}O_{58}$ to WO_2. According to Schubert[22], this is the most important path between 520 and 620°C. From their study under drier conditions, Wilken *et al.*[25] reported that it is the predominant reaction between 575 and 800°C. In relatively humid conditions and above about 560°C, $W_{20}O_{58}$ may be reduced to $W_{18}O_{49}$. Schubert[22] observed $W_{18}O_{49}$ above 570°C, when

it occurred simultaneously with the $W_{20}O_{58}$ ——▸ WO_2 reaction path. The reduction of $W_{20}O_{58}$ to $W_{18}O_{49}$ is the main reaction path above 700°C, although the formation of $W_{18}O_{49}$ can be prevented up to 800°C in dry conditions. Wilken *et al.*[25] and Charlton[28-29] obtained similar results, as did Fouad *et al.*[30], who observed the formation of $W_{18}O_{49}$ between 520 and 600°C as a distinct step in nonisothermal thermogravimetry (at a heating rate of 10°C min^{-1}).

The reduction of $W_{18}O_{49}$ to WO_2 occurs between about 570 and 1100°C[22,25]. Fouad *et al.*[30] reported that this reaction occurred between 600 and 655°C. The direct formation of α-W and β-W from $W_{18}O_{49}$ has been observed[22,26,29]. The reaction occurs under dry conditions and over a broad temperature range (570 to 1050°C)[22].

The reduction of WO_2 to α-W also occurs over a broad temperature range[3,22,25,26,29-33]. Fouad *et al.*[30], using nonisothermal thermogravimetry, reported that the reduction occurred from 713 to 875°C. It is a slow reaction and is rate-limiting. Zhiqiang and co-workers[34] have

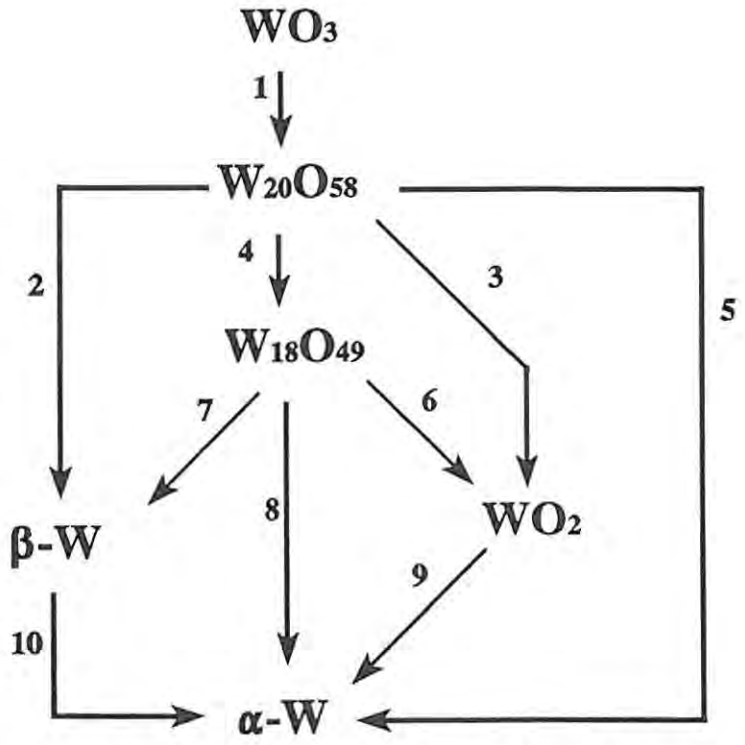

Fig. 2.6. The reaction scheme for the reduction of WO_3 with hydrogen, reported by Schubert[22].

reported the reduction of WO_2 to β-W. They found that moisture promoted this reaction and increased the temperature at which β-W was formed. They also observed that α-W is always formed shortly after β-W, and concluded that β-W is an unstable phase with a high activity.

2.2.4 Morphological and kinetic studies

Changes in the morphology of the tungsten oxide particles during reduction have been studied in detail. A characteristic of reduction of tungsten oxides with hydrogen is the retention of the shape of the original particles[25,35]. These "pseudomorphs", as they are called, are often composed of open agglomerates of small single crystals, and indicate significant physical contact between the particles comprising the pseudomorph. The porosity of these pseudomorphs decreases with temperature and humidity, because of a concomitant decrease in the transport of tungsten through the gas phase. A consequence of the formation of the pseudomorphs is that microporosity (within the pseudomorph) must be distinguished from macroporosity (between pseudomorphs). Both of these quantities change during the course of the reaction.

The first step in the reduction, $WO_3 \longrightarrow W_{20}O_{58}$, occurs without a change in morphology[22,25,31], and has been attributed to a solid state reaction. Whittingham and Dickens[26] have reported that the BET surface area of the particles does not change during this step, and that the rate at which this step occurs is proportional to the partial pressure of hydrogen. They proposed that oxygen ions diffuse to the surface where they are abstracted by molecular hydrogen.

Star-shaped cracks form on the surface of particles during the direct reduction of $W_{20}O_{58}$, $W_{18}O_{49}$, and WO_2 to α- and β-W[22,25,32], and also during the reduction of $W_{20}O_{58}$ to WO_2[22,25,36]. The development of these cracks has been attributed to local contraction arising from the formation of a more dense reduced phase[25].

The reduction of $W_{20}O_{58}$ to $W_{18}O_{49}$ is rapid, and results in the formation of long, needle-like crystals[21,22,32,35,36]. Both Taskinen *et al.*[33] and Sarin[21] regarded the rapidity with which these crystals formed as evidence for a vapour-to-solid mechanism. Sarin proposed that the gaseous tungsten hydroxide decomposed to form $W_{18}O_{49}$ needles. The needles grew by linking WO_6 octahedra in rows along the *b*-axis of the $W_{18}O_{49}$ monoclinic unit cell.

Different morphologies have been observed during the reduction of $W_{18}O_{49}$ to WO_2. Sarin[21] reported that spherical single crystals of WO_2 were formed, either by nucleation at the centre of needle clusters, or by converting individual $W_{18}O_{49}$ needles into WO_2. Basu and Sale[36] also observed the formation of rounded grains of WO_2. They also reported that the reduction from $W_{18}O_{49}$ to α-W occurred much more rapidly than reduction from WO_3, thereby indicating the importance of particle size, porosity, and morphology on the reaction rate. Schubert and co-workers[22,31] observed that the reduction started at distinct points in the $W_{18}O_{49}$ structure and propagated radially, forming WO_2 rosettes or longer WO_2 crystals at higher temperatures and humidities. A gap observed between the two phases was taken as evidence for a chemical vapour transport reaction.

The kinetics of the reduction of $W_{18}O_{49}$ to WO_2 have been studied by Taskinen *et al.*[33], who found that the reaction fitted a one-dimensional solid-state diffusion model. They observed a marked decrease in the reduction rate close to an O/W ratio of 2.72, and suggested that $W_{18}O_{49}$ acted as a barrier to the diffusion of oxygen. They found that the activation energy decreased at higher temperatures, which they believed was caused by differences in particle morphology at different temperatures.

In contrast to the rapid reduction of $W_{18}O_{49}$, the reduction of WO_2 to tungsten occurs slowly and is the rate-limiting step for the reduction process. There is little change in the morphology of the particles for this reduction under dry conditions[21,22,25,36]. At higher temperatures and under more humid conditions, the tungsten particles grow to form large, well-developed single crystals, often in polygonal or cubic shapes[31,35]. Marked growth steps, characteristic of gas phase condensation processes, have been observed on the surface of the tungsten crystals[35,32]. In particular, Taskinen and co-workers noticed that most particle growth occurred when large amounts of metallic tungsten were present in the system. They suggested that the gaseous tungsten hydroxide was reduced on the tungsten metal surface by hydrogen. Schubert[22] observed fine, ring-like structures of α-W under humid conditions. The growth of tungsten particles occurred simultaneously with the reduction process.

Taskinen and co-workers[32,33] found that the reduction of WO_2 to α-W fitted the R2 kinetic model. The reaction rate was also proportional to the hydrogen partial pressure below about $P(H_2) = 50$ kPa. With a water vapour partial pressure of 1.8 kPa, the reaction rate

increased for hydrogen concentrations of 45 to 98 vol.%, but decreased at lower hydrogen concentrations. Because the rate term of the contracting area model may be written as

$$k = \frac{k'P(H_2)}{r_0} \qquad (2.14)$$

(where r_0 is the initial radius of the particle, and k and k' are the rate coefficient and a constant respectively), the linear variation of the reduction rate with the partial pressure of hydrogen supports this model. Water vapour increased the reaction rate by facilitating the formation of $WO_2(OH)_{2(g)}$, which was reduced in the gas phase. Austin[37] found that the reduction of spherical pellets of WO_2 obeyed the R3 kinetic model.

Sarin[21] suggested that the final tungsten particle size was determined by the formation of $W_{18}O_{49}$ needles and nucleation of WO_2 from these needles. Taskinen and Tikkanen[32] observed that dilute mixtures of hydrogen with nitrogen produced larger tungsten particles with well-developed crystal morphologies, and that reduction of WO_2 resulted in larger particles. Schubert *et al.*[35] reported that at high temperatures tungsten pseudomorphs were comprised of completely intergrown crystals and were frequently hollow.

Schubert and co-workers[22,31] have proposed a detailed mechanism for the reduction. According to them, heterogeneous nucleation of a lower tungsten oxide or tungsten metal occurs below a particular H_2O/H_2 ratio (which is below the equilibrium ratio between the two phases). For example, in the reduction of WO_2 to W:

$$WO_{2(s)} + 2H_{2(g)} \longleftrightarrow W_{(s)} + 2H_2O_{(g)} \qquad (2.15)$$

This reaction increases the humidity in the system, and results in an increase in the amount of tungsten in the gas phase via the reaction:

$$WO_{2(s)} + 2H_2O_{(g)} \longleftrightarrow WO_2(OH)_{2(g)} + H_{2(g)} \qquad (2.16)$$

Growth of tungsten nuclei then takes place with the reduction of the gaseous tungsten hydroxide:

$$WO_2(OH)_{2(g)} + 3H_{2(g)} \longleftrightarrow W_{(s)} + 4H_2O_{(g)} \qquad (2.17)$$

As this dissolution-reduction sequence takes place, the gap between the two phases widens. This leads to a progressive lowering of the humidity at the phase being reduced, because less water

vapour formed in the reduction at the reduced phase is transported back to it. The H_2O/H_2 ratio drops at the phase being reduced until nucleation can occur, whereafter the cycle begins again.

If the humidity in the system is high enough, the reduction will follow a stepwise sequence through all the thermodynamically possible phases. At low humidities, simultaneous nucleation of more than one phase may occur during the desiccation stage. The phase with the highest nucleation rate will ultimately be favoured, although other phases may become dominant as the humidity changes during the course of the reduction. Thus, nucleation was considered to be of decisive importance. If the humidity increased above the equilibrium ratio between two phases, reoxidation could occur, as Schubert[22] observed.

Together with the above chemical vapour transport mechanism, Schubert[22] also recognised that solid state oxygen transport may constitute the reaction mechanism in some situations. This occurs via gas-solid or solid-solid interactions. For example:

$$WO_{3(s)} + 0.1H_{2(g)} \longrightarrow W_{20}O_{58(s)} + 0.1H_2O_{(g)} \qquad (2.18)$$

and

$$W_{20}O_{58(s)} + 0.45\beta\text{-}W_{(s)} \longleftrightarrow 1.45WO_{2(s)} \qquad (2.19)$$

Reactions occurring via this mechanism do not change the particle morphology.

From their investigations at low temperatures and humidities, Whittingham and Dickens[26] considered the direct reduction of $W_{20}O_{58}$, $W_{18}O_{49}$, or WO_2 to α- or β-W to consist of three major stages: (i) chemisorption of H_2; (ii) desorption of gaseous products; and (iii) diffusion of the reaction interface. They proposed that hydrogen first adsorbs on tungsten, and migrates over the surface to the reaction interface where it may form a hydroxide group. This occurs rapidly. The reduction of the oxides takes place by reaction of a hydroxide group with an adsorbed hydrogen atom, with tungsten acting as a source of hydrogen atoms. This mechanism is supported by their observation that the rate of reaction is proportional to the half-power of the hydrogen pressure, which indicates that hydrogen atoms are involved in the rate-determining step. Direct reduction resulted in a linear increase in the surface area of the sample, indicating that the reaction took place at an interface where the oxide lattice broke down and the tungsten lattice formed.

Charlton[28,29] has observed an induction period before the next phase in the reduction is formed. Water vapour increased the length of the induction period, probably by reoxidising nuclei of the next phase to be formed. Charlton also proposed that WO_2 and $W_{18}O_{49}$ are formed by the reoxidation of β-W. Wilken *et al.*[25] observed that moisture retards the reduction of WO_2 to α-W below 800°C. The retarding effect of water vapour on the reaction has also been reported by Zhiqiang and co-workers[34].

Bustnes and Du Sichen[20] observed that the reduction of WO_2 to tungsten occurred at a reaction front in the powder bed. Because the rate of reaction was approximately constant, they concluded that transport of H_2 or H_2O was not rate-controlling. These characteristics were not displayed in the reduction of WO_3 to WO_2.

In contradiction to the results of Bustnes and Du Sichen, Fouad *et al.*[30] observed that the reaction rate did depend on the hydrogen flowrate, and indicated the critical control of the H_2 surface reaction. According to them, dissociative chemisorption of hydrogen on tungsten is the rate-determining step. Autocatalysis occurred above about 700°C. Because the rate of the reaction was proportional to the mass of the WO_3 sample, diffusion of gaseous reagents was not rate-limiting.

From the above results, it is clear that the reaction mechanism is still unresolved. It also appears that different reaction mechanisms may operate under different conditions, as Schubert[22] has pointed out. However, contradictory observations and analyses of the system have been made, and need to be explained. The activation energies obtained by some workers are presented in Table 2.2.

Table 2.2. Activation energies for individual reaction paths in the reduction of tungsten oxides with hydrogen.

Reaction	Reaction Conditions	E_a /kJ mol^{-1}
WO_3 ⟶ $W_{20}O_{58}$		
Whittingham and Dickens[26]	300-400°C	96
Taskinen *et al.*[33]	560-660°C	146
	800-1000°C	50
Barret and Dufour[38]	480-720°C	92
$W_{20}O_{58}$ ⟶ β-W		
Barret and Dufour	<630°C	90
	>630°C	33
Whittingham and Dickens	350-550°C	108-113
$W_{20}O_{58}$ ⟶ $W_{18}O_{49}$		
Taskinen *et al.*	560-660°C	138
	800-1000°C	50
WO_3 ⟶ $W_{18}O_{49}$		
Austin[37]	580-850°C	85
WO_3 ⟶ WO_2		
Fouad *et al.*[30]	620-740°C	118 ± 5

Reaction	Reaction Conditions	E_a /kJ mol^{-1}
$W_{18}O_{49}$ ⟶ α-W		
Whittingham and Dickens	425-575°C	142
$W_{18}O_{49}$ ⟶ WO_2		
Taskinen *et al.*	560-660°C	84
	800-1000°C	63
Austin	670-850°C	65
WO_2 ⟶ W		
Whittingham and Dickens	400-700°C	164
Bustnes and Du Sichen	600-1000°C	83
Taskinen *et al.*	800-1000°C, from WO_3	104
	from WO_2	83
Lapostolle and Dufour[39]	520-760°C, 6.6 kPa H_2	138 ± 8
Austin	670-805°C	89

2.2.5 The effect of additives on the reduction

Considerable work has gone into studying the effects of various additives on the reduction of tungsten oxides with hydrogen. The focus has tended to be on so-called NS ("non-sag") dopants, which enhance the properties of tungsten for use in incandescent lamp filaments. Only general considerations will be discussed here.

An important aspect of the interaction of tungsten oxides with other metals is the ability to form tungsten bronzes (M_xWO_3, $x < 1$) and tungstates (M_yWO_4). The formation of these

compounds has a significant influence on the reduction. For instance, Qvick[40] has listed three reactions by which sodium tungsten bronzes might form tungsten metal. These reactions are additional paths to the formation of tungsten, other than the usual reduction of WO_2. They thus increase the overall reaction rate and consequently the humidity in the system. Gas phase transport of tungsten increases and hence larger tungsten particles are formed, as has often been observed[21,27,32,40]. Alkali tungsten bronzes enhance agglomeration of tungsten particles, possibly via a tungstate melt[40], or by diffusion of the alkali metal on the surface or in the bulk of the tungsten[26]. Alkali metals also stabilise β-W, and increase the temperature at which β-is transformed to α-W[27,32,40].

Zeiler *et al.*[41] have reviewed the influence of NS-dopants on the reduction of tungsten oxides with hydrogen. These dopants contain potassium, aluminium, and silicon. Silicates containing potassium and aluminium form in the oxide[41]. Because the dopant contains potassium, similar effects to those produced by alkali metals might be expected, as has indeed been observed. Thus, NS-dopants increase the final tungsten particle size and the rate at which WO_2 is reduced to tungsten[25,32,33,42] (except under very dry conditions[43]). Aluminium strongly retards the reaction above 500°C. The reaction course does not change with the introduction of the dopant, but the dopant does alter the temperature ranges in which particular reaction paths are followed[25,43].

The effect of platinum and palladium on the reduction has been studied. Hydrogen tungsten bronzes form slightly above room temperature in the presence of these metals[44,45]. Uvarova[46] observed that 0.1 % palladium decreased the induction period and increased the initial reaction rate. Bond and Tripathi[45] reported that palladium increased the rate of reduction of WO_3 to W_4O_{11} [this composition probably corresponds to $W_{18}O_{49}$], and suggested that only the hydrogen from the bronze takes part in the reduction. The reduction started at about 230°C when palladium was present, as compared to 480°C without a catalyst. Reduction beyond $W_{18}O_{49}$ proceeded in exactly the same way as in the absence of palladium. Fouad *et al.*[30] believed that this similarity indicated autocatalysis by tungsten formed in the reduction.

2.3 Reduction of metal oxides with carbon

2.3.1 Introduction

The reduction of metal oxides with carbon is of great practical importance, and is an integral part of the extraction of many metals from their ores. Much research, both fundamental and applied, has been done on the reduction of metal oxides with carbon, which is often referred to as "carbothermic" or "carbothermal" reduction. However, reduction with carbon is complicated, and a clear mechanistic picture of the process is still lacking.

Researchers agree that the reduction does not occur primarily by the reaction of solid carbon with the solid oxide, that is, by so-called "direct" reduction:

$$MO_{x(s)} + C_{(s)} \longleftrightarrow MO_{y(s,l)} + CO_{(g)}/CO_{2(g)} \qquad (2.20)$$

where $x > y$. Reaction (2.20) would occur at the points of contact between the reactants, followed by diffusion of the reactants across the product layer. Such a process is expected to be limited by the rate of diffusion of the reactants.

In carbothermal reduction, however, the contribution of reaction (2.20) to the overall process is probably small. Rather, the interaction between the solids is predominantly indirect and takes place via intermediate gases. This involves two gas-solid reactions:

$$MO_{x(s)} + CO_{(g)} \longleftrightarrow MO_{y(s)} + CO_{2(g)} \qquad (2.21)$$

and the "Boudouard" or "solution-loss" reaction:

$$C_{(s)} + CO_{2(g)} \longleftrightarrow 2CO_{(g)} \qquad (2.22)$$

The formation of $CO_{(g)}$ is a necessary first step in the process, and might result from direct reduction (reaction (2.20)), or from the reaction of carbon with oxygen (either residual oxygen or oxygen from the dissociation of the metal oxide). The process terminates when CO and CO_2 are removed from the sample[13].

A number of studies found that the diffusion models fitted the reduction. This is typified by the work of El-Guindy and Davenport[47], who found that the reduction of ilmenite ($FeTiO_3$) with graphite proceeded mainly by solid-solid reaction (i.e., reaction (2.20)) below 1020°C. Above this temperature the reaction rate increased considerably, and proceeded by reactions (2.21) and (2.22). The kinetics were described by the D4 model and CO was proposed to be

the diffusing species.

On the other hand, Rao[12] assumed that reaction (2.22) was rate-limiting in the reduction of hematite (Fe_2O_3) with carbon. This assumption was based on separate kinetic studies of reactions (2.21) and (2.22), which indicated that reaction (2.22) was slower than reaction (2.21). Eqn (2.13) fitted his experimental results and gave an activation energy of 301 kJ mol^{-1}. He suggested that iron catalysed reaction (2.22), as other studies had shown, and regarded the activation energy he obtained as reasonable compared with that of the uncatalysed reaction (360 kJ mol^{-1}) The addition of Li_2O increased the rate of the reduction process by catalysing reaction (2.22). The reduction results fitted the R3 model, indicating that the rate was limited by the reaction of CO_2 at the carbon surface, at which Li_2O would be active. An activation energy of 285 kJ mol^{-1} was obtained for the process with Li_2O as additive.

Bicknese and Clark[48] studied the reduction of FeO with CO in the presence of carbon. They observed that the rate was sensitive to the CO/CO_2 ratio below a certain value. Carbon increased the CO/CO_2 ratio via reaction (2.22), with the result that the reduction became insensitive to the flowrate of CO. The reduction results fitted an R3 model, modified to take the equilibrium concentrations of CO and CO_2 into account. An activation energy of 58 kJ mol^{-1} was calculated. In a similar investigation, Kawasaki *et al.*[49] studied the reduction of relatively large porous hematite pellets with CO and hydrogen. The reduction results fitted the R3 model, and occurred by the ingress of the reducing gas to the reaction interface. The rate of reduction was determined by equimolar countercurrent diffusion of the reactant and product gases. Reduction with hydrogen was about 5 times more rapid than with CO.

Mitchell and Parker[50] studied the reductions of FeO and SnO_2 with carbon. They calculated activation energies of 87 and 84 kJ mol^{-1} for the respective reductions with anthracite, and suggested that these values corresponded to the activation energy of reaction (2.22). The reduction of SnO_2 was much slower using graphite as the reductant, and an activation energy of 277 kJ mol^{-1} was calculated.

In a system analogous to that of the reduction of metal oxides with carbon, Maru and co-workers[51] showed that the reaction between $Cr_{23}O_6$ and Cr_2O_3 also took place via indirect gaseous reactions:

$$1/3Cr_2O_{3(s)} + CO_{(g)} \longleftrightarrow 2/3Cr_{(s)} + CO_{2(g)} \qquad (2.23)$$

and

$$1/6Cr_{23}C_{6(s)} + CO_{2(g)} \longleftrightarrow 23/6Cr_{(s)} + 2CO_{(g)} \qquad (2.24)$$

The similarity between these reactions and reactions (2.21) and (2.22) is readily apparent. For porous $Cr_{23}C_6$ particles, the reaction fitted the R3 model; however, this model applied only at low conversions when less porous $Cr_{23}C_6$ was used. The deviation from the R3 model was ascribed to increased resistance in particles of lower porosity to the transport of the diffusing species, and they suggested that the mechanism involved mixed control by both interfacial reaction (the R3 model) and diffusion. They used the following rate expression to analyse the mixed kinetics of the system:

$$1 - \tfrac{2}{3}\alpha - (1 - \alpha)^{\frac{2}{3}} + \beta\{1 - (1 - \alpha)^{\frac{1}{3}}\} = \gamma t \qquad (2.25)$$

where

$$\beta = \frac{2D_e(P_{CO})_0}{r_0 kRT} \qquad (2.26)$$

and

$$\gamma = \frac{2D_e(P_{CO_2})_0}{\rho_0 b r_0^2 RT} \qquad (2.27)$$

Thus, although there is general agreement that carbon reduces metal oxides indirectly, the rate-limiting step for the reduction varies from system to system. When reaction (2.21) is rate-limiting, the kinetics usually conform to the diffusion models. When reaction (2.22) is the slow step in the reduction, the reduction tends to be first-order with respect to carbon, except where promotive agents (such as Li_2O) are added, in which case the R3 model describes the process better.

2.3.2 Reduction of tungsten oxides with carbon and carbon monoxide

According to Elyutin *et al.*[52], WO_3 is reduced by lamp black below 700°C. CO was not observed and was not considered to take part in the reduction. They proposed that the oxide sublimed and reacted on the carbon surface, whereafter intermediate oxides diffused into the carbon particle, breaking up its structure. Gaseous products (CO and CO_2) were desorbed from the surface. Thus the rate of reaction was considered to depend on the volatility of the oxide. Increasing the flowrate of inert gas up to a certain point increased the reduction rate, after which any further increase in the flowrate decreased the reduction rate.

Miyake and Haka[53] observed that WO_3 sublimed above 1200°C and simultaneously decomposed when the oxygen potential of the atmosphere was low. In the early stages of the reaction WO_3 decomposed and subsequently reacted with carbon. They reported that reduction with carbon started after WO_3 had formed whiskers of $W_{18}O_{49}$.

The thermodynamics of the reduction of WO_3 using a mixture of hydrogen and CO were examined by Alekseev *et al.*[55]. They calculated that WC was formed at 530°C and transformed into W_2C at 730 to 1130°C. The amount of carbon in the gas phase depended on the H_2/CO ratio. Of particular relevance to this study is an article by Petukhov *et al.*[55] comparing the reducing potentials of CH_4, hydrogen, and hydrogen with carbon. They found that solid carbon improved the conditions of the reduction, in accordance with thermodynamic predictions.

The reduction and carburisation of tungsten oxides by CO was studied by Basu and Sale[56] between 600 and 1000°C. They found that gas transport limited the rate of reaction. At 1000°C and above, tungsten metal was formed in the reduction, possibly because the partial pressure of CO_2 was high enough to stabilise metallic tungsten. The product of the reaction consisted only of WC and free carbon—the fraction of WC in the sample was greater at higher temperatures. The reduction and carburisation of $W_{18}O_{49}$ and WO_2 took place more slowly than that of WO_3. Both $W_{18}O_{49}$ and WO_2 were observed as intermediate products in the reaction. They found that the morphology of WO_2 formed from WO_3 did not depend on the nature of the reducing gas used.

2.4 Reactions of carbon with carbon dioxide, water vapour, and hydrogen

The reactions of carbon with CO_2, H_2O, and H_2 have been reviewed by Walker *et al.*[57] Reaction (2.22) is obviously of crucial importance in the reduction of metal oxides with carbon. The variation of the CO/CO_2 equilibrium ratio with temperature is shown in Fig. 2.7[57]. The partial pressure of CO is much greater than that of CO_2 above 800°C, and the atmosphere becomes more reducing at higher temperatures. The rate equation for the reaction is given by:

$$rate = \frac{k_1 P_{CO_2}}{1 + k_2 P_{CO} + k_3 P_{CO_2}} \qquad (2.28)$$

CO retards the reaction by decreasing the fraction of surface covered by oxygen atoms. At low temperatures and high partial pressures of CO_2 the reaction is zero order, but becomes first order at high temperatures or at low CO_2 partial pressures. The activation energies determined for the reaction vary between 250 and 400 kJ mol^{-1}.

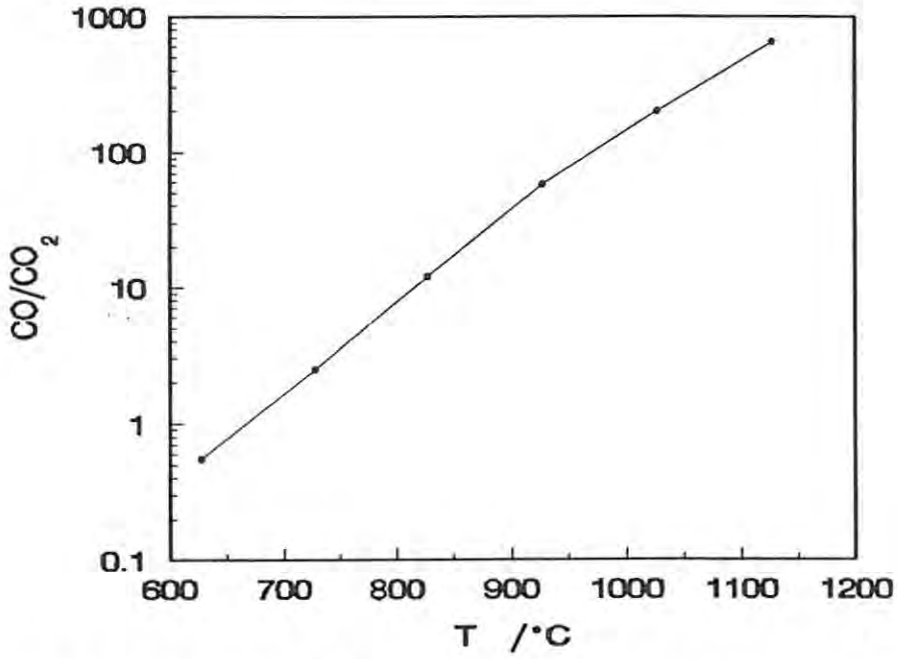

Fig. 2.7. The variation in the CO/CO_2 equilibrium ratio at 100 kPa as a function of temperature for the reaction $C_{(s)} + CO_{2(g)} \longleftrightarrow 2CO_{(g)}$.

The interaction of C and H_2O (the water-gas shift reaction) comprises four individual reactions:

$$C_{(s)} + H_2O_{(g)} \longleftrightarrow CO_{(g)} + H_{2(g)} \quad (2.29)$$

$$CO_{(g)} + H_2O_{(g)} \longleftrightarrow CO_{2(g)} + H_{2(g)} \quad (2.30)$$

$$C_{(s)} + CO_{2(g)} \longleftrightarrow 2CO_{(g)} \quad (2.22)$$

and

$$C_{(s)} + 2H_2(g) \longleftrightarrow CH_{4(g)} \quad (2.31)$$

The effect of temperature on the equilibrium ratios for these reactions is shown in Fig. 2.8[57]. At temperatures above 900°C, the reactions increase the reducing potential of the gas phase, and the partial pressures of CO and H_2 (both reducing agents) are considerably higher than the partial pressures of H_2O, CO_2, and CH_4. The partial pressures of H_2O, CO_2, and CH_4 are quite similar between 800 and 1000°C. The rate equation for reaction (2.29) is similar to that of reaction (2.22):

$$rate = \frac{k_1 P_{H_2O}}{1 + k_2 P_{H_2} + k_3 P_{H_2O}} \quad (2.32)$$

The reaction is zero order at low temperatures and high H_2O partial pressures, but becomes first order at higher temperatures or H_2O partial pressures. The activation energy for the reaction varies between 250 and 340 kJ mol^{-1}.

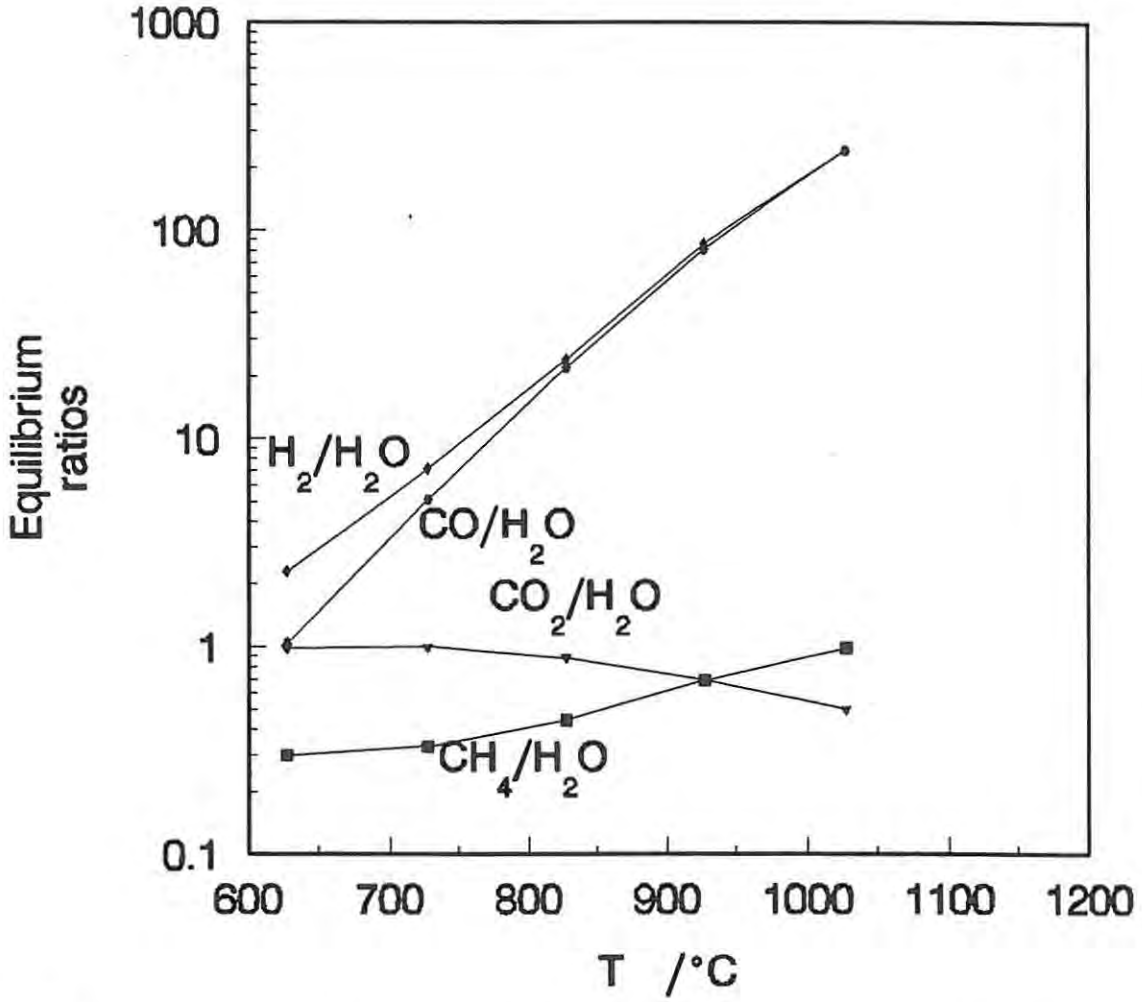

Fig 2.8. The temperature dependence of the equilibrium ratios between different gases and H_2O resulting from the interaction of carbon and water vapour (at 100 kPa).

The reaction of carbon and H_2 has been less extensively studied. From Fig. 2.9, we see that the reaction occurs only to a very slight extent above 900°C[57]. The rate equation above 900°C has been described by:

$$rate = \frac{k_1 k_2 A (P_{H_2})^2}{k_2 + k_3 P_{H_2}} \qquad (2.33)$$

The reaction order is 2 at low pressures and 1 at high pressures. The activation energy for the reaction is about 150 kJ mol^{-1}.

The relative rates of reactions (2.22), (2.28), and (2.30) are of considerable interest. At 800°C and about 10 kPa, the rate of reaction (2.29) is about 3 times greater than that of reaction (2.22), which in turn is about 300 times faster than reaction (2.31).

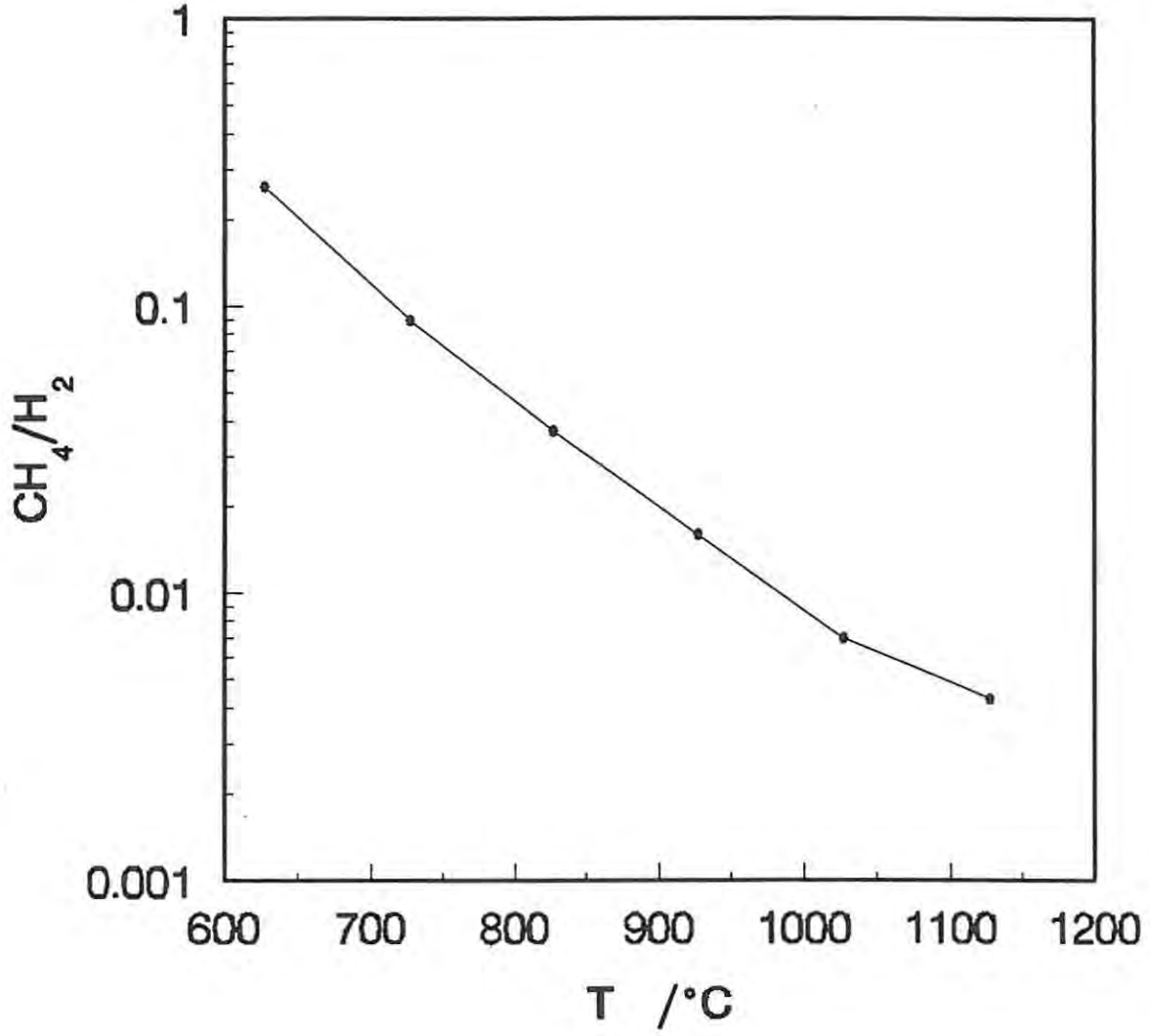

Fig. 2.9. The CH_4/H_2 equilibrium ratio at 100 kPa as a function of temperature for the reaction $C_{(s)} + 2H_{2(g)} \longleftrightarrow CH_{4(g)}$.

Chapter 3

EXPERIMENTAL

3.1 Materials

WO_3 (98% pure) was supplied by Saarchem and had a light pastel green colour. The size distribution of the particles (see section 3.4) is shown in Fig. 3.1a. Large particles were removed by sieving the powder through a 75 μm mesh, and smaller particles by sieving through a 53 μm mesh. Scanning electron micrographs showed WO_3 particles with simple cube-like shapes, Fig. 3.2a. The edges of the particles were rounded and the surface had a smooth texture; small cracks were often apparent. Some very small particles (less than 2 μm diameter) adhered to the larger particles.

Saarchem also supplied the graphite and lamp black (both 99% pure), which were used as the source of carbon. The size distribution of the graphite is shown in Fig. 3.1b. Large grains were removed by sieving through a 53 μm mesh. The graphite particles had jagged and irregular shapes (Fig. 3.2b). In contrast, the lamp black consisted of very small particles which formed fluffy agglomerates. The size distribution is shown in Fig. 3.1c.

WO_2 was prepared by reducing WO_3 at 800°C under hydrogen which had been bubbled through water. $W_{18}O_{49}$ was prepared in a similar manner at a temperature of 700°C. Except for WO_2, in which traces of $W_{18}O_{49}$ were observed, the X-ray powder diffraction patterns were exclusively those of the desired phase. Scanning electron micrographs of WO_2 and $W_{18}O_{49}$ are shown in Figs 3.2c and 3.2d. Some needles typical of $W_{18}O_{49}$ were observed in the WO_2 sample.

High purity argon and hydrogen gases were supplied by Fedgas. Both gases contained less than 3.0 vpm O_2 and 2.0 vpm H_2O. CO and CO_2 were also supplied by Fedgas.

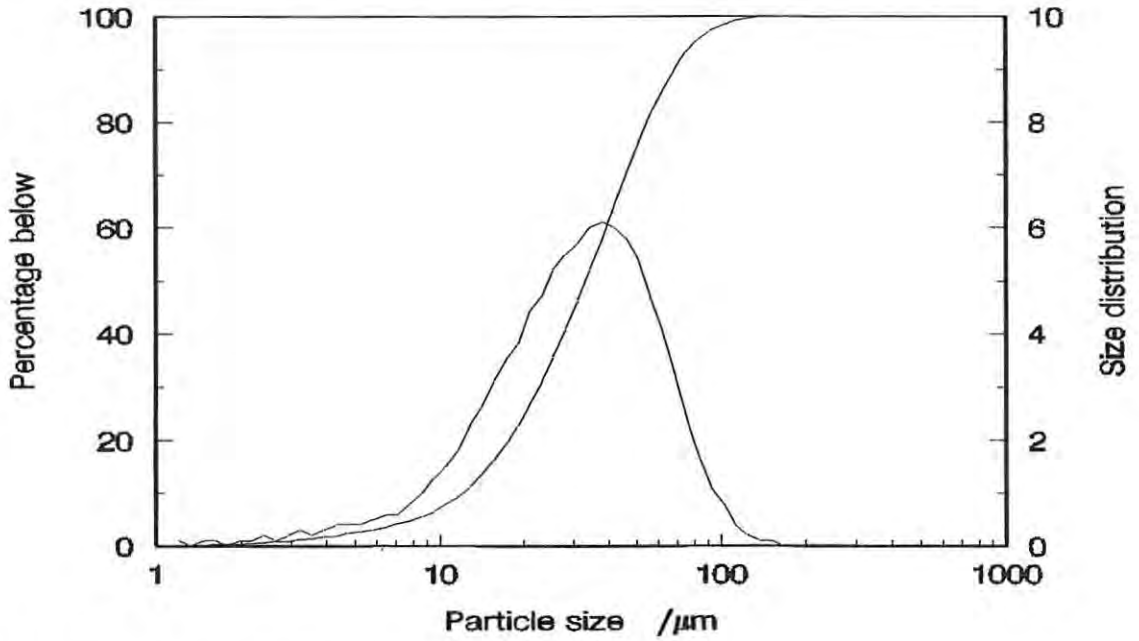

Fig. 3.1a. The size distribution of WO_3.

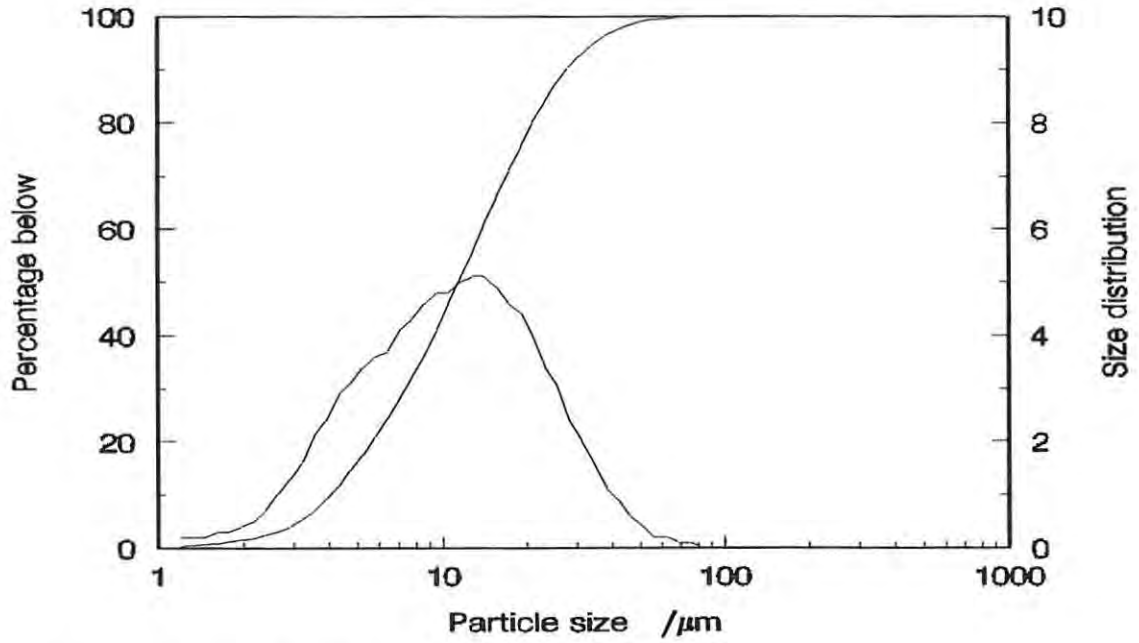

Fig. 3.1b. The size distribution of graphite.

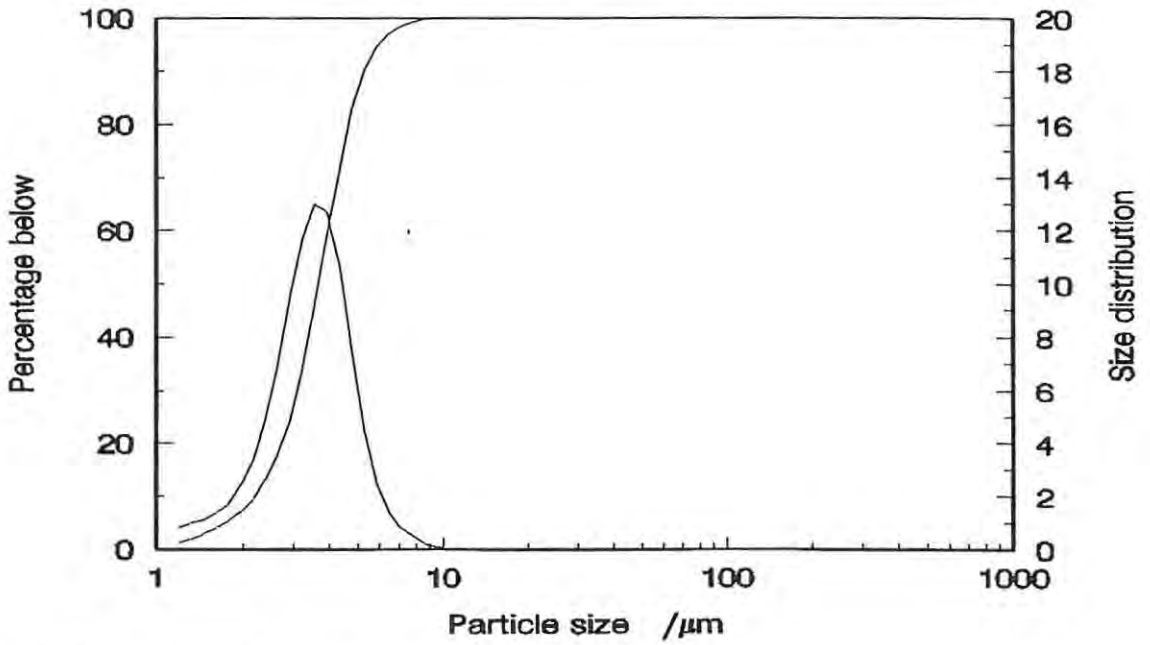

Fig. 3.1c. The size distribution of lamp black.

Mixtures of tungsten oxides and graphite or lamp black were made by weighing the constituents in the desired stoichiometric ratio, and then mixing the substances together. For thermogravimetric experiments, the mixing was carried out in a three-dimensional motion mixer over 18 hours. For other experiments, the mixing was achieved by end-over-end tumbling for at least 4 hours. Care was taken to ensure that the mixtures were not bumped, since they easily lost their homogeneity owing to the large difference in density between the carbon source and the tungsten oxides.

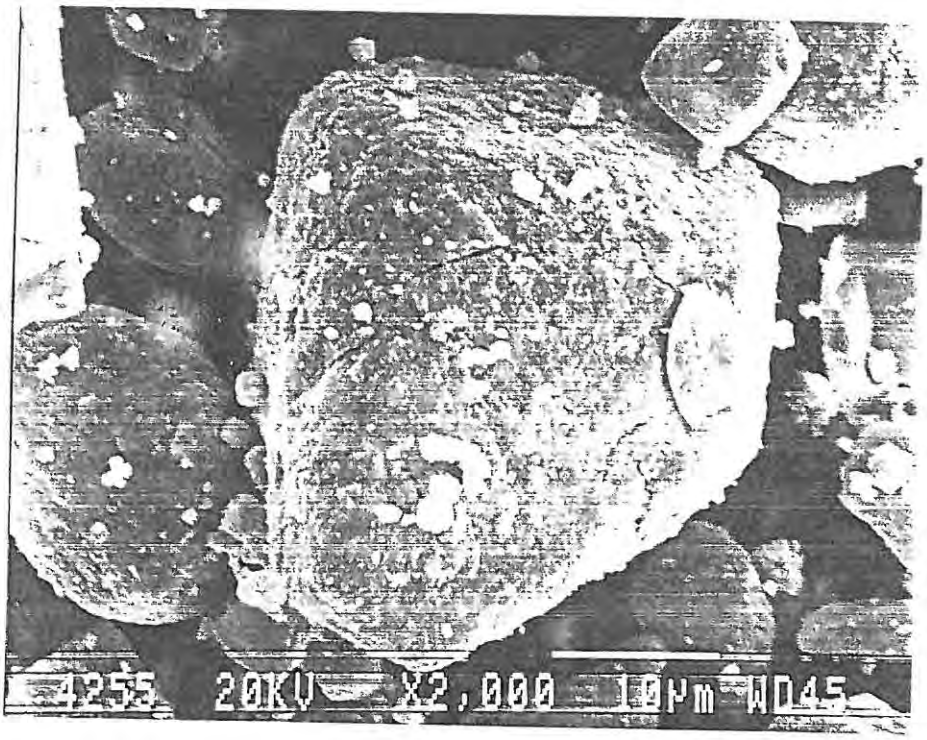

Fig. 3.2a. Scanning electron micrograph of the WO_3 reactant.

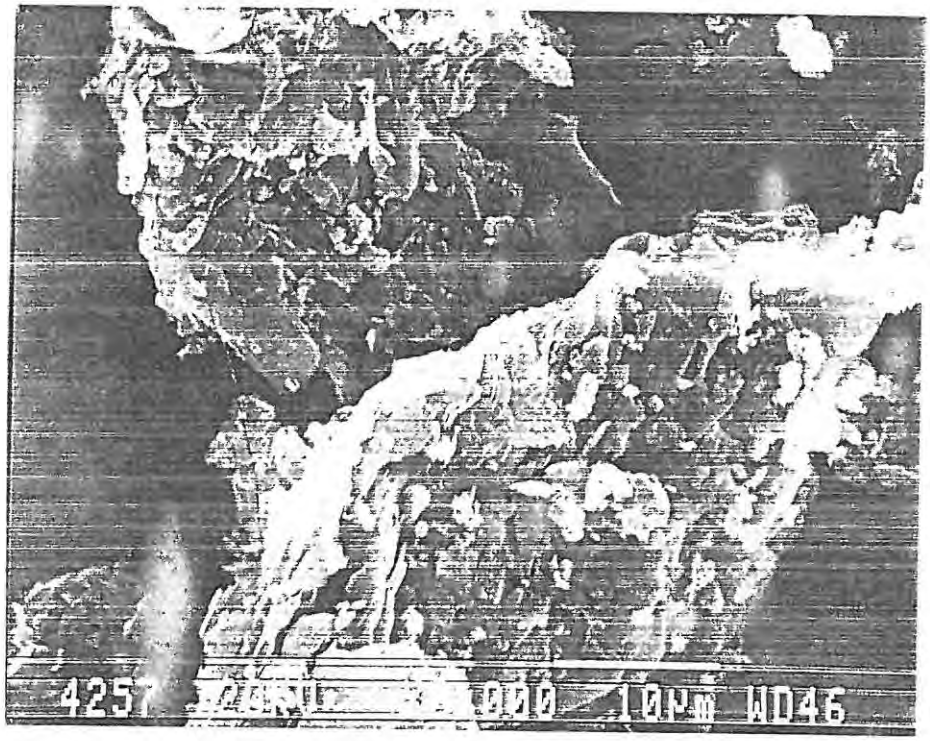

Fig. 3.2b. Scanning electron micrograph of the graphite reactant.

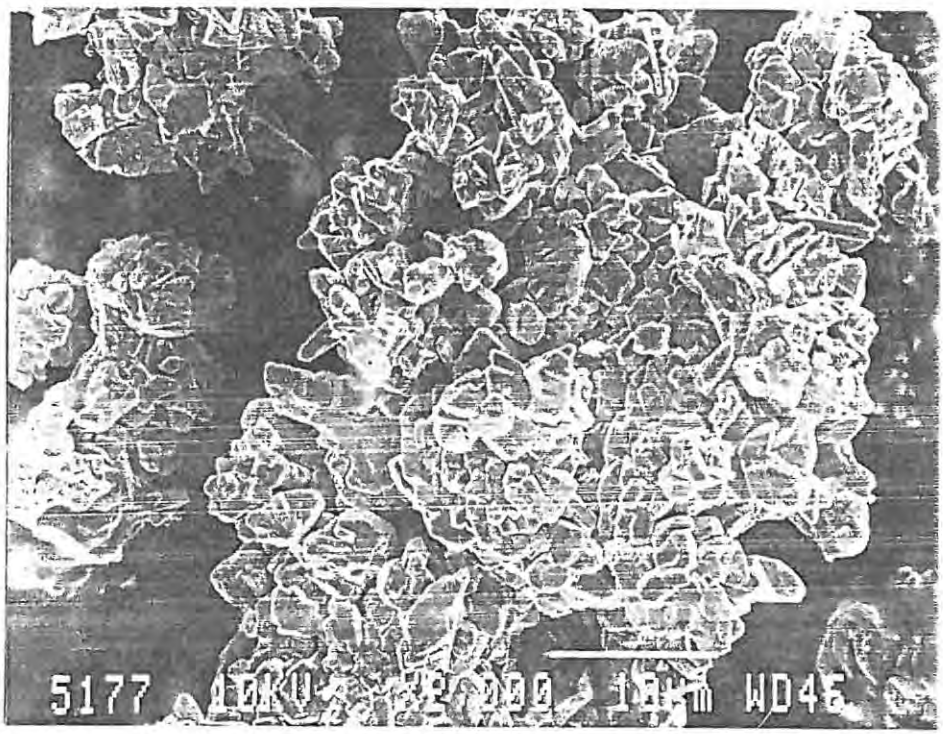

Fig. 3.2c. Scanning electron micrograph of the WO_2 reactant.

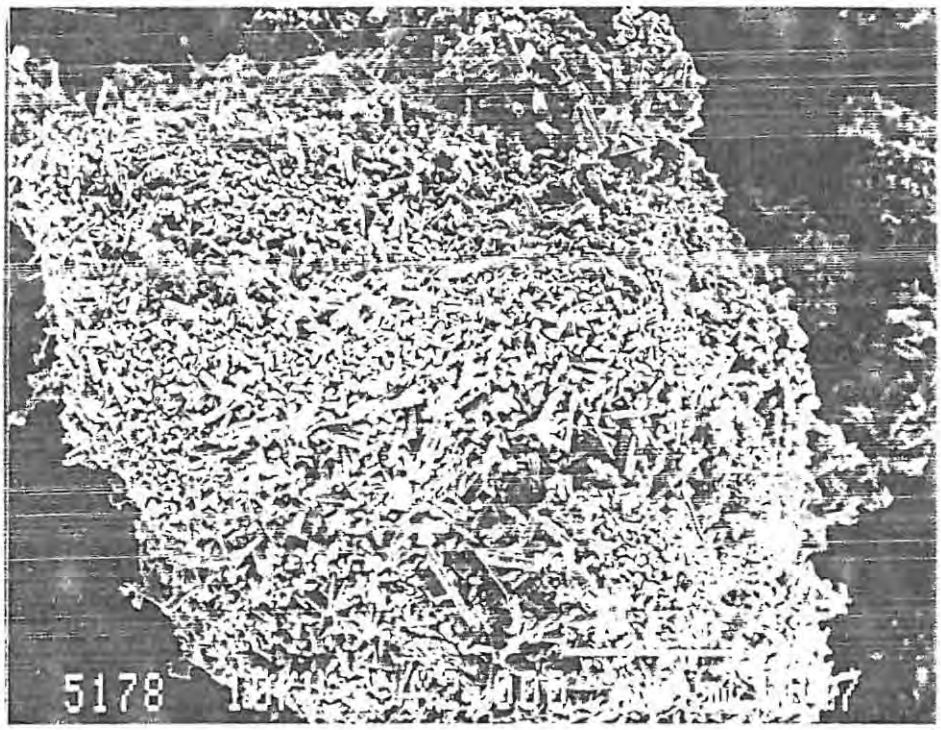

Fig. 3.2d. Scanning electron micrograph of the $W_{18}O_{49}$ reactant.

3.2 Thermal Analysis

3.2.1 Thermogravimetry

Investigations were performed using both isothermal and temperature-programmed thermogravimetry (TG). A Perkin-Elmer TGA-7 system was used for TG experiments below 900°C. Samples were contained in a platinum pan and were examined as loose powders; the sample mass varied between 5 and 40 mg, depending on the sample's density. The Curie point method was used to check the temperature calibration of the TG furnace. Nickel (354°C) and iron (780°C) were used to carry out two-point calibrations.

When experiments were conducted in argon, the system was flushed with nitrogen at a high flowrate (>600 mL min^{-1}) for about 40 min, and then with argon at about 60 mL min^{-1} for a further 20 min before commencing the experiment. Experiments with reactive gases, especially CO, were very sensitive to residual oxygen in the system. For experiments with these gases, the system was evacuated for 20 min, followed by flushing with the sample gas at a high flowrate (>600 mL min^{-1}). The flowrate was then adjusted to the desired flowrate, and the experiment was started.

Experiments at higher temperatures were carried out on a Setaram TGA 92 system. These experiments were done by Ian Sutherland and Ian Porée at AECI Ltd. Samples of 40 to 90 mg were held in an alumina crucible. The system was flushed with argon at 170 mL min^{-1} for at least 20 min before the experiment was started. A heating rate of 99°C min^{-1} was used to reach the desired temperature in isothermal experiments. In dynamic experiments, a heating rate of 5 or 10°C was used.

3.2.2 Differential Thermal Analysis

A Perkin-Elmer DTA 1700 system was used for differential thermal analysis (DTA) experiments. Sample masses of between 10 and 60 mg were held in an alumina crucible and studied in argon. The flowrate was less than 60 mL min^{-1}. The DTA system was flushed for about 20 min prior to starting an experiment.

3.3 Tube Furnace and Gas Detection System

3.3.1 Description of the system

Reactions of larger masses (0.25 to 5.0 g) of samples were studied in a Carbolite MTF 12/38B tube furnace, which had a maximum temperature of 1200°C. Fig. 3.3 shows the tube furnace and the gas detection system. The sample was enclosed in a stainless-steel tube, which was positioned in the furnace and connected to the gas supply. The temperature in the reaction tube was approximately constant (± 5°C) at the position of the sample. Flexible tubing on both sides of the reaction tube allowed the tube to be rapidly inserted into or removed from the furnace. By so doing, rapid heating and cooling of the sample was achieved. The temperature measured at the sample's position is shown in Fig. 3.4 during heating to, and cooling from, 900°C.

The exhaust gas from the reaction tube passed through a filter and then though a Servomex MK158 thermal conductivity detector (TCD), which was enclosed in an oven at 150°C. To prevent condensation of water vapour before the TCD, the exhaust line between the tube furnace and TCD was heated with a heating coil. A reference gas stream was also fed to the TCD. The pressure of the gas in the system was controlled by a pressure regulator, and was usually between 1.2 and 1.4 bar. Needle valves were used to adjust the flowrates of the sample and reference gas streams. The flowrate was determined with a digital flowmeter. After the TCD, the sample gas passed through an infrared CO_2 detector and then an infrared CO detector, both from Edinburgh Sensors (see Appendix A). The CO_2 detector had a range of 0 to 1 vol.% CO_2, and the CO detector had a range of 0 to 10 vol.% CO. The exhaust gas was directed out of the building.

The voltage across the TCD filaments and the bridge balance could be adjusted at the TCD control unit. Output from the TCD was amplified 500 times, and recorded by an 8088 IBM PC using a PC-26 analogue-to-digital (A-to-D) board. The Turbo C program, ATOD2 (Appendix B) collected the data at a sampling interval between 0.01 and 10 s. Up to 10000 readings could be collected. The data were saved to a file for further processing.

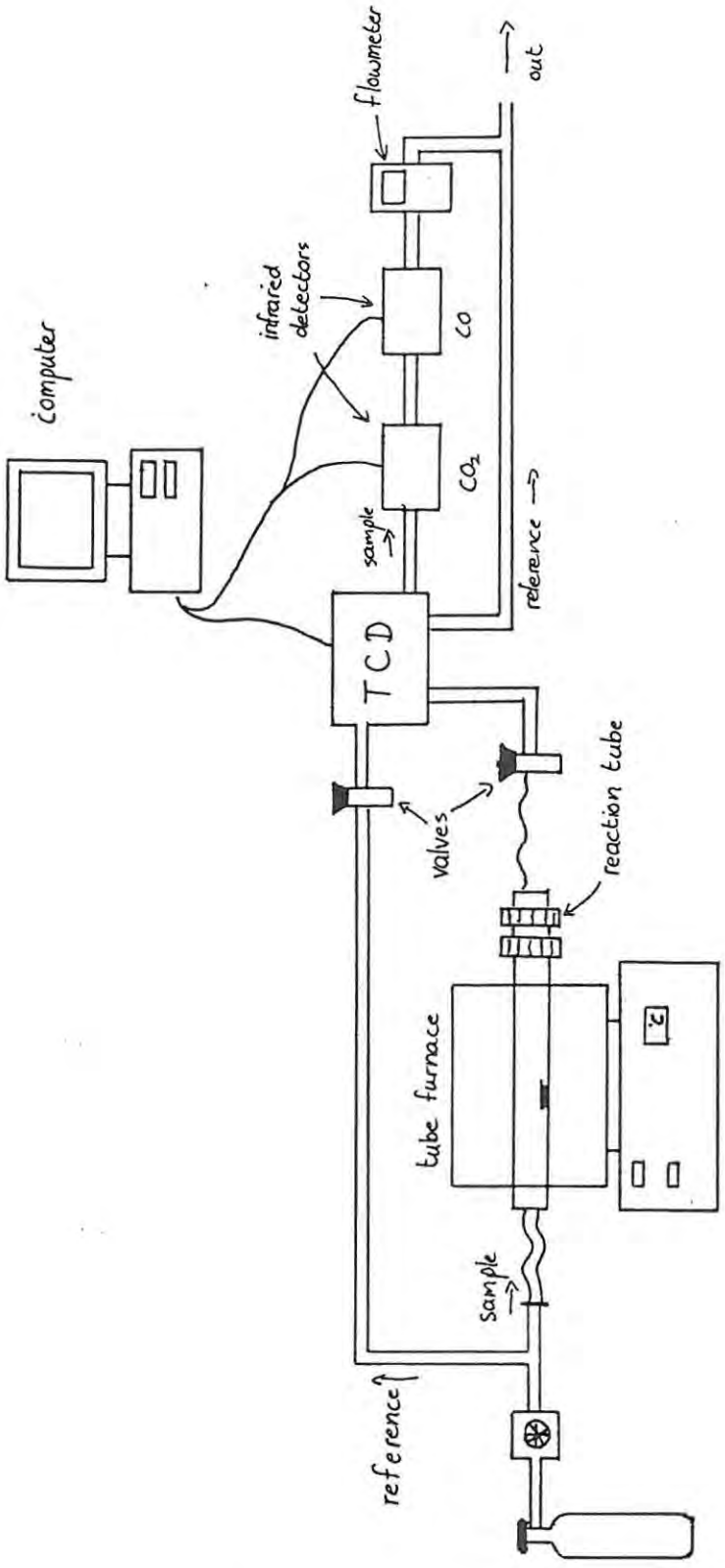

Fig. 3.3. The tube furnace and gas detection system.

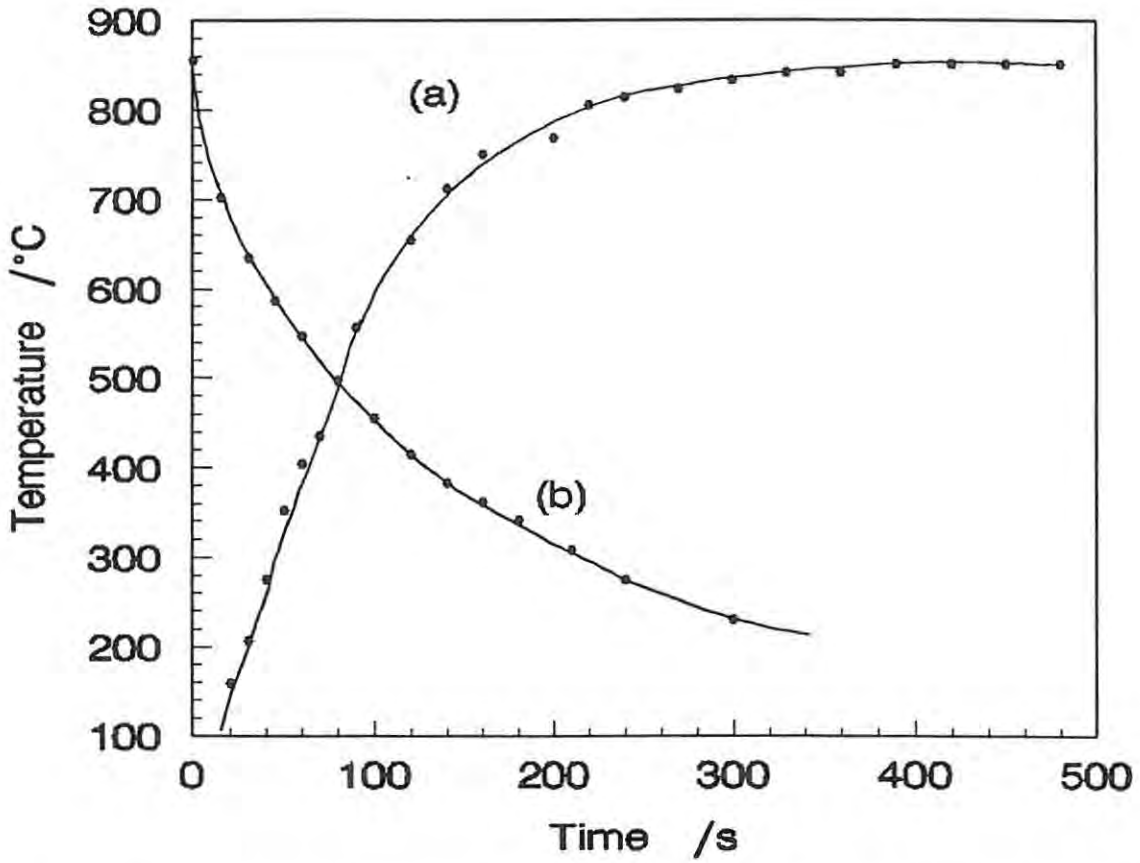

Fig. 3.4. The temperature measured at the sample's position during (a) heating and (b) cooling in the tube furnace (set at 900°C).

3.3.2 Experimental procedure

The experimental procedure was as follows: the samples were placed in a porcelain boat and the mass was determined to 0.1 mg. The reaction tube was clamped at a fixed position in the furnace, and the boat was pushed a fixed distance into the reaction tube. The sample and reference gas streams were adjusted to the desired flowrate. Argon was used as the flushing gas for reduction with carbon; all other experiments were carried out in hydrogen. The system was flushed for about 10 to 15 min before the furnace was heated. To determine whether this flushing time was adequate, a sample of iron powder was placed in the reaction tube and flushed with argon for 30 min at a flowrate of 200 mL min^{-1}. The sample was then heated to 900°C

for about 3 hours. There was no change in mass or colour, indicating that minimal oxygen was present in the system.

Because reduction with hydrogen begins at lower temperatures than reduction with carbon, the procedure followed for hydrogen reduction differed slightly from that for carbon reduction. In hydrogen, the furnace was initially heated to 200°C, whereas in argon the furnace was heated to 500°C. In both systems the temperature was maintained for 10 to 15 min, after which the reaction tube was removed from the furnace, and the furnace was heated to the desired temperature for the experiment.

The filament voltage of the TCD was set to 4.0 V in argon, and 6.0 V in hydrogen. When the signal had stabilised and the TCD bridge had been balanced, the reaction tube was pushed into the furnace and the time was noted. After the reaction time had elapsed, the reaction tube was removed from the furnace, and the furnace turned off. When the TCD signal had returned to the baseline, the sampling was stopped and the data saved. The boat was removed and weighed once the reaction tube had cooled. The sample was collected and stored in a desiccator for further analysis by SEM and XRD.

For experiments carried out in argon, the flowrate remained reasonably constant during the experiment, but in hydrogen the flowrate often fluctuated considerably during the experiment, and had to be constantly adjusted. This fluctuation in the flowrate was probably caused by condensation of water vapour in the unheated exhaust line from the TCD. The condensate obstructed the gas flow and thus reduced the flowrate. This effect was greater at higher reaction rates: that is, at higher temperatures, and over the initial part of the reaction.

Because water vapour formed in the reduction condensed before reaching the flowmeter, the flowrate in the system was higher than that measured by the flowmeter. However, the actual flowrate in the system at a given time could be easily determined from the rate of water production, which was calculated from the area under the TCD curve at that time, since the total area of the curve and the mass of the sample were also known. Fig. 3.5 shows the percentage increase of the calculated flowrate from the desired flowrate. As Fig. 3.5 shows, the flowrate probably varied within about 20% of the desired flowrate for the initial part of the reaction, and within 10% of the desired flowrate for the remainder of the reaction.

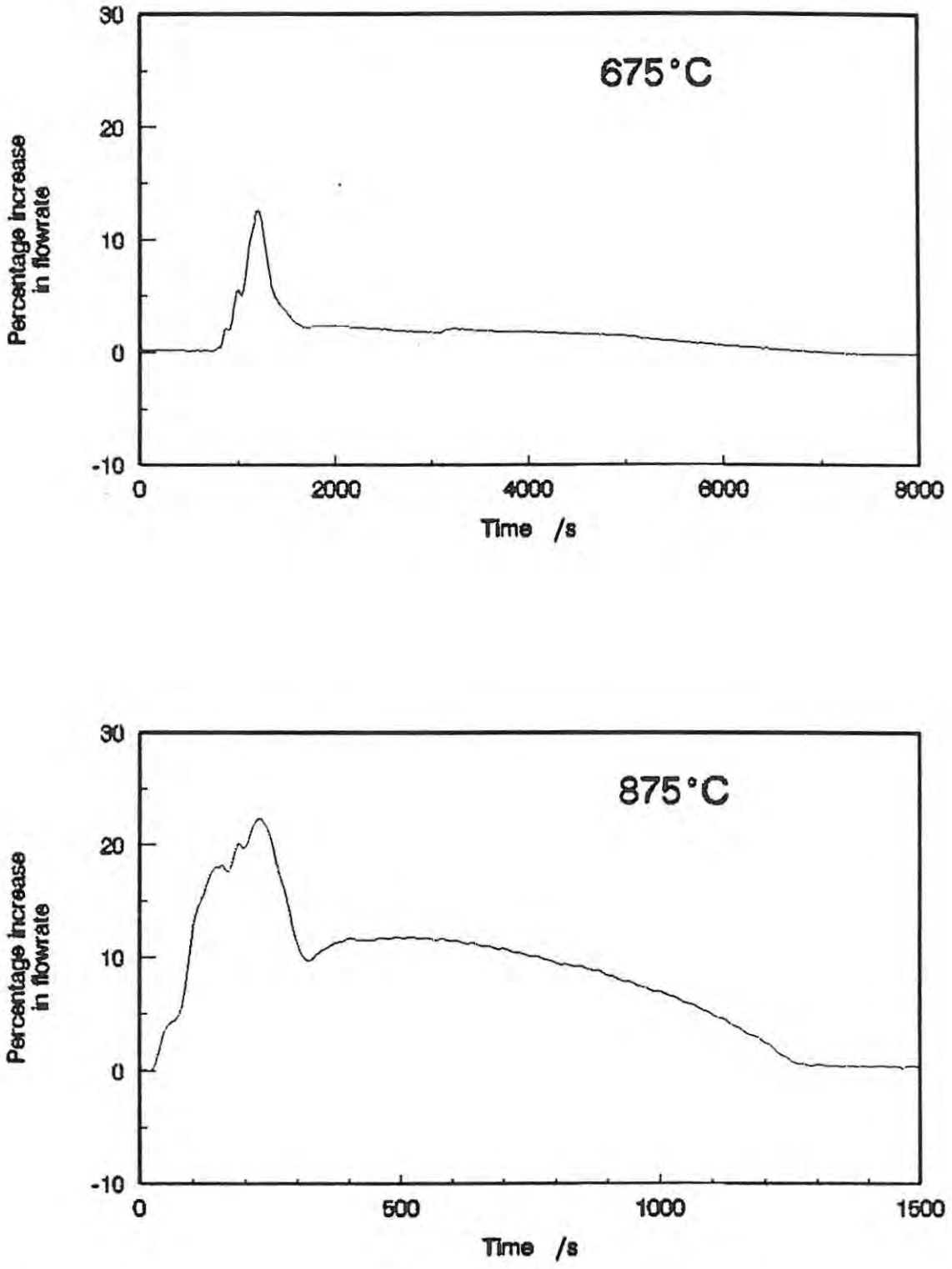

Fig. 3.5. The calculated increase in the flowrate above the observed flowrate (200 mL min^{-1}) for the reduction of WO_3 with hydrogen.

3.4 Scanning Electron Microscopy (SEM) and Particle Sizing

The size and morphology of the reactant and product powders were studied using a JEOL JSM-840 scanning electron microscope. The size distributions of WO_3, graphite, and lamp black powders were determined by laser diffraction in a Malvern Instruments MasterSizer at AECI Ltd.

3.5 X-Ray Powder Diffraction

X-Ray diffractometry (XRD) was used to analyse the composition of the sample at various stages of the reduction. XRD allows both the identity and the concentration of crystalline phases in the sample to be determined. A Phillips diffractometer was used for the analyses. The detector was a scintillation counter, and the time constant was set to 4 seconds. The primary X-ray beam was collimated through a 1° slit, and the diffracted beam was passed through a 0.2° slit and then a 1° slit before reaching the detector. The XRD pattern was recorded from 5 to 100°, at a scanning rate of 2° min^{-1}.

The small number of possible solid phases in the reaction system made qualitative analysis straightforward. The most important diffraction lines for the phases expected in the system are listed in Appendix C. Care was taken to ensure that samples were as homogeneous as possible. This was especially important when the sample contained graphite, because it is much less dense than the tungsten-containing compounds.

3.6 Processing of Data

TG, DTA, and TCD data were processed using a spreadsheet. A Savitsky-Golay[58,59] smoothing routine (in the program ALTDATA, Appendix B) was applied to TCD data. Because a large number of data were collected, a 35-point quadratic smoothing routine was used. Fig. 3.6 compares the smoothed and the unsmoothed data from a TCD experiment. The amount of data could be decreased by an integer factor to make processing easier.

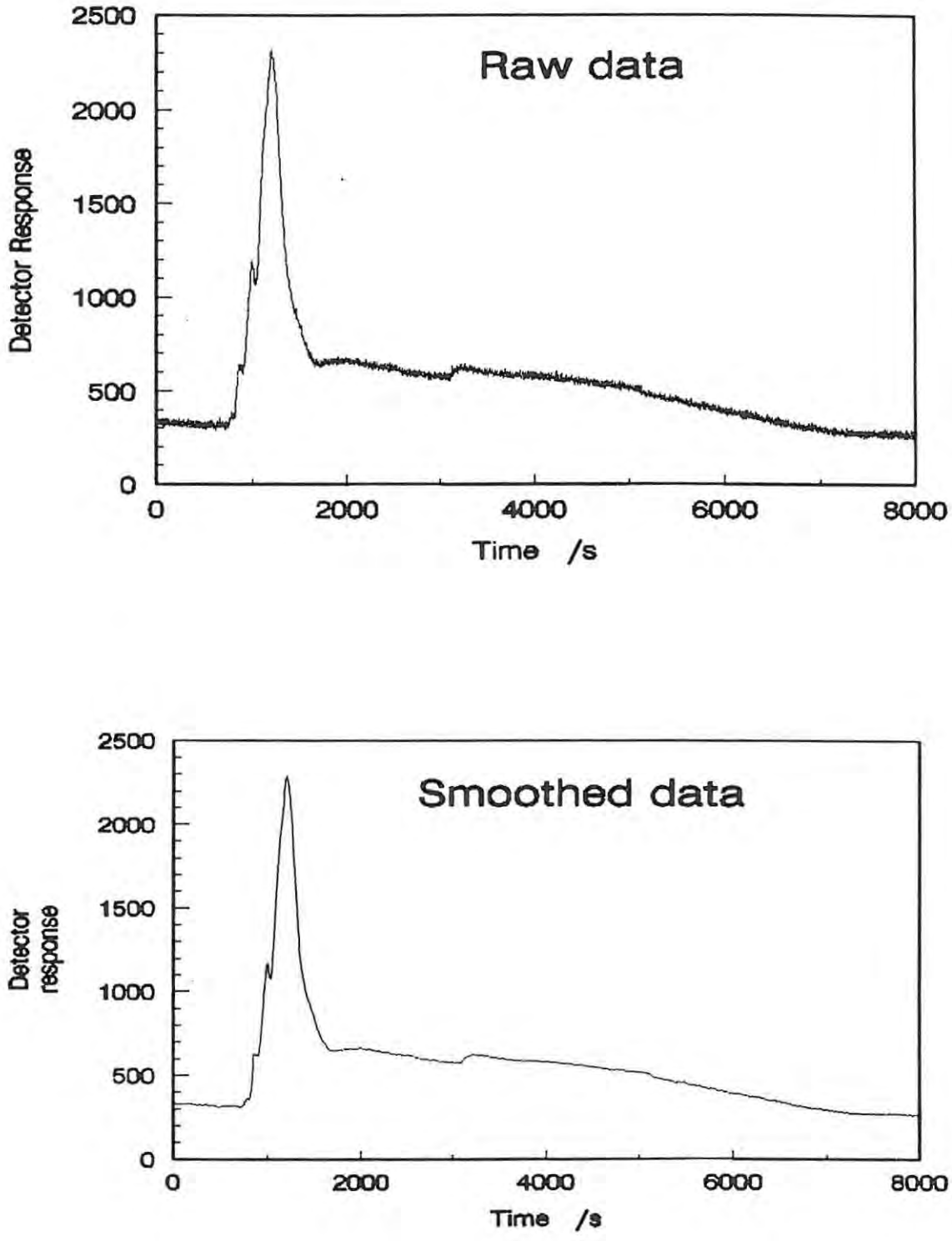

Fig. 3.6. Comparison of the raw TCD data with the data smoothed using the program ALTDATA.

Chapter 4

THERMODYNAMICS OF THE W-O-H-C SYSTEM

4.1 Introduction

Thermodynamic analysis of a system can be used to predict the behaviour of its constituent species under different conditions. Depending on the reliability of the data and the completeness of the analysis, the thermodynamic results closely describe the equilibrium state of a closed, isothermal system. Results are less precise when applied to closed systems which are not at equilibrium, and to open systems such as used in this investigation; nonetheless, tendencies in the system's behaviour can be investigated. However, the state of the system is ultimately a function of both kinetic and thermodynamic factors, both of which must be considered to describe the system accurately. This analysis is based on the standard Gibbs functions of the reactions, $\Delta_r G°$. Differences between the standard Gibbs function and the true Gibbs function at temperatures above 25°C are ignored for the purposes of this analysis.

Table 4.1 lists the standard enthalpies of formation and the standard entropies of the most important species expected in this system. Oxidation-reduction processes can be conveniently represented in an Ellingham diagram[60]. This diagram depicts the competition by different reactions for a common species in terms of $\Delta_r G°$ of the reactions. In considering competing reactions, the reaction with the most negative standard Gibbs function will take place by reversing the other reactions. The standard Gibbs functions of reactions also have value for calculating equilibrium constants.

Table 4.1. The standard enthalpies of formation and the standard entropies of the elements and compounds expected in the system.

	$\Delta_f H^\circ$ /kJ mol^{-1}	S° /J K^{-1}mol^{-1}		$\Delta_f H^\circ$ /kJ mol^{-1}	S° /J K^{-1}mol^{-1}
$WO_{3(s)}$	-842.9	75.90	$W_2C_{(s)}$	-26	-
$WO_{3(l)}$	-771.8	116.90	$WC_{(s)}$	-40.5	41.8
$W_{20}O_{58(s)}$	-820.1	73.39	$H_{2(g)}$	0.0	130.6
$W_{18}O_{49(s)}$	-781.2	68.41	$H_2O_{(g)}$	-241.8	188.7
$WO_{2(s)}$	-589.7	50.54	$C_{(s)}$	0.0	5.74
$WO_{2(l)}$	-541.6	81.71	$CO_{(g)}$	-110.5	197.6
$O_{2(g)}$	0.0	205.0	$CH_{4(g)}$	-74.81	186.2

Some of the reactions in the W-O-H-C system which compete for oxygen are listed in Table 4.2, and the Ellingham diagram based on these reactions is shown in Fig. 4.1. Of the tungsten oxides, only the formation of WO_3 from WO_2, and WO_2 from W are shown in the Ellingham diagram. The formation of $W_{20}O_{58}$ and $W_{18}O_{49}$ may be analysed in a similar manner.

Table 4.2. The standard reaction enthalpies and entropies of some reactions which involve competition for oxygen.

Reaction	$\Delta_r H°$ /kJ mol^{-1}	$\Delta_r S°$ /J K^{-1}mol^{-1}
1. $\frac{1}{2}W_{(s)} + \frac{1}{2}O_{2(g)} \longleftrightarrow \frac{1}{2}WO_{2(s)}$	-294.9	-93.53
$\frac{1}{2}W_{(s)} + \frac{1}{2}O_{2(g)} \longleftrightarrow \frac{1}{2}WO_{2(l)}$	-270.8	-77.75
2. $WO_{2(s)} + \frac{1}{2}O_{2(g)} \longleftrightarrow WO_{3(s)}$	-253.2	-77.14
$WO_{2(l)} + \frac{1}{2}O_{2(g)} \longleftrightarrow WO_{3(s)}$	-301.3	-108.31
$WO_{2(l)} + \frac{1}{2}O_{2(g)} \longleftrightarrow WO_{3(l)}$	-230.2	-67.31
3. $C_{(s)} + \frac{1}{2}O_{2(g)} \longleftrightarrow CO_{(g)}$	-110.5	+89.36
4. $CO_{(g)} + \frac{1}{2}O_{2(g)} \longleftrightarrow CO_{2(g)}$	-283.0	-86.50
5. $H_{2(g)} + \frac{1}{2}O_{2(g)} \longleftrightarrow H_2O_{(g)}$	-241.8	-44.40
6. $\frac{1}{2}C_{(s)} + \frac{1}{2}O_{2(g)} \longleftrightarrow \frac{1}{2}CO_{2(g)}$	-196.8	+1.43

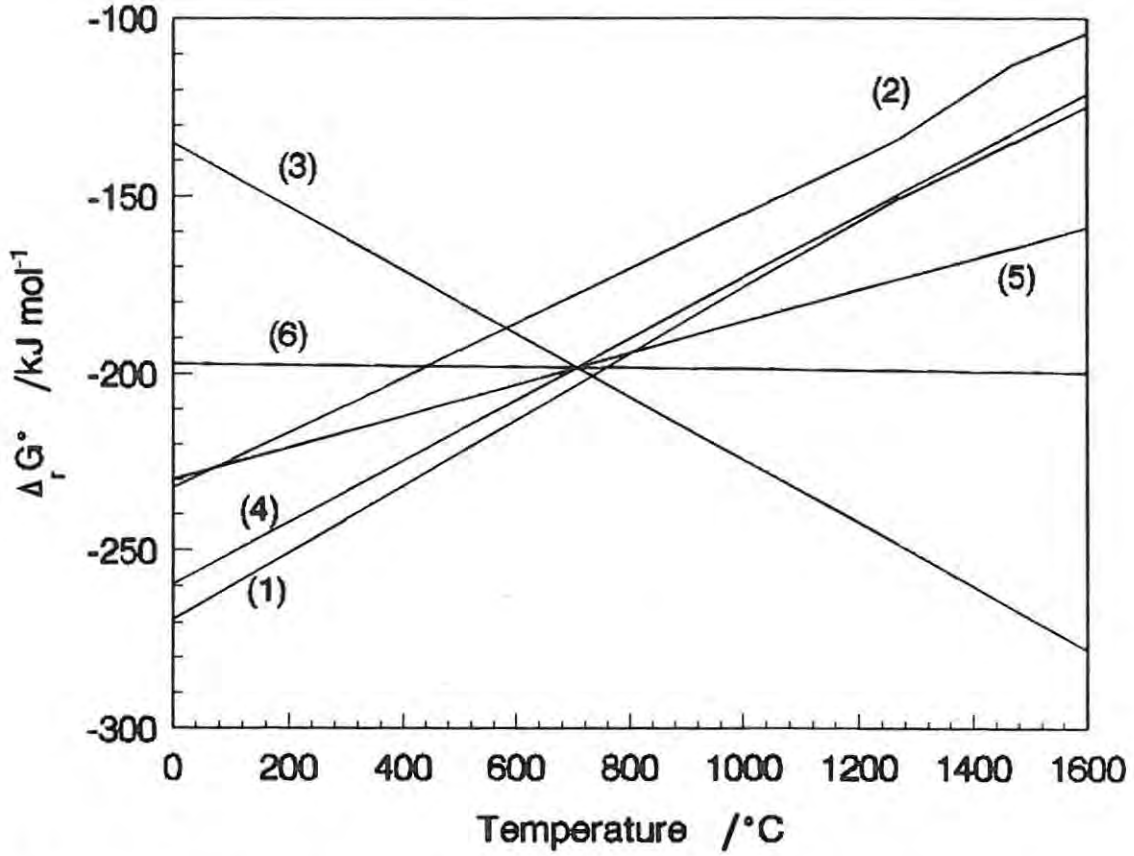

Fig 4.1. The Ellingham diagram for the reactions listed in Table 4.2.

4.2 Reduction of tungsten oxides using hydrogen, carbon, or carbon monoxide

Referring to the Ellingham diagram, we see that the reduction of WO_3 to WO_2 with hydrogen becomes possible above 75°C, and the reduction of WO_2 to tungsten is possible in hydrogen above 800°C:

$$WO_{3(s,l)} + H_{2(g)} \longleftrightarrow WO_{2(s,l)} + H_2O_{(g)} \quad (4.1)$$

$$WO_{2(s,l)} + 2H_{2(g)} \longleftrightarrow W_{(s)} + 2H_2O_{(g)} \quad (4.2)$$

The individual reduction steps from the reaction scheme of Schubert [22] were also analysed, and the temperatures at which $\Delta_r G°$ becomes zero are shown in Table 4.3.

Table 4.3. Individual reaction steps from the reaction scheme of Schubert[22] for hydrogen reduction, and the temperatures at which $\Delta_r G°$ for these reactions becomes negative.

Reaction step	$\Delta_r S°$ /J $K^{-1}mol^{-1}$	Temperature above which $\Delta_r G° < 0$ /°C
$WO_3 \longleftrightarrow W_{20}O_{58}$	3.28	always negative
$W_{20}O_{58} \longleftrightarrow W_{18}O_{49}$	5.39	always negative
$W_{18}O_{49} \longleftrightarrow WO_2$	24.06	428
$W_{18}O_{49} \longleftrightarrow W$	122.33	732
$WO_2 \longleftrightarrow W$	98.26	807

The reducing action of carbon differs considerably from that of hydrogen. If solid carbon is considered as the reductant, then WO_3 can be reduced to WO_2 above 470°C:

$$WO_{3(s,l)} + \tfrac{1}{2}C_{(s)} \longleftrightarrow WO_{2(s,l)} + \tfrac{1}{2}CO_{2(g)} \qquad (4.3)$$

although at temperatures above 680°C the thermodynamically preferred product is CO:

$$WO_{3(s,l)} + C_{(s)} \longleftrightarrow WO_{2(s,l)} + CO_{(g)} \qquad (4.4)$$

Solid carbon can reduce WO_2 above 740°C; although carbon may be oxidised to either CO or CO_2, the thermodynamically favoured product is CO:

$$WO_{2(s,l)} + 2C_{(s)} \longleftrightarrow W_{(s)} + 2CO_{(g)} \qquad (4.5)$$

Carbon usually reduces metal oxides indirectly, via CO which is formed as an intermediate in the reduction. The CO_2 product then reacts with solid carbon to regenerate CO according to the Boudouard reaction, eqn (2.22). The Boudouard reaction is a combination of

reactions 3 and 4 in Table 4.2, and $\Delta_r G°$ becomes negative above 700°C. A point to note is that these are both gas-solid reactions. This has important consequences for the kinetics of the reduction, because gas-solid reactions are usually more rapid than solid-solid reactions.

$\Delta_r G°$ for the reduction of WO_3 with CO to either WO_2 or to tungsten is always negative:

$$WO_{3(s,l)} + CO_{(g)} \longleftrightarrow WO_{2(s,l)} + CO_{2(g)} \quad (4.6)$$

$$WO_{3(s,l)} + 3CO_{(g)} \longleftrightarrow W_{(s)} + 3CO_{2(g)} \quad (4.7)$$

On the other hand, the reduction of WO_2 by CO always has a positive standard Gibbs function:

$$WO_{2(s,l)} + 2CO_{(g)} \longleftrightarrow W_{(s)} + 2CO_{2(g)} \quad (4.8)$$

although the CO_2/CO equilibrium ratio for the reaction is quite close to unity ($CO_2/CO = 0.62$ at 800°C and 0.76 at 1000°C). Therefore, CO will reduce WO_2 to W when the partial pressure of CO is slightly higher than that of CO_2. These conditions may be achieved in a stream of CO, or in the presence of solid carbon above about 700°C.

4.3 Simultaneous use of hydrogen and carbon in the reduction

When both hydrogen and carbon are present in the system, the reduction will be primarily achieved by the reaction which is thermodynamically and kinetically favoured. Based on these considerations, WO_3 will be mainly reduced by hydrogen, especially below 700°C, where reduction by carbon would have to occur by a slow solid-solid reaction. Even above this temperature, reduction by carbon will probably be limited by the Boudouard reaction, which is reported to be slow below about 1000°C[61].

The reduction of WO_2 will probably also be largely accomplished by hydrogen, although at substantially higher temperatures than the reduction of WO_3. At these temperatures, reduction by carbon is thermodynamically feasible, but the kinetic constraints mentioned above are likely to limit its importance in the reduction below about 1000°C. Direct reduction of WO_3 to tungsten by hydrogen has been observed, but appears to be much less important than reduction via WO_2. The direct reduction of WO_3 by carbon is also unlikely to be important.

The main effect of carbon in the system probably lies in its interactions with H_2O produced in the reduction of tungsten oxides with hydrogen. These interactions may be seen in the Ellingham diagram, which shows that H_2O may be reduced by solid carbon above 720°C

by either the "shift" reaction:

$$C_{(s)} + H_2O_{(g)} \longleftrightarrow H_{2(g)} + CO_{(g)} \quad (4.9)$$

or

$$\tfrac{1}{2}C_{(s)} + H_2O_{(g)} \longleftrightarrow H_{2(g)} + \tfrac{1}{2}CO_{2(g)} \quad (4.10)$$

Thus, in the temperature range in which WO_2 is reduced by solid carbon or by hydrogen, the H_2O produced in the reaction can reform H_2 by reaction with carbon. Because the formation of CO is favoured above that of CO_2, both reducing agents are likely to be regenerated, which might increase the rate of reduction.

A more important consequence is that a decrease in the H_2O partial pressure should also lead to a decrease the amount of tungsten transported by the species $WO_2(OH)_{2(g)}$. This may result in significantly smaller tungsten particles, which are desirable for the manufacture of WC. This effect might be negated to some extent by the reduction of CO_2 by H_2:

$$H_{2(g)} + CO_{2(g)} \longleftrightarrow CO_{(g)} + H_2O_{(g)} \quad (4.11)$$

which becomes thermodynamically feasible above 700°C.

The carbon and hydrogen in the system may react together to form CH_4:

$$C_{(s)} + 2H_{2(g)} \longleftrightarrow CH_{4(g)} \quad (4.12)$$

$\Delta_r G°$ for this reaction is positive above 650°C, and therefore the concentration of CH_4 will be quite low above this temperature. Nonetheless, this heterogeneous reaction might be a means of transporting solid carbon to other reaction sites. A reaction involving methane is

$$CH_{4(g)} + H_2O_{(g)} \longleftrightarrow CO_{(g)} + H_{2(g)} \quad (4.13)$$

for which $\Delta_r G°$ is negative above 700°C. This reaction will also reduce the concentration of H_2O at elevated temperatures. Considering the low equilibrium concentrations of CH_4, though, reactions with CH_4 are unlikely to influence the overall process significantly.

4.4 Carbide formation

Unfortunately, no value was found for the standard entropy of W_2C, and we will therefore only consider the more important carbide species, WC. The standard enthalpies and entropies for some of the reactions in which WC is formed are listed in Table 4.4.

Table 4.4. The standard enthalpies and entropies of reactions in which WC is formed.

Reaction	$\Delta_r H°$ /kJ mol^{-1}	$S°$ /J $K^{-1}mol^{-1}$
1. $W_{(s)} + C_{(s)} \leftrightarrows WC_{(s)}$	-40.5	3.5
2. $W_{(s)} + CO_{(g)} \leftrightarrows WC_{(s)} + ½O_{2(g)}$	70.0	-85.9
3. $W_{(s)} + 2CO_{(g)} \leftrightarrows WC_{(s)} + CO_{2(g)}$	-213.0	-172.4
4. $WO_{2(s)} + 4CO_{(g)} \leftrightarrows WC_{(s)} + 3CO_{2(g)}$	-189.3	-158.3
5. $W_{18}O_{49(s)} + 85CO_{(g)} \leftrightarrows 18WC_{(s)} + 67CO_{2(g)}$	-201.5	-164.7

The direct reaction of tungsten and carbon to form WC (reaction (1)) is thermodynamically favoured at the temperatures considered in this study. WC may also be formed when CO is the source of carbon. For the carburisation of tungsten metal by CO (reaction (2)), $\Delta_r G°$ is always positive and the equilibrium constant for the reaction is very small ($K = 4.4 \times 10^{-8}$ at 1000°C). In contrast, reaction (3) is thermodynamically feasible, and the $\Delta_r G°$ only becomes positive above 960°C.

The Kellogg, or predominance area diagram, quoted by Basu and Sale[56] and shown in Fig. 4.2, suggests that WC may also be formed directly from WO_2 and $W_{18}O_{49}$. Considering reactions in which CO_2 is the product, namely reactions (4) and (5), we see that $\Delta_r G°$ for reaction (4) is negative below 920°C, and that $\Delta_r G°$ for reaction (5) is negative below about 950°C.

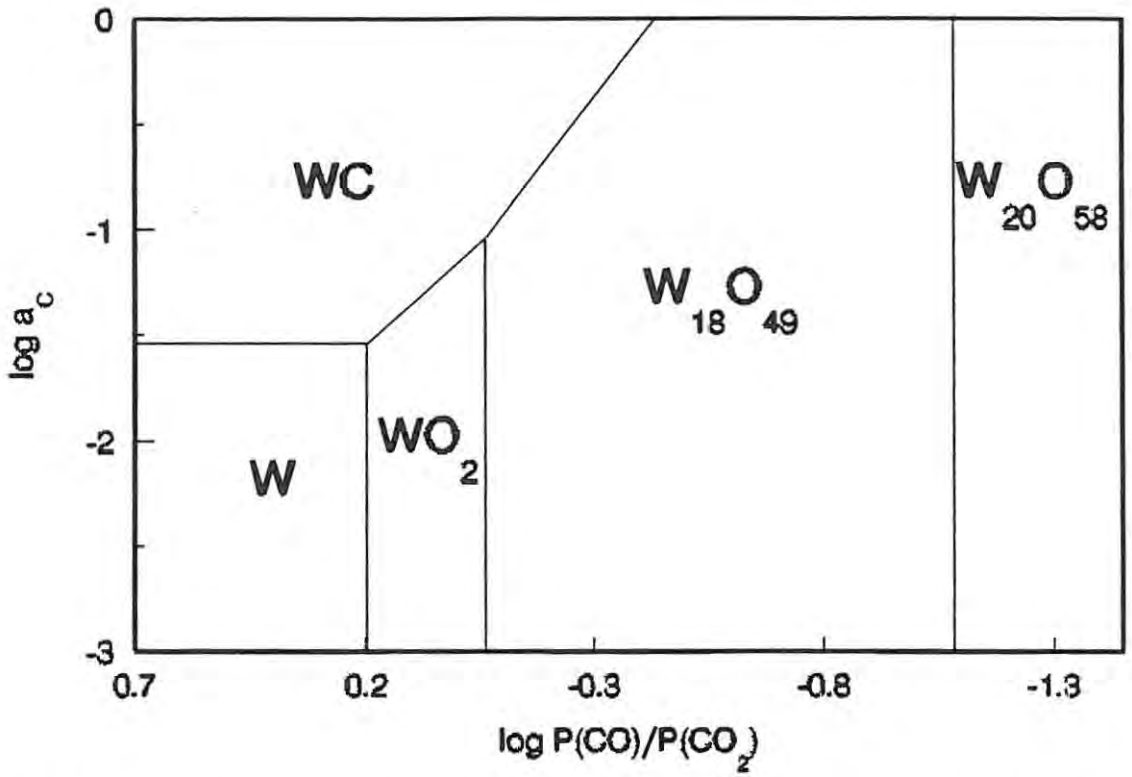

Fig 4.2. Kellogg diagram for the W-C-O system at 927°C (quoted in Basu and Sale[56]).

Chapter 5

THERMAL BEHAVIOUR OF INDIVIDUAL REACTANTS

A TG curve (Fig. 5.1) of a sample of WO_3 heated to 900°C at 10°C min^{-1} in an argon atmosphere showed that the sample lost about 0.7% of its mass below 450°C, whereafter the mass remained constant. Graphite decreased about 1.9% in mass up to 400°C when studied under identical conditions, Fig. 5.2. These mass losses probably correspond to removal of moisture and other volatile species from the samples. DTA curves of the same substances indicated that there were no significant endo- or exothermic events up to 1200°C (Figs 5.3 and 5.4). The broad variations in the height of the DTA trace are probably caused by changes in the baseline and by the differences between the heat capacities of the sample and of the Al_2O_3 reference material.

This investigation of the individual reactants identifies the relatively minor changes which must be taken into account when examining the thermal behaviour of mixtures.

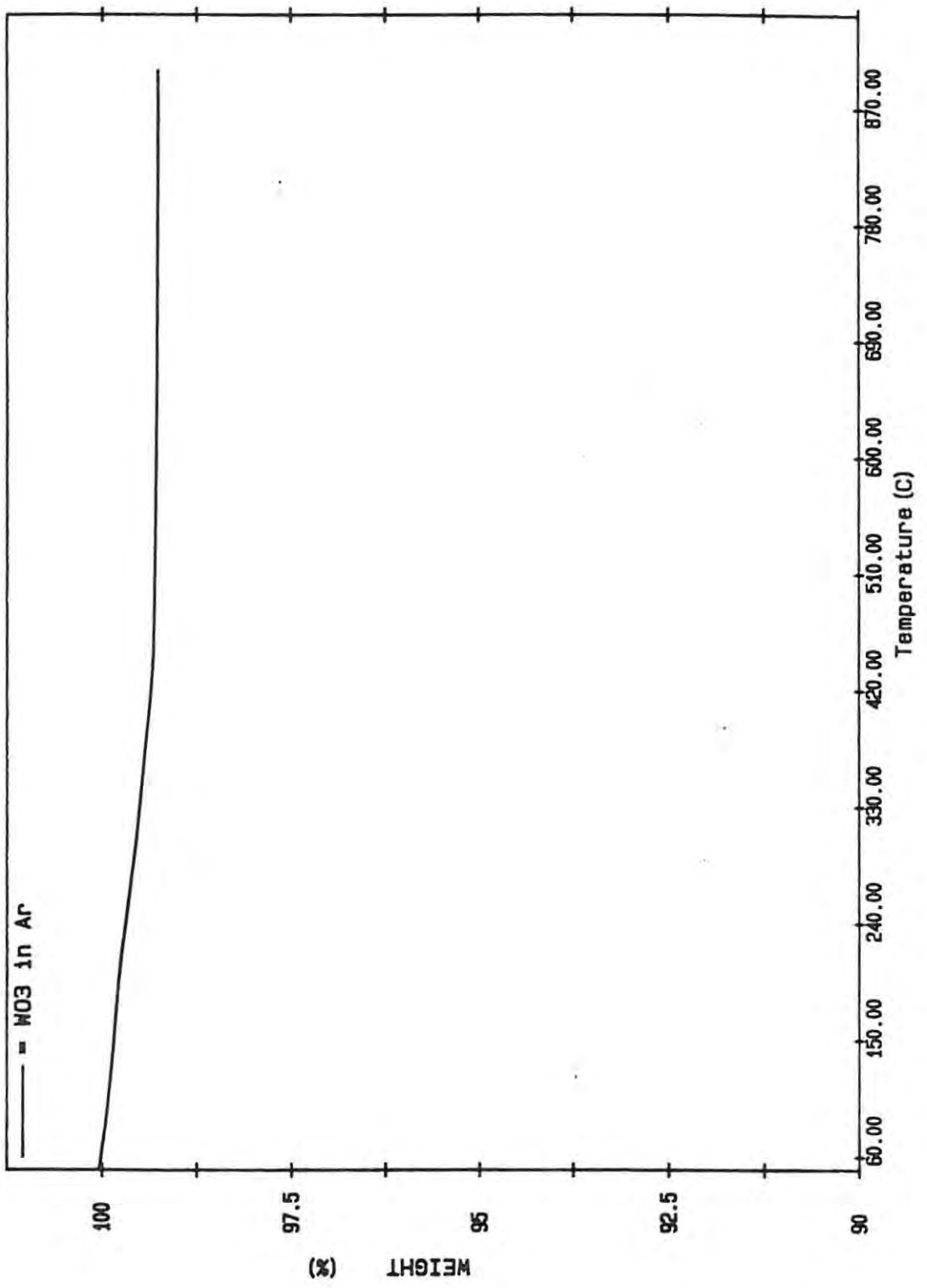

Fig. 5.1. Thermogravimetric trace of the WO_3 reactant heated in argon at 10°C min^{-1}.

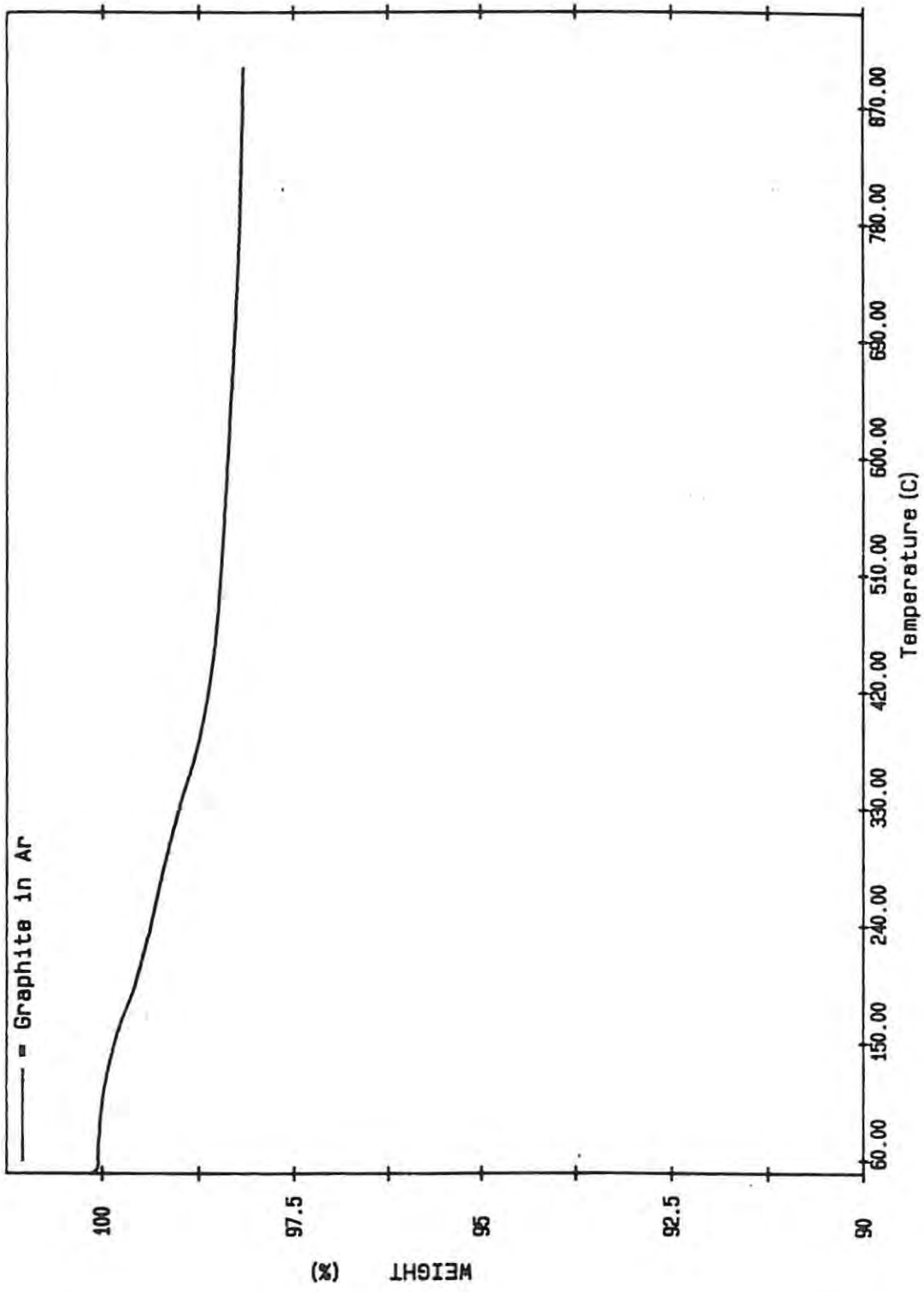

Fig. 5.2. Thermogravimetric trace of the graphite reactant heated in argon at 10°C min^{-1}.

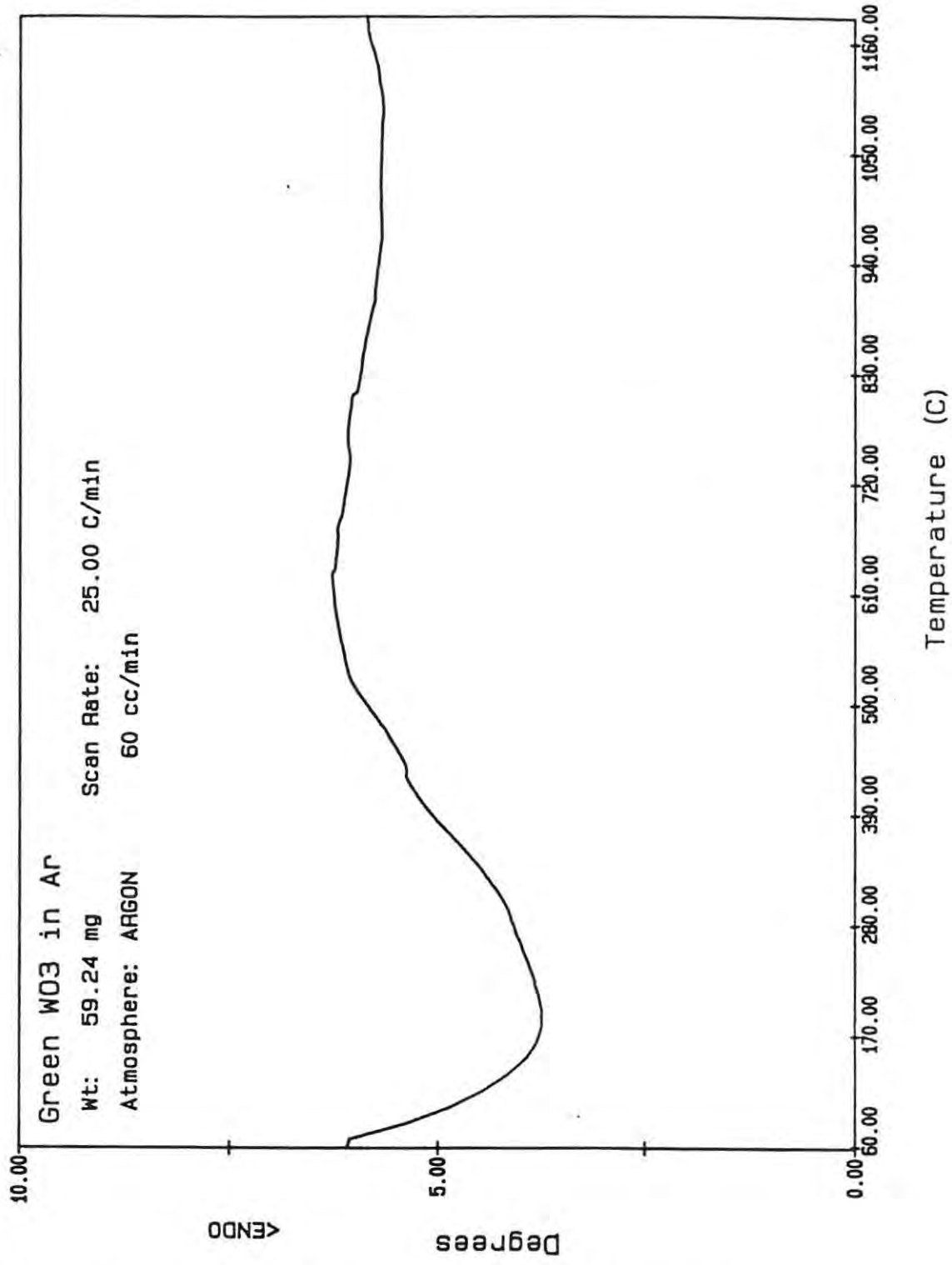

Fig. 5.3. DTA trace of the WO_3 reactant heated in argon at 25°C min^{-1}.

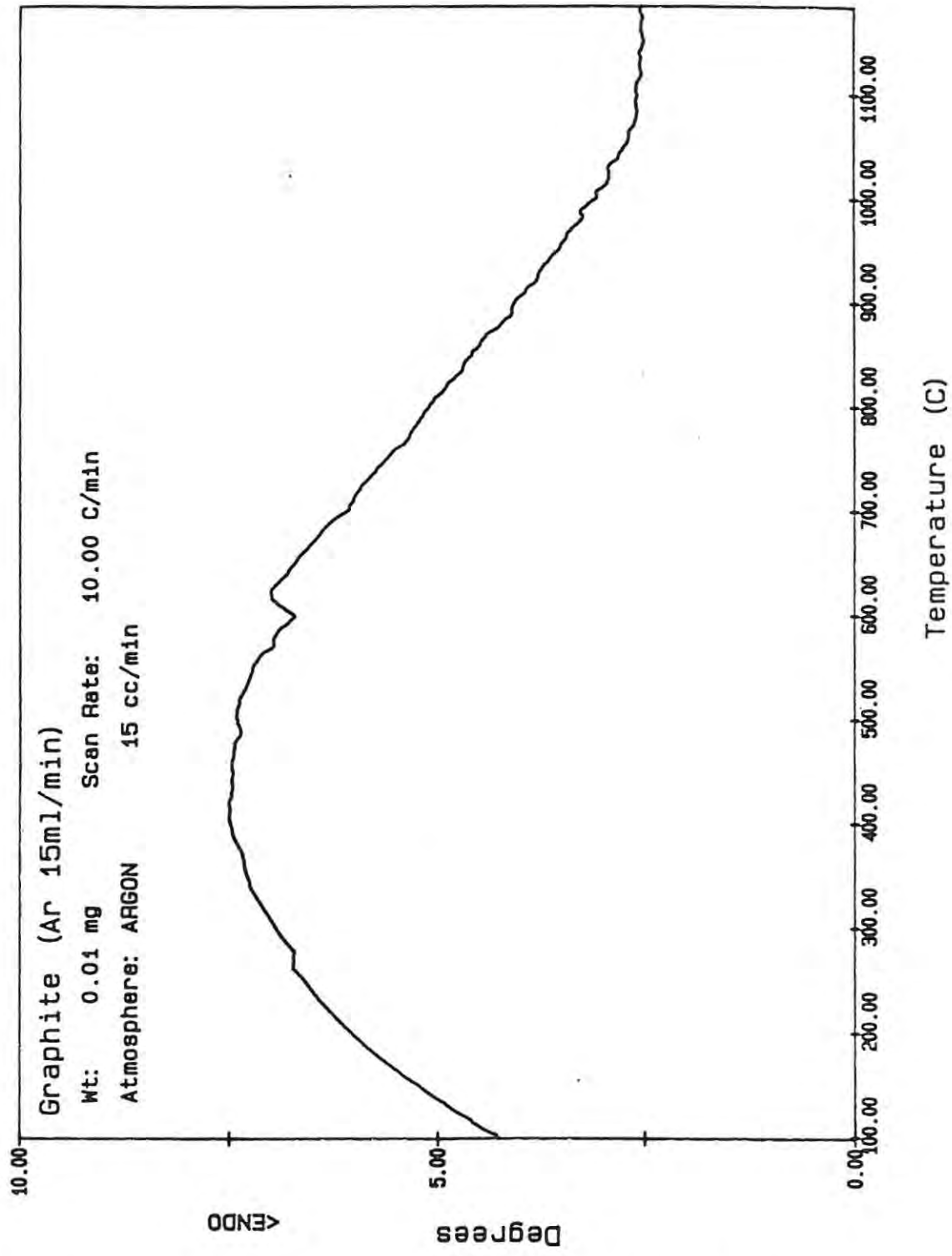

Fig. 5.4. DTA trace of the graphite reactant heated in argon at 10°C min^{-1}.

Chapter 6

REDUCTION OF TUNGSTEN OXIDES WITH CARBON MONOXIDE

6.1 Introduction

The reduction of metal oxides with carbon usually occurs via formation of CO as an intermediate. Thus, the reactions

$$WO_{x(s)} + CO_{(g)} \longleftrightarrow WO_{y(s)} + CO_{2(g)} \qquad (6.1)$$

(where $x > y$), and

$$C_{(s)} + CO_{2(g)} \longleftrightarrow 2CO_{(g)} \qquad (6.2)$$

could occur if the usual reduction mechanism holds. The reduction of tungsten oxides with CO was thus studied so that results could be compared with the reactions of mixtures of carbon and tungsten oxides.

6.2 Isothermal reduction of WO_3 with carbon monoxide

The isothermal TG curves for the reduction of WO_3 with CO over the temperature range 650 to 900°C are shown in Figs 6.1 and 6.2. The final product of the reaction was determined by XRD to be WC. The reaction was quite sensitive to the flowrate of CO, as is shown in Fig. 6.3. A temperature calibration of the TG done at high flowrates indicated a slight decrease in temperature.

At flowrates above the critical flowrate (i.e., the flowrate above which the transfer of gases to or from the solid is no longer rate-limiting), the reaction was broadly divided into two steps: a small initial mass loss, and a second step which had a much a larger mass loss. (These mass losses occurred after an initial decrease in mass of about 0.4% while heating to the reaction temperature.) A small gain in mass after the second step was recorded at all temperatures above 650°C. This increase in mass took place at a moderate rate for a short while, but then

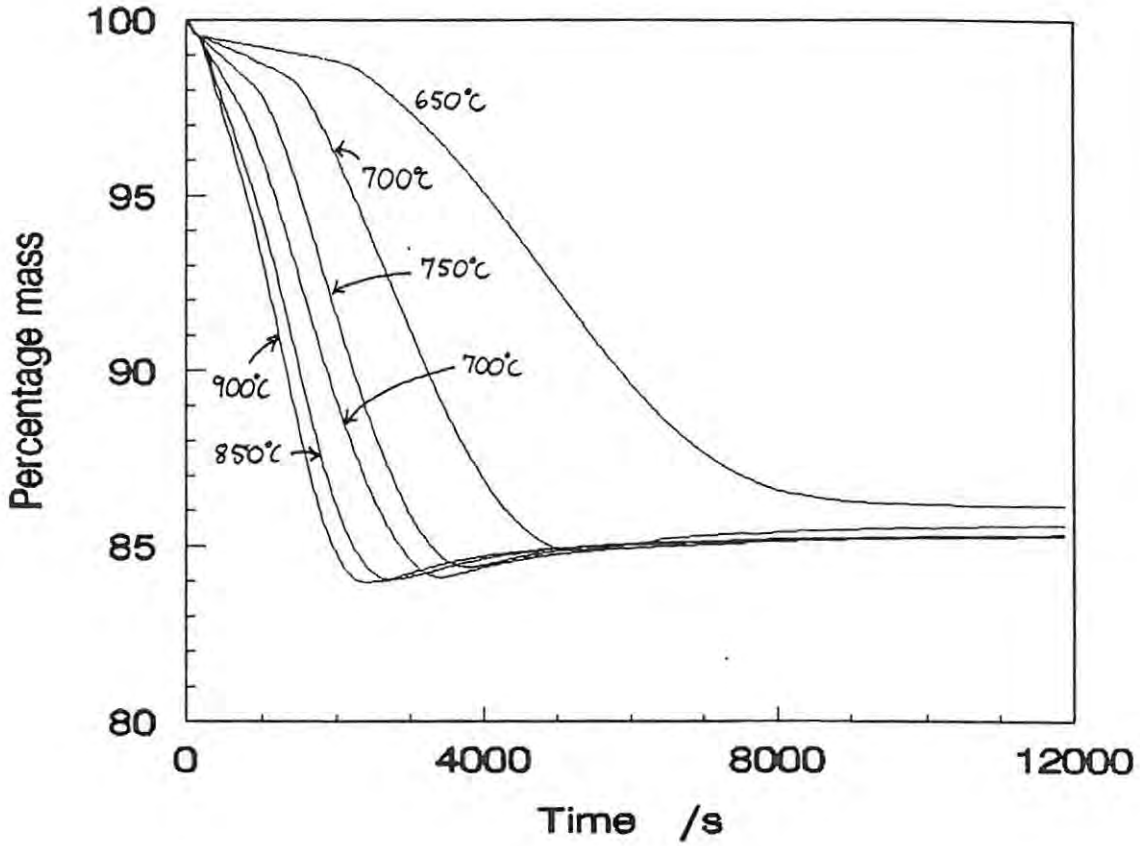

Fig. 6.1. The mass loss curves for the reduction of WO_3 with CO at a high flowrate.

decreased to a slow, constant rate. The constant mass gain almost certainly results from the deposition of carbon by the reverse of reaction (6.2). Similar observations were reported by Basu and Sale[56].

The first step appeared to be zero order up to 750°C, and the products were $W_{20}O_{58}$ and $W_{18}O_{49}$. The mass loss for this step increased with temperature, and thus the composition of the sample at the end of this step probably varied from predominantly $W_{20}O_{58}$ at 650°C, to predominantly $W_{18}O_{49}$ at 750°C. From 800 to 900°C the first stage of the process was still distinguishable by its lower rate of mass loss compared with the main reaction. An examination of the rate of mass loss showed that this initial step actually consisted of two small maxima, suggesting that the reaction took place in discrete steps.

The second step of the reaction corresponded to a large mass loss, and the curve of the rate of mass loss against time showed a single peak. Thus, this second step — the reduction

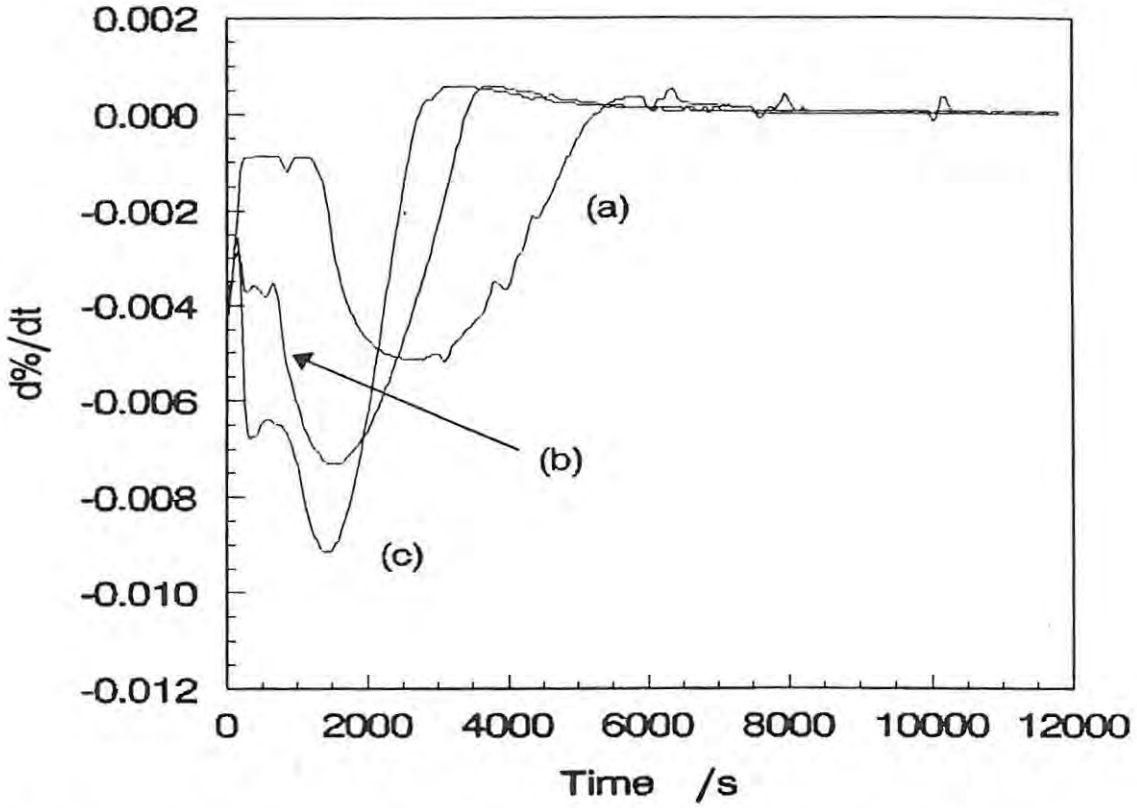

Fig. 6.2. The rate of mass loss for the reduction of WO_3 with CO at high flowrates at (a) 700°C, (b) 800°C, and (c) 900°C.

from $W_{20}O_{58}$ and $W_{18}O_{49}$, to WC — appeared to take place in a single stage.

To determine the composition and morphology of the sample during the course of the reaction, a number of experiments were carried out at 900°C in which the reaction was interrupted at different times. The amount of reaction during cooling was probably small because the sample cooled rapidly. The samples observed at room temperature were therefore assumed to be reasonably representative of the composition and morphology of the samples at the time the reaction was interrupted. This is not always true, however, and the effects of cooling and the vacuum in the electron microscope are difficult to determine. In this particular system, however, the solids have relatively low mobility at ordinary temperatures and the assumption seems reasonable.

Table 6.1 lists the colour of the samples and the phases identified by XRD in each sample. No more than two phases were observed in any sample; therefore, the amount of each

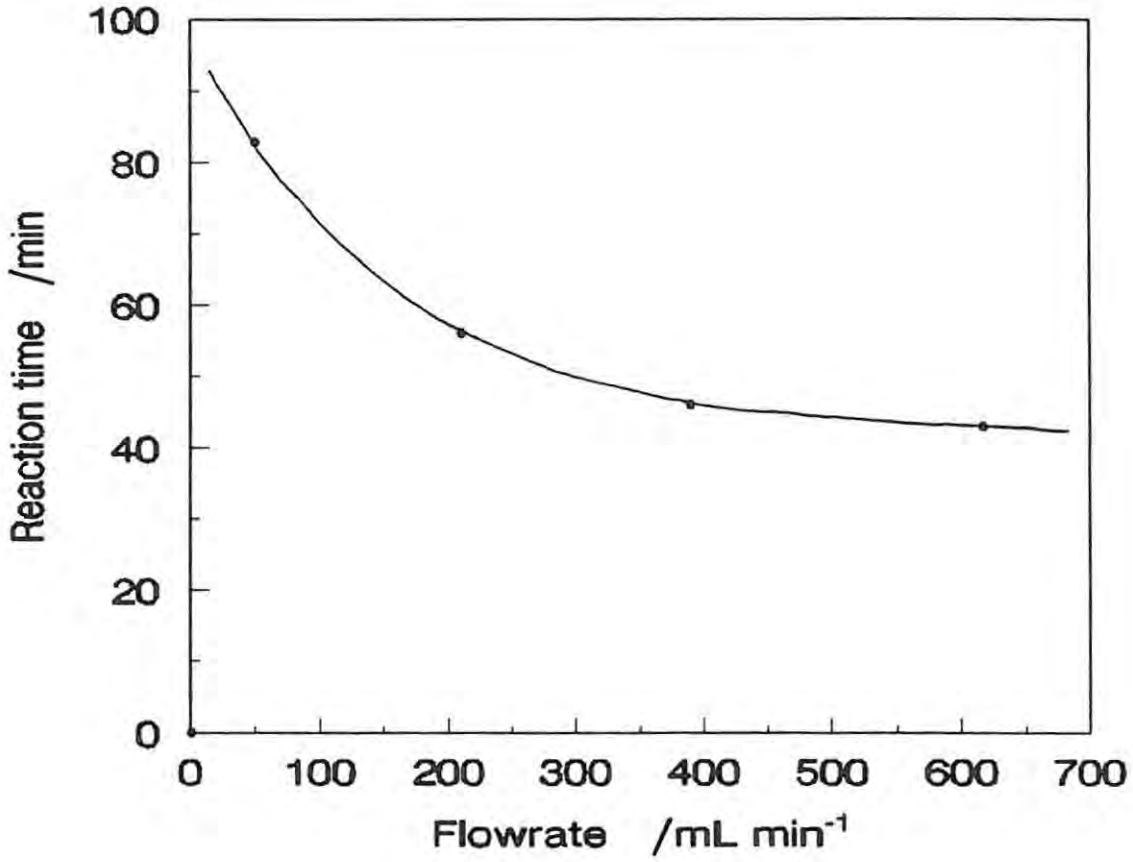

Fig. 6.3. The effect of the flowrate on the time for the complete reduction of WO_3 with CO.

phase could be estimated from the mass loss at the end of the experiment (excluding the initial mass loss on heating). A further experiment, interrupted after about 27 min at 800°C, indicated that only α-W and $W_{18}O_{49}$ were present in significant quantities in the sample (approximately 30% α-W and 70% $W_{18}O_{49}$).

Table 6.1. Intermediate phases in the isothermal reduction of WO_3 in CO at 900°C.

Time /min	Mass Loss /%	Colour	Phases present	Estimated Amount
3	0.4	blue-green	WO_3	100%
6	1.5	deep blue	$W_{20}O_{58}$	70%
			$W_{18}O_{49}$	30%
8	2.4	dark purple	$W_{20}O_{58}$	traces
			$W_{18}O_{49}$	100%
16	5.0	deep purple	$W_{18}O_{49}$	90%
			α-W	10%
29	10.9	not recorded	WO_2	70%
			α-W	30%
47	16.2	grey	WC	100%
>120	15.4	grey	WC	100%

From the phases observed at up to 8 min, and their relative quantities, it seems reasonable to predict the following initial steps in the reduction:

$$WO_3 \xrightarrow{(1)} W_{20}O_{58} \xrightarrow{(2)} W_{18}O_{49}$$

The product of the first step in the reduction therefore appears to be $W_{18}O_{49}$, and perhaps includes some $W_{20}O_{58}$ at temperatures below 800°C. Thereafter, $W_{18}O_{49}$ is reduced directly to α-W, as observed after 16 min:

$$W_{18}O_{49} \xrightarrow{(3)} \alpha\text{-W}$$

After about 29 min, the sample contained no $W_{18}O_{49}$ but consisted predominantly of WO_2 and

lesser amounts of α-W. This means that either $W_{18}O_{49}$ was also reduced to WO_2 by the reaction:

(4)

$$W_{18}O_{49} \longrightarrow WO_2$$

which became the dominant reaction, or that step (3) occurred together with the reaction of α-W and $W_{18}O_{49}$ to give WO_2:

$$11\alpha\text{-W} + 2W_{18}O_{49} \longleftrightarrow 49WO_2$$

The second possibility is unlikely to be significant because the reaction of tungsten with tungsten oxides to form oxides of intermediate stoichiometry is extremely slow compared with the relatively short reduction time with CO. (For example, the reaction of tungsten with WO_3 to form WO_2 takes 40 hours at 950°C[16].)

An obvious question at this point is what determines the relative importance of steps (3) and (4)? At 800°C, WO_2 was not observed after about 27 min, which suggests that step (4) is not significant at this temperature. Step (4) was observed only at a relatively high reaction rate, and consequently at relatively high partial pressures of CO_2. A graph of the CO/CO_2 equilibrium ratios for some of the reactions in the system (Fig. 6.4) shows that the reduction of $W_{18}O_{49}$ to α-W (step (3)) requires a higher CO/CO_2 ratio than the reduction of $W_{18}O_{49}$ to WO_2 (step (4)). Thus, at the start of the reduction (when the CO/CO_2 ratio in the system is high), step (3) dominates the reduction sequence, but is suppressed as the amount of CO_2 increases in the atmosphere around the sample. Thereafter, the reaction proceeds mainly by step (4).

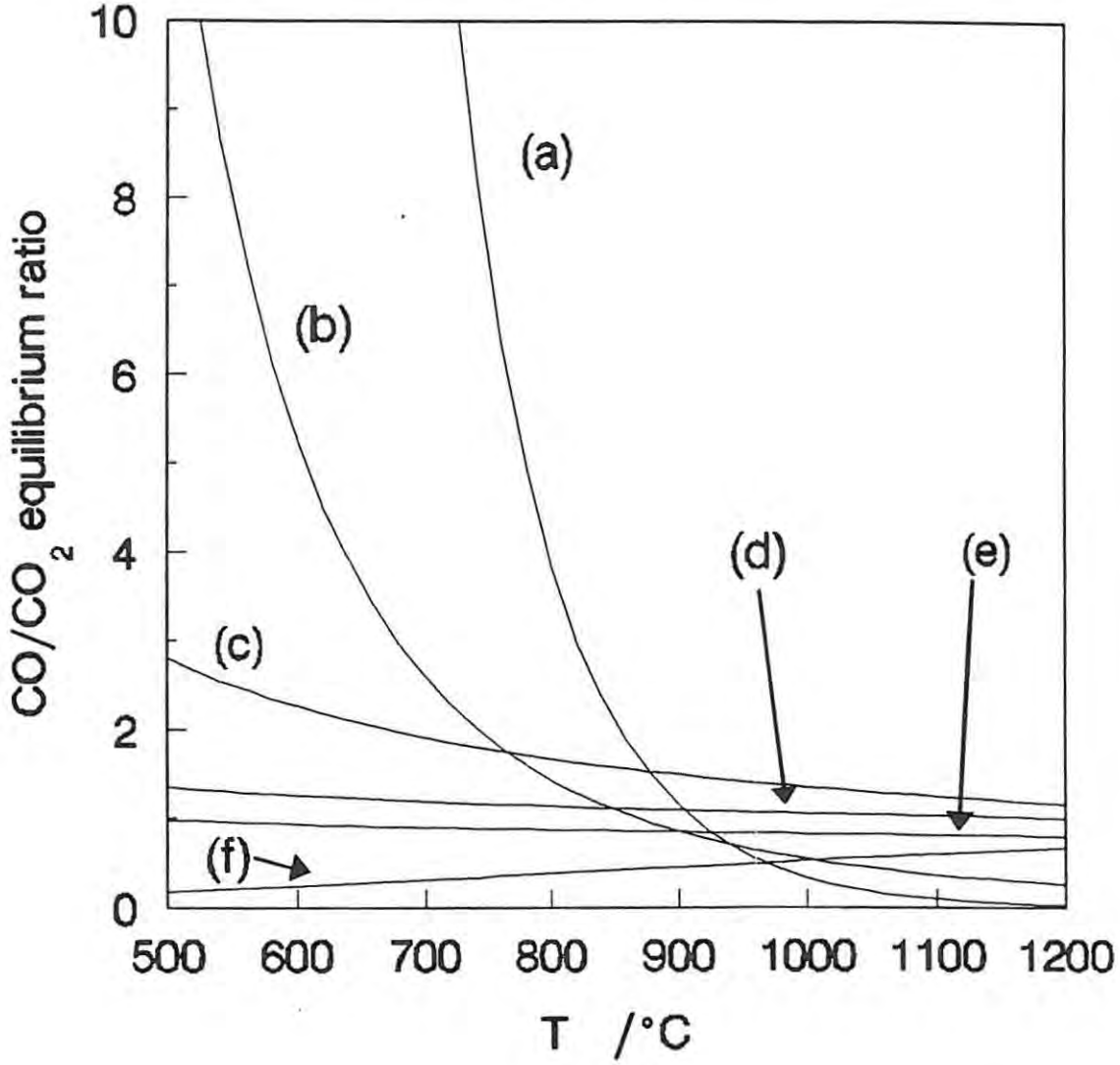

Fig. 6.4. The equilibrium ratios for the reactions: (a) $W + 2CO \leftrightarrows WC + CO_2$; (b) $WO_2 + 4CO \leftrightarrows WC + 3CO_2$; (c) $WO_2 + 2CO \leftrightarrows W + 2CO$; (d) $W_{18}O_{49} + 49CO \leftrightarrows 18W + 49CO_2$; (e) $W_{18}O_{49} + 85CO \leftrightarrows 18WC + 67CO_2$; and (f) $W_{18}O_{49} + 13CO \leftrightarrows 18WO_2 + 13CO_2$.

The transformation of WO_2 to WC may be either indirect, via:

(5)

$$WO_2 \longrightarrow \alpha\text{-}W$$

followed by:

(6)

$$\alpha\text{-}W \longrightarrow WC$$

or direct, according to:

(7)

$$WO_2 \longrightarrow WC$$

Referring to Fig. 6.4, it is clear that high CO/CO_2 ratios are required for step (6) to occur below 850°C. Consequently, the tungsten formed during the reduction will probably only form WC once the reaction is almost complete. There was a mass gain towards the end of the reaction which was more rapid than the subsequent deposition of carbon. This mass gain can be attributed to step (6), which is the only reaction path resulting in an increase in mass. An experiment to investigate the carburisation of tungsten (step (6)) at 900°C showed that the reaction was initially rapid, but slowed down markedly after a mass gain of about 1.2% (Fig. 6.5).

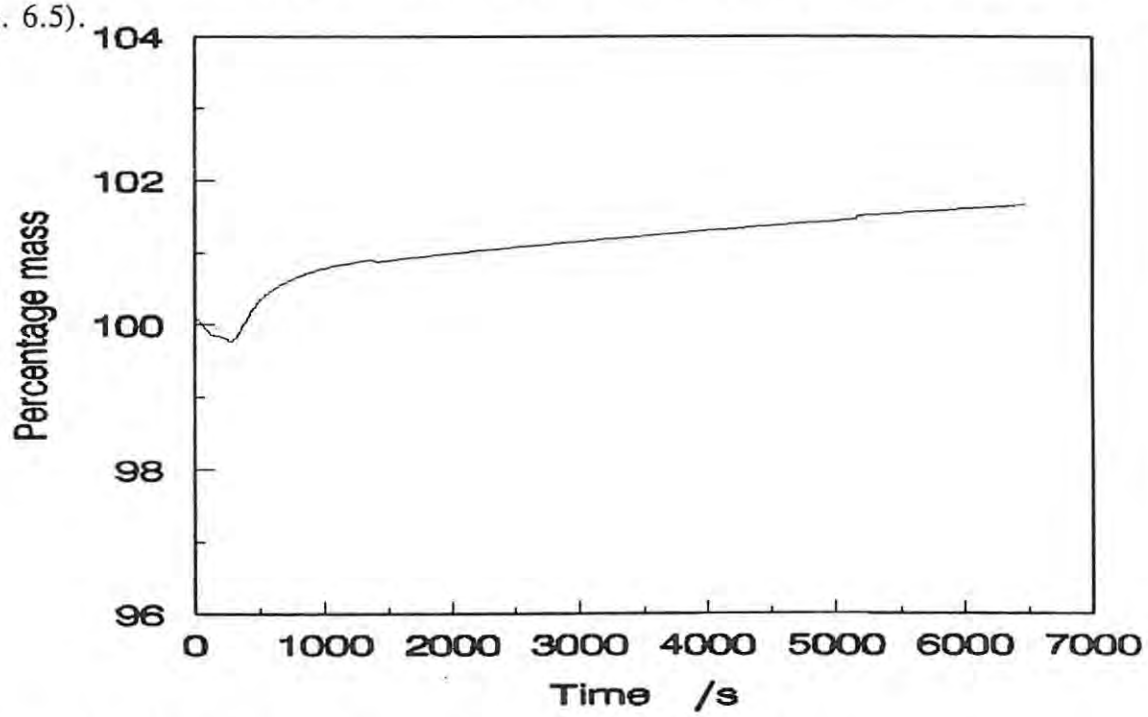

Fig. 6.5. The reaction of tungsten metal with CO at 900°C.

The reaction scheme inferred from the above observations is shown in Fig. 6.6.

At a flowrate of 50 mL min^{-1} the reduction was appreciably slower than at 500 ml min^{-1} (Fig 6.7), indicating that mass transport controlled the reaction at low flowrates (Fig. 6.3). Because the sample was small, reacted slowly, and the gas was pure CO, the reaction could not be limited by lack of CO at the sample. Instead the reaction was probably limited by the reducing potential of the gas, which decreased as CO_2 formed in the reduction.

Since the calculated CO/CO_2 equilibrium ratio for the reduction of WO_3 to WO_2 is small, the first stage of reaction might be limited by some other factor associated with the reduction. Nonetheless, the first stage of the reaction was also much longer at low flowrates than at high flowrates, which suggested that the reverse reaction was significant at low flowrates. The temperature dependence of the first stage of the reaction was greater than that of the main stage so that at high temperatures and low flowrates the rate of the first stage of the reaction surpassed that of the second stage (Fig. 6.7), possibly because the rate of the second stage was more affected by the higher CO/CO_2 equilibrium ratio.

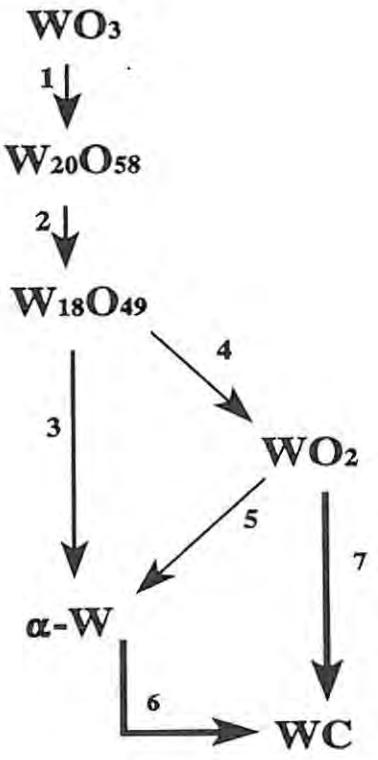

Fig. 6.6. The reaction scheme for the reduction of WO_3 with CO at 900°C and at a high flowrate.

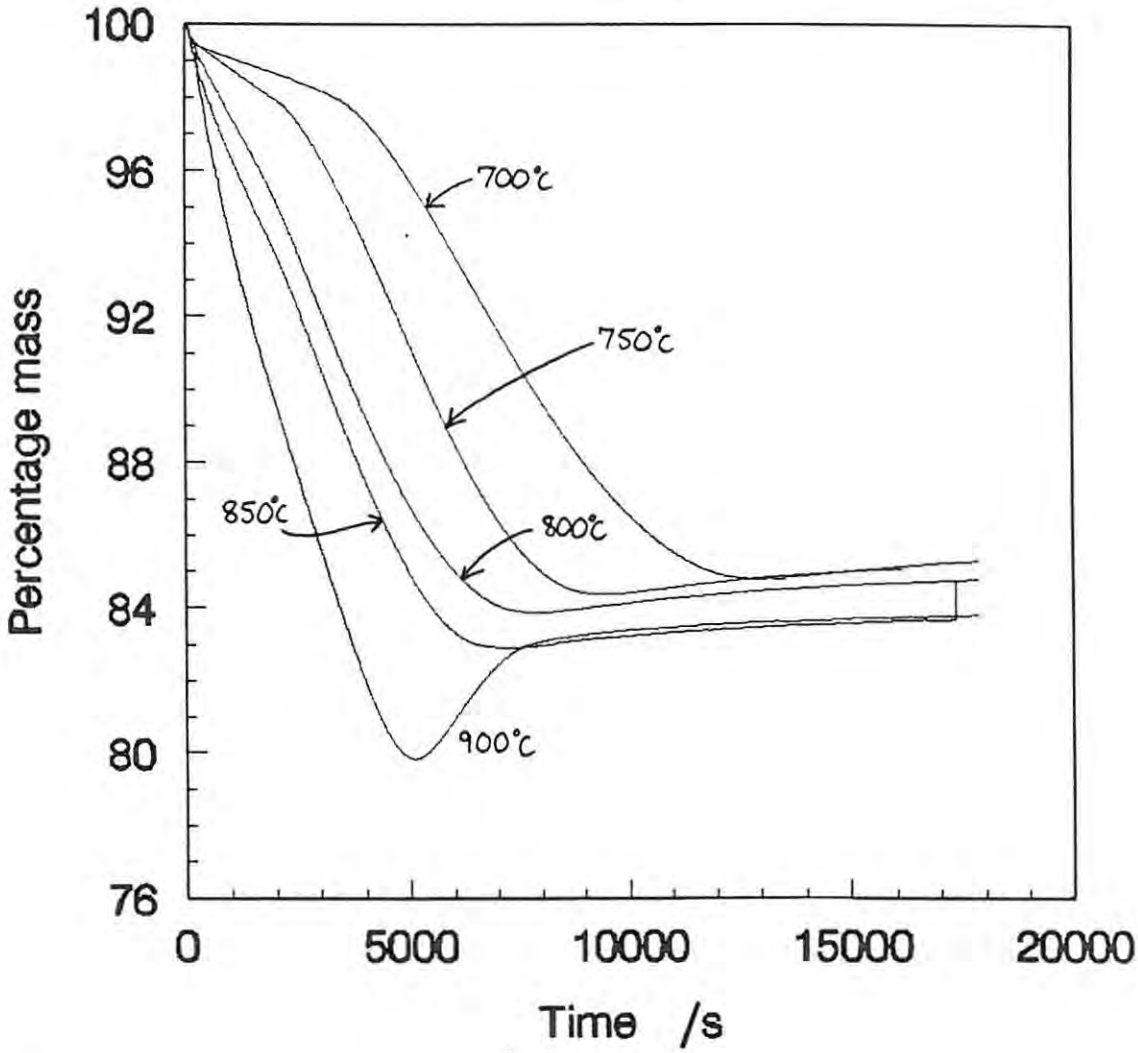

Fig. 6.7. The reduction of WO_3 with CO at a flowrate of 50 mL min^{-1}.

At 900°C, the maximum mass loss corresponded to that expected for the formation of metallic tungsten, and was followed by a considerable gain in mass as carburisation took place. (This mass gain was larger than that observed in the experiment to study the carburisation of tungsten.) The maximum mass loss was much smaller at high flowrates, thereby indicating the importance of the CO/CO_2 ratio on the reaction.

An unusual phenomenon in the reductions of WO_3 and WO_2 with CO, is that the reactions appeared to proceed from the bottom of the sample upwards, and from the sides inwards. Often the top centre of the surface retained the original colour of the sample for a

considerable length of time, whereas the sides and bottom of the powder layer were the colour of the product. This is contrary to expectations, because the atmosphere at the bottom of the powder layer tends to be more oxidising than that at the surface, where the CO_2 produced is removed and replaced by CO. When iron powder was heated under similar conditions it increased in mass, indicating that traces of oxygen were in the system. Small amounts of oxygen would explain the observed tendency for the reaction to start from the bottom of the sample.

6.3 Reduction of $W_{18}O_{49}$ with carbon monoxide

The isothermal reductions of $W_{18}O_{49}$ with CO at 900°C and at 750°C at a high flowrate are shown in Figs 6.8 and 6.9. There was a short induction period at 750°C, which probably signifies the formation of stable nuclei of the product phase. Judging from the rate of mass loss curve, the main mass loss occurs in a single step.

The reaction at 900°C did not have an induction period. Inspection of the rate of mass loss showed two peaks, where the first peak was small and appeared to be superimposed on the larger peak. This suggests two alternative reaction paths — possibly steps (3) and (4) from the reaction scheme for the reduction of WO_3 (Fig. 6.6). As in the reduction of WO_3, step (3) is likely to occur only at the beginning of the reaction, and would then be superseded by step (4) as the partial pressure of CO_2 increased.

6.4 Reduction of WO_2 with carbon monoxide

The isothermal reduction of WO_2 with CO was also studied at a high flowrate, and the results are shown in Figs 6.10 and 6.11. An induction period was observed over the whole temperature range studied. As was found for $W_{18}O_{49}$, no mass loss accompanied this period, which suggested that nucleation took place before the reaction proceeded. The rate of mass loss showed that the main reaction takes place in a single stage at and below 750°C. At 850 and 900°C, however, there were indications of overlapping peaks in the rate of mass loss curve. These could indicate that there are two reaction paths in the system, possibly the two alternative

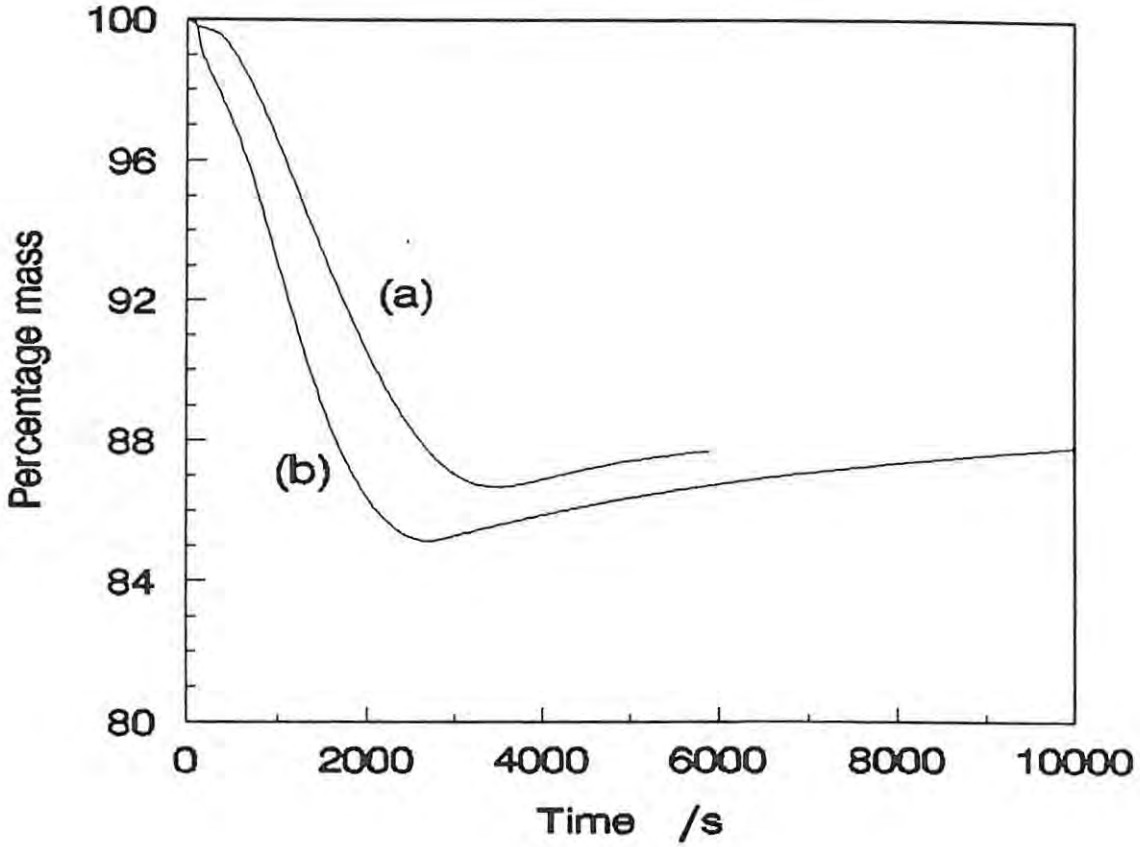

Fig. 6.8. The reduction of $W_{18}O_{49}$ with CO at (a) 750°C and (b) 900°C and at high flowrates.

paths whereby WO_2 can be reduced to WC, that is, either step (7), or steps (5) and (6).

In an attempt to establish the reaction paths more precisely, the reduction of WO_2 with CO was interrupted after 12 min at 900°C and after 25 min at 850°C. These times correspond approximately to the first and second peaks in the rate of mass loss curve. At 900°C, the sample consisted primarily of WO_2, with small amounts of both α-W and WC also present, thus suggesting occurrence of both pathways. At 850°C, the sample was predominantly WC, with smaller quantities of WO_2, implying that either step (6) is rapid compared to step (5), or that step (7) dominates the reduction sequence.

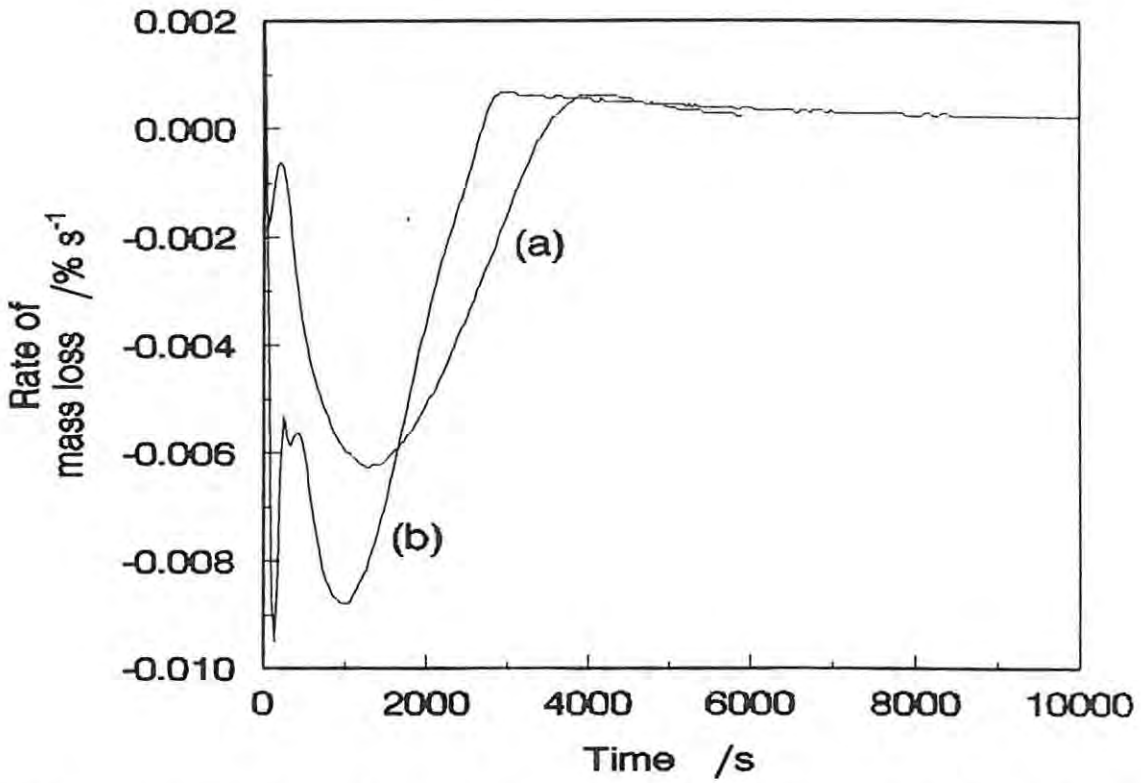

Fig. 6.9. The rate of mass loss for the reduction of WO_3 with CO at (a) 750°C and (b) 900°C (at a high flowrate of CO).

6.5 Morphological changes

The morphologies of the samples interrupted during reduction (Table 6.1), as well as a few other samples, were examined using SEM. The sample after 3 min was very similar to the starting WO_3, but reduction for a slightly longer time resulted in marked changes. The smooth surface of the WO_3 particles was converted to a surface covering of small needles after about 6 min. These needles are typical of the formation of $W_{18}O_{49}$, and were quite flat and randomly oriented on the face of the pseudomorph, Fig. 6.12. Extensive cracking was apparent.

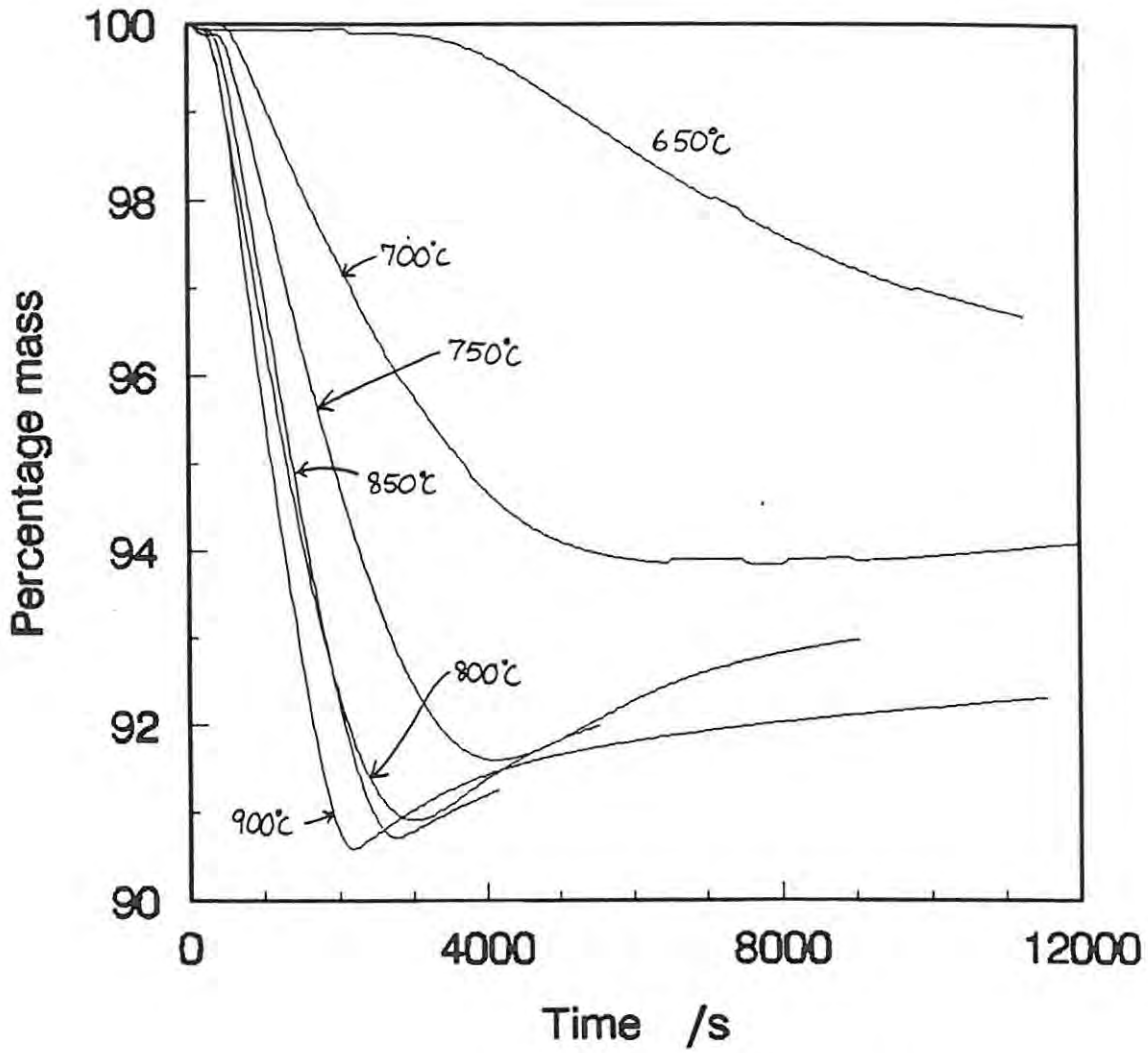

Fig. 6.10. The mass loss curves for the reduction of WO_2 in CO at high flowrates.

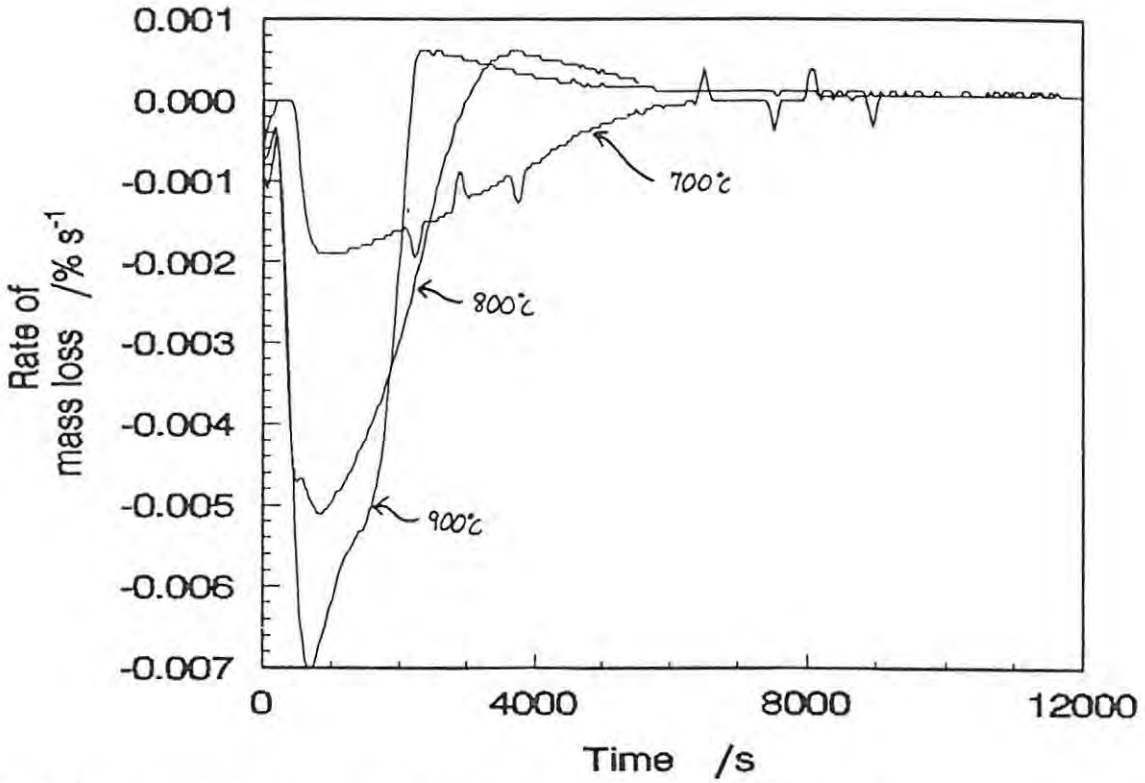

Fig. 6.11. The rate of mass loss of WO_2 in CO at a high flowrate.

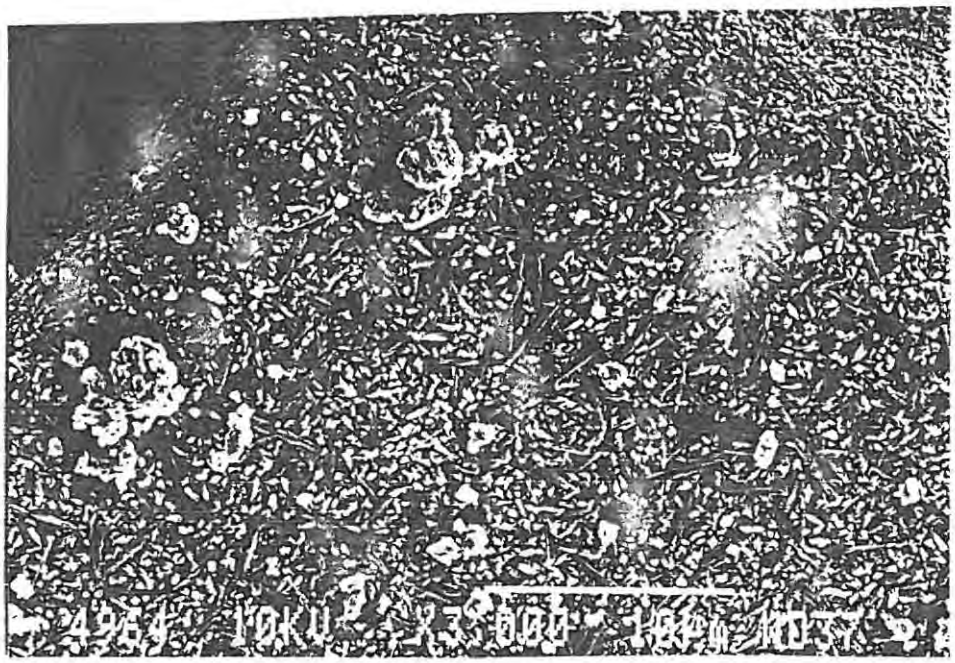

Fig. 6.12. Scanning electron micrograph of a WO_3 sample after reduction in CO for 6 min at 900°C.

The morphology of the particles observed after 6 min was retained during the course of the reduction, indicating that the strong tendency of $W_{18}O_{49}$ to form needles dictates the morphology of the subsequent phases and also that of the final product. The pseudomorphs appear to increase in porosity as the reaction progresses, as is expected from the decrease in the molar volume of the more reduced phases. The well-defined shape of the needles is lost somewhat towards the end of the reaction and the needles appear to be shorter and more rounded.

A similar morphology was observed for the final reduction product at 800°C, However, at 650°C the development of the needles appears to be retarded and the surface of the particles was only slightly textured. The product of the reduction of WO_2 at 650°C was unchanged from the WO_2 starting material. Particles from the carburisation of tungsten were very similar to the starting material.

6.6 Kinetic analysis

6.6.1 Introduction

As the reaction scheme in Fig. 6.6 shows, there are a number of possible reaction steps in the process. This complicates the kinetic analysis, because different reactions will generally occur at different rates, with different temperature dependencies, and may occur simultaneously or consecutively, or both. The kinetics of the reduction of WO_2 (which has fewer reaction steps) will be considered before examining the kinetics of the reduction of WO_3.

6.6.2 Tungsten carburisation

The results for the carburisation of tungsten were analysed to determine the mechanism of the reaction. A comparison of the mass at the end of the experiment (2.0%) with the expected mass gain of 6.5% shows that the reaction was only about a third complete when the experiment was stopped. It is also apparent that reaction is very slow after the rapid initial mass gain. The slowness of the reaction at 1000°C has been reported[56].

The kinetics were evaluated on the basis that reaction was complete at a mass increase of 6.5%. None of the kinetic models fitted the extent of reaction curve below about $\alpha = 0.17$. At high values of α, the diffusion models fitted the data quite well, and better than the geometric and order-of-reaction models. The fit of the diffusion models to the experimental curve is shown in Fig. 6.13.

The lack of agreement between the fit of the kinetic models and the initial part of the extent of reaction curve excludes a conventional solid state mechanism for this part of the reaction. A possible alternative explanation is that CO initially reacts rapidly at reactive sites, such as the surface and defects in the crystal lattice. These sites are used up quickly, and further

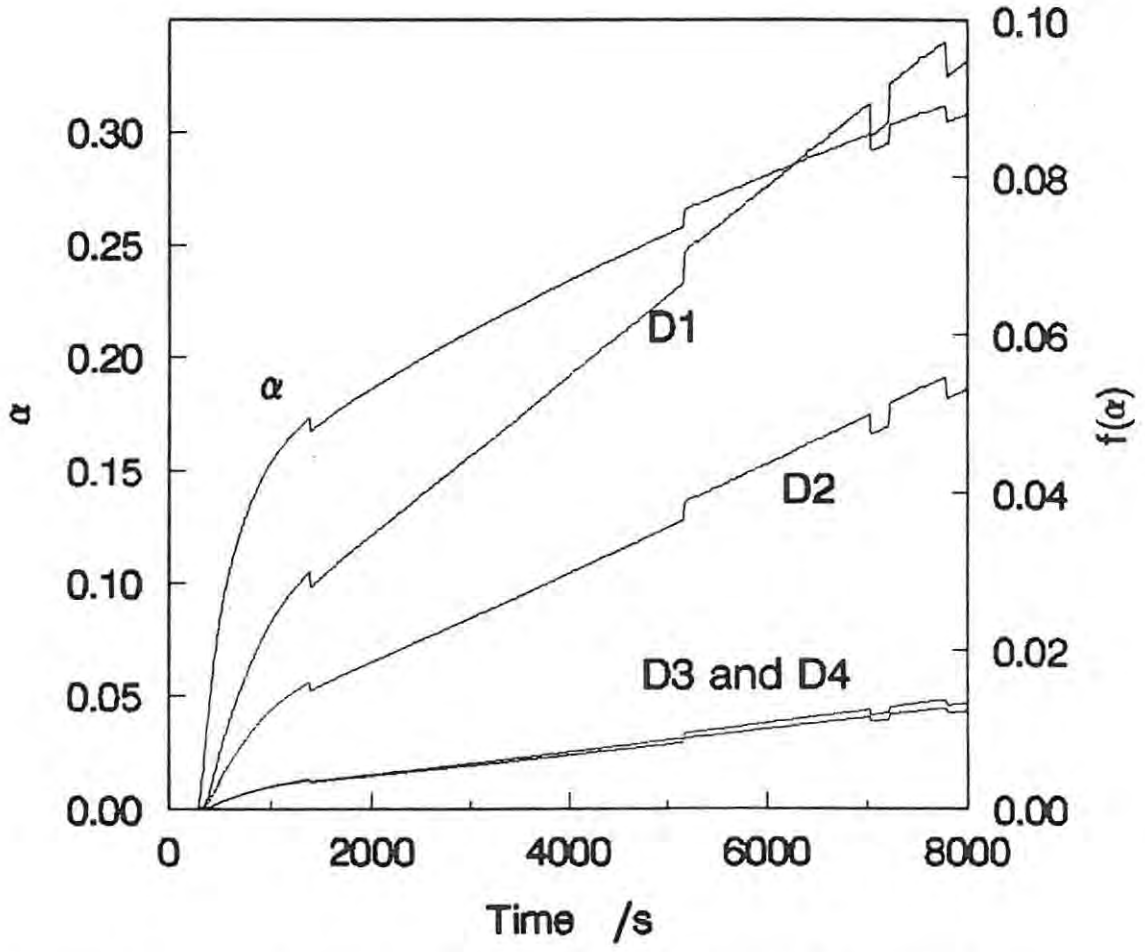

Fig. 6.13. The fit of the diffusion models to the carburisation of tungsten metal in CO at 900°C.

reaction has to proceed by diffusion of CO and CO_2 through a protective product layer of WC.

These proposals are speculative, but the main part of the reaction does seem to be diffusion controlled, as is usual with a protective product layer. Scanning electron microscopy showed that the particles of partly reacted sample have the smooth surface and facets typical of tungsten. XRD proved that the sample was predominantly α-W with significant amounts of WC. The presence of WC and the appearance of the sample particles suggest that WC is formed as a protective layer on the tungsten particles.

6.6.3 Kinetics of the reduction of WO_2 with carbon monoxide

The possible reactions whereby WO_2 may be reduced to form WC are shown in Fig. 6.14. If reaction (5) were to go to completion in a separate stage, the expected mass loss would be 14.83% of the original mass of WO_2. In none of the experiments illustrated in Fig. 6.10 is this value even remotely approached. The maximum recorded mass losses and the estimated final mass losses after carburisation for these experiments are given in Table 6.2.

Table 6.2. Maximum mass losses in the reduction of WO_2 by CO.

Temperature /°C	Maximum mass loss /%	Final mass loss /%
650	-	-
700	6.2	6.2
750	8.4	7.1
800	9.1	7.9
850	9.3	(incomplete)
900	9.5	8.4

Complete conversion of WO_2 to WC would correspond to a mass loss of 9.3%. The final mass losses after carburisation fall well short of the above value, although the maximum mass losses approach this value at and above 800°C. Incomplete reduction of WO_2 is probably the main reason for the smaller than expected mass losses, although carbon deposition in a separate process may also decrease the observed mass losses slightly. Basu and Sale[56] have reported similar results for the reduction of WO_2.

There are three main possibilities in considering the kinetics of the reaction:

(1) Step (7) is very slow compared to the alternative path (5) and (6);

(2) Step (7) is the more rapid path;

(3) Both pathways contribute significantly to the formation of WC as the final product.

No evidence from the WO_2/CO experiments indicates that step (5) is dominantly rapid under the conditions investigated.

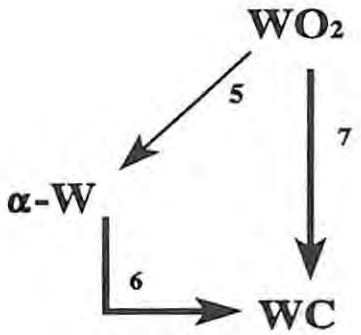

Fig. 6.14. The reaction paths for the transformation of WO_2 into WC.

The progress of the reduction process is depicted in Fig. 6.15. The process may be considered as being composed of a mass loss and a mass gain component, which when combined result in the experimental mass loss curve. The limits of the mass loss component fall between 9.3% (for conversion to WC with no intermediate tungsten formed) and 14.8% (for complete conversion to tungsten with no WC being formed). Depending on the extent to which tungsten is formed, the carburisation of tungsten results in an increase in mass of up to 5.6% of the original mass of WO_2. If the experimental mass loss curve could be deconvoluted to give the separate mass loss and mass gain curves, then in principle the kinetics of these components could be analysed separately. However, such a procedure requires detailed knowledge of the course of reaction. Therefore, a kinetic analysis can only proceed on the basis of several assumptions.

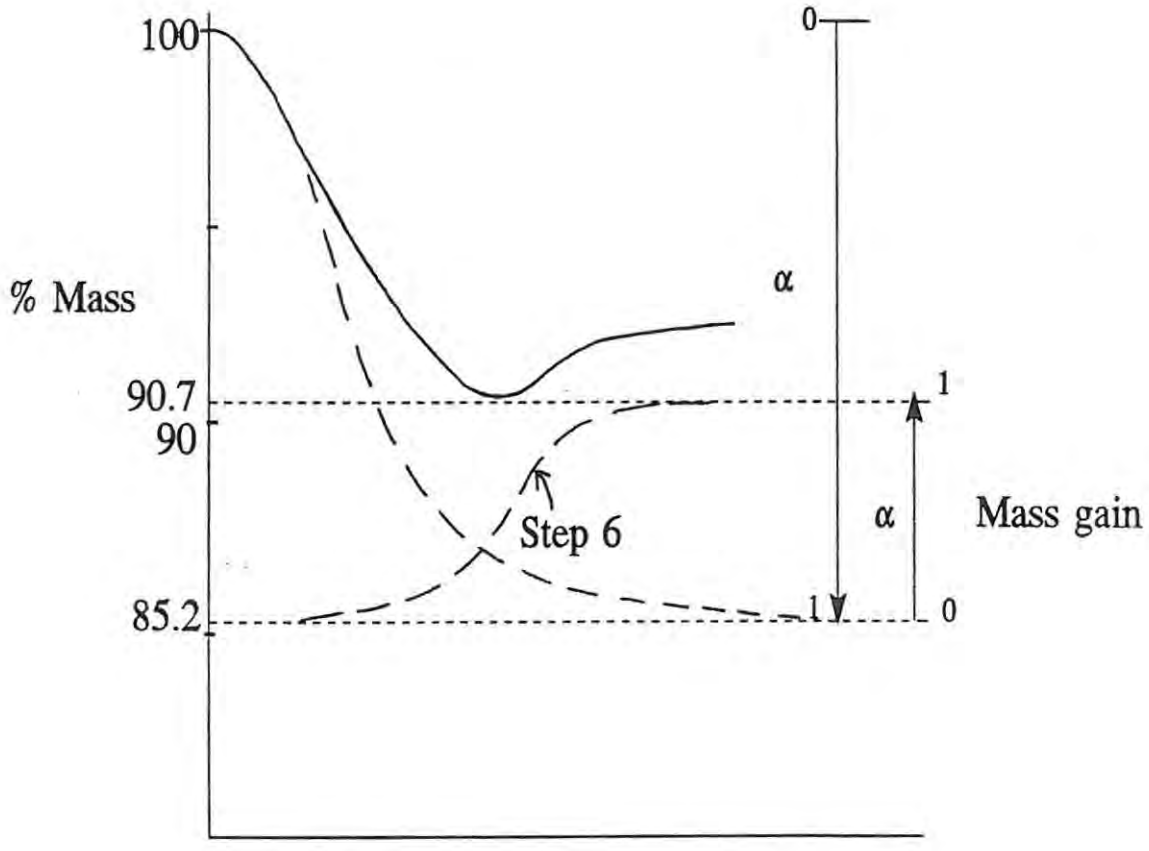

Fig. 6.15. Schematic representation of the progress of the overall reaction as a function of the mass loss and mass gain components.

There are essentially three ways to define α.

(1) $\alpha = 1$ at the final mass loss after carburisation;

(2) $\alpha = 1$ at the maximum mass loss;

(3) $\alpha = 1$ at the theoretical mass loss for the conversion of WO_2 to WC.

Of these options, (1) is the least satisfactory, since α will reach unity well before the final mass loss is attained, when the reaction is obviously incomplete. Option (2) is a better estimate of α from a theoretical point of view, although the same problem arises as in the first option when the maximum mass loss exceeds 9.3% (as happens at 850 and 900°C). Furthermore, it is perhaps better to measure the extent of reaction in terms of when the reaction ends, instead of at the complete conversion of products into reactants. This is especially true if the equilibrium amount of the reactants is significant, or if other stable phases are formed in the reaction.

The third option seems to give the most useful definition of α. As has been discussed, the carburisation of tungsten (step (6)) is more likely to occur towards the end of reaction, so that at the maximum mass loss all the reactions in which mass is lost will probably be virtually complete. According to this definition, α is essentially a measure of the extent to which the reactions involving mass losses are complete, and excludes the contribution of much of step (6) to the overall process. The effect of carbon deposition on the process is ignored in the kinetic analysis, as the mass gains are quite small. Furthermore, the higher CO_2 partial pressure in the system during the main stages of reaction will suppress the deposition of carbon to some extent.

The induction period and short acceleratory part of the reaction are usually indicative of the formation and growth of nuclei, and suggest that the process is not exclusively controlled by diffusion or by reaction at a boundary between two phases. Another possible explanation for the acceleratory period is the reaction did not occur uniformly over the sample, but started at the bottom of the sample and progressed upwards, as was observed. In this case, the acceleratory period is caused by increasing amounts of the powder layer contributing to the reaction as time progresses.

The reaction kinetics were analysed by comparing the linearity of the kinetic models in Table 2.1 using the experimental α,t data. Since the α,t curves had a brief acceleratory period, the sigmoid group of models (i.e., Avrami-Erofe'ev equation and the Prout-Tompkins model) were tested and fitted the data reasonably well. The deceleratory models were also examined

since the major portions of the α,t curves were deceleratory. Table 6.3 lists the correlation coefficients, R^2, determined for the models which gave the best fit to the data at the temperatures studied. The linearity of the R2 and A2 models is shown in Figs 6.16 and 6.17 at 750 and 850°C.

Table 6.3. The correlation coefficients for the kinetic models which gave the best fit to the experimental data for the reaction of WO_2 with CO over the range $0.05 < \alpha < 0.99$.

Temperature /°C	R2	R3	A2	A3	Prout-Tompkins
700	0.9977	0.9972	0.9979	0.9930	0.9898
750	0.9979	0.9854	0.9924	0.9920	0.9779
800	0.9968	0.9821	0.9904	0.9929	0.9785
850	0.9880	0.9648	0.9811	0.9914	0.9733
900	0.9859	0.9607	0.9792	0.9891	0.9698

The experimental curve is compared with the curves predicted by the R2 and A2 models at 750°C in Fig. 6.18. As might be expected, the R2 model fits the experimental data over the main deceleratory region better than the A2 and A3 models. Fig. 6.19 shows the Arrhenius plot using the values of the rate coefficients determined by the R2 model. An activation energy of 62 ± 5 kJ mol^{-1} and a frequency factor of 3.9 ± 0.3 s^{-1} were calculated using rate coefficients determined from application of the R2 model over the parts of the α,t curve which the model fitted best.

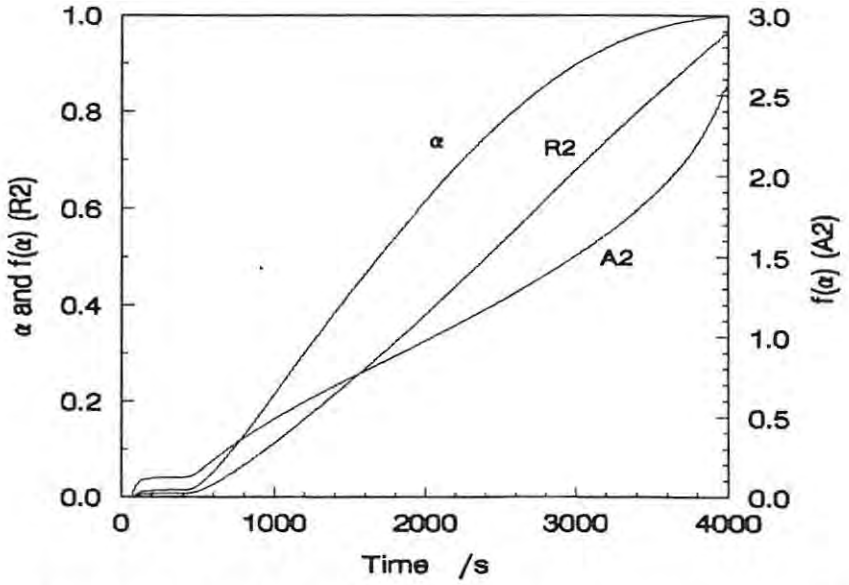

Fig. 6.16. The fit of the R2 and A2 models to the experimental data for the reduction of WO_2 with CO at 750°C.

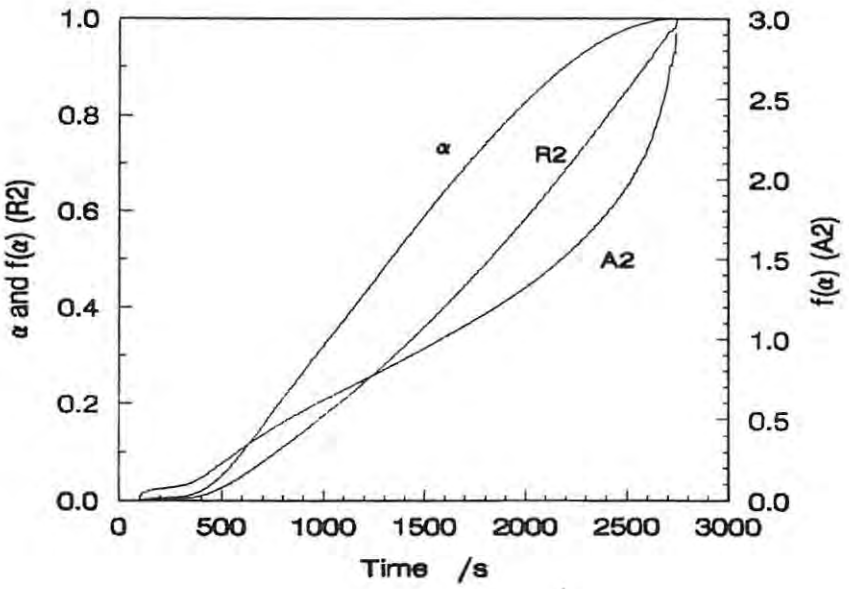

Fig. 6.17. The fit of the R2 and A2 models to the experimental curve for the reduction of WO_2 with CO at 850°C.

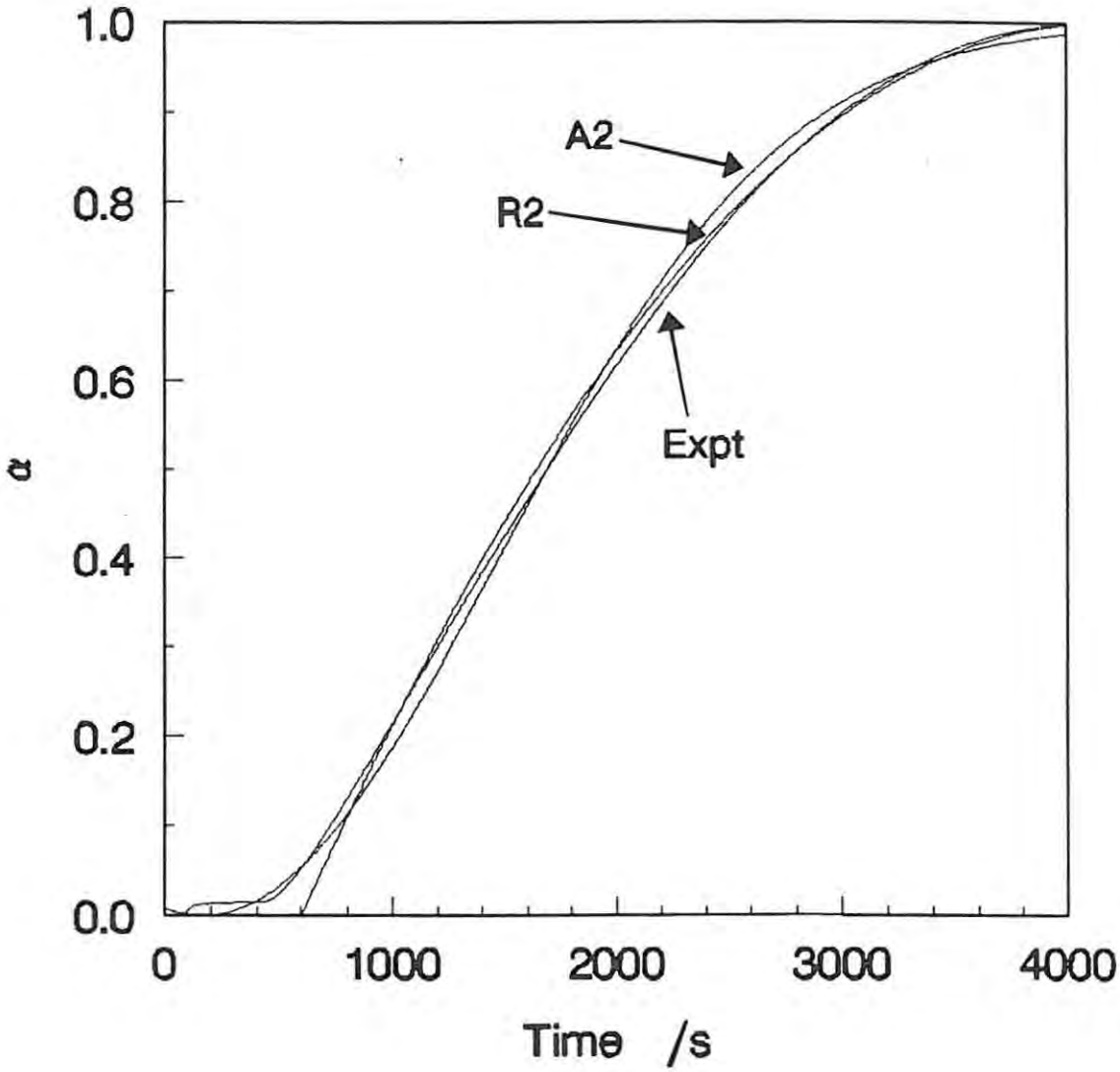

Fig. 6.18. Comparison of the experimental α values with those calculated using the R2 and A2 models.

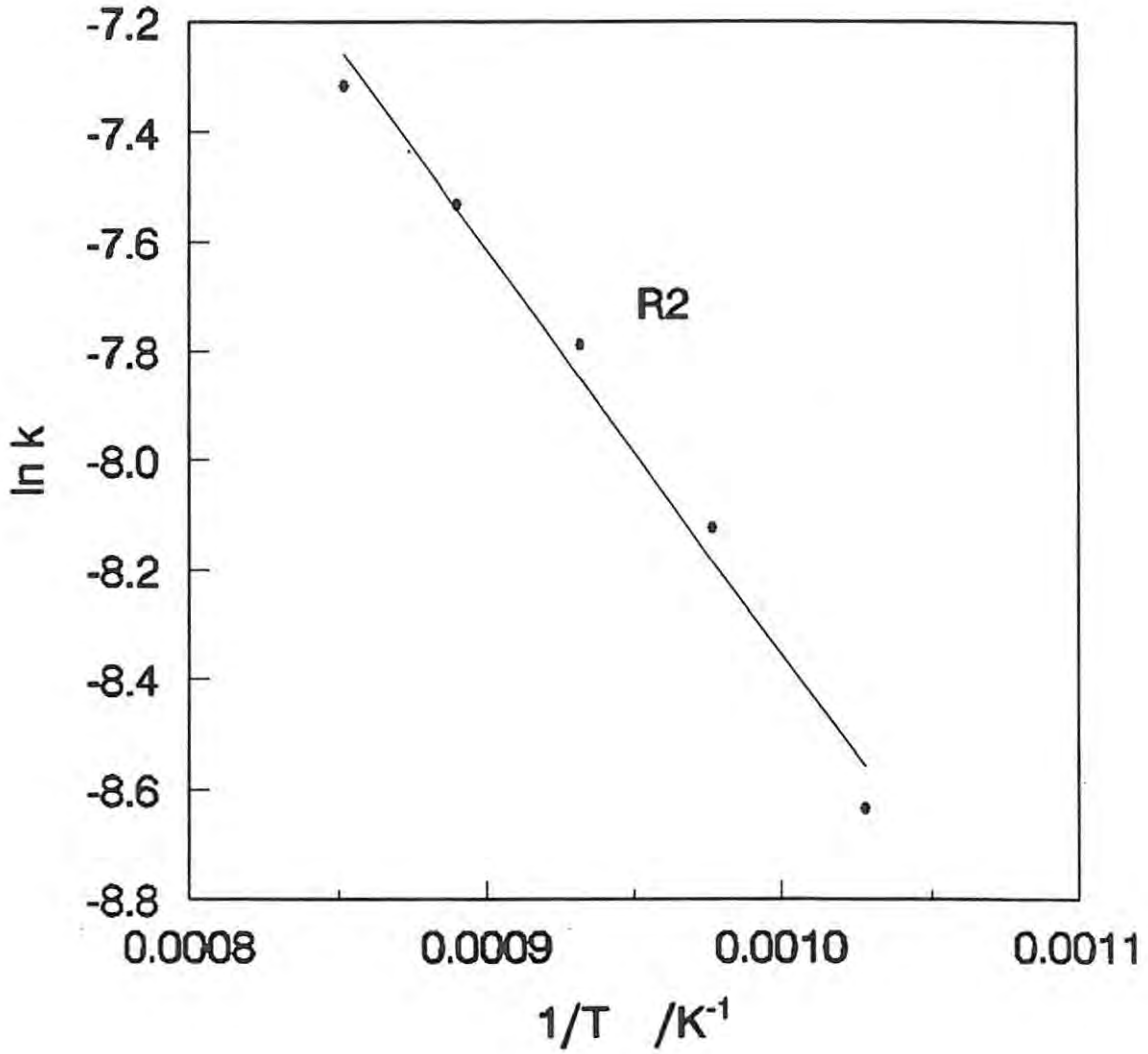

Fig. 6.19. The Arrhenius plot for the reduction of WO_2 with CO with the rate coefficients calculated by application of the R2 model.

6.6.4 Kinetics of the reduction of WO_3 with carbon monoxide

Unlike the reduction of WO_2, the reduction of WO_3 with CO took place in two main reaction stages. These stages were analysed separately for reactions below 800°C because: (1) the transition from the first to the second stage is readily identified; (2) the reaction products of the first stage are $W_{20}O_{58}$ and $W_{18}O_{49}$; and (3) the first stage of the reaction appears to take place in a single stage (up to 750°C).

From 800 to 900°C, only the kinetics of the second stage of the reaction were analysed. As with the reduction of WO_2, the reaction was assumed complete at the maximum mass loss. The α,t curve included both stages of the process because the first and second stages of the reduction could not be separated accurately. The error introduced by using a different starting point for the reaction is probably small since the mass loss of the first stage was only about 10% of the total mass loss. Table 6.4 list the mass losses at the end of the first and second stages.

Table 6.4. The mass losses taken to be the end of the first and second stages of the reaction, for the reduction of WO_3 with CO.

	Mass lost from the starting mass	
Temperature /°C	First stage /%	Second stage /%
650	1.3	13.9
700	1.8	15.1
750	2.3	15.6
800	-	15.9
850	-	16.0
900	-	16.0

The first stage of the reaction took place at an approximately constant rate, which indicates a zero-order reaction. The correlation coefficients and the rate constants calculated for a zero-order reaction are listed in Table 6.5. An activation energy and frequency factor of 66 ± 2 kJ mol^{-1} and 2.41 ± 0.04 s^{-1} were calculated for the first stage of reaction.

Table 6.5. The correlation coefficients and rate constants calculated for the first stage of the reduction of WO_3 by CO, for a zero-order reaction rate.

Temperature /°C	R^2	k /10^{-4} s^{-1}
650	0.9996	4.69
700	0.9985	7.42
750	0.9989	10.8

The reliability and meaning of the kinetic parameters are questionable when applied to a process involving a number of steps. In the reaction being studied, the process is probably:

$$WO_3 \xrightarrow{(1)} W_{20}O_{58} \xrightarrow{(2)} W_{18}O_{49}$$

as has been discussed. However, the extent to which this process is complete decreases at lower temperatures, and the extent to which steps (1) and (2) are complete is not known. If the product of first stage is $W_{18}O_{49}$, then it would be more accurate to calculate α assuming that $\alpha = 1.00$ at the mass loss expected for the formation of $W_{18}O_{49}$. Calculations using this definition of α gave an activation energy of 128 ± 6 kJ mol^{-1}, which differs considerably from the activation energy calculated previously.

Another method of calculating the rate constant for the process is from the reciprocal time of the induction period, which is independent of the mass loss. The results obtained using this method were very similar to those determined using the first estimate of α: the activation energy was 65.65 ± 0.02 kJ mol^{-1}, and the frequency factor was 2.6702 ± 0.0005 s^{-1}. These

values support the assumption that the process was complete at the end of step (1).

From the above conclusions regarding the definition of α, and the observed variation in the mass loss at the end of the first stage, the zero-order behaviour of the process is probably attributable to the formation of $W_{20}O_{58}$, since only step (1) could occur completely at the observed mass losses for first stage. Furthermore, the reduction of WO_3 to $W_{20}O_{58}$ by hydrogen has also been reported to take place at a constant rate[38], which suggests that the nature of the process is influenced more by the structure of the solids (especially that of $W_{20}O_{58}$) than by the particular reducing agent. Since the extent of reaction of the first stage represents the extent of formation of $W_{20}O_{58}$, the calculated activation energy of 65 kJ mol^{-1} is proposed to be that of the reduction of WO_3 to $W_{20}O_{58}$.

The greater mass loss at higher temperatures indicates the extent to which $W_{18}O_{49}$ is formed. The zero-order nature of the process appears to apply to the formation of $W_{18}O_{49}$ too, possibly because the formation of $W_{20}O_{58}$ and $W_{18}O_{49}$ occur in tandem.

For the second stage of reaction, the geometric models (especially R2) gave the best fit to the experimental data, although it was apparent that the middle of the α,t curve was approximately linear, i.e., a zero-order process. Table 6.6 lists the correlation coefficients for the R2 model and the zero-order rate equation at the temperatures studied.

Table 6.6. The correlation coefficients of the R2 model and the zero-order rate equation. The R2 model was analysed over most of the α,t curve; the zero-order rate equation was only analysed over the middle of the curve.

Temperature /°C	Correlation coefficients	
	Zero-order rate equation	R2
650	0.9998	0.9711
700	1.0000	0.9863
750	0.9996	0.9847
800	0.9998	0.9823
850	0.9998	0.9827
900	1.0000	0.9814

Figs. 6.20 and 6.21 show the fit of the R2 model to the experimental data at 700 and 850°C. The fit of the model is better towards the end of the reduction ($\alpha > 0.70$), and rate coefficients were calculated from correlations carried out over this section of the α,t curve. The Arrhenius plot using the rate constants calculated from the R2 model and the zero-order rate equation is shown in Fig. 6.22. An activation energy of 40 $\pm$ 7 kJ mol^{-1} and a frequency factor of (3.7 $\pm$ 0.6) $x10^{-2}$ s^{-1} were calculated using the R2 model; the zero-order rate equation gave values of 33 $\pm$ 8 kJ mol^{-1} and (2.0 $\pm$ 0.4) $x10^{-2}$ s^{-1} for the activation energy and frequency factor.

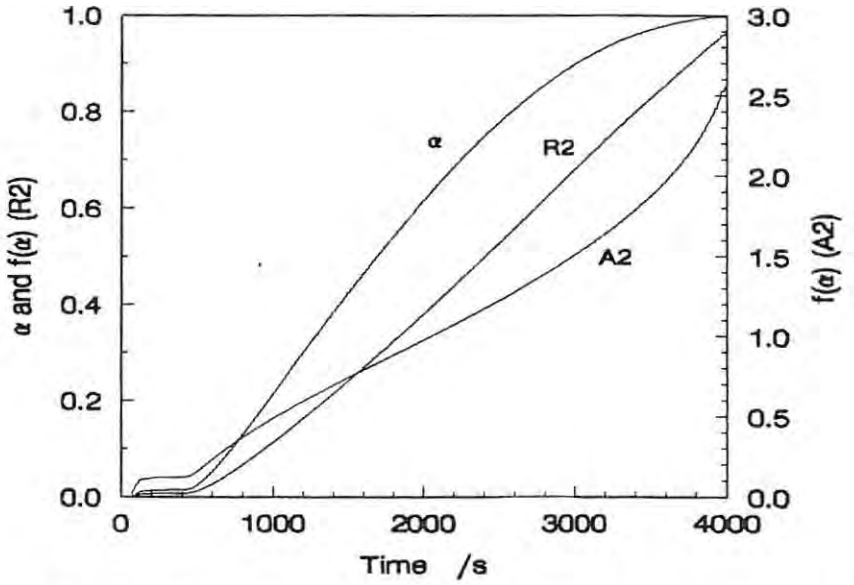

Fig. 6.20. The fit of the R2 and A2 models to the experimental data for the reduction of WO_3 with CO at 750°C.

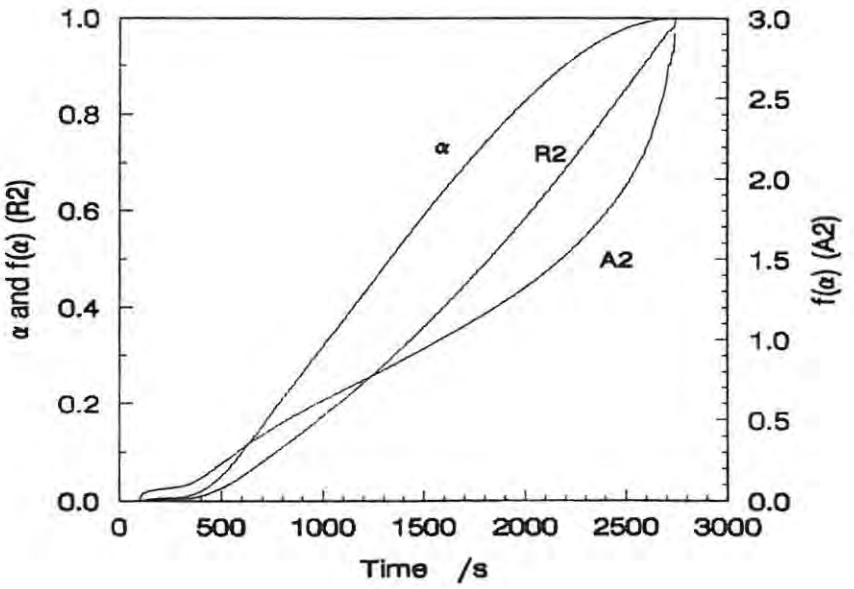

Fig. 6.21. The fit of the R2 and Avrami-Erofe'ev models to the reduction of WO_3 with CO at 850°C.

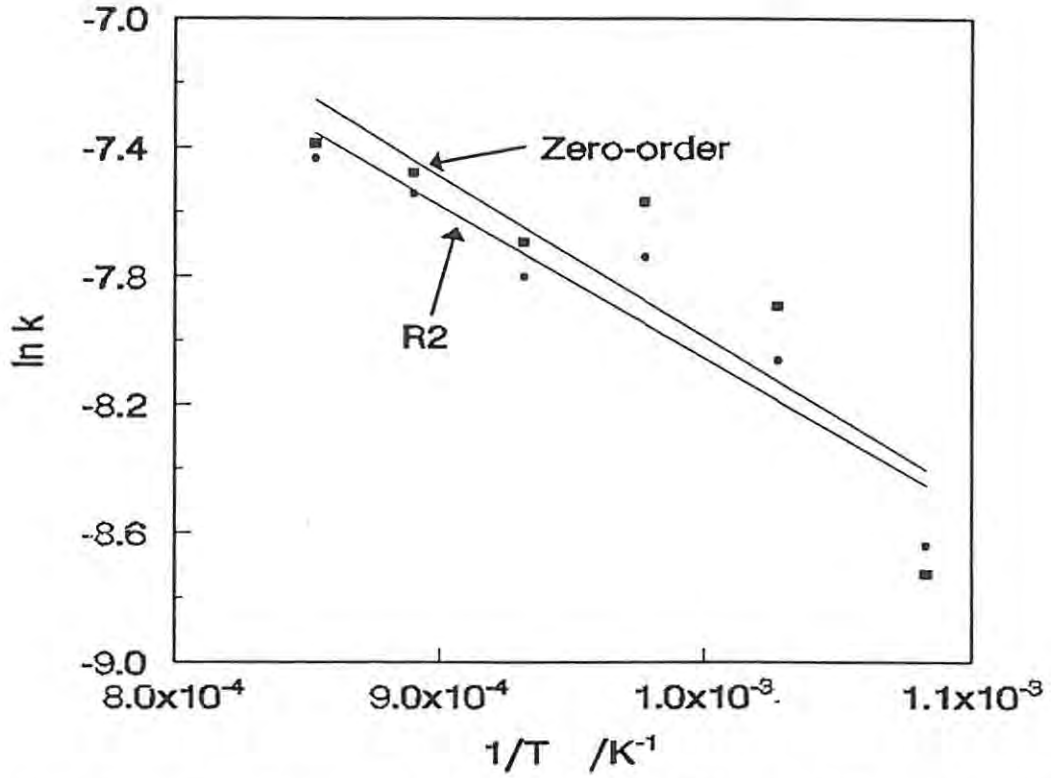

Fig. 6.22. The Arrhenius plot for the reduction of WO_3 with CO, using the rate coefficients calculated using the zero-order rate equation and the R2 model.

The good fit of the R2 model to the later stages of reduction suggests that the reaction occurred at a phase boundary which advanced inwards at a constant rate towards the end of the reduction. The beginning and middle of the reduction are less certain, and seem to involve some acceleratory process, perhaps nucleation and growth, or reaction starting from the bottom of the sample pan.

6.6.5 Discussion of kinetic results

Despite the difficulty in choosing a suitable definition of α, the kinetics were quite consistent for the reductions of WO_3 and WO_2. The good agreement of the geometric models suggests that the reaction occurs at an interface which advances into the particle. The induction period suggested that nucleation of the phase being formed may occur. The reduction was controlled by mass-transfer at low flowrates, as Basu and Sale[56] also found.

The kinetics of the reduction with CO are similar to those reported for the reduction

hydrogen. In particular, Taskinen *et al.*[33] reported that the reduction of WO_2 with hydrogen fitted the R2 model, and an induction period during reduction with hydrogen has been observed by Charlton[28,29].

The initial zero-order reaction in the reduction of WO_3 is probably associated with the reduction of $W_{20}O_{58}$. If this is the case, then the constant rate at which $W_{20}O_{58}$ is formed may be related to the formation or migration of crystallographic shear planes in the WO_3 lattice.

The formation of α-W during the reduction may result from reduction of $W_{18}O_{49}$ or of WO_2. Most carburisation seems to takes place towards the end of the reaction, when the CO/CO_2 ratio is relatively high. Although the investigation into the carburisation of tungsten powder indicated that reaction was very slow after about $\alpha = 0.20$, the tungsten produced during the reduction of tungsten oxides will probably be much more reactive and is likely to react to completion. The mass loss curves in the reductions of WO_3 and WO_2 and the results of Basu and Sale[56] suggest that this is the case.

The Arrhenius plots of the reductions of WO_3 and WO_2 are quite curved, possibly indicating that the reaction mechanism changes with temperature. This change may result from the variations in the structure of the particles at different temperatures. Alternatively, differences in the CO/CO_2 ratios at different temperatures may alter the reactions which take place during the overall process. If the reaction mechanism does change, then the activation energy will be higher at low temperatures than the calculated activation energy, and at high temperatures the activation energy will be lower than the calculated activation energy.

Chapter 7

REDUCTION OF TUNGSTEN OXIDES WITH CARBON

7.1 High-temperature thermogravimetric studies

7.1.1 Preliminary observations on the interaction of WO_3 with graphite

The reaction of a 1:3 mole ratio mixture of WO_3 and graphite was studied in argon by heating the sample at 2°C min^{-1} up to 950°C (Fig. 7.1). The mass decreases very slowly from 750 to 900°C, and starts decreasing more rapidly above 900°C. A DTA curve of the same mixture up to 1200°C shows a shallow endotherm from about 930 to 1110°C (Fig. 7.2). The endotherm is initially small, but increases significantly above 1000°C. These observations indicate that the reaction between WO_3 and graphite is only significant above 900°C, and may take place in two stages.

7.1.2 Isothermal reduction of WO_3 with graphite

Only a very limited number of TG experiments could be done, through a combination of limited time available on the instrument and the considerable wear-and-tear on the instrument under the experimental conditions required. Choices thus had to be made, in advance, of aspects to be studied.

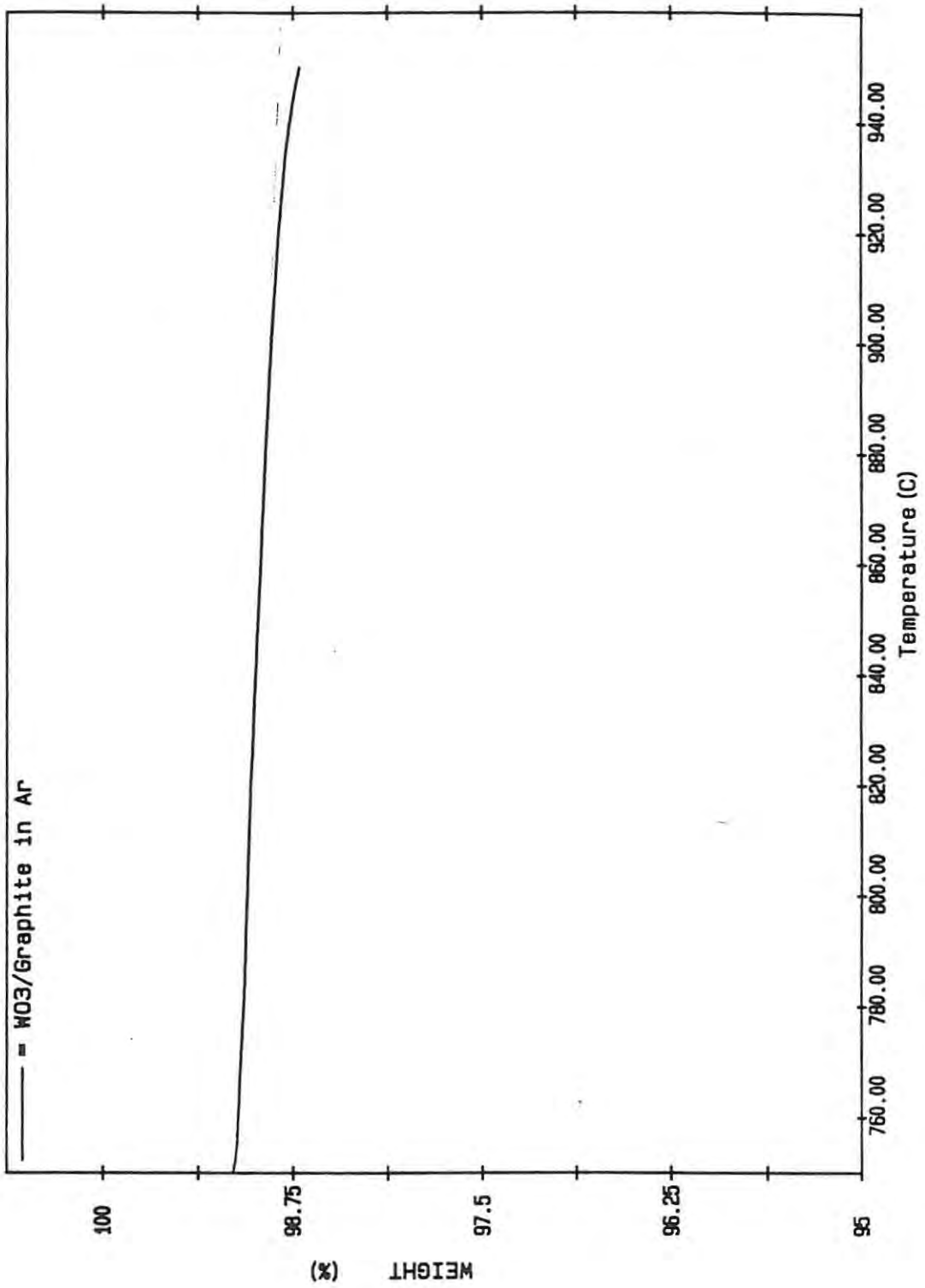

Fig. 7.1. Thermogravimetric trace of a WO_3/graphite mixture (in a 1:3 mole ratio) heated in argon at 2°C min^{-1}.

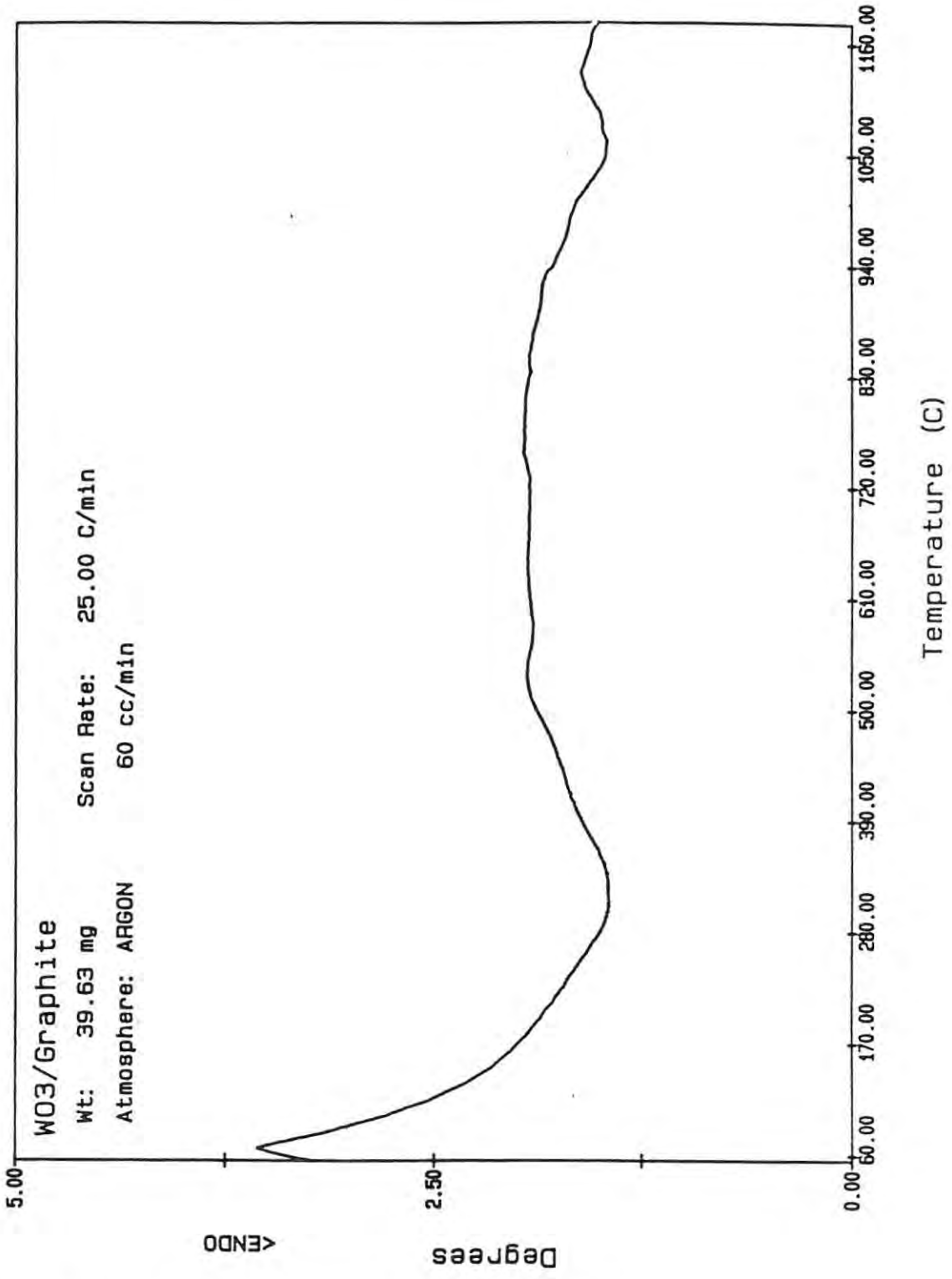

Fig. 7.2. DTA curve of the interaction of a mixture of WO_3 and graphite in a 1:3 mole ratio, heated at 25°C min^{-1} in an argon atmosphere.

Mixtures of WO_3 and graphite in a 1:3 mole ratio were studied at 950, 1050, and 1100°C. The mass loss curves are displayed in Fig. 7.3, and indicate that the course of reaction changes dramatically with temperature. At 950°C the mass loss describes a smooth curve and the reaction is about a third complete after about 4 hours. The mid-temperature range (1050°C) shows overlapping processes, which are less evident at higher temperatures (1100°C). The transition between the first and second stages occurs between 8 and 13% mass loss, suggesting a two stage reduction:

$$WO_3 \longrightarrow WO_2$$

followed by

$$WO_2 \longrightarrow W$$

The mass losses of these steps (as a percentage of the original WO_3/graphite mixture) vary from 8.2 to 10.5% for the first stage, and 16.4 to 20.9% for the second stage, depending on the

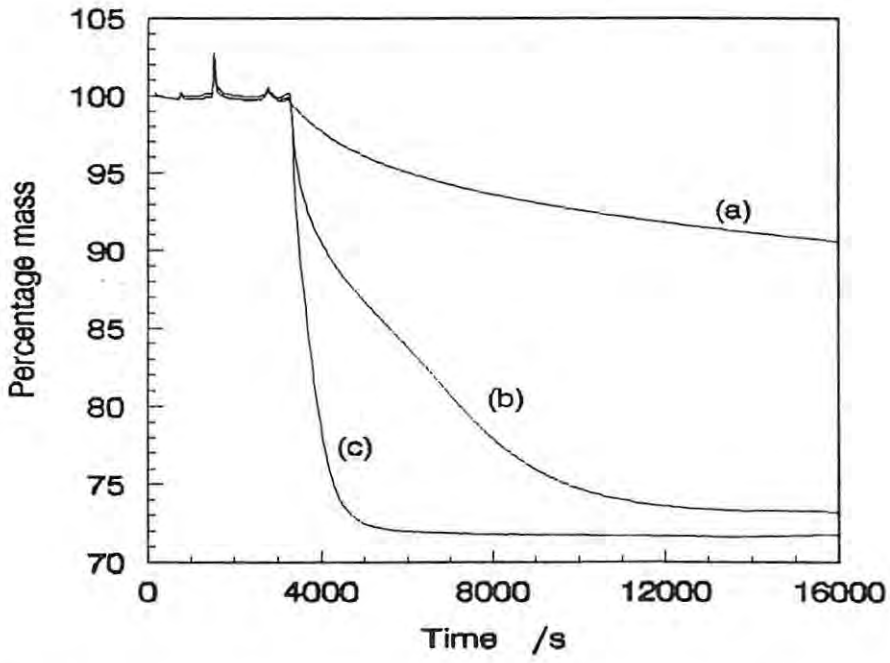

Fig. 7.3. The mass loss curves of WO_3/graphite mixtures at 950, 1000, and 1100°C.

relative amounts of CO and CO_2 formed in the reaction. Thus, the total mass loss for complete reaction ranges from 24.6 to 31.4%.

If the reduction is accomplished by CO, then from the reaction scheme given in Fig. 6.6 the reaction should proceed by $W_{20}O_{58}$ and $W_{18}O_{49}$. However, these phases were not apparent as separate stages in the reduction, and their participation in the reduction was not considered further. The reduction of WO_3 via WO_2 has been proved in the reduction by CO, and a similar reaction path may be expected here.

The actual reactions which can take place in the reduction are determined by the CO/CO_2 ratio in the system. It seems likely that the CO/CO_2 ratio in the system would be quite low, in which case the reduction would be more likely to proceed by reduction to WO_2 than directly to tungsten metal (Fig. 6.4). The reduction of WO_2 to tungsten requires a relatively high CO/CO_2 ratio.

The kinetics of the first and second stages of the reaction were analysed separately. The reaction rate was deceleratory over the course of the reaction; thus, only the deceleratory models (Table 2.1) were examined. The extent of reaction based on the completion of the first stage (taken as 10.5%) will be designated as α', whereas α will indicate the extent of the overall reaction. At 950 and 1050°C the reaction was taken to be complete at 26.9% (the final mass loss at 1050°C), and at 1100°C the reaction was assumed complete at 28.4%, the final mass loss at that temperature. Only the rate coefficients determined from α values were used for activation energy calculations.

Fig. 7.4 shows how α and α' vary with time at 950°C. The Ginstling-Brounshtein (D4) and one-dimensional diffusion (D1) models gave the best fit to the experimental data (Fig. 7.5), whereas the R2, R3, and F1 models did not fit the data well (Fig. 7.6).

Using $f(\alpha) = kt$ and $f(\alpha') = k't$, and decreasing the range of the regressions to $0 < \alpha < 0.29$, the rate constants shown in Table 7.1 were obtained. Using these values, the experimental times are compared with the time values calculated using the D1 and D4 models in Fig. 7.7.

Table 7.1. The rate constants and correlation coefficients calculated using the D1 and D4 models for the WO_3/graphite system at 950°C for $\alpha < 0.29$.

	D1 /10^{-6} s^{-1}	R^2	D4 /10^{-6} s^{-1}	R^2
k'	61.3 ± 0.3	0.9885	15.0 ± 0.1	0.9942
k	11.1 ± 0.1	0.9950	1.43 ± 0.01	0.9974

At 1050°C the D4 model gave the best fit to the initial part of the curve ($\alpha < 0.60$), and at higher α values the F1 model fitted the curve well ($0.78 < \alpha < 0.97$). The applicability of the D4 model extended over a larger range of α than that expected if the reduction of WO_3 to

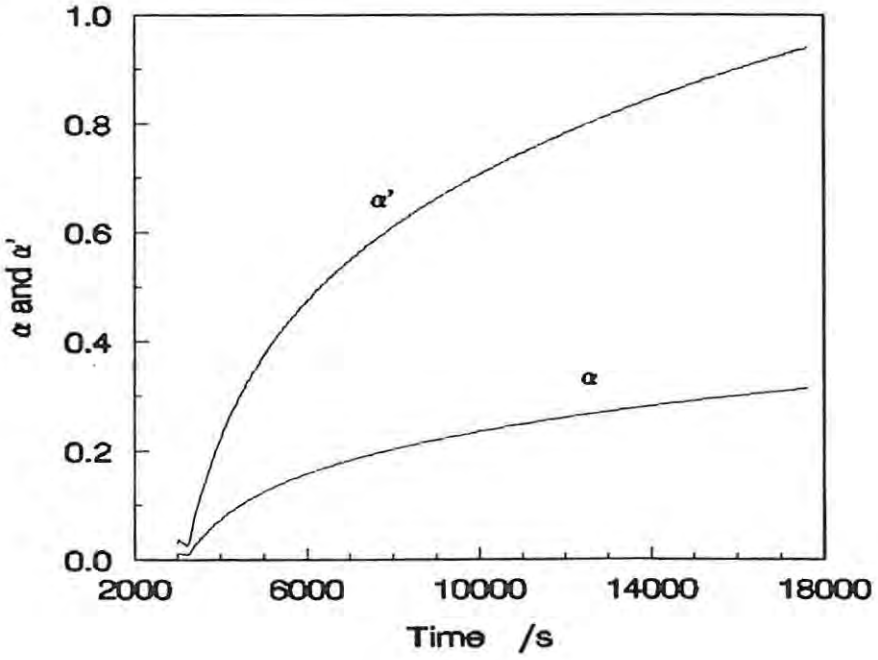

Fig. 7.4. Comparison of α and α' for the reduction of WO_3 with graphite as a function of time at 950°C.

well, so it is not clear whether the diffusion-limiting process applies to complete reduction, or only the reduction to WO_2. Fig. 7.8 shows the α and $f(\alpha)$ curves for the D4 and F1 models, scaled for comparison. The calculated rate coefficients are $(234.9 \pm 2.9)\ x10^{-7}\ s^{-1}$ for the D4 model, and $(560 \pm 2)\ x10^{-6}\ s^{-1}$ for the F1 model. Using these values, and taking the start of applicability of the models at $t = c/k$ (where c is the intercept and k is the rate coefficient calculated in the linear regression), we obtain Fig. 7.9 which compares the experimental α,t curve with the curves calculated using the D4 and F1 models. The transition from the D4 to the F1 model occurs at about $\alpha = 0.67$.

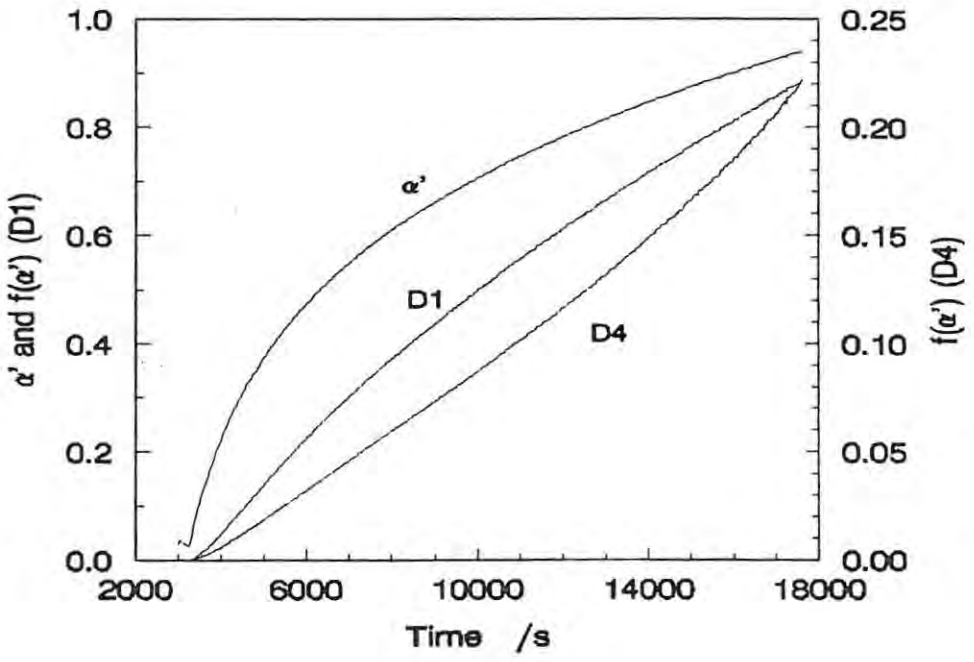

Fig. 7.5. The closeness of fit of the D1 and D4 models to the α' values for the reaction of WO_3 and graphite at 950°C.

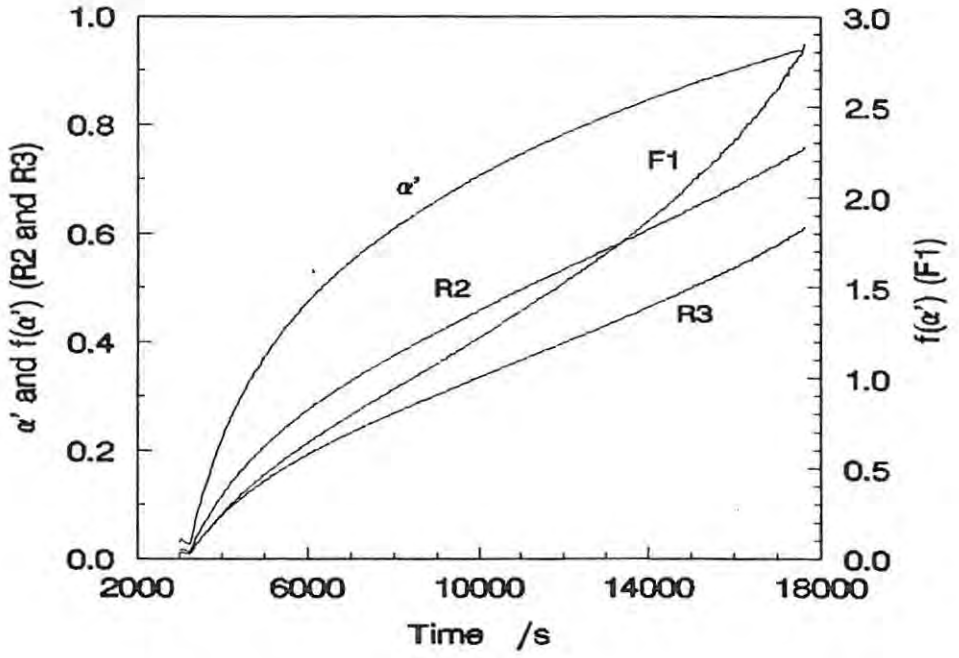

Fig. 7.6. The closeness of fit of the R2, R3, and F1 models to the α' values for the reduction of WO_3 with graphite at 950°C.

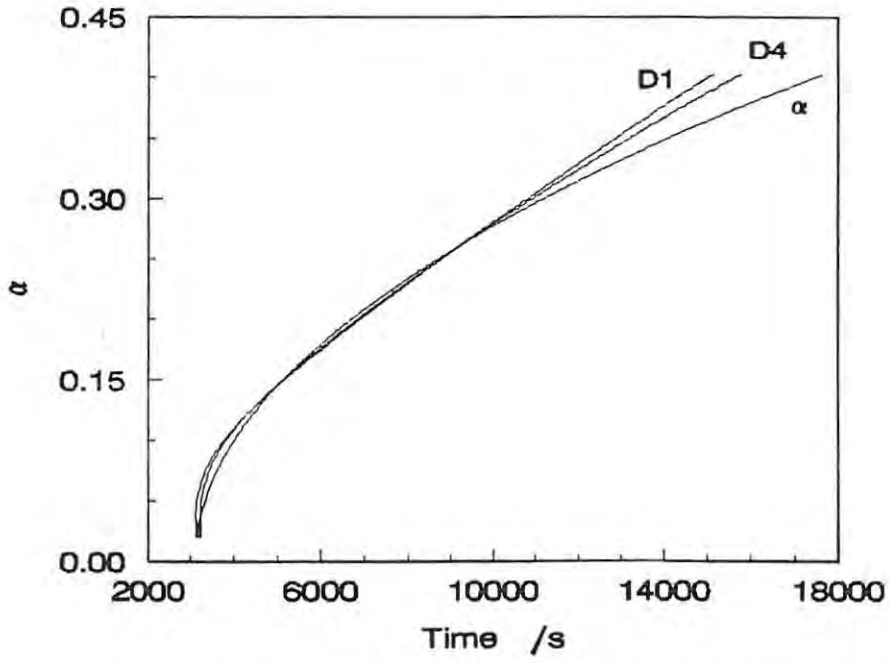

Fig. 7.7. Comparison of the experimental α,t curve (for the reduction of WO_3 with graphite at 950°C) with the α,t curves calculated using the D1 and D4 models.

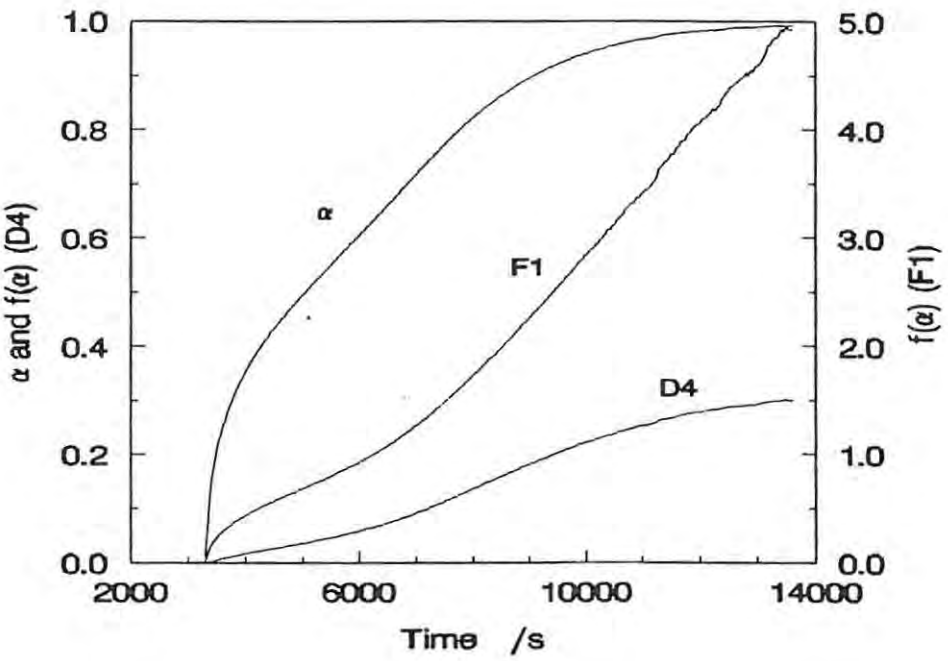

Fig. 7.8. The closeness of fit of models D4 and F1 to the α values for the reduction of WO_3 with graphite at 1050°C.

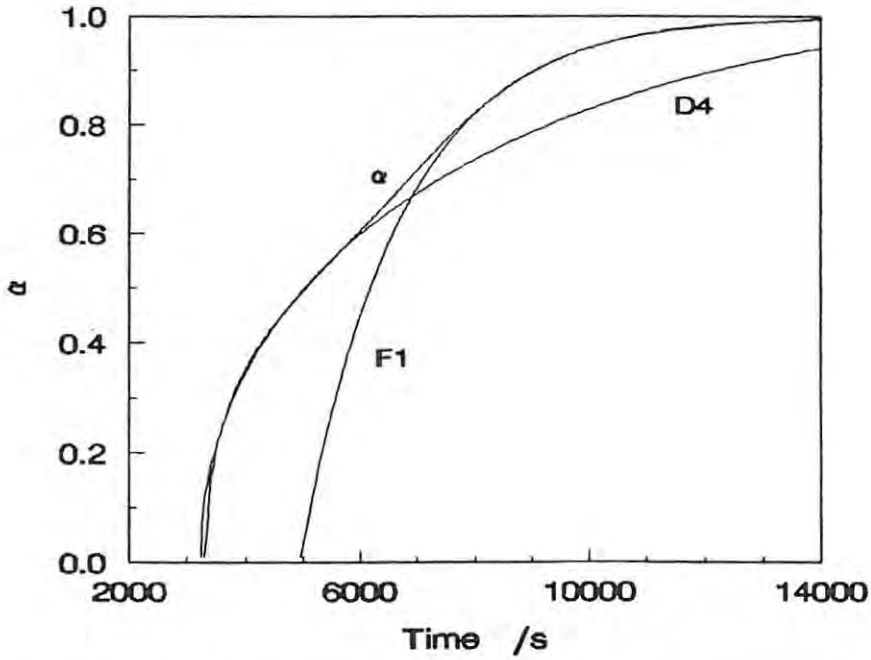

Fig. 7.9. Comparison of the experimental α,t curve for the reduction of WO_3 with graphite at 1050°C with the α,t curves calculated using the D4 and F1 models.

At 1100°C the first stage of the reaction was completed very rapidly ($\alpha < 0.40$) and did not permit a meaningful comparison of models. A D4 model was assumed based on the results at 950 and 1050°C, and gave $k = (9.25 \pm 0.57)\ x10^{-5}\ s^{-1}$ for $\alpha < 0.40$. For the second stage of the reaction, the F1 model gave the best fit to the data; for $0.65 < \alpha < 0.95$ the value of k was $(239 \pm 1)\ x10^{-5}\ s^{-1}$. Fig. 7.10 shows α and $f(\alpha)$ for the D4 and F1 models, and the α,t curves calculated using these models are plotted with the experimental curve in Fig. 7.11. The transition between models takes place at about $\alpha = 0.47$.

The k values calculated using the D4 and F1 models were incorporated in an Arrhenius plot, shown in Fig. 7.12. The values calculated for the activation energy and the frequency factor were 386 ± 9 kJ mol^{-1} and $(4.36 \pm 0.3)\ x10^{10}\ s^{-1}$ for the D4 model, and 438 kJ mol^{-1} and $1.13\ x10^{14}\ s^{-1}$ for the F1 model.

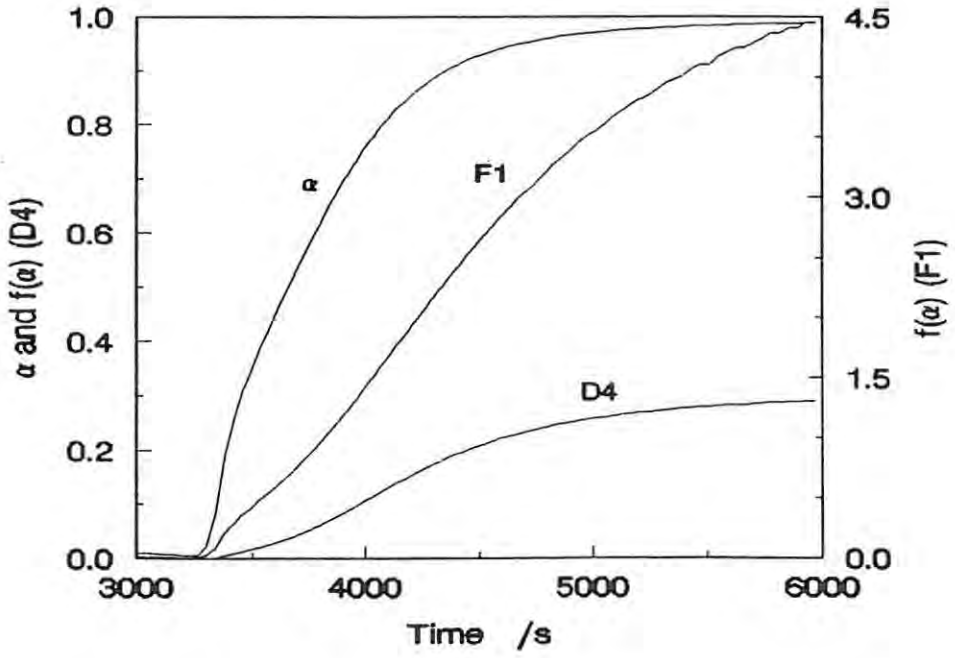

Fig. 7.10. The closeness of fit of the D4 and F1 models to the α values for the reduction of WO_3 with graphite at 1100°C.

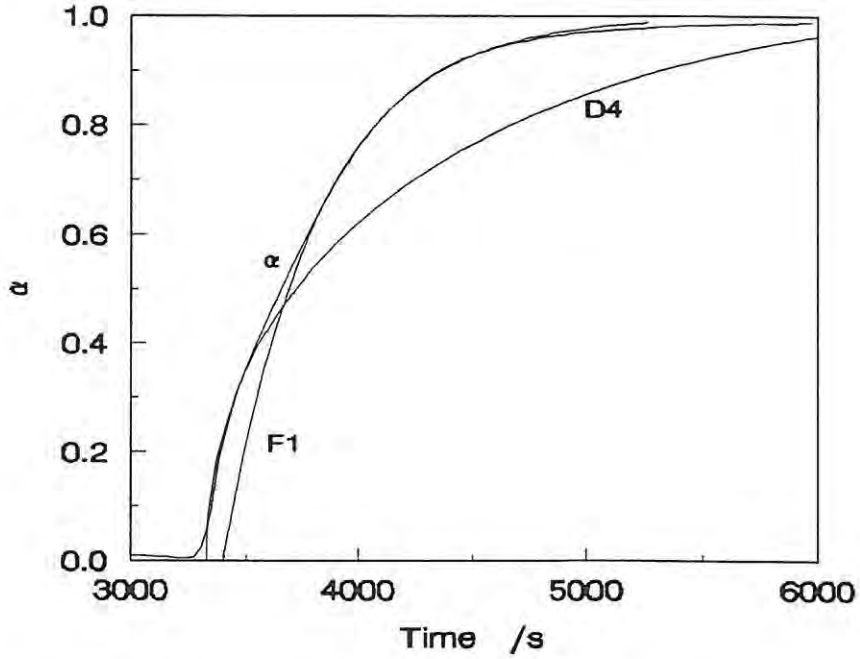

Fig. 7.11. Comparison of the α,t curves calculated using the D4 and F1 models, with the experimental curve for the reduction of WO_3 with graphite at 1100°C.

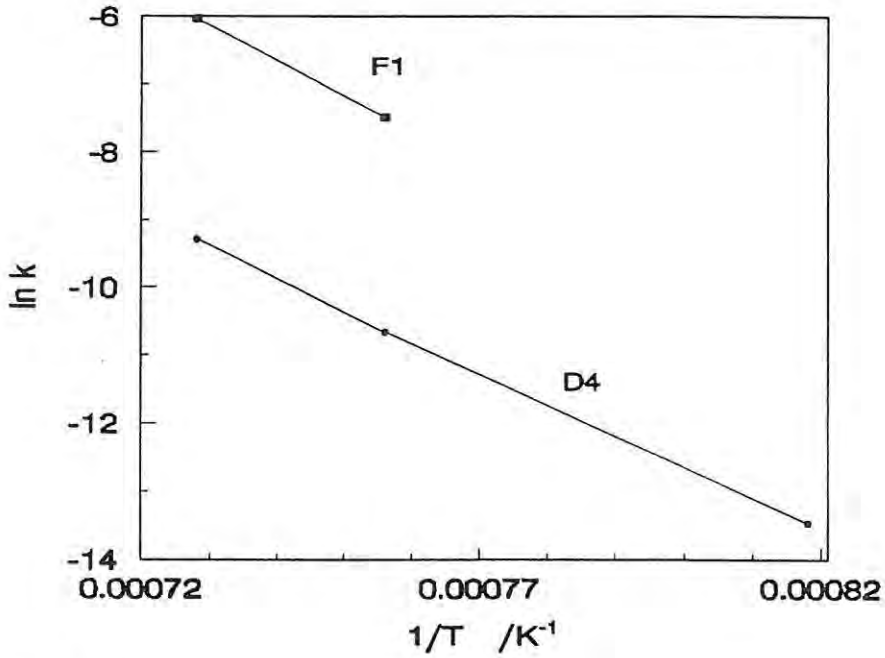

Fig. 7.12. The Arrhenius plots for the first and second stages of the reduction of WO_3 with graphite, using the rate constants calculated from application of the D4 and F1 models, respectively.

The small number of experimental curves decreases the certainty of the results, and hence the value of the analysis. Some further experiments were performed later to investigate intermediate temperatures, but the results suggested that significant changes in the calibration of the thermogravimetric analyser had occurred.

7.1.3 Isothermal reduction of WO_3 with lamp black

The mass loss curves obtained at 950°C using graphite and using lamp black were similar (Fig. 7.13), and increasing the temperature to 1000°C gave no indication of a two stage process. The extent of reaction was defined such that $\alpha' = 1$ at 10.5% mass loss (for the first stage), and $\alpha = 1$ at 31.4% (for the complete reaction).

At 950°C the tests of the diffusion models showed good linearity using the values of α'. The linearity improved on going from the D1 to D4 model (Fig. 7.14). The experimental and the D4 model curves are compared in Fig. 7.15, and the calculated rate coefficients are listed in Table 7.2. Other models did not fit the data well.

Table 7.2. The rate coefficients calculated using the D3 and D4 models for the WO_3/lamp black system at 950°C.

Rate Coefficient	D3 $/10^{-7}$ s^{-1}	D4 $/10^{-7}$ s^{-1}
k'	110 ± 1	80.1 ± 0.1
k	6.22 ± 0.03	6.99 ± 0.03

The diffusion models also gave good agreement with the experimental α values at 1000°C. The D4 model, in particular, showed excellent agreement with the data (Fig. 7.16), and gave a value of 4.22 $x10^{-6}$ s^{-1} for the rate constant. An activation energy of 465 kJ mol^{-1} and a frequency factor of 5.21 $x10^{13}$ s^{-1} were calculated using the D4 model.

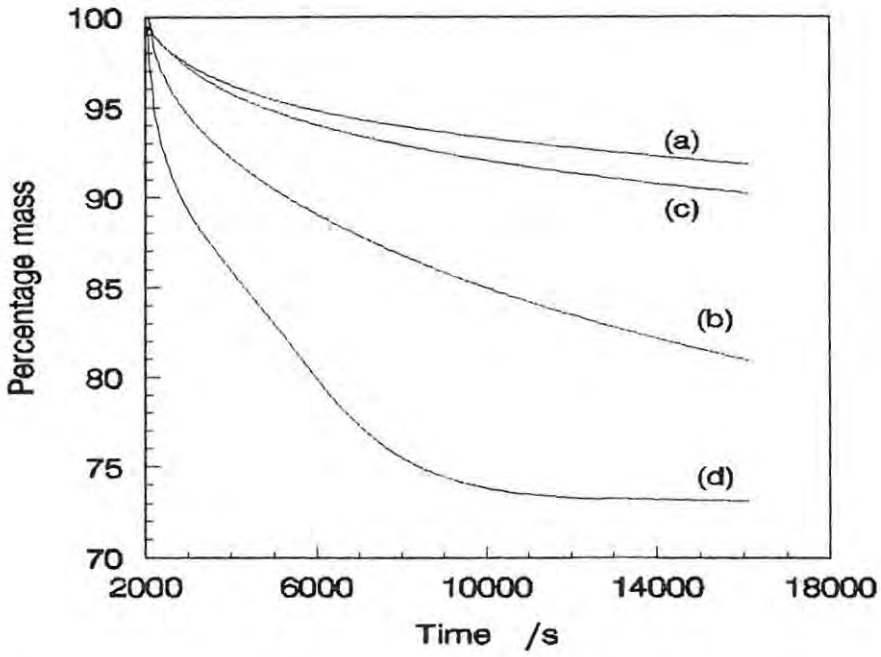

Fig. 7.13. Mass loss curves of the reduction of WO_3 with lamp black at (a) 950°C and at (b) 1000°C; the mass loss curves for the reduction using graphite at (c) 950°C and at (d) 1050°C are shown for comparison.

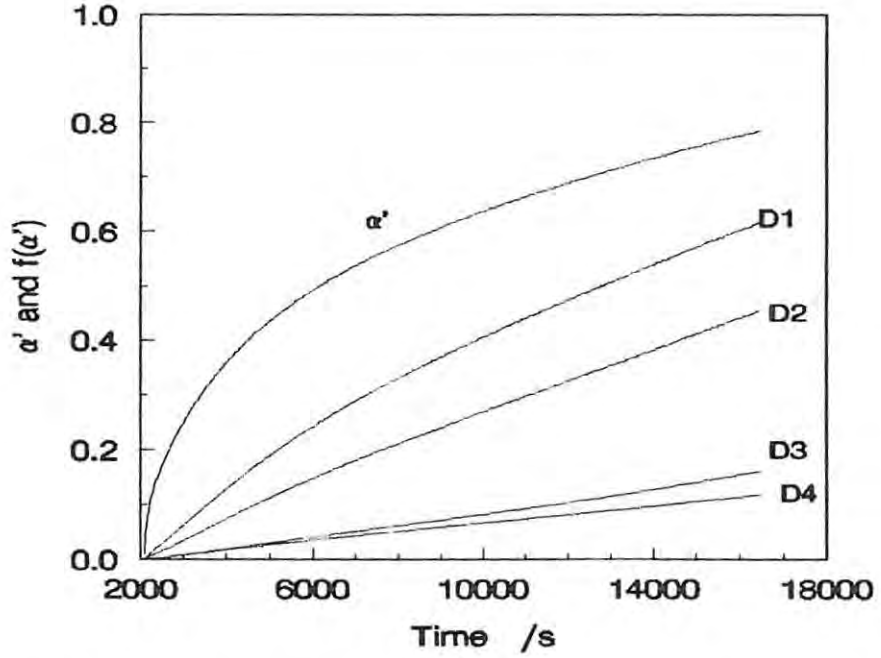

Fig. 7.14. The closeness of fit of the diffusion models to the α values for the reduction of WO_3 with lamp black at 950°C.

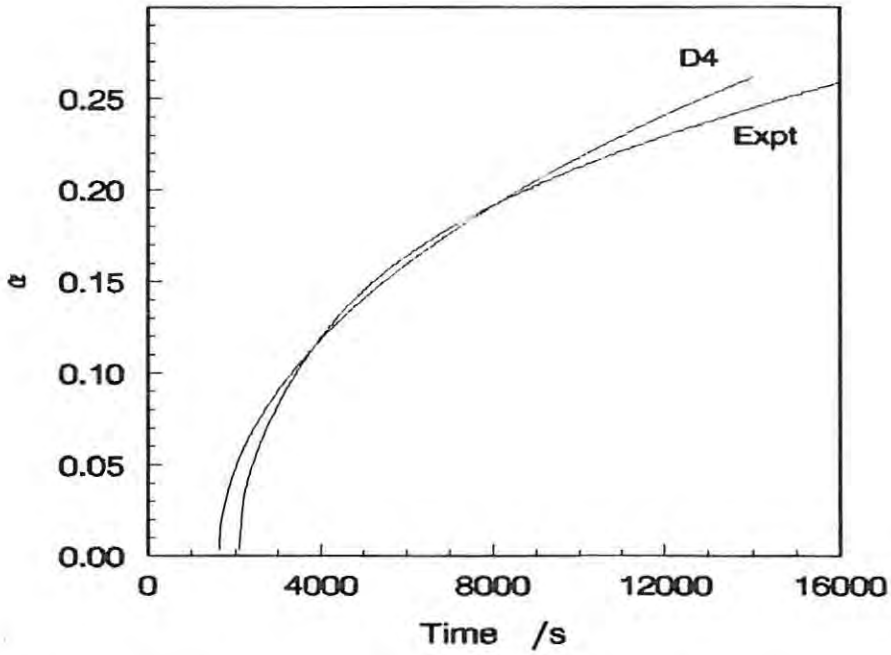

Fig. 7.15. Comparison of the experimental and the calculated α values for the reduction of WO_3 with lamp black at 950°C.

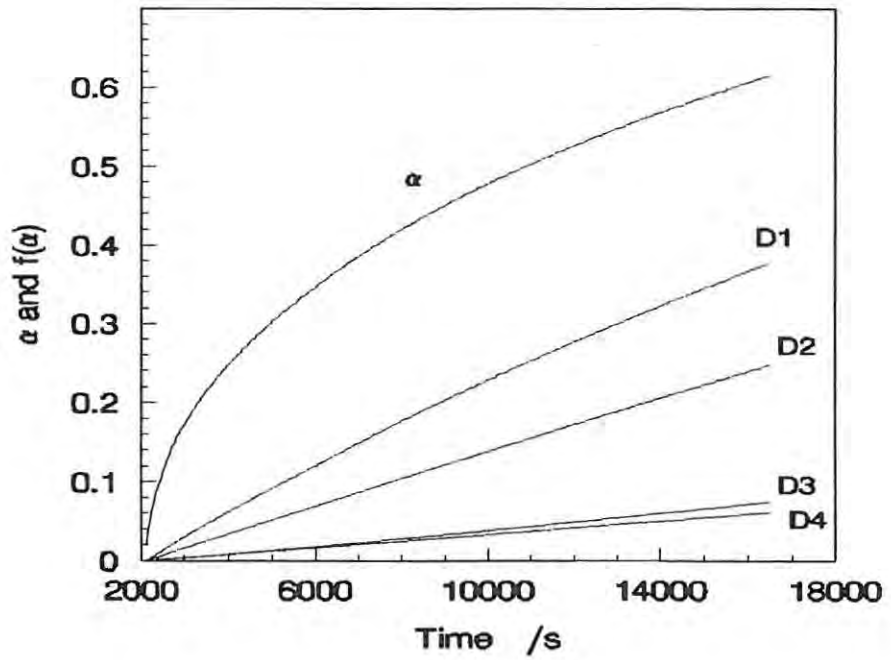

Fig. 7.16. The closeness of fit of the diffusion models to the α values for the reduction of WO_3 with lamp black at 1000°C.

7.1.4 Dynamic experiments

The kinetics of the reactions were examined using the Borchardt-Daniels model[62],

$$k = \frac{d\alpha}{dt} \cdot \frac{1}{(1 - \alpha)^n}, \tag{7.1}$$

where n is the "order of the reaction". Thus, k values can be directly incorporated in an Arrhenius curve by plotting $\ln k$ against $1/T$. The values of n considered were 0.333, 0.5, 0.667, 1, 1.5, and 2. A 7-point cubic Savitzky-Golay smoothing routine was used to smooth the data and compute the first derivative for the analysis.

For the WO_3/graphite system, in which two experiments were carried out at different heating rates, the method of Gyulai and Greenhow[63] was also used to analyse the data. This method does not assume a particular form for f(α) but uses an approximation for the temperature integral:

$$f(\alpha) = \frac{A}{\phi} \int_{T_0}^{T} e^{-E/RT} dT \simeq \frac{A}{\phi} b \tag{7.2}$$

where

$$b = \int_0^T e^{-E/RT} dT. \tag{7.3}$$

At a given $\alpha = \alpha_i$, $T = T_1$ at heating rate ϕ_i, and $T = T_2$ at heating rate ϕ_i. Thus

$$f(\alpha) = \frac{A}{\phi_1} b_1 = \frac{A}{\phi_2} b_2. \tag{7.4}$$

The log (b_1/b_2) ratio is

$$\log\frac{b_1}{b_2} = -1.916\log\frac{T_1}{T_2} - 0.2254\,E_a\left[\left(\frac{1000}{T_1}\right)^{0.980} - \left(\frac{1000}{T_2}\right)^{0.980}\right] \qquad (7.5)$$

and hence this ratio can be plotted against activation energy. The activation energy of the process is taken from the point on the graph at which log (b_1/b_2) = log (ϕ_1/ϕ_2).

Fig. 7.17 shows how α and $d\alpha/dt$ vary with temperature for the reduction of WO_3 with graphite at a heating rate of 5°C min^{-1}. The plot of ln k against $1/T$ is shown in Fig. 7.18. Disregarding the initial, erratic values for α, the curve divides into two sections. The first section occurred from about 915 to 1050°C, followed by a steeper slope from 1050 to 1125°C. α = 0.27 at the transition temperature (1050°C), which is quite close to α = 0.33, the transition point expected for a two-step process proceeding via reduction of the dioxide. Higher orders of reaction fitted the data best for temperatures below 1050°C, whereas from 1050 to 1125°C the lower orders give the best fit (Table 7.3).

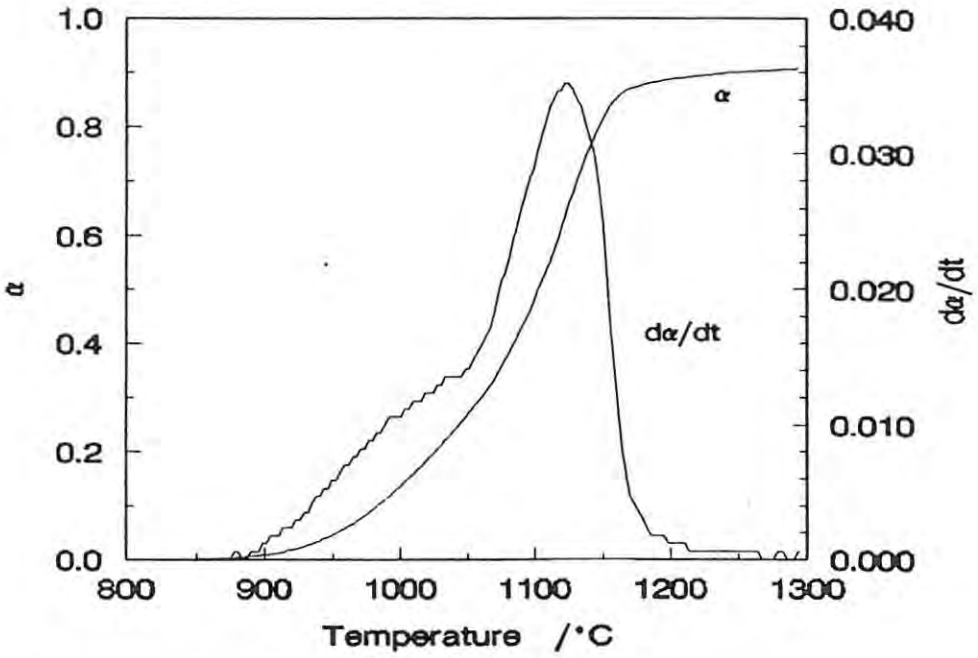

Fig. 7.17. The variation of α and $d\alpha/dt$ as a function of temperature for a mixture of WO3 and graphite heated at 5 °C min^{-1}.

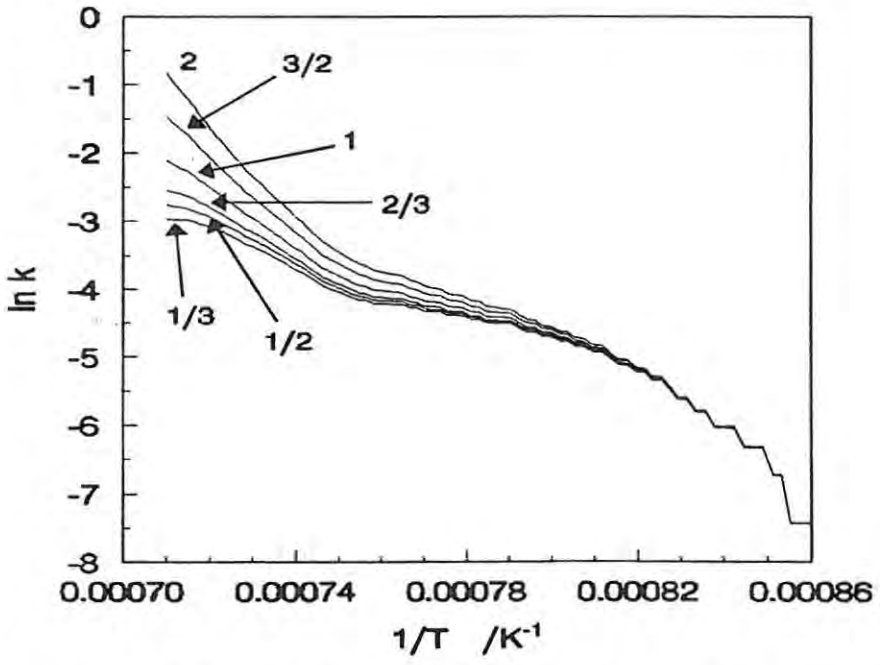

Fig. 7.18. Plot of ln k at different orders of reaction for a WO_3/graphite mixture heated at 5 °C min^{-1}.

Table 7.3. The calculated activation energies for different orders of reaction for WO_3/graphite, heated at 5°C min^{-1}.

	915 to 1050°C		1050 to 1125°C	
n	E_a /kJ mol^{-1}	R^2	E_a /kJ mol^{-1}	R^2
0.333	174 ± 7	0.9281	255 ± 3	0.9953
0.5	179 ± 7	0.9343	279 ± 3	0.9970
0.667	184 ± 7	0.9401	304 ± 3	0.9973
1.0	194 ± 7	0.9501	352 ± 4	0.9960
1.5	208 ± 6	0.9621	424 ± 8	0.9919
2.0	222 ± 6	0.9713	496 ± 11	0.9874

Similar results were obtained for an experiment at 10°C min^{-1}, and the ln k versus $1/T$ curves also divided into two sections: from 932 to 1058°C, and from 1058 to 1121°C (Fig. 7.19). At the transition temperature, $\alpha = 0.25$. The results of the regressions over these temperature ranges are displayed in Table 7.4. A reaction order of 2 gave the best fit at low temperatures, and above 1058°C orders of 1 and 1.5 gave the closest fit.

The Gyulai-Greenhow method was applied to the 5 and 10°C min^{-1} experiments. The α values chosen for the analysis were 0.05, 0.10, and 0.20 for the first stage of the reduction, and 0.40, 0.50, and 0.60 for the second stage. Fig. 7.20 shows the graph for the first stage: an activation energy of between 300 and 360 kJ mol^{-1} was calculated. The activation energy for the second stage of the reduction varied considerably with the value of α and was also very high (well above 600 kJ mol^{-1}).

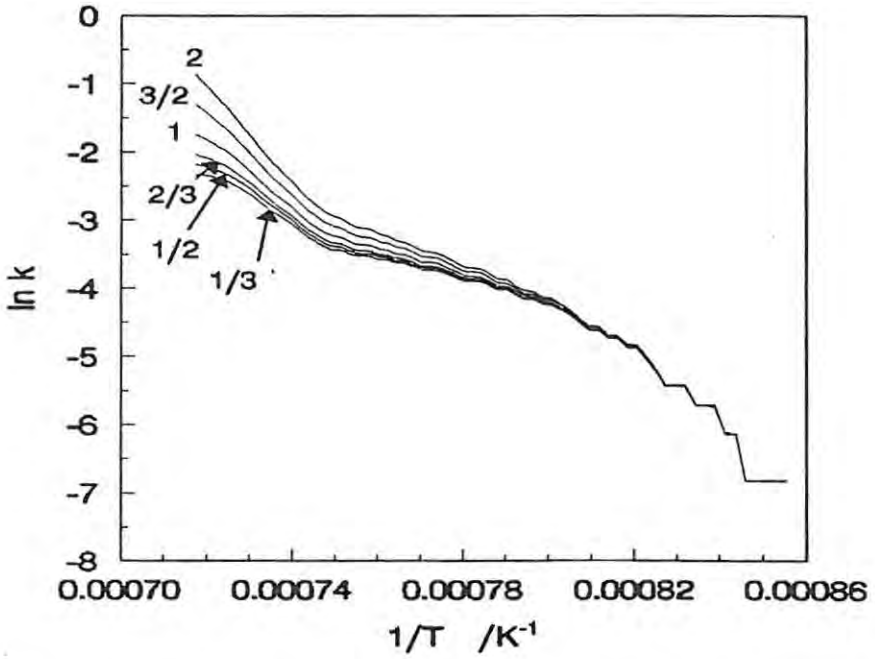

Fig. 7.19. Variation of ln k at different orders of reaction as a function of $1/T$ for a WO_3/graphite mixture heated at 10°C min^{-1}.

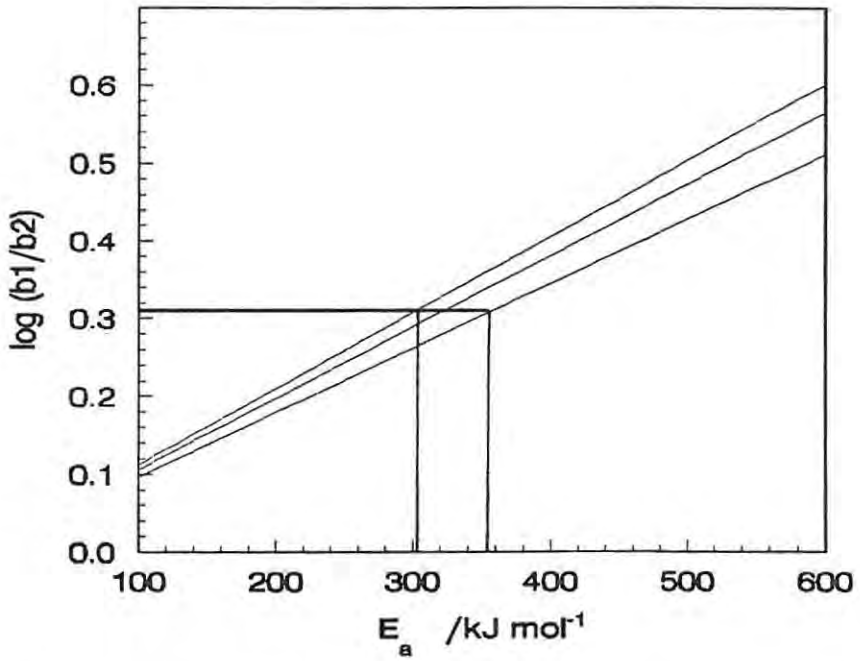

Fig. 7.20 The Gyulai-Greenhow plot for the first stage of the reaction of WO_3 and graphite.

Table 7.4. The calculated activation energies for different orders of reaction for WO_3/graphite, heated at 10°C min^{-1}.

	932 to 1058°C		1058 to 1121°C	
n	E_a /kJ mol^{-1}	R^2	E_a /kJ mol^{-1}	R^2
0.333	194 ± 8	0.9421	313 ± 10	0.9826
0.5	199 ± 8	0.9468	337 ± 9	0.9875
0.667	203 ± 8	0.9511	361 ± 8	0.9908
1.0	213 ± 7	0.9588	408 ± 7	0.9943
1.5	226 ± 7	0.9681	479 ± 8	0.9951
2.0	240 ± 6	0.9754	549 ± 10	0.9836

For the reduction of WO_3 with lamp black, the reaction mixture was heated at 5°C min^{-1} and the results were analysed in the same manner as above. Fig. 7.21 shows the variation of α and $d\alpha/dt$ with temperature, and the ln k values are plotted against $1/T$ in Fig. 7.22. As with the graphite mixture, the ln k plot also formed two parts. The transition temperature was at about 1040°C, at which α was about 0.30. The curves were analysed between 900 and 1040°C and between 1040 and 1140°C; the results are shown in Table 7.5. As for the WO_3/graphite mixtures, a reaction order of 2 fitted the data best at lower temperatures; low reaction orders fitted the data well at higher temperatures. The activation energies calculated for the lamp black system were significantly lower than for the graphite system.

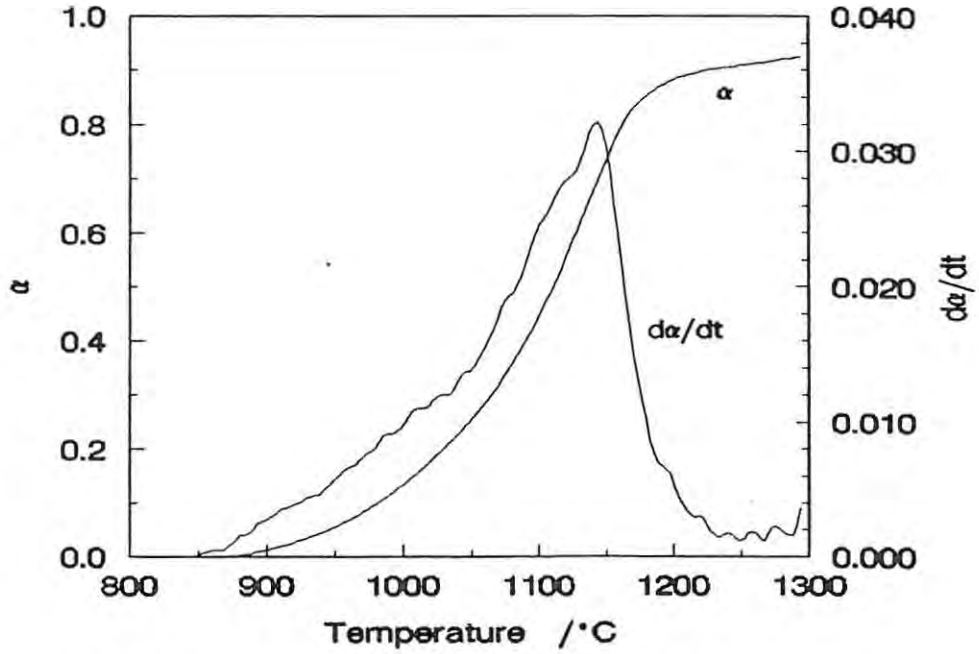

Fig. 7.21. The variation of α and $d\alpha/dt$ as a function of temperature for WO_3/graphite mixtures heated at 5°C min^{-1}.

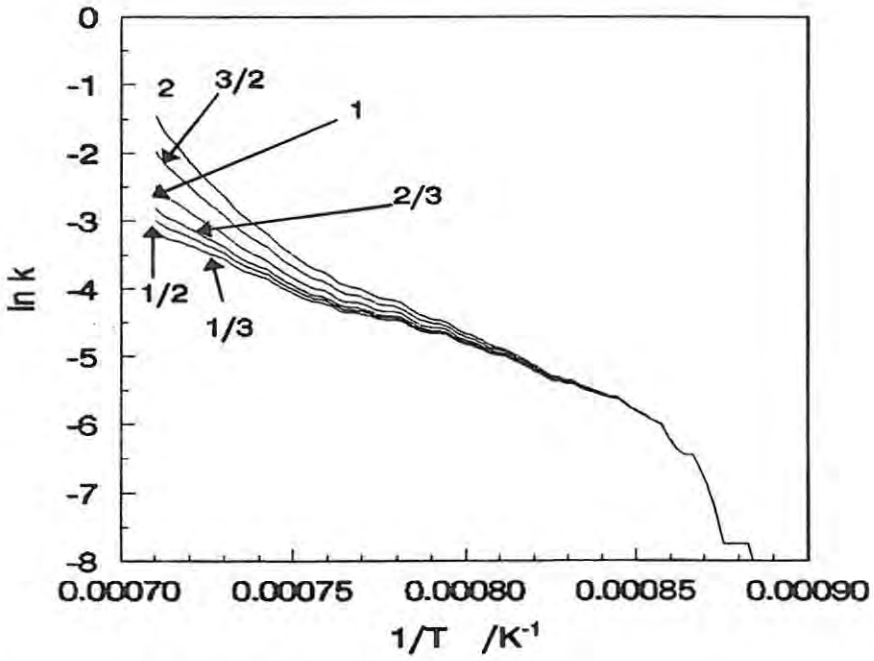

Fig. 7.22. Plot of ln k for WO_3/graphite mixtures heated at 5°C min^{-1} against $1/T$ for different reaction orders.

Table 7.5. The calculated activation energies for different orders of reaction for WO_3/lamp black mixtures, heated at 5°C min^{-1}.

	900 to 1040°C		1040 to 1140°C	
n	E_a /kJ mol^{-1}	R^2	E_a /kJ mol^{-1}	R^2
0.333	152 ± 2	0.9892	184 ± 2	0.9973
0.5	155 ± 2	0.9906	203 ± 2	0.9976
0.667	159 ± 2	0.9919	223 ± 2	0.9969
1.0	165 ± 2	0.9940	262 ± 4	0.9939
1.5	175 ± 2	0.9962	321 ± 6	0.9884
2.0	186 ± 1	0.9975	380 ± 9	0.9833

7.1.5 Morphological changes during reduction

After incomplete reduction with graphite at 950°C for 240 min, the WO_3 particles had been converted to porous clusters of randomly-oriented needles (Fig. 7.23a). The diameters and lengths of these needles varied substantially. A number of agglomerates of small, rounded particles were also observed on the surface of the needle clusters.

The product of the reaction of WO_3 with graphite at 1050°C for 240 min is shown in Fig. 7.23b. No needles were observed, but the product consisted of rounded particles which had smooth faces and well-defined facets. The sizes of these particles ranged from less than 0.5 μm to about 10 μm. Small particles, joined together in slightly porous agglomerates, were found in an open network of much larger particles.

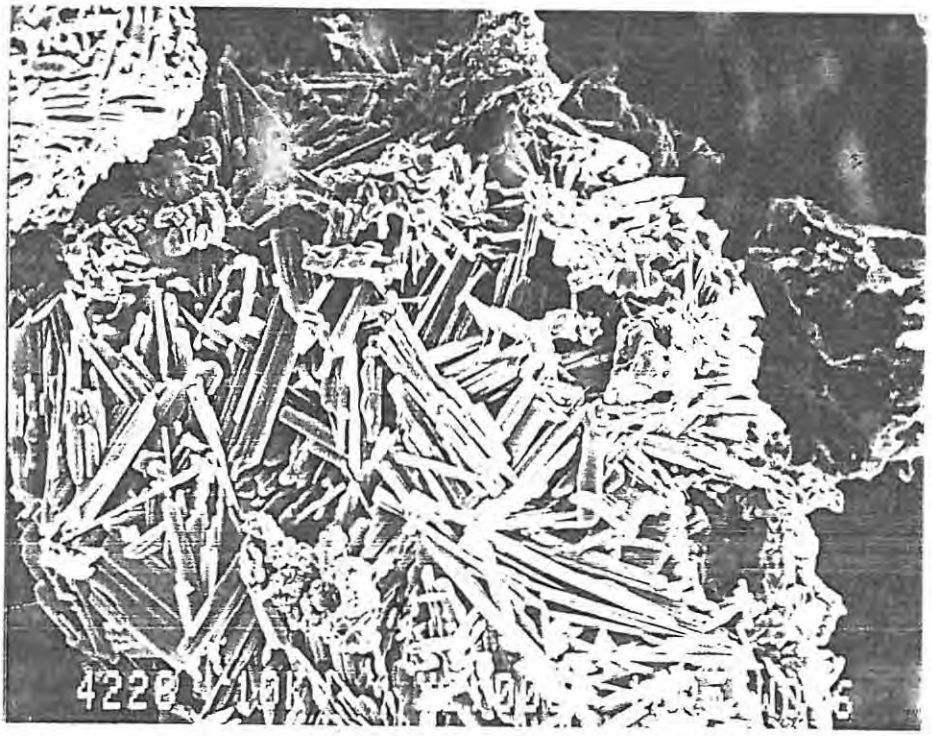

Fig. 7.23a. Scanning electron micrograph of a WO_3/graphite mixture after 4 hours at 950°C.

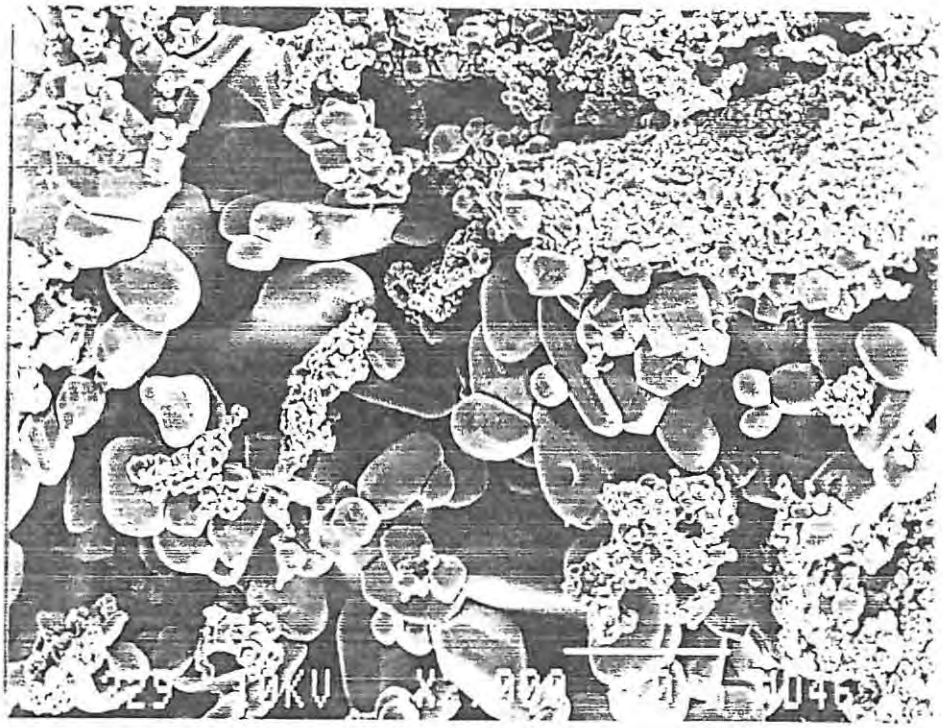

Fig 7.23b. Scanning electron micrograph of a sample of WO_3/graphite after 4 hours at 1050°C.

Needle clusters were also observed in the reduction of WO_3 with lamp black at 1000°C. The surfaces of these clusters were covered with tiny lamp black particles.

The occurrence of needles in the reduction is evidence for the formation of $W_{18}O_{49}$, which was also observed in the reduction with CO. The products of reduction with solid carbon were much more porous than when CO was the reducing agent. This difference may merely be an effect of temperature, as the reduction with CO was carried out at 900°C and below, whereas reduction with carbon was studied from 950°C.

7.1.6 Discussion

In isothermal experiments, two distinct stages were observed in the reduction at 1050°C and 1100°C, with the transition between stages occurring between $0.2 < \alpha < 0.4$. Dynamic experiments also showed a transition in the kinetics of the reduction occurring at about 1040 to 1060°C, corresponding to α between 0.25 to 0.30. These results are consistent with a two-stage reduction of WO_3. WO_2 seems to be the most likely intermediate based on the mass losses, although the formation of $W_{20}O_{58}$ and $W_{18}O_{49}$ may also be inferred from the reaction scheme for the reduction with CO, and from the morphology of the products. It was not possible to stop the TG experiments during the course of reaction and thus the reaction scheme could not be determined. As was observed for the reduction of WO_3 in CO, there may be a number of possible steps in the overall process. The first stage of the reduction took place slowly at about 950°C; the second stage of reduction only started above 1000°C.

The D4 (Ginstling-Brounshtein) model gave the closest fit to the first stage of the reduction in isothermal experiments. The diffusion may be either that of gases through the pores of the solid, or diffusion of species through the crystal lattice. In the present study, the reaction must be limited by pore diffusion, and not by diffusion in the crystal lattice, because, as shown by electron microscopy, the structure of the reactant particles changes from nonporous WO_3, to a more porous structure for $W_{18}O_{49}$ and WO_2. Thus, a reacting WO_3 particle will have a nonporous core of WO_3 or $W_{20}O_{58}$ surrounded by a porous layer of product, probably WO_2 and $W_{18}O_{49}$. CO and CO_2 would be able to diffuse much more rapidly through the pores in the particle than by diffusion through the crystal structure of the product. Access to the reaction

interface by CO, or to the outside of the particle by CO_2, would be relatively easy. Consequently, any diffusion through the crystal lattice which contributed to the reaction process would only occur at a receding reaction interface. However, such a mechanism is described by the contracting-area or contracting-volume models (i.e., R2 and R3), and not by a diffusion model.

The D4 model could therefore describe diffusion of CO and CO_2 through the pores of the reacting tungsten oxides. The activation energy calculated for the first stage would then correspond to the activation energy for pore diffusion, and not the reaction between WO_3 and CO. The kinetic parameters of the actual chemical reaction could then only be determined indirectly, by studying the reaction of WO_3 with CO separately, at temperatures at which the chemical reaction is much slower than pore diffusion.

Because the first stage of the process is limited by pore diffusion, the deviation in the rates of reaction of WO_3 with graphite and with lamp black is probably caused by different CO/CO_2 ratios in these systems. At 960°C, the lamp black is not as reactive as graphite towards CO_2, Fig. 7.13. Considering that the temperature is the same and that the CO/CO_2 ratios in the systems are unlikely to differ substantially, it seems improbable that the different reaction rates are caused by dissimilarities in the structures of the reacting tungsten oxide particles. Since the source of carbon does not affect the CO/CO_2 equilibrium ratio[57], the CO/CO_2 ratios in the system must be significantly below the equilibrium concentration in at least some of the experiments.

The activation energies determined for the first step are therefore related to the reactivities of graphite and lamp black towards CO_2, but are unlikely to be directly related to reaction (6.2). Lamp black is less reactive towards CO_2 than graphite at low temperatures, but the higher activation energy for the lamp black system implies a higher temperature dependence of the reaction than the graphite system. Using the kinetic parameters determined above, the rate of the first stage of reaction of WO_3 with lamp black should exceed that with graphite above 1070°C. Variations in the reactivities of different forms of carbon are well documented[61].

The second stage of reaction can be described by a first-order rate equation. The reaction of CO_2 with CO, reaction (6.2), is known to be first-order[12,56,61] which suggests that the second stage of reaction is also limited by reaction (6.2), and not by the reduction of a

tungsten oxide. Indeed, it is difficult to conceive a process whereby the reduction depends solely on the amount of tungsten oxide. Such a reaction mechanism implies that CO has access to all the tungsten oxide over the duration of the second stage. It does appear that such is the case, but the observation is only superficially correct because the tiny particles comprising the pseudomorph are themselves nonporous. In effect, the reaction still takes place between CO and nonporous particles, and reaction must start at the external surface of these particles.

If we accept that the second stage of the reaction is limited by the rate of reaction (6.2), then the relative rates of the first and second stages seem anomalous. For, if reaction (6.2) limits the rate of the second stage of the process, then it should also be rate-limiting for the first stage of the reaction, because the second stage of reaction occurs more slowly than the first stage.

The difficulty can be resolved by considering the effect of the CO/CO_2 ratio on the reduction of WO_3 and WO_2. The rate of reaction of CO_2 with C must be known as a function of the CO/CO_2 ratio. Referring to Fig. 6.4, it is clear that the CO content in the gas phase must be much higher to reduce WO_2 to tungsten than to reduce WO_3 to WO_2. For instance, at 1000°C the concentration of CO must be above 58% to reduce WO_2 (if the remainder of the gas is CO_2), whereas to reduce WO_3 to WO_2 requires a CO/CO_2 ratio above 0.19 (that is, at least 16% CO in CO_2).

The rate equation for reaction (6.2) is given by eqn (2.28) and indicates that the rate of reaction depends strongly on the CO/CO_2 ratio. This dependence is shown in Fig. 7.24, which is from the work of Turkdogan and Vinters[63]. Using the above example, at 1000°C the rate of reaction at a CO/CO_2 ratio of 0.19 is about three times higher than at a CO/CO_2 ratio of 1.37. The rate of reaction (6.2) will also decrease as carbon is used up during the reaction. These general considerations explain how the rate may be limited by different processes during the reduction.

Although the activation energies of the graphite and lamp black systems differed significantly for the first stage of reduction (386 compared to 465 kJ mol^{-1}), the systems were examined at different temperatures. These activation energies are high for a diffusion process, and may be inflated by changes in the structure of the product and the CO/CO_2 equilibrium ratio as the temperature increases. The structure of the product is more open at higher temperatures,

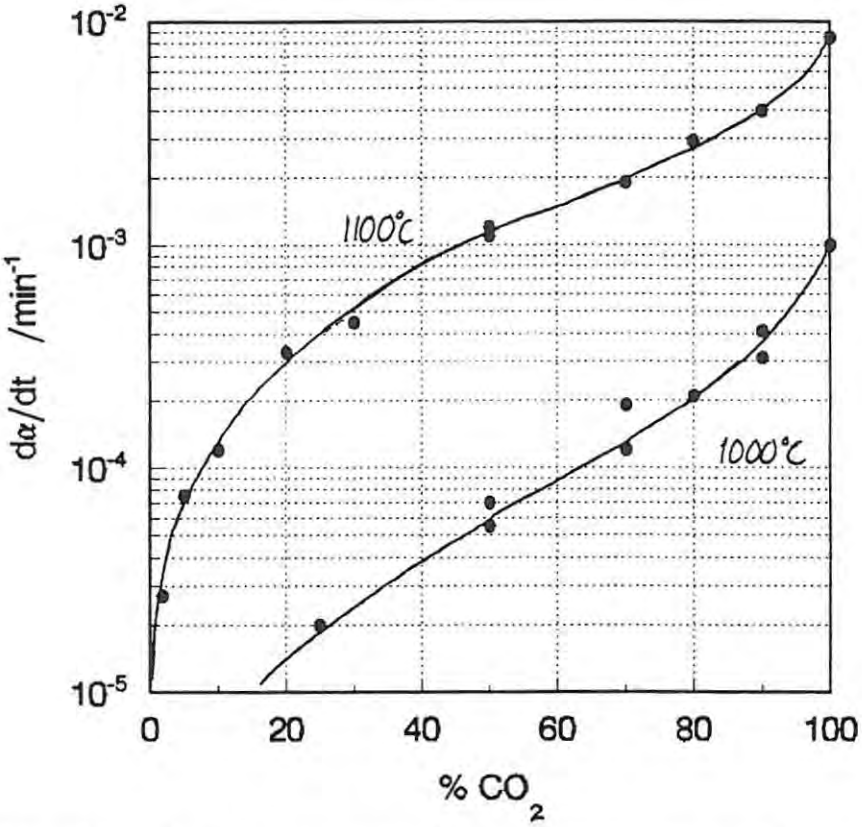

Fig. 7.24. The effect of the temperature and the gas composition on the rate of reaction (6.22) in CO_2/CO mixtures (from Turkdogan and Vinters[61]).

which would facilitate the diffusion of gases in the tungsten oxide and thus increase the rate constant for the reaction. The higher CO/CO_2 ratio in the powder layer might also result in a significant increase in the rate of reduction.

The first order reaction model, F1, described the second stage of the reaction and gave an activation energy of 438 kJ mol^{-1}. This activation energy is slightly higher than the reported values for reaction (6.2), which range up to 400 kJ mol^{-1}. Considering the complexity of the system and that only two points were used to calculate the activation energy, this discrepancy is not significant.

As is almost always found, the results obtained from the dynamic experiments were less consistent than the isothermal results. A second-order rate equation fitted the data best at low temperatures, and gave an activation energy of between 220 and 240 kJ mol^{-1} for the graphite system, compared to 186 kJ mol^{-1} for the lamp black system. Above the transition temperature,

reaction orders between 0.5 and 1.5 fitted the data well. Changing the reaction order made little difference to the fit of the equation, but altered the value of the activation energy considerably. Thus, the activation energies calculated for n = 0.5 to 1.5 varied between 300 and 480 kJ mol^{-1}. The activation energy for the reaction using lamp black was considerably lower, between 180 and 225 kJ mol^{-1} for reaction orders of 0.333 to 0.667. Better results from the dynamic experiments were obtained using the Gyulai-Greenhow approach. For the first stage of the reduction the activation energy was between 300 and 360 kJ mol^{-1}, which compares favourably with the isothermal results. However, the results for the second stage were poor.

In conclusion, the results from isothermal experiments were more reliable than dynamic results. They provided a model of the process and a plausible explanation of the rate determining step, and showed good agreement with the data.

7.2 Tube furnace experiments

7.2.1 Effect of temperature

Mixtures of WO_3 and graphite in a 1:4 mole ratio were reacted in the tube furnace system (described in section 3.3) at 935, 960, 985, 1010, 1035, and 1060°C in a stream of argon flowing at 100 mL min^{-1}. As with the TG experiments, the final mass loss for complete reaction may vary between 23.6 and 30.0%, depending on the relative amounts of CO_2 and CO formed. The CO_2/CO ratio is determined by the rate of reaction (6.2) over the course of the entire process. A high reaction rate favours CO formation and hence a greater mass loss.

Fig. 7.25 shows the percentage mass lost as a function of time at the temperatures investigated. At temperatures below 1000°C, the mass loss is slow and well below the mass loss expected for complete reaction. At and above 1000°C, however, the mass eventually becomes constant, indicating that the process is complete. As would be expected, the mass loss at the end of the process also increases with temperature because reaction (6.2) is very dependent on the temperature. Thus, at higher temperatures CO_2 will react more rapidly with graphite, resulting in a higher ratio of CO to CO_2. The mass losses at the end of the process are listed in Table 7.6.

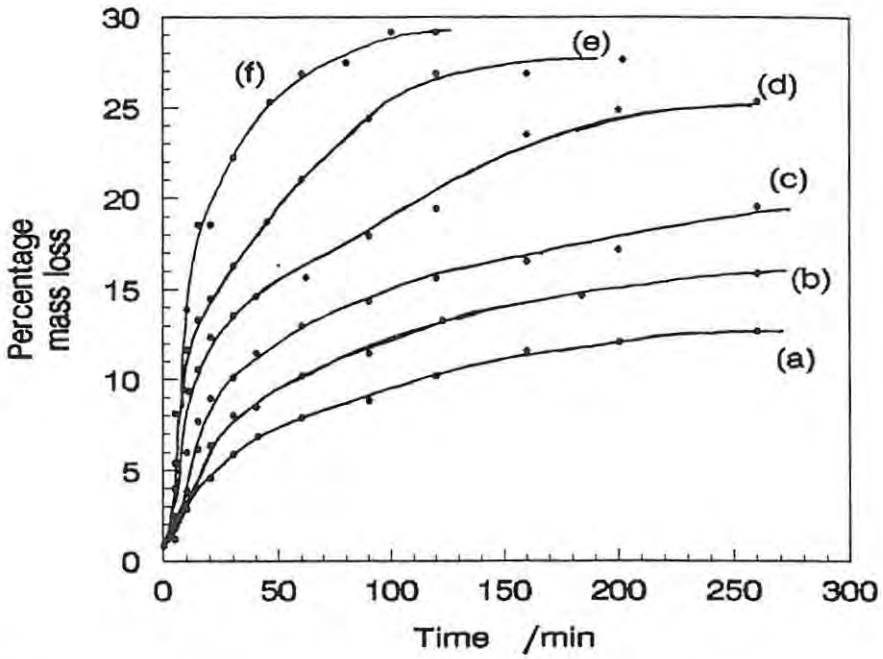

Fig. 7.25. The mass loss curves for the reaction of WO_3/graphite mixtures in a 1:4 mole ratio at (a) 1060°C, (b) 1035°C, (c) 1010°C, (d) 985°C, (e) 960°C, and (f) 935°C.

Table 7.6. The mass losses at various temperatures for complete reaction of WO_3 with graphite in a 1:4 mole ratio and in a stream of argon flowing at 100 mL min^{-1}.

Temperature /°C	Mass loss for complete reaction /%
935	incomplete
960	incomplete
985	incomplete
1010	25.4
1035	27.7
1060	29.2

The rate of mass loss is high initially, but decreases considerably after a mass loss of from 8 to 18%. The rate of mass loss is displayed in Fig. 7.26 and shows two maxima, which implies a change in the reactions or in the reaction mechanism. The mass loss corresponding to the change in reaction rate falls broadly in the range at which the formation of WO_2 would occur (7.9 to 10.0% mass loss), although the higher mass losses observed at higher temperatures suggest that the first stage of reaction may also include some reduction to tungsten.

7.2.2 Reaction scheme

The products at various times during the reaction at 935, 985, and 1035°C were analysed using XRD, and are listed in Table 7.7. These results suggest the reaction scheme shown in Fig. 7.27, which is similar to that observed at 900°C for the reduction using CO (Fig. 6.6). XRD patterns also indicated that some W_2C may have formed in small quantities, but this phase could not be conclusively identified. Unlike during the reduction with CO, no WC was formed during the reaction with carbon.

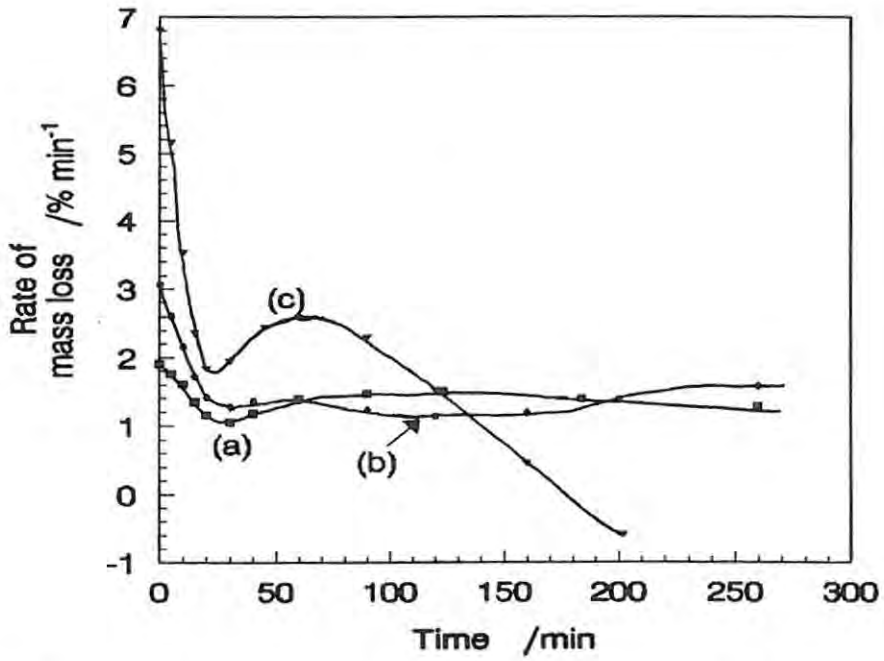

Fig. 7.26. The rate of mass loss curves for the reduction of WO_3 with graphite at (a) 960°C, (b) 985°C, and (c) 1035°C.

Table 7.7. Phases identified at different times in the reduction of WO_3 with graphite at 935, 985, and 1010°C.

Time /min	Mass lost /%	Phases identified
935°C		
5	1.2	Mostly WO_3; small amounts of $W_{20}O_{58}$
10	2.8	Mostly $W_{20}O_{58}$; small amounts of $W_{18}O_{49}$
40	6.5	$W_{18}O_{49}$; α-W; small amounts of WO_2
160	11.5	α-W; WO_2; small amounts of $W_{18}O_{49}$
985°C		
5	2.5	Mostly $W_{20}O_{58}$; possibly $W_{18}O_{49}$ and WO_3
10	6.0	$W_{18}O_{49}$; α-W; small amounts of WO_2
20	9.0	α-W; WO_2; $W_{18}O_{49}$
40	11.4	α-W; WO_2; small amounts of $W_{18}O_{49}$
260	19.5	Mostly α-W; small amounts of WO_2
1035°C		
5	5.4	$W_{18}O_{49}$; α-W; small amounts of WO_2
10	11.6	α-W; WO_2; small amounts of $W_{18}O_{49}$
30	16.2	α-W; WO_2
60	21.0	α-W; WO_2
120	26.8	Mostly α-W; small amounts of WO_2

The reaction scheme and the mass loss curves indicate that considerable amounts of α-W are formed in the first stage of reduction. Similar results have been obtained in the reduction with hydrogen[22], and were attributed to the relatively high reactivity of $W_{18}O_{49}$. The extent to which $W_{18}O_{49}$ is reduced directly to α-W is probably related to the CO/CO_2 ratio, as has been discussed. The variation in the partial pressures of CO and CO_2 in the system during reduction

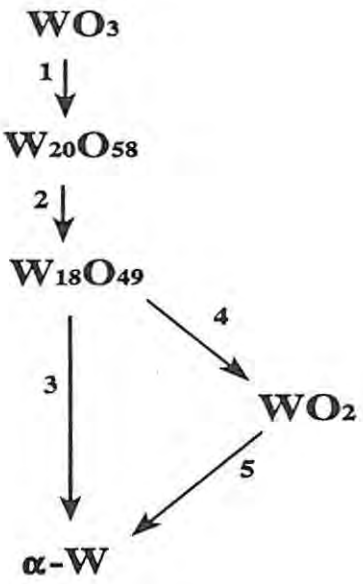

Fig. 7.27. The reaction scheme inferred in the reduction of WO_3 with graphite.

will be analysed in section 7.2.5.

The second stage of the reduction appears to be solely associated with the reduction of WO_2 to α-W, and occurs very slowly. Similar observations have been made in the reduction with hydrogen[22], and indicate that WO_2 is relatively unreactive compared to other tungsten oxides.

7.2.3 Effect of the flowrate

The flowrate of inert gas affects the concentration of gaseous species in the system, which may in turn influence the reaction rate. If the reaction occurs between two solids and forms a gaseous product, then higher flowrates will tend to increase the reaction rate by minimising the reverse reaction. On the other hand, if the solids react via intermediate gases, then diluting the reactant and product gases is likely to have a large effect on the reaction rate. Whether the overall reaction rate increases or decreases depends on how the rates of the gas-solid reactions in the system are affected by the concentrations of the different gaseous species.

Experiments were performed at 985°C and at flowrates of 25, 50, 100, and

150 mL min^{-1}. An inspection of the mass loss curves (Fig. 7.28) shows that decreasing the flowrate results in a large increase in the mass lost during the reaction. The mass loss curves at 100 and 150 mL min^{-1} are very similar and it appears that increasing the flowrate above 100 mL min^{-1} has little effect on the reaction rate. Thus, maximum flushing of the sample is achieved at about 100 mL min^{-1}, and the concentrations of CO_2 and CO in the system are not significantly affected at higher flowrates.

Below 100 mL min^{-1}, the rate of reduction and the total mass loss which occurs during reduction increase with decreasing flowrate. The reduction rate is increased over both stages of the reduction, although the start of reaction is somewhat delayed at lower flowrates. This delay may be caused by an initially oxidising atmosphere, possibly from the transformation of WO_3 to $W_{20}O_{58}$. (The calculated CO/CO_2 equilibrium ratio for this transformation is very low; thus, this reaction may proceed even when the CO_2 partial pressure in the sample is too high for other reductions to occur.) If this is so, a slower flowrate will prolong the oxidising conditions and hence result in a lower rate of mass loss. This initial difference should be regarded as a separate phenomenon from the rest of the reduction.

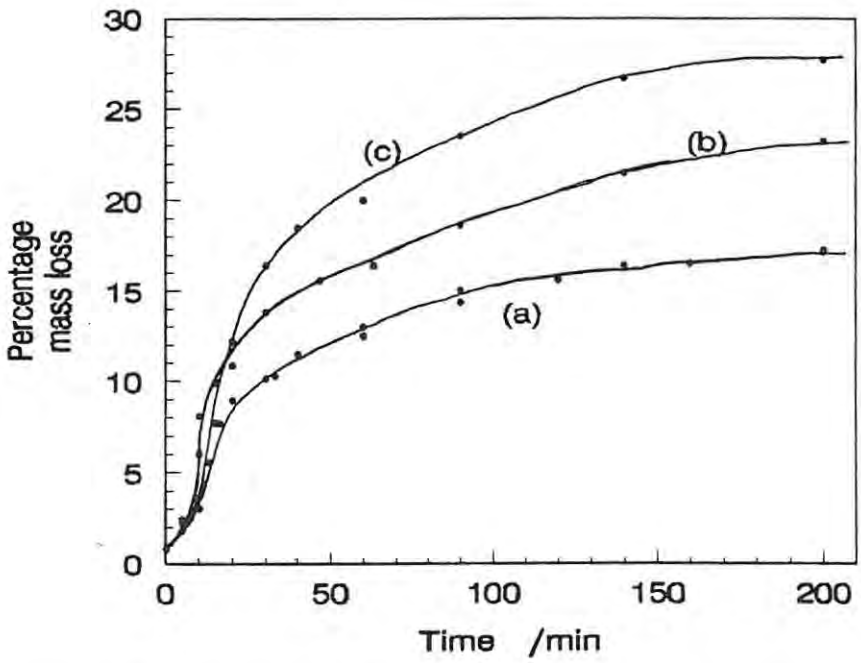

Fig. 7.28. The effect of the flowrate on the reduction of WO_3 with graphite at 985°C: (a) 100 and 150 mL min^{-1}, (b) 50 mL min^{-1}, and (c) 25 mL min^{-1}.

The increased mass loss at lower flowrates proves conclusively that the reaction is not predominantly a solid-solid reaction, but instead must involve gaseous intermediates. As has been found for the reduction of other metal oxides with carbon, the reduction is almost certainly by reactions (6.1) and (6.2). The reduction process thus proceeds via two simultaneous gas-solid reactions. The solid-solid reaction between the tungsten oxides and graphite cannot be excluded, although the large dependence of the reaction rate on the flowrate indicates a predominantly gas-solid process.

It is also apparent that the final mass loss is significantly higher at low flowrates. This means that more CO is formed at lower temperatures and that the atmosphere is more reducing.

7.2.4 Effect of the stoichiometry of the mixture

Mixtures of WO_3 and graphite of 1:2 and 1:8 mole ratio were compared to the standard mixture (1:4 mole ratio) at 985°C and 100 mL min^{-1}. Sample masses were the same as used in other experiments; compared to the standard mixtures, however, the sample volumes were 20% larger for the 1:8 mole ratio mixtures, and 12% smaller for the 1:2 mole ratio mixtures. This may alter the flushing of the samples slightly and hence affect the final CO/CO_2 ratio. Fig. 7.29 shows the percentage mass loss curves as a function of time.

As would be expected, the final mass losses of the different mixtures vary with the amount of carbon present. Thus, comparing the mass losses directly with each other is not very meaningful, and it would be better to compare the extent to which the reactions are complete. The calculated final mass losses for the different mixtures are shown in Table 7.8. The extent of reaction was estimated by assuming that all the oxygen in WO_3 was removed as CO; the $\alpha.t$ curves obtained on this basis are shown in Fig. 7.30. As expected, increasing the amount of graphite in the system results in a final mass loss which is closer to the maximum mass loss attainable.

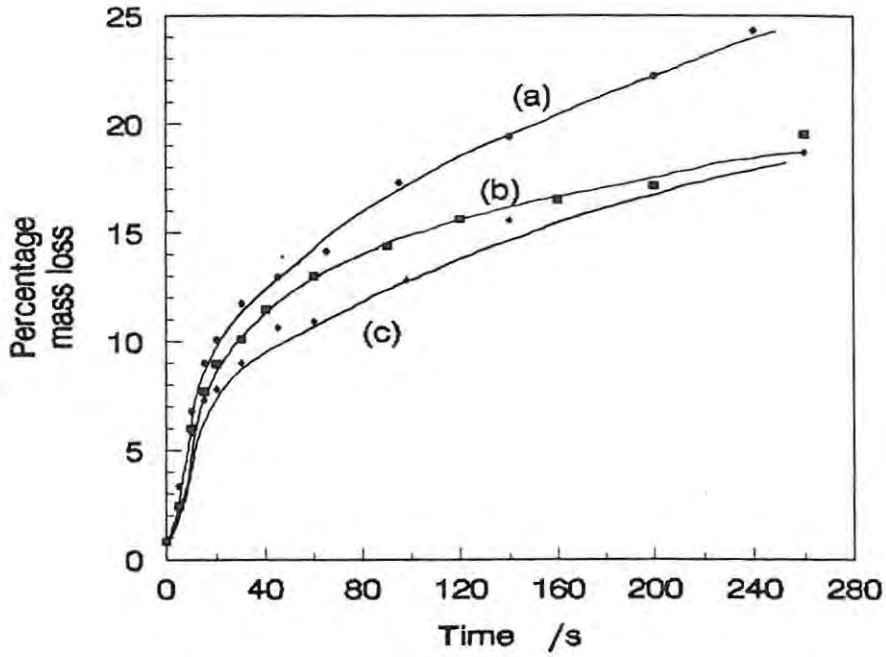

Fig. 7.29. The mass loss curves for WO_3/graphite mixtures at 985°C, at mole ratios of (a) 1:8, (b) 1:4, and (c) 1:2.

Table 7.8. The calculated final mass losses of WO_3/graphite mixtures in different stoichiometric proportions.

	Ratio of WO_3 to graphite		
Gas produced	1:2 moles	1:4 moles	1:8 moles
CO only	21.9% (incomplete)	30.0%	25.6%
CO_2 only	25.8%	23.6%	20.1%

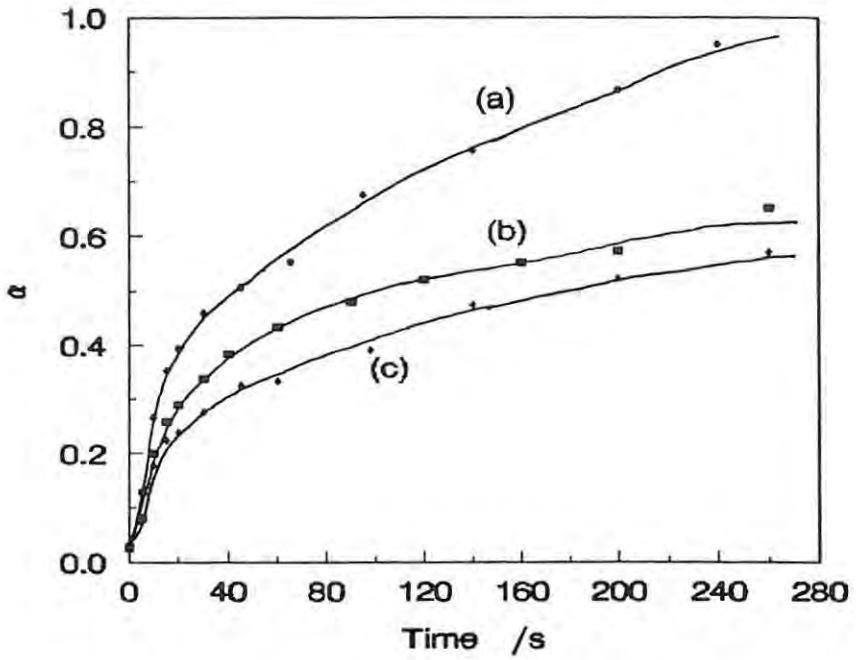

Fig. 7.30. The extent of reaction as a function of time at 985°C for WO_3/graphite in mole ratios of (a) 1:8, (b) 1:4), and (c) 1:2.

7.2.5 Evolved gas analysis

The influences of the temperature, stoichiometry, and flowrate on the gases evolved from the reduction were studied using the TCD and infrared detectors described in section 3.3. There were problems with these detectors in that parts of the CO and CO_2 concentration curves exceeded the range of the detectors in some experiments, and sometimes the CO and CO_2 concentrations changed suddenly and spuriously, possibly as a result of inhomogeneities in the gas concentrations in the exhaust stream. In such cases the most probable concentrations are estimated by a dashed line. The TCD was less sensitive to the concentration of the gases, and it was difficult to determine the baseline of the curve. Consequently, only the results from the CO and CO_2 infrared detectors are considered below.

The reaction at 935°C clearly shows three peaks in the CO_2 evolution trace (Fig. 7.31). Each succeeding peak shows a lower rate of CO_2 evolution, but increases in duration and in the total amount of CO_2 formed. After the third peak, the concentration of CO_2 drops considerably,

and then decreases very slowly as the reaction progresses. The CO concentration in the system shows only one large peak which occurs simultaneously with the three peaks in the CO_2 trace. The concentration of CO then tapers off to a slow rate, as in the evolution of CO_2. The peaks for the evolution of CO_2 indicate discrete steps in the reduction of WO_3. The size and order of occurrence of these peaks suggest the reduction sequence:

$$WO_3 \longrightarrow W_{20}O_{58} \longrightarrow W_{18}O_{49} \longrightarrow WO_2$$

which agrees with the XRD analysis of the sample.

It seems conceptually unlikely that direct reduction between two solids could effect a

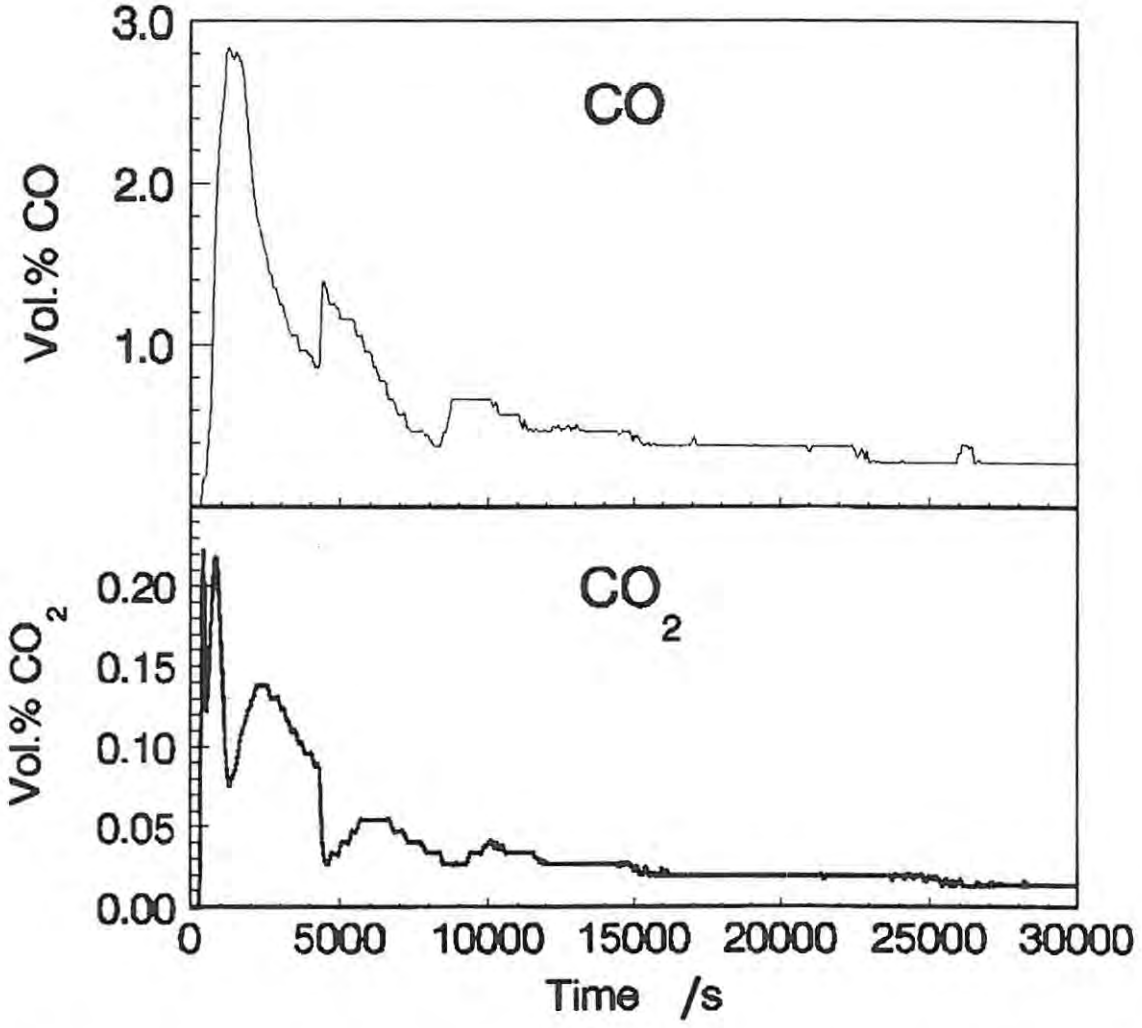

Fig. 7.31. The CO and CO_2 concentrations during the course of the reduction of WO_3 with graphite at 935°C (in argon flowing at 100 mL min^{-1}).

sequential reduction in which one phase is almost completely reduced to the next lower oxide, before reduction of the lower oxide can take place. Direct interaction between solids must necessarily be localised at points of contact, and thereafter occurs by diffusion or surface migration. Such a mechanism is unlikely to result in a sequential reduction, and thus the sequential nature of the reduction is further evidence for reaction taking place via intermediate gases.

In contrast to the CO_2 concentration, the single CO peak indicates that the rate of reaction (6.2) is relatively insensitive to the WO_3 reduction sequence, even though the concentration of CO_2 in the system undoubtedly influences the reaction rate (Fig. 7.24).

The CO and CO_2 traces for the reaction at 985°C (Fig. 7.32) have the same general features as at 935°C, although the relative sizes of the peaks in the CO_2 trace have changed and are less distinguishable. At 1035°C both CO and CO_2 concentrations exceed the range of the detectors during the first part of the reduction, Fig 7.33.

Decreasing the flowrate at 985°C to 50 mL min^{-1} also resulted in the CO and CO_2 concentrations exceeding the limits of the detectors, Fig. 7.34, and the resultant curves were similar in form to those at 1035°C. Particularly apparent at low flowrates is that the conditions in the powder layer are initially oxidising, and that CO takes some time to reach reasonable levels. This is probably related to the formation of $W_{20}O_{58}$, which can be formed under quite oxidising conditions (e.g., the CO/CO_2 equilibrium ratio is about 0.01 at 900°C), and explains the observed delay in the start of the reaction at 50 and 25 mL min^{-1}.

The stoichiometric ratio influenced the relative sizes of the second and third peaks considerably at 985°C. In a 1:2 mole ratio mixture, the size of the third peak was considerably larger than the second peak (Fig. 7.35), whereas the opposite was true at a 1:4 mole ratio. At a 1:8 mole ratio, the second and third peaks were not distinguishable, Fig. 7.36. These observations suggest that different stoichiometries change the reaction path by affecting the CO/CO_2 ratio in the system. The size and duration of the CO peaks increased with increasing amounts of graphite in the system. Compared with the CO_2 peaks, the duration of the CO peak was shorter for a 1:2 mole ratio, approximately equal for a 1:4 mole ratio, and considerably longer for at 1:8 mole ratio.

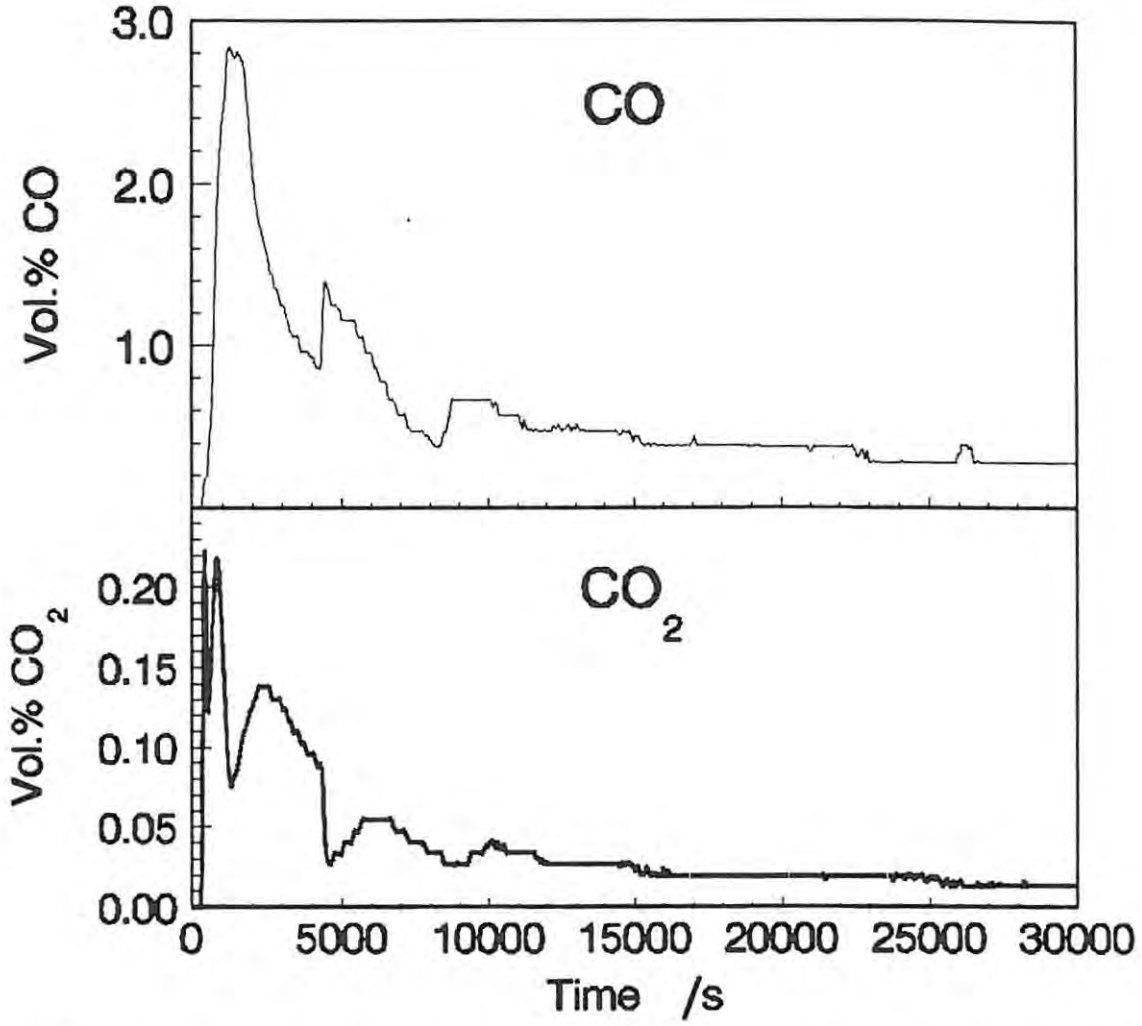

Fig. 7.32. The CO and CO_2 concentrations during the course of the reduction of WO_3 with graphite, in a 1:4 mole ratio, at 985°C in argon flowing at 100 mL min^{-1}.

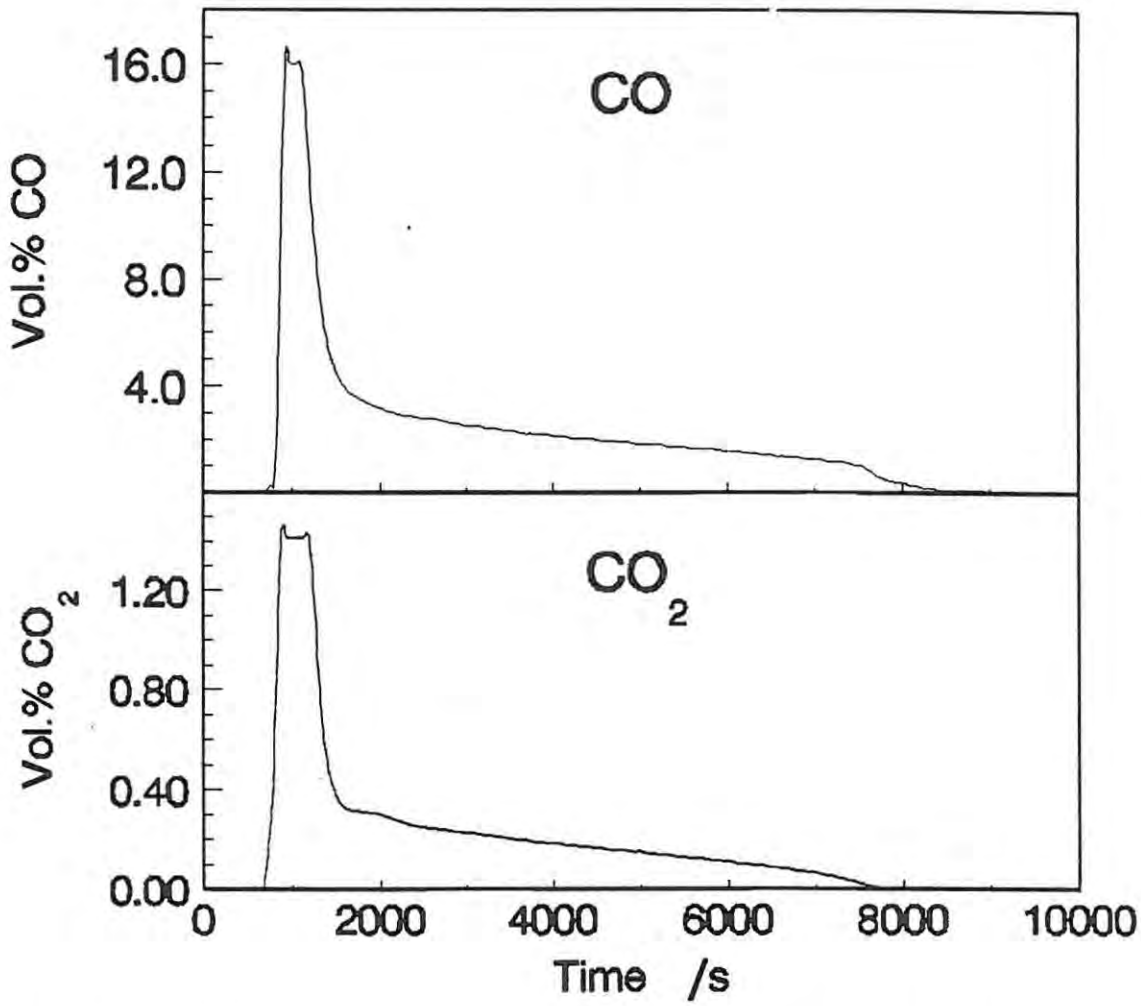

Fig. 7.33. The CO and CO_2 concentrations during the reduction of WO_3 with graphite (in a 1:4 mole ratio) at 1035°C in argon flowing at 100 mL min^{-1}.

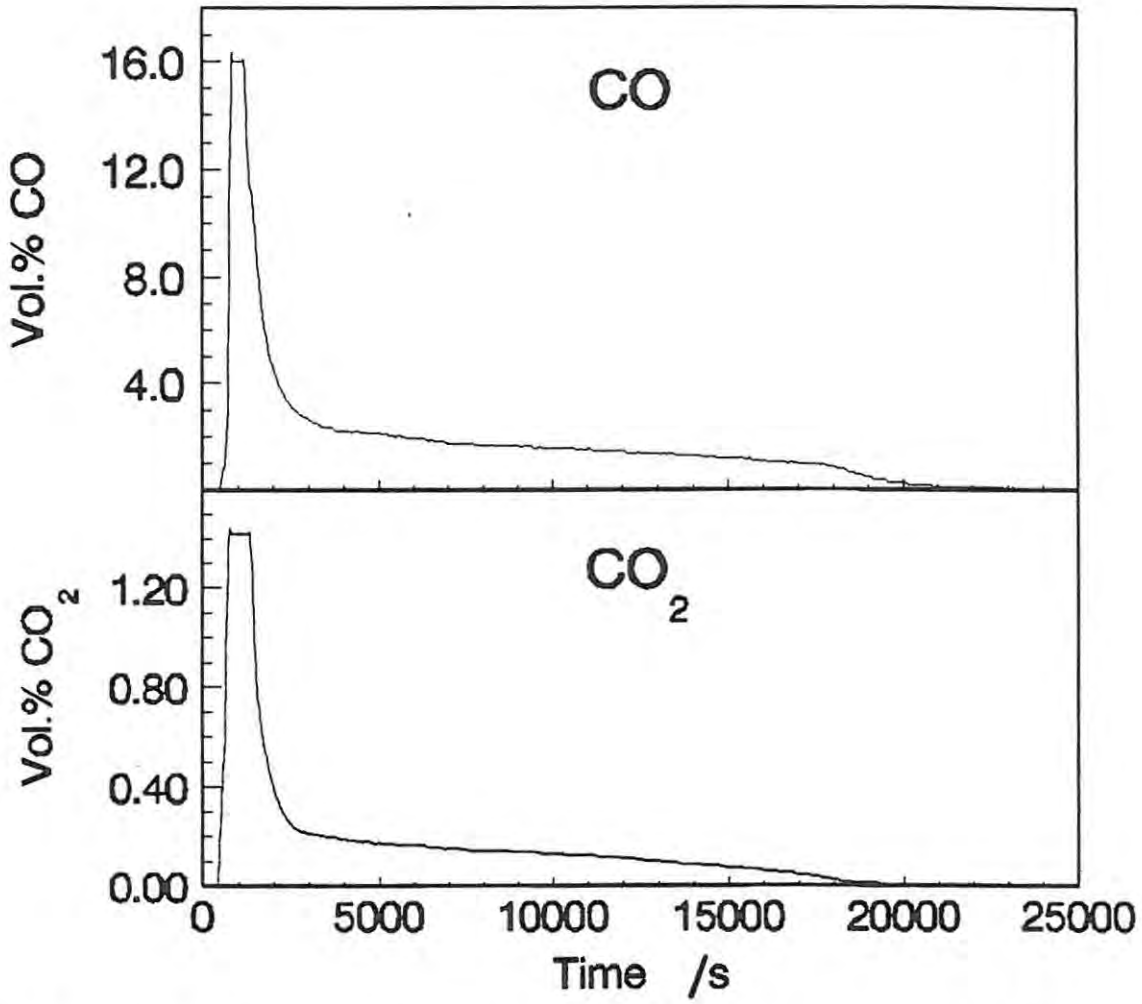

Fig. 7.34. The CO and CO_2 concentrations during the reduction of WO_3 with graphite (in a 1:4 mole ratio) at 985°C in argon flowing at 50 mL min^{-1}.

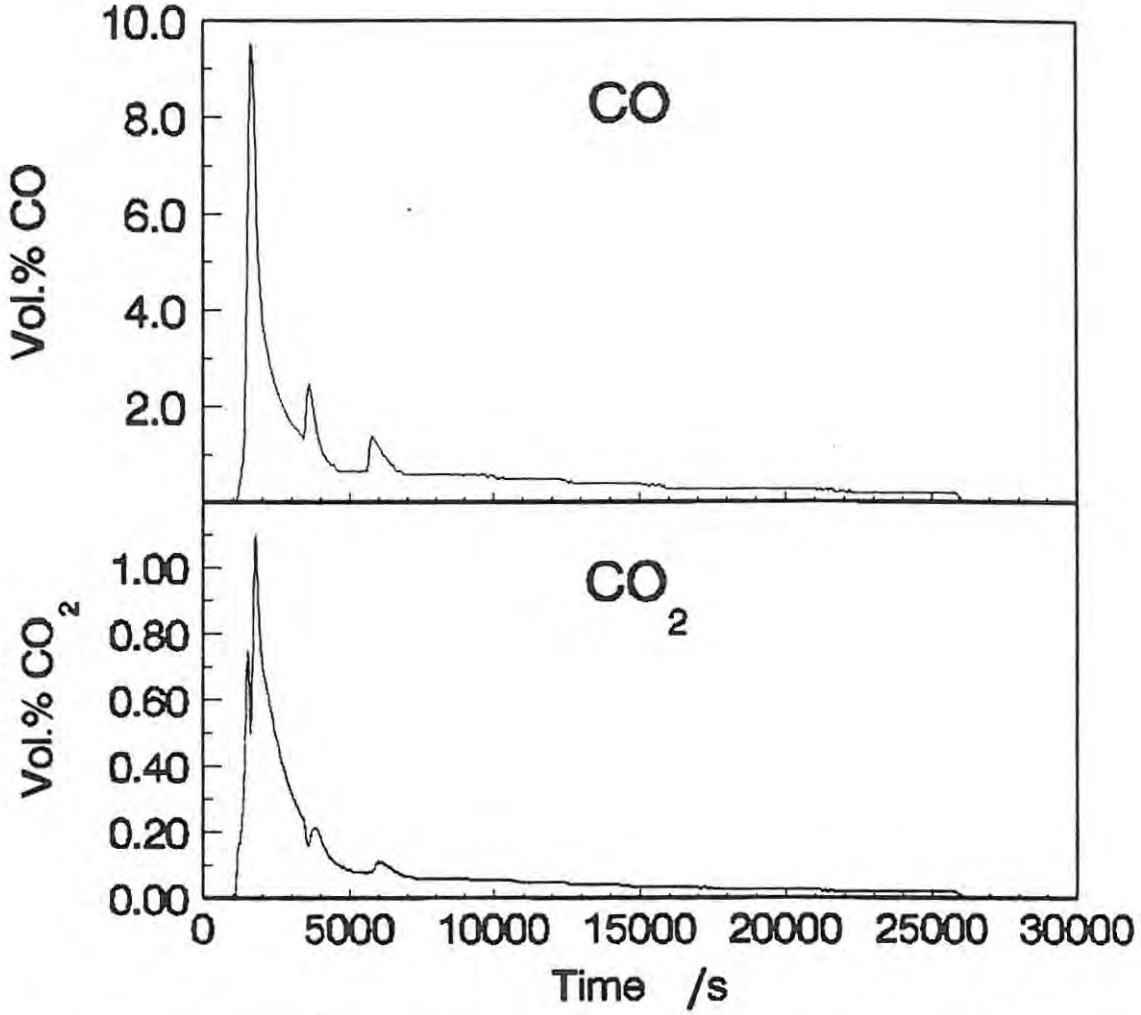

Fig. 7.35. The CO and CO_2 concentrations during the reduction of WO_3 with graphite in a 1:2 mole ratio at 985°C (in argon flowing at 100 mL min^{-1}).

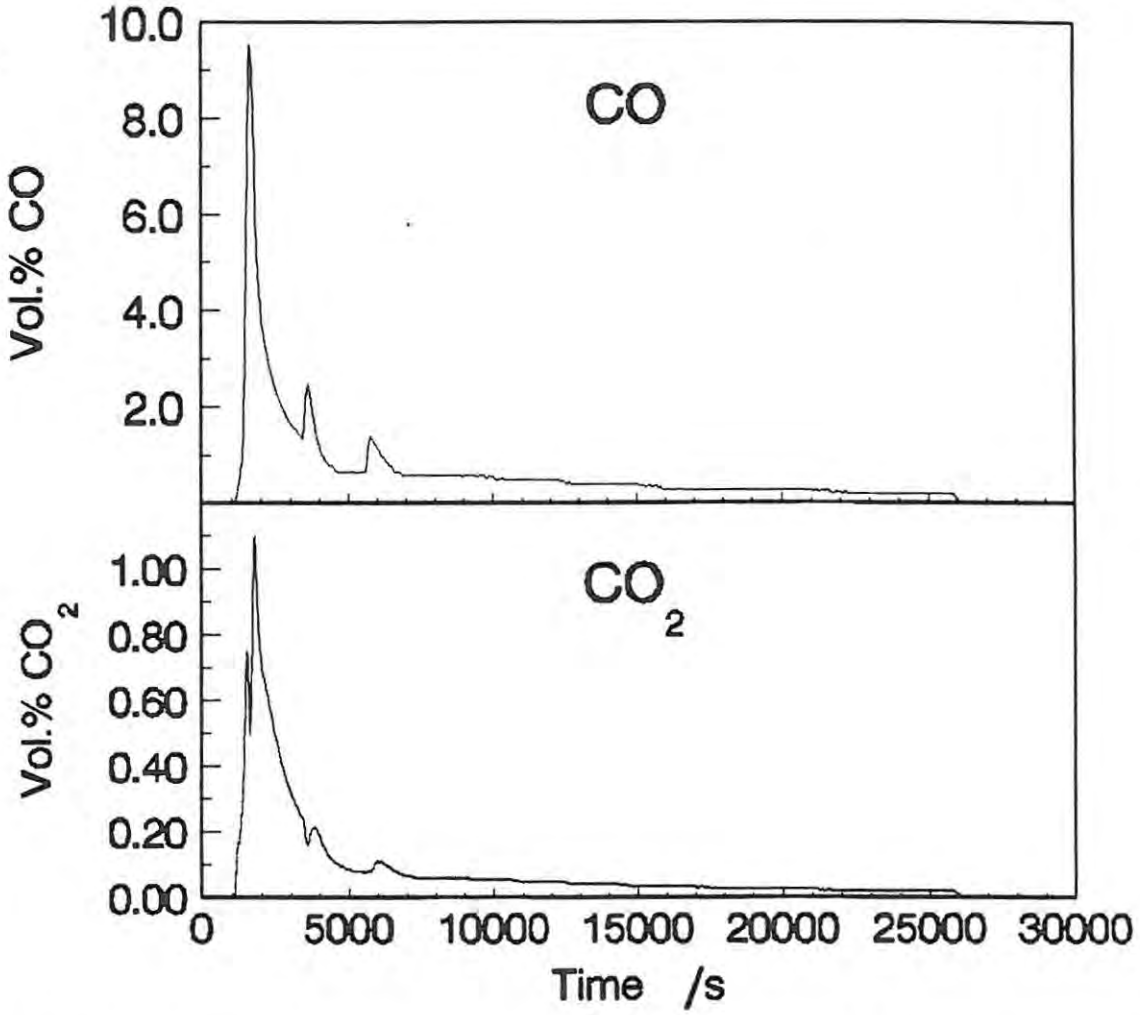

Fig. 7.36. The CO and CO_2 concentrations during the reduction of WO_3 with graphite in a 1:8 mole ratio at 985°C (in argon flowing at 100 mL min^{-1}).

7.2.6 Morphological studies

The morphological changes observed in the reaction between WO_3 and graphite were very similar to those observed when CO was the reducing agent. The shape of the original WO_3 particles was retained during the reduction but became porous as the molar volumes of the phases decreased. Needles characteristic of $W_{18}O_{49}$ were observed after reduction for 10 min at 935°C, and were randomly-orientated and flat on the surface of the pseudomorphs. The length and diameter of the needles increased as the reaction progressed, and they also protruded more from the surface, Fig. 7.37a. Intergrowth of needles parallel to each other resulted in twins or parallel growths, which had the appearance of thicker, column-like crystals. After reduction for 120 min, the needles on the surface of the pseudomorphs were starting to disintegrate into small spherical and worm-like particles of less than 1 μm (Fig. 7.37b).

A similar morphological pattern was observed at 985°C, with needles observed after 10 min of reduction. Crystal intergrowth was already visible at this early stage. After 20 min, it was apparent that tungsten or tungsten oxide was migrating onto the surface of graphite particles with which it was in contact. Fig. 7.37c shows the sample after 180 min, which had not changed much in its appearance from the sample after 20 min.

A sample of WO_3 investigated after reduction at 1035°C for 180 min (at which time the reaction was effectively complete), showed the presence of tightly packed clusters of crystals, presumably tungsten. The size of particles in these clusters varied considerably.

A particularly interesting phenomenon is that tungsten or tungsten oxides seem to form a thin layer on the surface of the graphite particles, which spreads over the whole graphite surface. This is shown in Fig 7.37d which displays the atomic number contrast and ordinary secondary electron images. This phenomenon was also observed at 985°C, and its appearance is strongly indicative of surface diffusion. Impurities in the sample, which might form a tungstate melt[40] or diffuse on the surface of tungsten[26], are a possible explanation for the observed effect. Enhanced diffusion also explains the large differences in particle sizes that were observed in the reduction in the TG. Evidence for the presence of significant impurities is that small indentations in the surface of tungsten crystals were observed; such holes have been associated with the presence of impurities[41].

Fig. 7.37a. Scanning electron micrograph of a WO_3/graphite mixture after 60 min at 935°C.

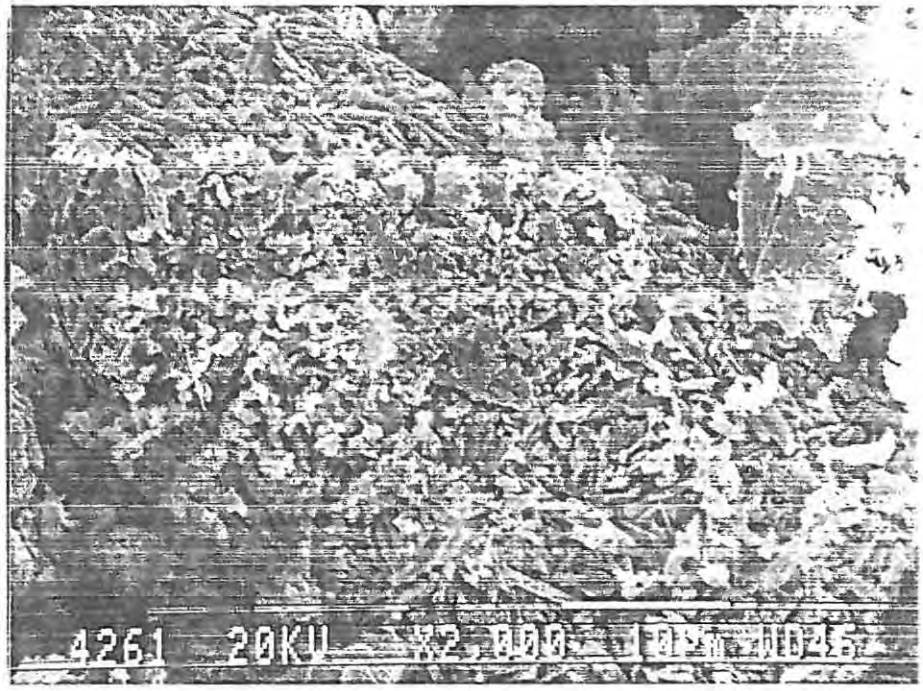

Fig 7.37b. Scanning electron micrograph of a sample of WO_3/graphite after 120 min at 935°C.

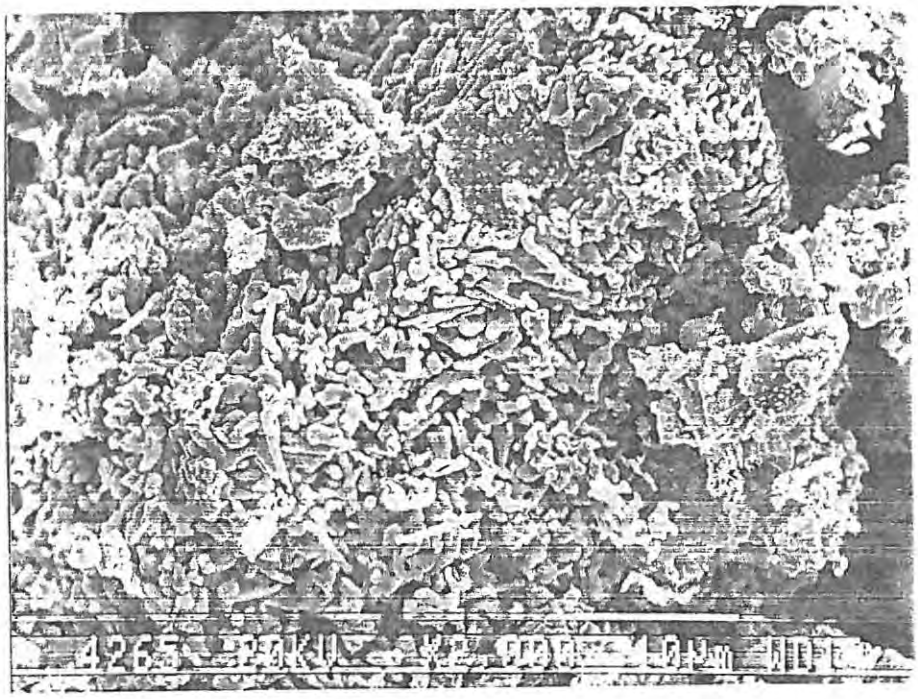

Fig. 7.37c Scanning electron micrograph of a WO_3/graphite mixture after 180 min at 985°C.

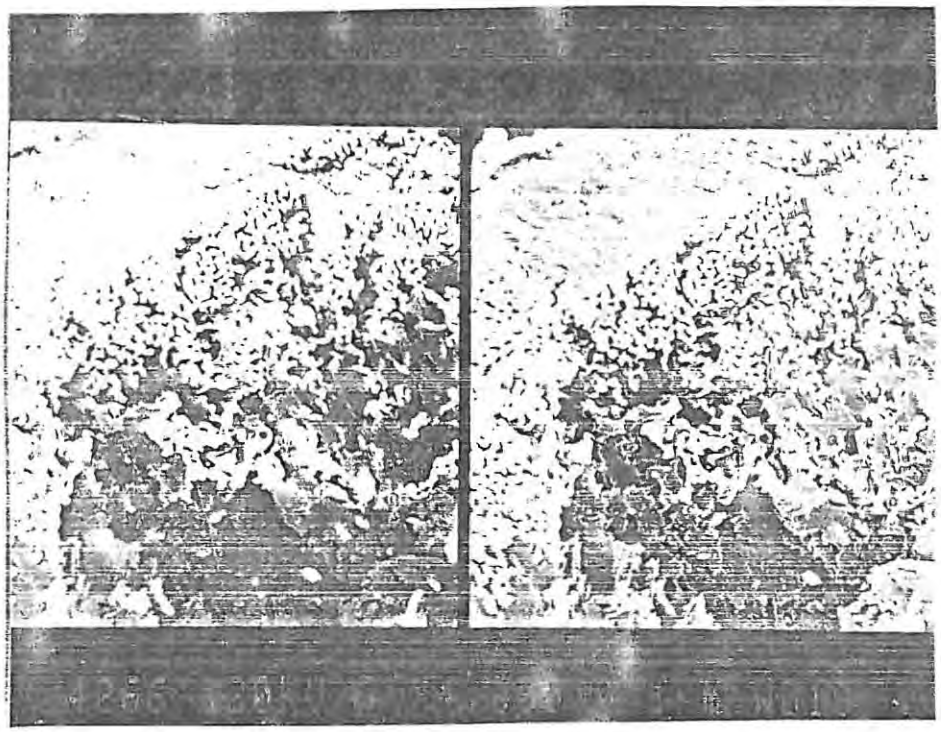

Fig 7.37d. Scanning electron micrograph of a WO_3/graphite sample after 180 min at 1035°C, showing the atomic number contrast image (left) and the secondary electron image (right). The bright surfaces are tungsten.

The morphological changes observed in the tungsten oxide particles were similar to those occurring when reduction took place in CO. The morphology appears to be dictated initially by the formation of needles of $W_{18}O_{49}$ at the start of the process. Later on in the reduction these needles fragment to form small, rounded particles which grow considerably at higher temperatures and result in a wide range of sizes.

7.2.7 Kinetic analysis

As in the TG study, the extent of reaction, α, was defined such that $\alpha = 1.00$ at the mass loss corresponding to complete reaction (see Table 7.6). Below 1010°C the reaction was not finished in the time studied, but following the trend of decreasing final mass loss with decreasing temperature, the analysis was based on a mass loss of 25.4% for complete reaction. Each isotherm was analysed in two stages. The transition between the first and second stages occurred for α values between 0.30 and 0.50, as is apparent by the change in slope of the $f(\alpha)$ function.

The results from the first stage of reaction indicated that the diffusion models gave a consistently better fit than any of the other models. Among the diffusion models, the D3 and D4 models fitted the data best. The correlation coefficients and rate constants calculated from the D3 and D4 models are listed in Table 7.9, and Fig. 7.38 shows the fit of the D3 and the D4 model to the experimental curve at 985°C. The Arrhenius plot of the D4 model is shown in Fig. 7.39; an activation energy of 374 ± 2 kJ mol^{-1} and frequency factor of $(3.59 \pm 0.05)\times10^{12}$ min^{-1} were calculated.

Table 7.9. The rate constants and correlation coefficients calculated using the D3 and D4 models.

	D3		D4	
Temperature /°C	k /10^{-3}min^{-1}	R^2	k /10^{-3}min^{-1}	R^2
935	0.250	0.9938	0.230	0.9919
960	0.544	0.9682	0.499	0.9660
985	1.15	0.9984	1.04	0.9969
1010	2.40	0.9929	2.06	0.9900
1035	4.55	-	3.98	-

The applicability of these models implies that the reaction is limited by diffusion in 3 dimensions, as was inferred from the TG study. Again, the diffusion referred to is almost certainly diffusion of gases through the pores of the product layer, and not diffusion through the crystal lattice.

A kinetic analysis of the second stage of reaction was also attempted. However, it was apparent that no model fitted the experimental data very well, and no model was consistently better than any others. The quality of the data was clearly not good enough to discern meaningfully between different kinetic models.

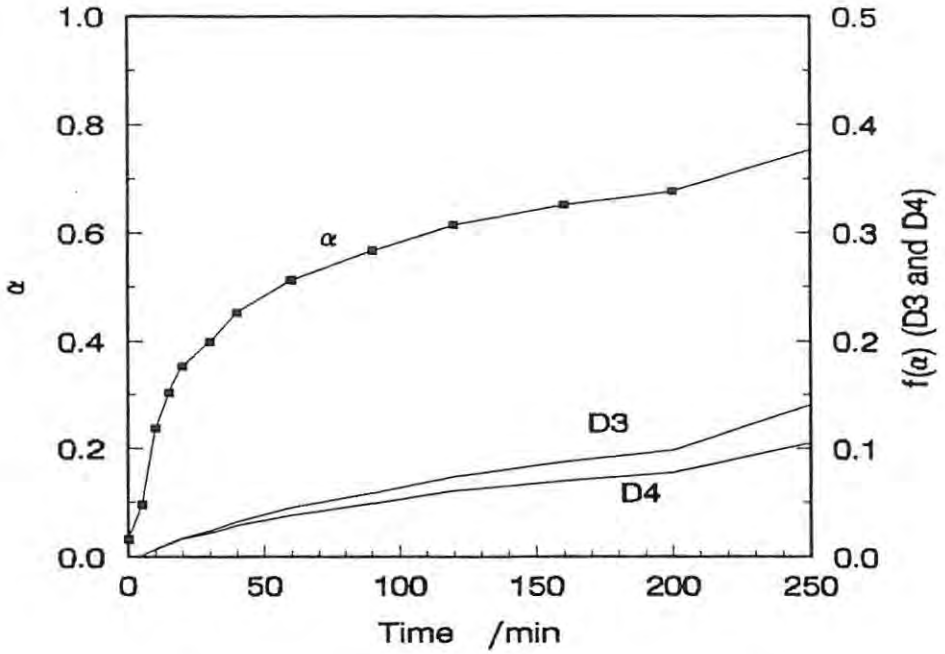

Fig. 7.38. The fit of the D3 and D4 models to the α,t curve for WO_3/graphite mixtures at 985°C.

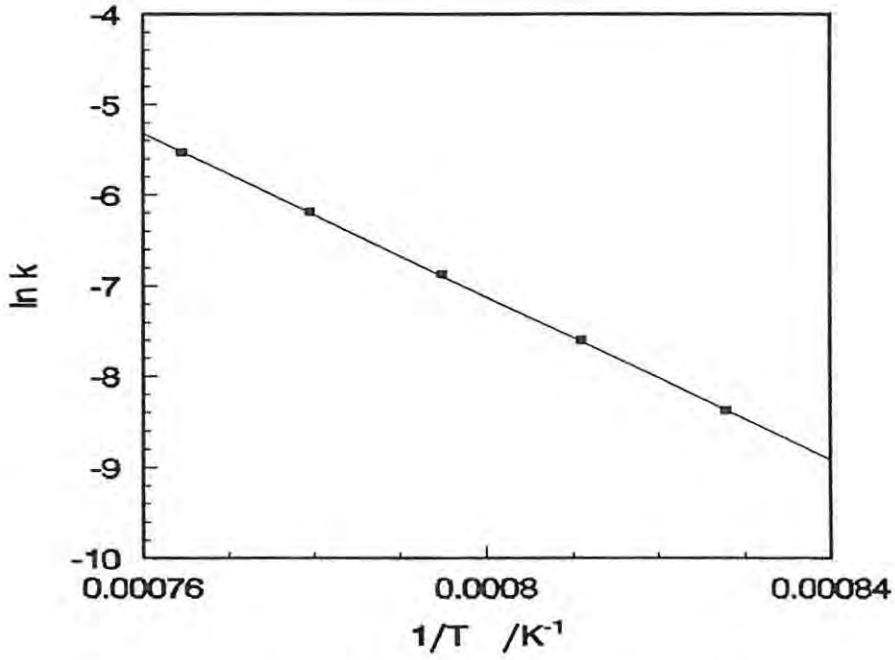

Fig. 7.39. The Arrhenius plot for the reduction of WO_3 with graphite in a 1:4 mole ratio and in argon flowing at 100 mL min^{-1}.

7.2.8 Discussion

The reaction scheme for the reduction of WO_3 with graphite is similar to that for the reduction with CO. The reaction occurs predominantly by gaseous intermediates, which is in accordance with the reduction of other metal oxides with carbon.

The rate of the first stage of the reduction is best described by a diffusion-limited kinetic model, as was also found in the analysis of the data from TG experiments. The diffusion models have often been applicable to the reduction of other metal oxides with carbon. The porous structure of the tungsten oxide pseudomorphs suggests that the diffusion being described is pore diffusion, as opposed to solid state diffusion. Diffusion is probably rate-limiting because the CO/CO_2 ratio in the powder is moderately low. Since the rate of diffusion increases with the concentration gradient of the diffusing species, a small difference between the CO/CO_2 equilibrium ratio for the reaction taking place, and the CO/CO_2 ratio in the powder layer, will result in a slow rate of diffusion, which may become rate-limiting.

The conformity of the reduction of WO_3 by CO to a kinetic model which is not based on a diffusion-limited process is explained by the much higher CO/CO_2 ratio in the powder layer. In this situation, the CO/CO_2 ratio at the reaction interface (as for the geometric models) would be greater than the equilibrium ratio, and diffusion would therefore not be rate-limiting. The proposed mechanism for the reductions of WO_3 with CO and with carbon are depicted in Fig. 7.40.

Although the intermediate oxides $W_{20}O_{58}$ and $W_{18}O_{49}$ were identified in the reduction with carbon, the first stage of the process is limited by a physical mechanism which is largely independent of the specific chemical reactions. Consequently, the rate of reaction does not show any features which might be identified with a particular reaction. In the reduction with CO, on the other hand, the rate of reaction curve does show distinct peaks which were attributed to the formation of particular phases.

The gravimetric measurements from the tube furnace experiments were insufficient to analyse the kinetics of the second stage of reaction. The data from the TG experiments suggested that this part of the process was limited by a first-order rate of reaction, which indicates that the reaction of CO_2 with graphite was probably rate-limiting. Many other metal

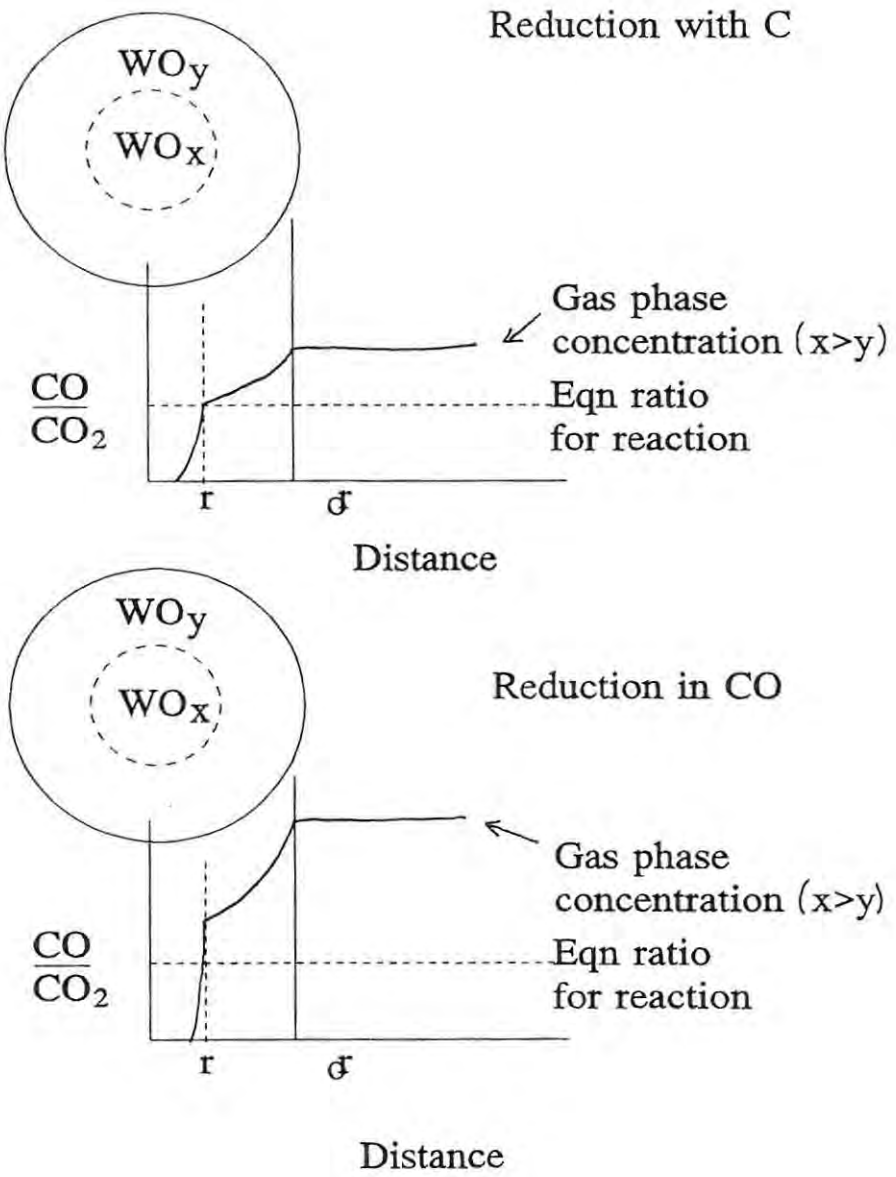

Fig. 7.40. Schematic representation of the CO/CO_2 ratio in the reacting pseudomorphs during the reduction of WO_3 with carbon and with CO..

oxide reductions with carbon have also found that this reaction is rate-limiting.

The morphology of the reduction has been described. The retention of the shape of the starting oxide particles (pseudomorphs) throughout the process and the presence of tungsten or tungsten oxide on graphite particles are particularly relevant in relation to the results of Elyutin *et al.*[52] In their study of the reduction of WO_3 with lamp black below 700°C, they proposed that tungsten oxides sublimed and reacted on the carbon surface. The results presented in this work, particularly the effect of the flowrate, are consistent with the reduction taking place via CO. Furthermore, tungsten oxides within the pseudomorph are completely reduced by the end of the process. Because the particles within the pseudomorph are not in contact with carbon, the mechanism proposed by Elyutin *et al.* could not occur in this study. The differences between this work and the work of Elyutin *et al.* are possibly a result of the different temperature ranges considered (above 900°C in this work, compared to their study of the reaction below 700°C).

The appearance of tungsten and tungsten oxides on the graphite particles indicates that tungsten oxides have considerable mobility, and could result from sublimation, which has been reported by Elyutin *et al.* and Miyake and Haka[53]. The localised sheets of tungsten or tungsten oxides are indicative of surface diffusion, which is enhanced by impurities in the sample, as has been discussed. This high mobility explains the substantial growth of tungsten particles during the reduction process, and also implies that grain growth during hydrogen reduction is partly attributable to the inherent mobility of the tungsten oxides, and not just to tungsten transport by the species $WO_2(OH)_{2(g)}$.

Chapter 8

REDUCTION OF TUNGSTEN OXIDES WITH HYDROGEN

8.1 General observations

Samples of WO_3 of 1.2 to 1.3 g were reduced in the tube furnace (section 3.3) in hydrogen at different temperatures and flowrates. The product of the reduction was identified as α-W by XRD. The mass losses at the end of the reduction process ranged from 20.7 to 21.4%, which is close to the expected mass loss of 20.70% for the reduction of WO_3 to tungsten metal.

The TCD traces of the reduction of WO_3 at different temperatures and in hydrogen flowing at 200 mL min^{-1} are shown in Figs 8.1 and 8.2, and are similar to the CO_2 traces described in section 7.2.5, which again indicates the sequential nature of the reduction. Four parts of the TCD profile were identified: there are two small peaks at the start of the reaction, a large peak indicating a high rate of reaction, and finally a considerably slower reaction. At high temperatures, the first and second stages are not readily distinguishable from the third peak, and the fourth stage also increases in rate relative to the preceding stages of the reaction (Table 8.1).

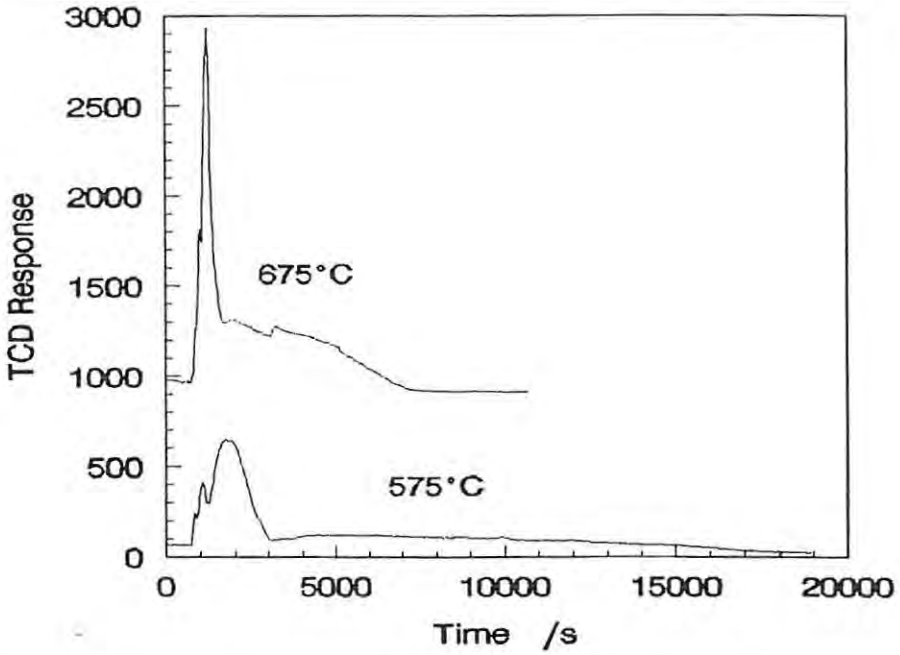

Fig. 8.1. TCD traces of the reduction of WO_3 in hydrogen flowing at 200 mL min^{-1} (at 575 and 675°C).

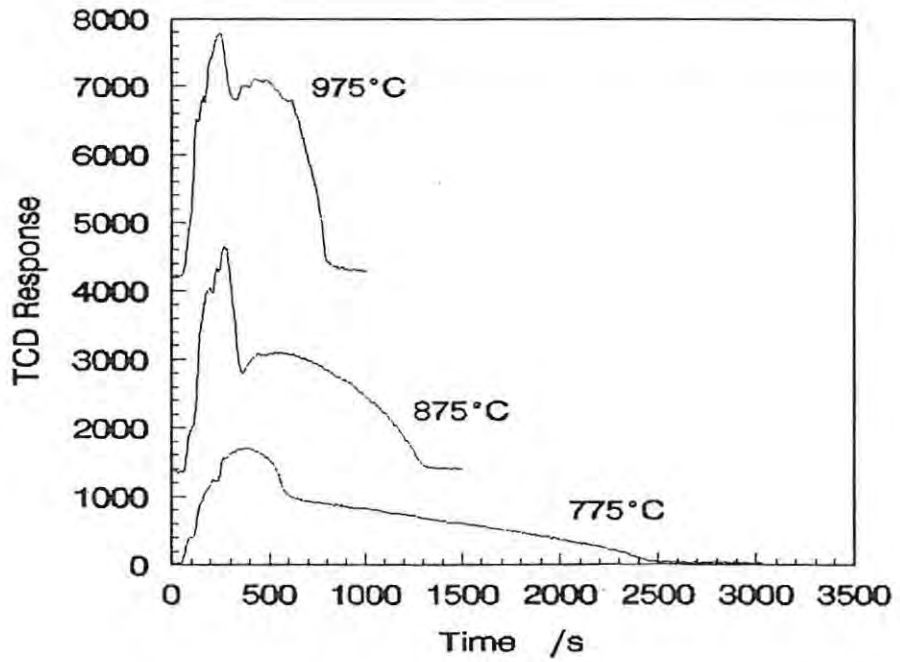

Fig. 8.2. TCD traces of the reduction of WO_3 in hydrogen flowing at 200 mL min^{-1} (at 775, 875, and 975°C).

Table 8.1. The duration of the first three stages of the reaction, the fourth stage of reaction, and the total reaction. The ratio of the duration of the first three stages to the fourth stage of reaction is also shown. The hydrogen flowrate was 200 mL min^{-1}.

Temperature /°C	Stages 1-3 /s	Stage 4 /s	Complete reaction /s	Time Ratio (1-3)/4
575	2380	incomplete	incomplete	-
675	960	7140	8100	7.4
775	540	1860	2400	3.4
	450	1730	2180	3.8
875	290	940	1230	3.2
975	250	490	740	2.0

The composition of the sample was examined at different stages of the process at 675 and 875°C, and the results are shown in Table 8.2. When no more than two phases were present the approximate composition was calculated. (These calculations assumed that 0.7% mass was lost before the reduction started, based on the TG studies of the WO_3 reactant in chapter 5.) The reaction scheme inferred from these results is shown in Fig. 8.3 and is very similar to the reaction schemes for the reductions with CO and with solid carbon (Figs 6.6 and 7.27). Not all the phases and reactions reported by Schubert[22] (Fig. 2.6) were identified in this study, most notably the direct reduction of $W_{18}O_{49}$ to tungsten metal. β-W was only identified in trace amounts at 575°C.

Table 8.2. The composition of the sample at different times in the reduction at 675 °C and at 875 °C.

Time /min	Mass Loss /%	Phases identified and approximate composition
675 °C		
5	2.35	80% $W_{18}O_{49}$; 20% $W_{20}O_{58}$
12	8.50	90% WO_2; 10% α-W
40	13.97	50% α-W; 50% WO_2
875 °C		
1.5	1.34	$W_{20}O_{58}$
2.5	3.73	80% $W_{18}O_{49}$; 20% WO_2
3.5	5.49	60% WO_2; 40% $W_{18}O_{49}$
5	8.44	90% WO_2; 10% α-W
8	11.81	70% WO_2; 30% α-W
12	17.12	70% α-W; 30% WO_2
16	20.09	90% α-W; 10% WO_2

The number of steps in the reaction and the amount of oxygen removed in each step suggests that the four parts of the TCD trace may be identified with each of the steps in Fig. 8.3. Samples in which the reactions were interrupted at the end of the third stage at 575 to 975 °C all consisted predominantly of WO_2; α-W was the only other phase present, but usually in small quantities. Thus, the fourth stage in the TCD trace can be identified with the reduction of WO_2 to α-W. From the approximate position on the TCD traces of the samples interrupted at various times during the process, the first three peaks in the TCD trace may be

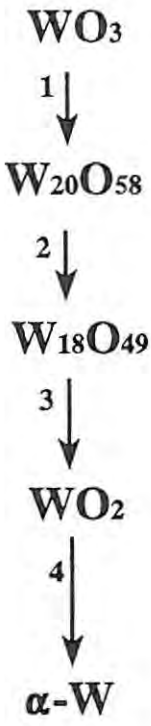

Fig. 8.3. The reactions observed in the reduction of WO_3 with hydrogen.

similarly associated with the first and third reactions in the scheme shown in F[illegible]. The relative areas of the peaks in the TCD traces for the four stages of the reaction a[illegible]nd 875 °C also correspond quite closely with the proportion of the overall reaction of each of the reactions in the reduction, Table 8.3.

Table 8.3. Relative areas of the peaks under the TCD traces at 675 and at 875 °C, compared with the proportion of the overall process of each of the four reactions in Fig. 8.3.

Stage of reaction	Relative area of peak		
	675 °C /%	875 °C /%	Calculated /%
First	1.2	1.2	3.3
Second	4.7	11.1	5.9
Third	31.0	22.9	24.1
Fourth	63.1	64.8	66.7

A number of experiments were conducted in which the hydrogen flowrate was varied. Fig. 8.4 shows the duration of the first to third stages, and of the fourth stage of the process at 675, 875, and 975 °C. It is apparent that the flowrate has a marked influence on the reaction rate, and increasingly so as the temperature in the system is lowered.

The H_2/H_2O equilibrium ratios for each of the four steps in the reaction (Fig. 8.5) help to explain the effect of the flowrate on the system. The H_2/H_2O equilibrium ratios for the first and second stages of the reduction are less than 0.01 at all the temperatures considered in this study, and thus the flowrate is unlikely to influence these reactions. However, the equilibrium ratio for the reduction of $W_{18}O_{49}$ to WO_2 is significant, and increases slightly as the temperature is lowered, which accounts for the greater effect of the flowrate on the reduction than at higher temperatures.

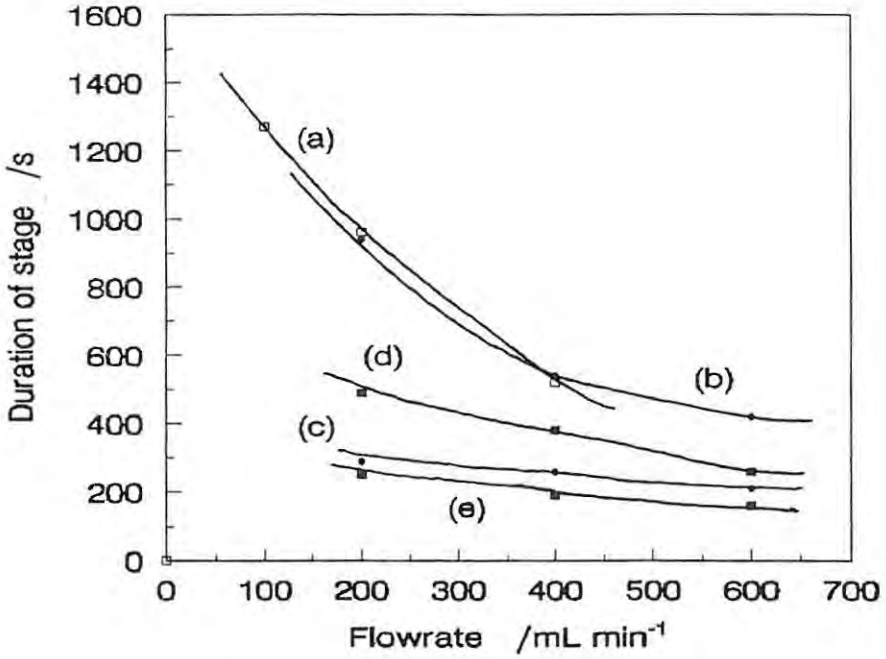

Fig. 8.4. Effect of the flowrate on the duration of the reduction of WO_3 with hydrogen: (a) stages 1 to 3, 675°C; (b) stage 4, and (c) stages 1 to 3, at 875°C; (d) stage 4 and (e) stages 1 to 3, at 975°C.

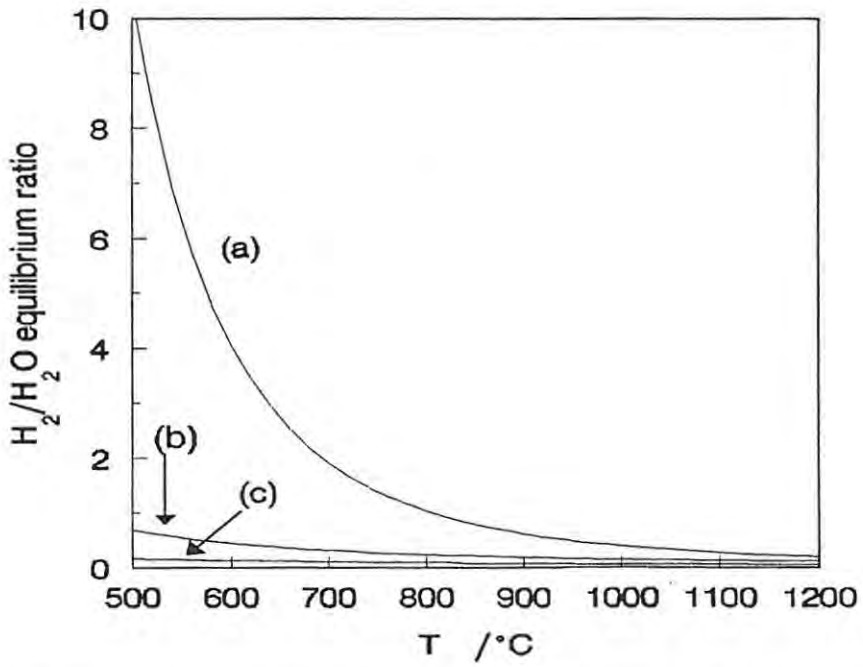

Fig. 8.5. The H_2/H_2O equilibrium ratios for the reduction of (a) WO_2 to tungsten metal, (b) $W_{18}O_{49}$ to WO_2, and (c) $W_{20}O_{58}$ to WO_2.

The temperature has an even larger bearing on the value of the H_2/H_2O equilibrium ratio for the reduction of WO_2 to tungsten, and an increasingly reducing atmosphere is required for the reduction to proceed as the temperature in the system is lowered. Thus, the reduction of WO_2 will become more dependent on the flowrate at low temperatures, especially below about 775°C. The variation of the equilibrium ratios of the four reactions with temperature also explains the observed increase in the duration of the fourth stage relative to the preceding three stages at lower temperatures, Table 8.1.

The situation normally encountered in gas-solid reactions is that the reaction is influenced less by the flowrate at lower temperatures. Because the rate of reaction decreases with temperature, the ratio of reactant to product gases in the system decreases relative to the equilibrium concentration and mass-transfer becomes relatively less important in the reaction. The kinetic parameters of the reaction are therefore often obtained by decreasing the temperature until the reaction is no longer controlled by mass-transfer[9]. In the present system, though, the large increase in the H_2/H_2O ratio required to bring about reduction at low temperatures opposes the decrease in the reduction rate.

The observed dependence of the reaction rate on the flowrate indicates that mass-transfer plays an important part in the reduction at the temperatures and flowrates investigated. Samples interrupted during reduction were often different colours at the front and at the back of the boat. The more reduced phase was always found towards the end of the boat facing the incoming hydrogen stream, which is the more reducing end of the boat. These observations are additional evidence for a mass-transfer-controlled process.

Because the TCD system could not be operated at higher flowrates, a meaningful investigation of the kinetics of the system (that is, in the regime where the reaction is not controlled by mass-transfer) could not be undertaken.

8.2 Morphological changes

The changes in the morphology of WO_3, which was reduced at 875°C in hydrogen flowing at 200 mL min^{-1}, were studied at different times during the reduction. The original particles were unchanged after reduction for 1.5 min, at which stage the sample was almost entirely $W_{20}O_{58}$. Small textured patches were observed on the surfaces and may have indicated nucleation of $W_{18}O_{49}$, the next phase to be formed.

After 2.5 min, the surfaces of the original particles were covered in a network of thin needles, which were randomly oriented in the plane of the pseudomorph's surface. The needle network was little changed after reduction for 3.5 and 8 min, although some small, circular aggregates of elongated particles — "tufts" — were apparent. Rounded mounds of coral-like clusters were observed in a sample reduced for 5 min, Fig. 8.6a; these are almost certainly clusters of WO_2, which was the main constituent of the sample.

After 12 to 16 min of reduction, the morphology of the particles had changed enormously. Many pseudomorphs of the starting WO_3 particles had broken into smaller agglomerates. These agglomerates were composed of approximately spherical particles of differing sizes among which coral-like clusters were scattered, Fig. 8.6b. The spherical particles were multi-facetted; growth ledges were apparent on some of the particles, and are indicative of gas-phase crystal formation[32,35]. The spherical particles are almost definitely tungsten, which was the major constituent of the sample, and appear very similar to the particles which other researchers have identified as tungsten[31,35]. The coral-like clusters are probably WO_2, which was present in the sample in lesser quantities.

The effect of the temperature on the morphology was studied by examining the samples at the start of the last stage of reduction, which corresponds to the reduction of WO_2 to tungsten metal. XRD of the samples showed that they consisted primarily of WO_2. At low temperatures (575 and 675°C) the shapes of the original WO_3 particles were retained, but they had become somewhat porous. Star-shaped cracks were apparent, and small needles were observed at 675°C. At 775°C and above, particles were more rounded and appeared to merge into one another to form quite dense clusters (Fig. 8.6a). The shapes of the pseudomorphs lost much of their definition and also increased in porosity. The rounding off of the WO_2 particles indicates

increased mobility of the tungsten and oxygen atoms, perhaps through the gas phase (via $WO_2(OH)_{2(g)}$ or gaseous tungsten oxides), or by surface diffusion.

The hydrogen flowrate and the sample size exerted a large influence on the morphology. Adjusting these variables affects the water vapour partial pressure in the powder, as well as the time required for the reaction to go to completion. In very dry conditions (400 mL H_2 min^{-1} and 0.25 g WO_3), needles were still evident by the time the sample was mainly WO_2, at which stage the pseudomorphs were only slightly porous. The pseudomorphs increased in porosity in more humid conditions and became quite rounded. The sizes of the tungsten crystals were larger when the conditions were more humid. In very dry conditions (400 mL H_2 min^{-1} and 0.25 g WO_3) there were no distinct tungsten single crystals as were observed under other conditions.

The transformation of one phase into another was sometimes observed. At 975°C and 200 mL H_2 min^{-1}, for instance, a number of dense clusters of rounded particles were observed in the needle network, which is consistent with the formation of WO_2 from $W_{18}O_{49}$, Fig. 8.6c. The rounded shapes of the WO_2 clusters contrast with the well-defined needles of $W_{18}O_{49}$, again suggesting that WO_2 has relatively high mobility. Textured patches similar to those observed at 875°C were also apparent at 675°C, which also suggested the formation of $W_{18}O_{49}$ on the surface of $W_{20}O_{58}$ particles.

The size and shape of the final products of the reduction varied considerably under different experimental conditions. At 875°C in very dry conditions (400 mL H_2 min^{-1} and 0.25g WO_3), the pseudomorphs were composed of very small crystals of tungsten, usually less than 0.5 μm in diameter (Fig. 8.6d). More humid conditions (875°C, 200 mL H_2 min^{-1}, and 1.2 g WO_3) resulted in formation of much larger tungsten crystals in open skeletal networks, shown in Fig 8.6e.

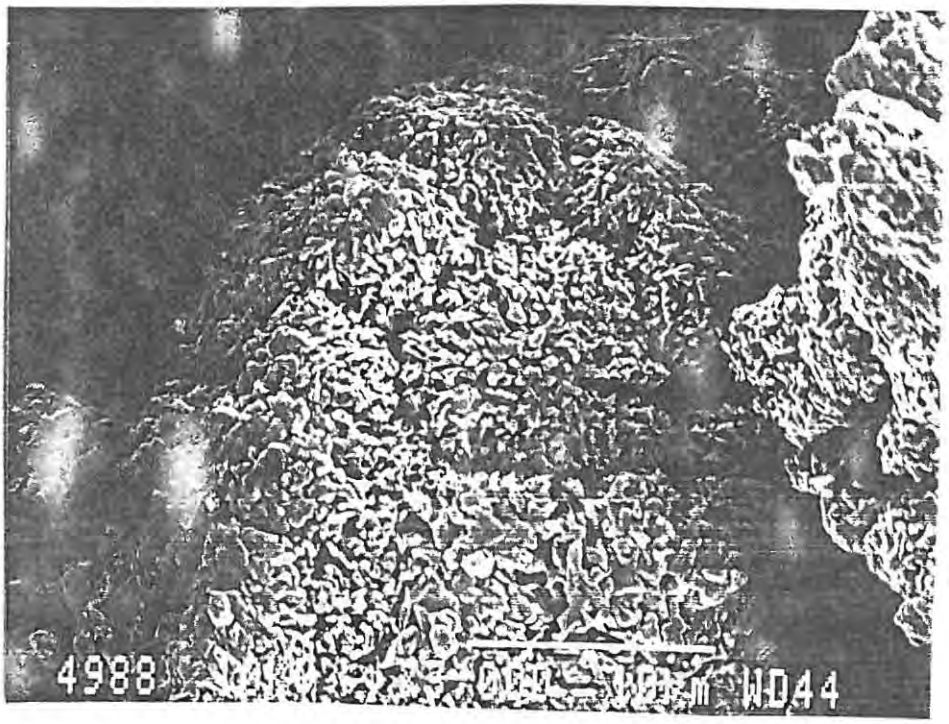

Fig. 8.6a Scanning electron micrograph of a WO_3 sample after heating for 5 min at 875°C in hydrogen flowing at 200 mL min^{-1}.

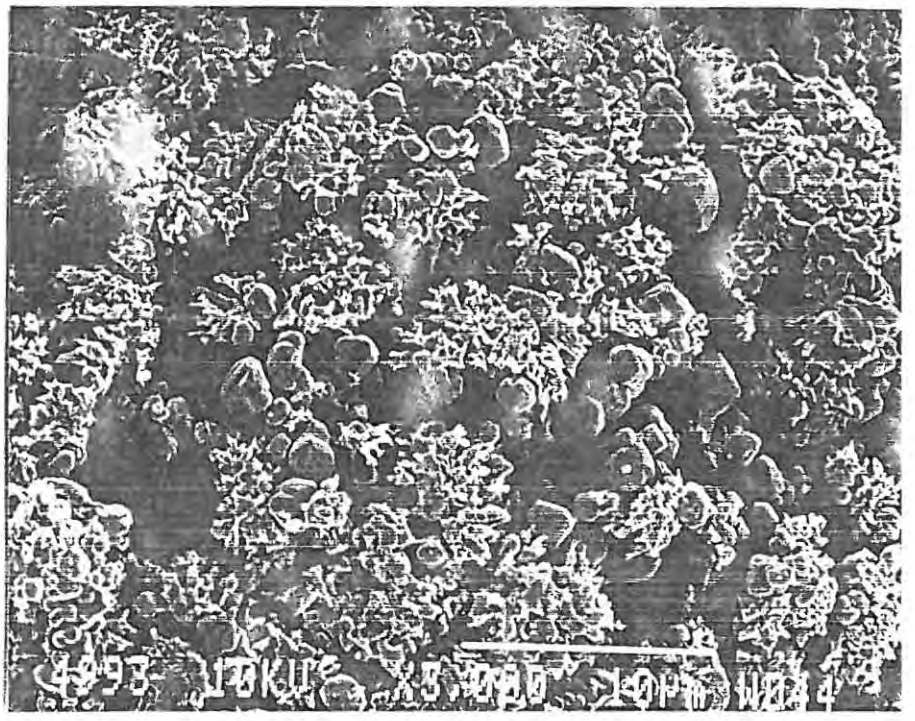

Fig 8.6b. Scanning electron micrograph of a WO_3 sample after 12 min at 875°C in hydrogen (200 mL min^{-1}).

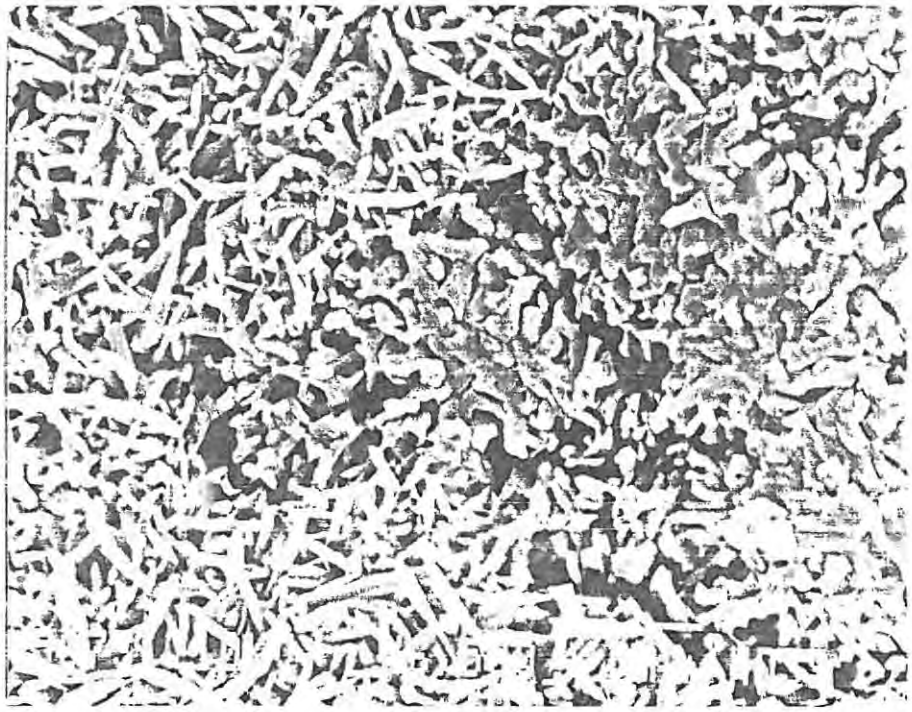

Fig. 8.6c Scanning electron micrograph of a WO_3 sample after 2.5 min at 975°C (in hydrogen flowing at 200 mL min^{-1}).

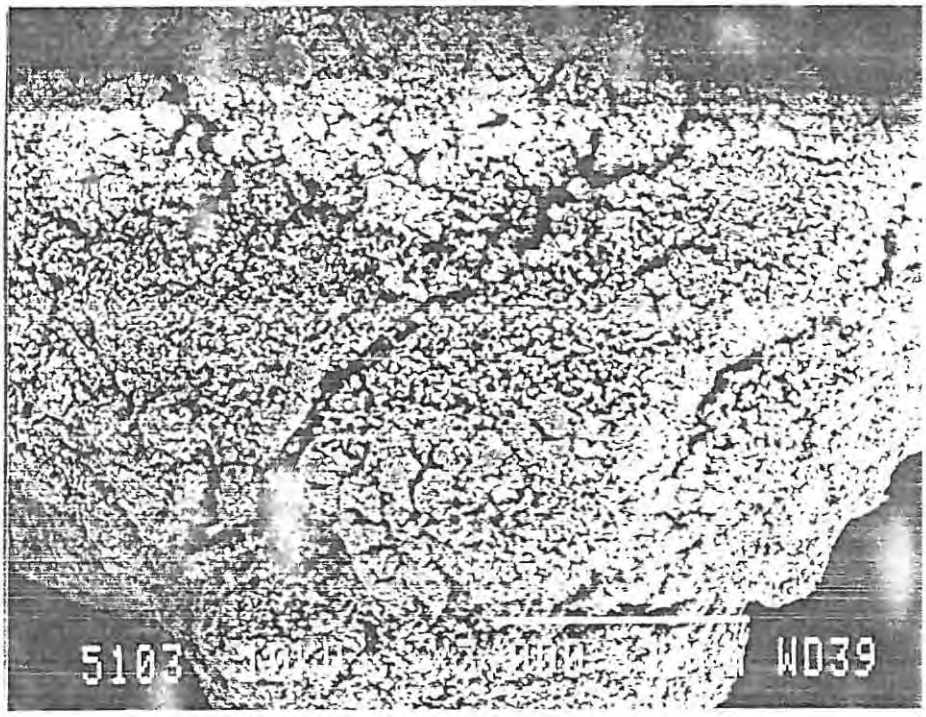

Fig 8.6d. Scanning electron micrograph of the product of a sample of WO_3 reduced in hydrogen at 875°C under dry conditions (0.25 g WO_3, 400 mL H_2 min^{-1}).

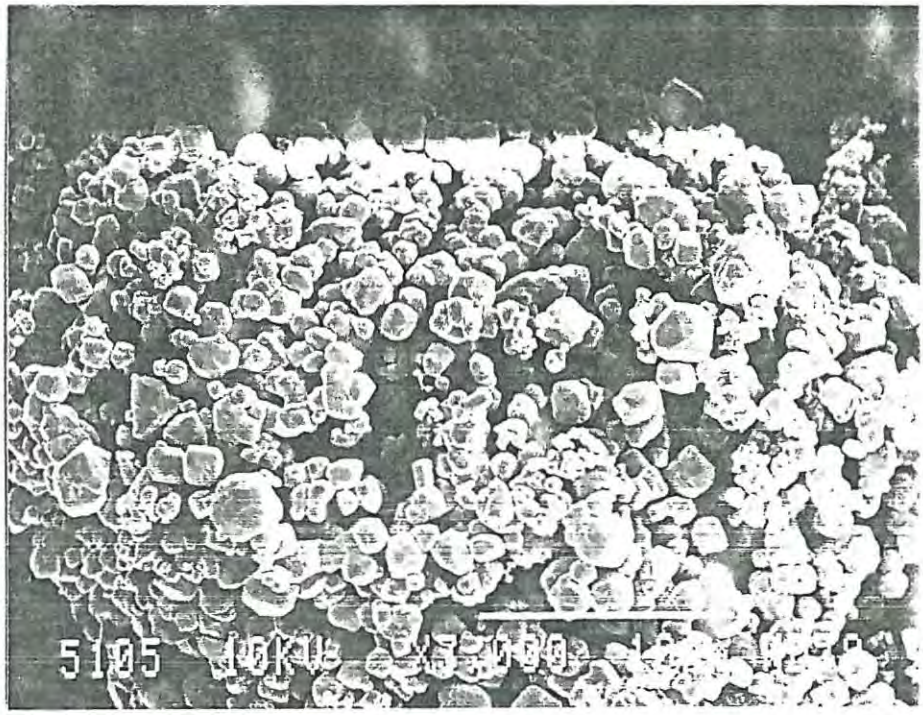

Fig. 8.6e Scanning electron micrograph of the product of the reduction of WO_3 in hydrogen at 875 °C, under the usual conditions studied (1.2 g WO_3, 200 mL min^{-1}).

Chapter 9

REDUCTION OF TUNGSTEN OXIDES WITH CARBON AND HYDROGEN

9.1 General observations

The simultaneous use of graphite and hydrogen in the reduction of WO_3 was studied in the tube furnace under similar conditions to the reductions when only one reducing agent was used. Samples were usually 1.2 to 1.3 g in mass, and a flowrate of 200 mL min^{-1} and a stoichiometric ratio of 1 mole WO_3 to 4 moles graphite were used in most experiments. Compared to WO_3 samples used in the reduction with hydrogen, the samples of 1:4 mole mixtures of WO_3 and graphite, of the same mass, were about 13% larger, but contained only 83% WO_3 by mass. These differences will have opposite effects: smaller amounts of WO_3 produce less water vapour, which leads to a higher H_2/H_2O ratio in the powder layer; on the other hand, a higher powder layer will decrease the rate at which H_2 diffuses into the powder layer, thus lowering the H_2/H_2O ratio. Nonetheless, there will inevitably be differences in the porosities and diffusivities of WO_3 and WO_3/graphite mixtures.

The reduction of WO_3/graphite mixtures by hydrogen at 675°C was virtually identical to the reduction of WO_3 by hydrogen alone, as would be expected from thermodynamic and kinetic considerations. At 775°C, however, the graphite containing mixtures (Fig. 9.1) are reduced considerably more rapidly than WO_3 alone, Fig. 8.2. The traces of the CO_2 and CO concentrations showed that these gases were only evolved in noticeable quantities over the first two stages of the reduction. At 875 and 975°C, similar features to the reduction at 775°C were observed, as well as a significant increase in the CO concentration towards the end of the reduction (Figs 9.2 and 9.3). The transition from the third to the fourth stage was also more marked in the TCD trace than when graphite was not present.

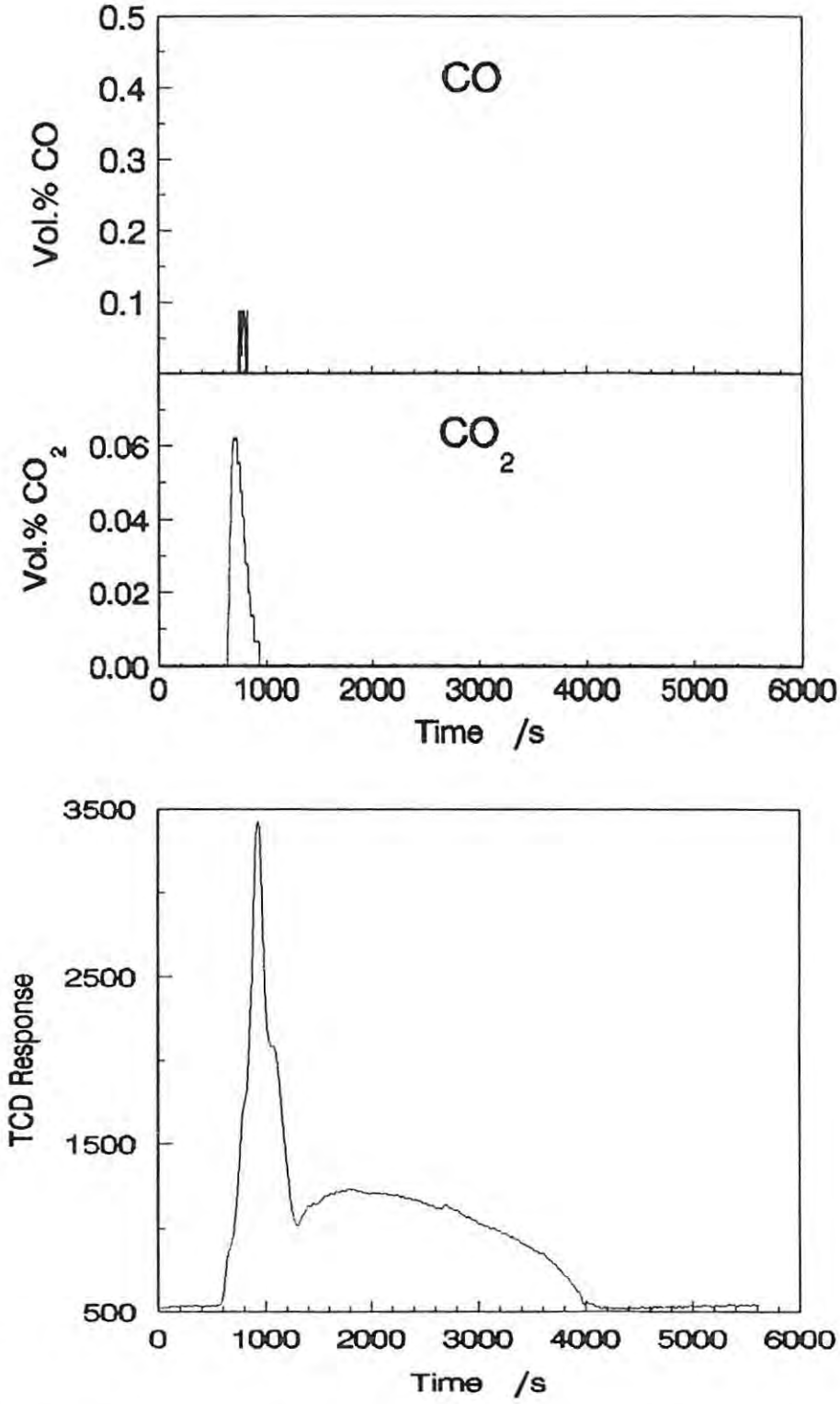

Fig. 9.1. The concentrations of evolved gases during the reaction of WO_3/graphite mixtures (in a 1:4 mole ratio) with hydrogen (200 mL min^{-1}) at 775°C.

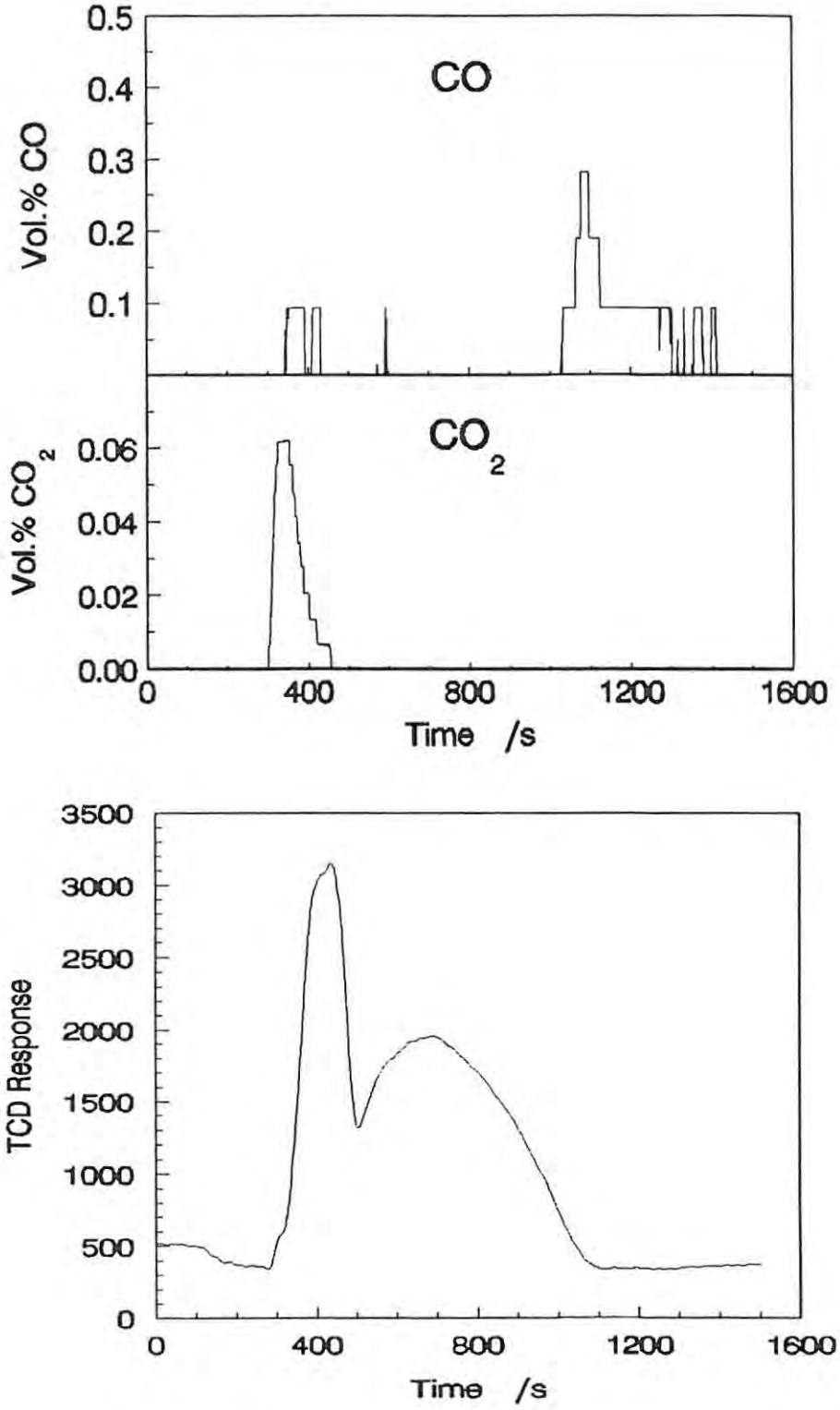

Fig. 9.2. The concentrations of evolved gases during the reaction of WO_3/graphite mixtures (in a 1:4 mole ratio) with hydrogen (200 mL min^{-1}) at 875°C.

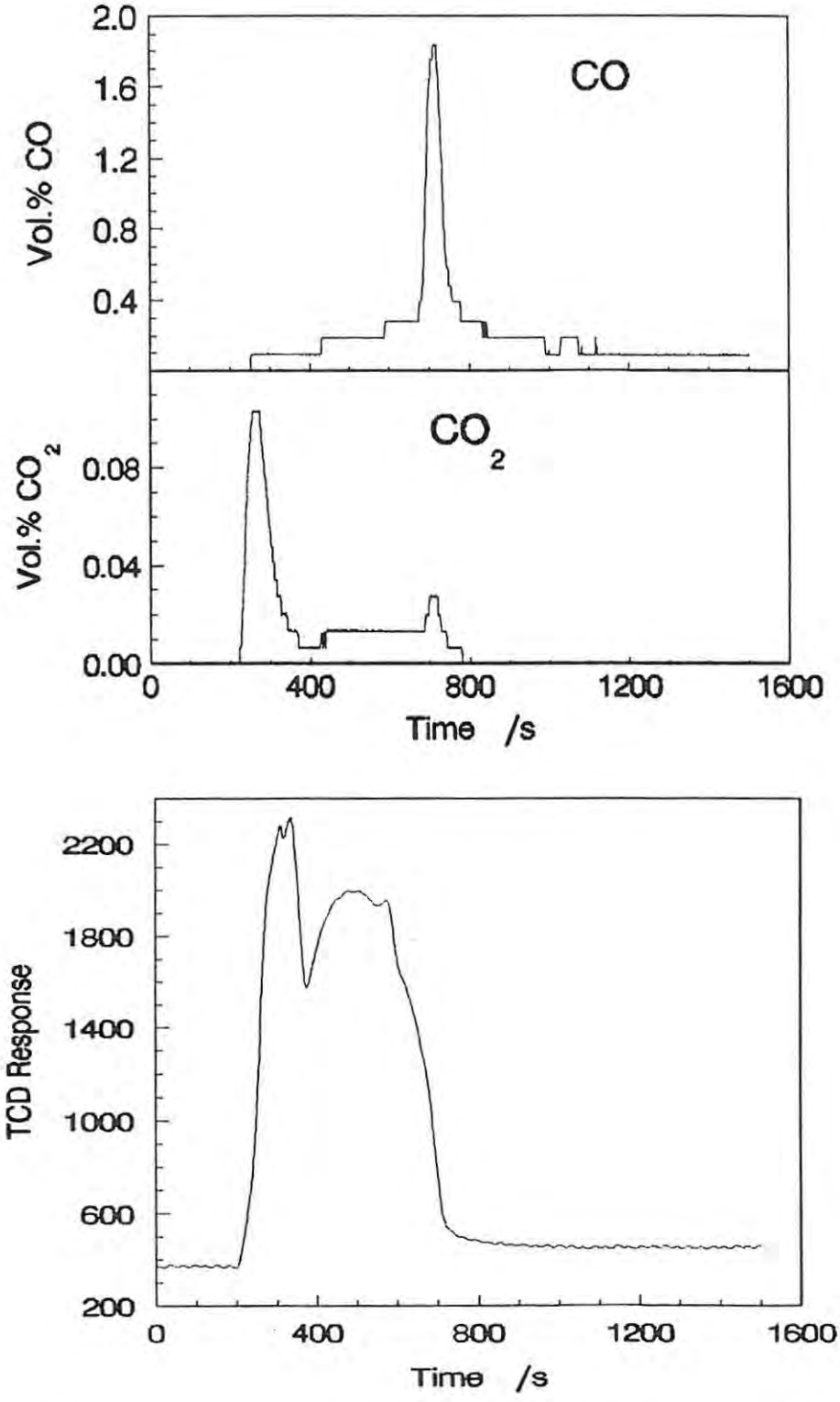

Fig. 9.3. The concentrations of evolved gases during the reaction of WO_3/graphite mixtures (in a 1:4 mole ratio) with hydrogen (200 mL min^{-1}) at 200 mL min^{-1}.

The CO_2 concentration increased sharply for a short while at the beginning of the reduction. After reaching a minimum at the transition from the third to the fourth stages of the reduction, the concentration increased slowly and reached a small second maximum at the same time as the CO concentration reached its maximum.

The concentration of CO_2 evolved from the sample is only appreciable at the start of the reduction. The CO_2 is probably not formed from the reduction of WO_3 with CO, since the concentration of CO in the sample is very low initially. The CO_2 is also not likely to be formed by the reduction of water vapour (e.g., reaction (4.10) and the reverse of reaction (4.11)), because the water vapour concentration is reasonably high throughout the reduction process, which implies that the concentration of CO_2 should also be significant throughout the process.

A more likely explanation for the formation of CO_2 is that WO_3 dissociates at high temperatures, and the oxygen from the dissociation reacts with carbon to form CO_2. Another possibility is that the CO_2 is formed from reaction at the points of contact between the WO_3 and the graphite particles. The duration of the first peak in the reduction of WO_3 with graphite (in the absence of hydrogen) was of approximately the same duration as when the reduction took place in hydrogen, which suggests that CO_2 results from the interaction of WO_3 and carbon, and does not involve participation by hydrogen or water vapour.

The peak in the CO concentration at the end of the reduction process is not so readily explained. The reaction of water vapour with CO is almost certainly appreciable (Fig. 2.8), and one would expect that CO is evolved in reasonable quantities throughout the reduction. If CO is formed throughout the process, then it must be retained in the sample, and released only at the end of the reduction. CO may be retained in the sample either by adsorption or by reaction to form a carbide. If CO is adsorbed, then the evolution of CO at the end of the process might result from the change in the H_2/H_2O ratio facilitating the desorption of CO from the tungsten surface. Alternatively, if CO reacts to form a carbide, then towards the end of the process the surface of all the freshly-generated tungsten may have reacted with CO to form a carbide. If this occurs, further reaction of CO with tungsten would have to take place across a protective layer of carbide (section 6.6.2), and would occur slowly. Thus, the remaining CO in the system would not be consumed as rapidly and would be removed in greater quantities from the powder layer.

The products of the reductions of WO_3/graphite mixtures at 875 and 975°C were analysed using XRD. The samples consisted predominantly of α-W and small peaks indicating W_2C were also observed.

The durations of the first to the third, and of the fourth stages in WO_3/graphite mixtures are compared to the durations of these stages in the absence of graphite, Table 8.1. The relative increase in the reaction rates appears to be quite similar for the first to the third, and for the fourth stages of the process, Table 9.1.

Table 9.1. The duration of the first three stages, and of the fourth stage, of reaction, for the reaction of WO_3/graphite mixtures in hydrogen. The relative duration of these stages to the corresponding stages in the absence of graphite are also reported.

Temperature /°C	Stages 1-3 /s	Relative duration /%	Stage 4 /s	Relative duration /%
775	355	72	1346	75
875	181	62	586	62
	216	74	622	66
975	176	70	345	70
	181	72	415	85

The composition of the sample at different times in the reduction was analysed for 1:4 mole WO_3/graphite mixtures at 875 and 975°C in hydrogen flowing at 200 mL min^{-1}. The results are presented in Table 9.2. The reaction paths are the same as in the absence of graphite, Fig. 8.3, but may also include the reduction of $W_{20}O_{58}$ to WO_2. No W_2C was observed during these experiments, and is probably only formed right at the end of the reduction, when the CO concentration is highest.

Table 9.2. Composition of WO_3/graphite mixtures after reduction in hydrogen (200 mL min^{-1}) at 875 and 975°C.

Time /s	Mass Loss /%	Phases identified besides graphite
875°C		WO_3
1	0.71	
2	2.33	$W_{20}O_{58}$; WO_2; small amounts $W_{18}O_{49}$
3.5	4.15	WO_2; $W_{18}O_{49}$
6	9.12	Mostly WO_2; some α-W
10	15.17	Mostly α-W; some WO_2
975°C		
2	4.59	Mostly WO_2; some $W_{18}O_{49}$
5	11.12	α-W; WO_2

As in the absence of graphite, the flowrate had a considerable influence on the rate of reduction. Table 9.3 lists the duration of the first to the third, and of the fourth stages of the reduction for different flowrates. The fourth stage of the reaction is more affected by the flowrate than the preceding stages, as is expected from the higher H_2/H_2O equilibrium ratio (Fig. 8.5). In samples interrupted during the course of the reaction, the colour of the sample often varied across the length of the boat. These observations again indicate that reaction was limited by mass-transfer.

Table 9.3. Effect of the flowrate on the duration of the first to the third stages, and of the fourth stage of the reduction of a 1:4 mole ratio mixture of WO_3 and graphite.

		Duration of stage	
Temperature /°C	Flowrate /mL min^{-1}	Stages 1-3 /s	Stage 4 /s
875	200	216	586
		216	622
	400	207	425
975	200	176	345
		181	415
	400	150	252

The effect of varying the amount of graphite in the system was studied by examining WO_3/graphite mixtures in 1:2 and 1:8 mole ratios. The mixtures examined were the same mass as used previously (i.e., 1.2 g). The mass of WO_3 in the sample is likely to affect the rate of the reduction because more water vapour will be formed when the sample contains larger amounts of WO_3. This will lower the H_2/H_2O ratio, and hence may decrease the rate of reduction. The duration of stages one to three, and of stage four of the process as a function of the WO_3 mass in the sample is shown in Fig. 9.4 for reaction at 875°C. The duration of the stages being measured is also shown for a 0.5 g sample of WO_3.

The duration of the first three stages of reaction is noticeably shortened by the presence of graphite. Increasing the proportion of graphite in the sample does not have much effect above a 1:4 mole ratio. The duration of the same stage for a 0.5 g sample of WO_3 was longer than that of the mixtures, which proves that decreasing the WO_3 mass in the sample at different mixtures was not solely responsible for the increased rate of reduction, and that graphite increased the rate of reduction.

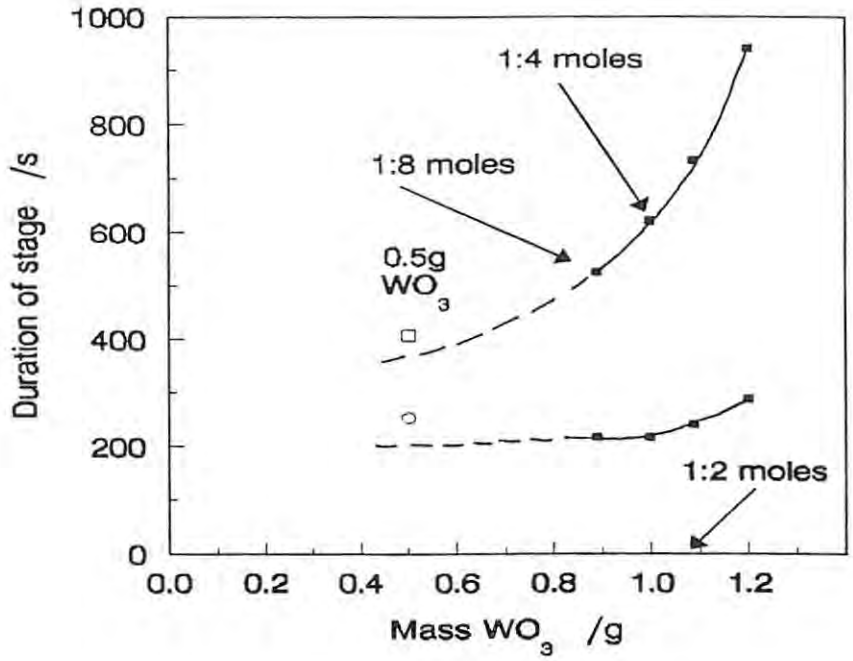

Fig. 9.4. The effect of the mass of WO_3 in the sample on the duration of the first three stages, and of the fourth stage. The points at 0.5 and 1.2 g correspond to samples containing WO_3 only.

The fourth stage of the process was considerably shorter when graphite was present, but the effect might also be caused by the associated decrease in the WO_3 mass of the sample as the stoichiometric ratio increases. For example, the duration of the fourth stage in the reduction of 0.5 g of WO_3 was similar to that expected by extrapolating the curve of WO_3/graphite mixtures to the composition which would correspond to 0.5 g of WO_3 in a 1.2 g WO_3/graphite mixture. The stoichiometric ratio of WO_3 to graphite in a 1.2 g mixture which contained 0.5 g WO_3 would be 1:27, which corresponds to a 1:4.4 volume ratio. This increase in the volume of the mixture is likely to decrease the rate of transport of hydrogen through the powder layer, which would attenuate the observed effect of graphite on the duration of the fourth stage. Therefore, the fourth stage is probably accelerated by graphite, but this assertion could not be definitely proved without a more detailed knowledge of the effective diffusivities in the system and how they affect the reduction rate.

The amount of graphite which reacted during the process was taken as the difference between the mass loss from the sample and the theoretical mass of oxygen in the sample.

Results are listed in Table 9.4 for reactions under different conditions. These results show a reasonably consistent increase in the amount of graphite reacted as the temperature and stoichiometric ratio of the mixtures are increased. Less graphite reacts when the flowrate is increased, probably because the reaction time is shorter.

Table 9.4. The mass and percentage mass of graphite reacted during the reduction.

Temperature /°C	Flowrate /mL min^{-1}	Stoich. ratio	Mass Loss /10^{-3} g	Mass loss /%
775	200	1:4	1.1	0.6
875	200	1:4	2.3	1.3
	400	1:4	1.5	0.9
	200	1:2	0.5	0.4
	200	1:8	2.0	0.6
975	200	1:4	1.9	1.1
			1.9	1.1
	400	1:4	1.9	1.1

9.2 Morphological changes

The appearance of WO_3/graphite mixtures was relatively unchanged after heating in the furnace for 1 min at 875°C in a flowrate of 200 mL H_2 min^{-1}, although patches of the WO_3 surface had started to become textured. Needles were visible after 2 min, but were much less extensive than in the absence of graphite, and were interspersed between relatively smooth round regions of up to 3 μm in diameter (Fig. 9.5a). These round patches (which were often cracked in the centre) were probably the WO_2 which was present in the sample. After 3.5 min, the needles were

longer and covered a larger proportion on the surface.

The less extensive formation of needles of $W_{18}O_{49}$ when graphite was present probably indicates that the water vapour concentration in the system was lower. Similar morphologies were seen when the flowrate was decreased, and Schubert[22] has also observed the reduction of $W_{20}O_{58}$ to WO_2 in dry conditions.

Reduction for 6 min resulted in the disintegration of needles to form small particles which were sometimes clustered into mounds. The surfaces of pseudomorphs after reduction for 10 min were quite similar, although the growth of crystals with clear facets was observed in cracks. Patches of small elongated tungsten or tungsten oxide particles were often observed on the surface of the graphite particles. These observations are similar to those reported for the reduction of WO_3 in the absence of graphite.

At 975°C, the morphologies of tungsten oxide particles at different times during the reduction were similar to those observed at 875°C. Small nodules of tungsten or tungsten oxides were seen on the graphite particles. Increasing the stoichiometry did not have much effect on the morphology of the tungsten oxide particles.

At the end of the process, the tungsten particles were collected in loose, open networks; small graphite particles were sometimes incorporated on the surface of these structures. Tungsten nodules were often observed on the surfaces of the graphite particles (Fig. 9.5b). The tungsten particles were up to 2 μm in diameter at 875°C, Fig. 9.5c. Similar morphologies were observed at 975°C; in some places a sheet of tungsten particles was observed on the graphite surface. The shapes and sizes of the final products of the reduction were quite similar, and altering the flowrate, stoichiometric ratio, or temperature did not seem to have much effect.

Compared to the product in the absence of carbon, the tungsten particles appeared to be slightly smaller, but the size difference was not marked. Owing to variations in particle sizes at different heights in the powder layer, it was not possible to ascertain the precise extent to which the particle sizes changed. To do so would require grinding the product of both systems to separate the individual tungsten crystals from the pseudomorphs, and then determining a size distribution of the particles in each system. Facilities were not available for such a study.

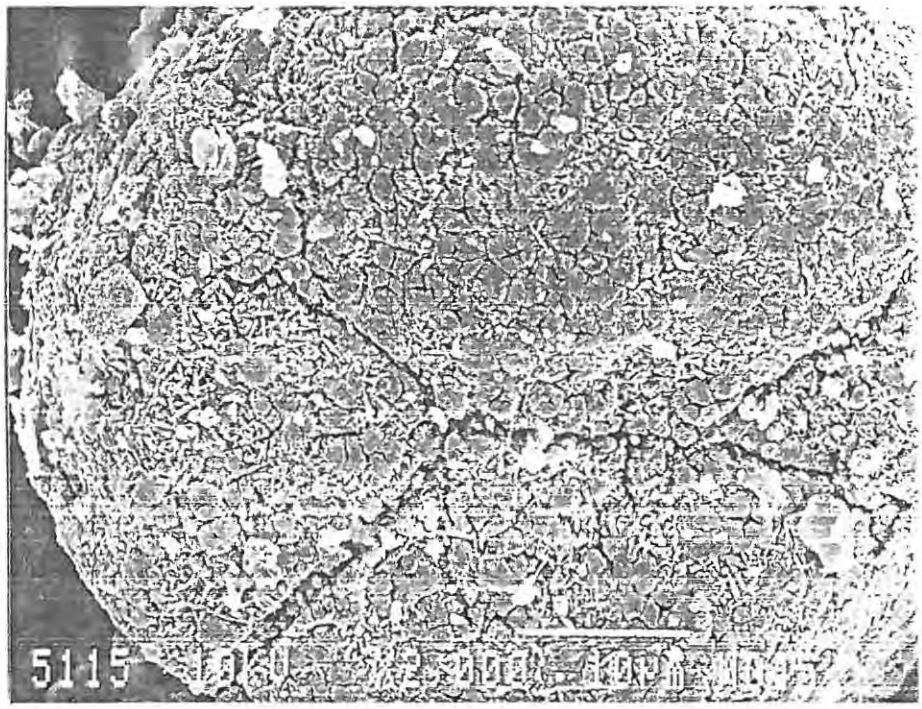

Fig. 9.5a. Scanning electron micrograph of a WO_3/graphite mixture (1:4 mole ratio) after heating for 2 min at 875 °C in hydrogen flowing at 200 mL min^{-1}.

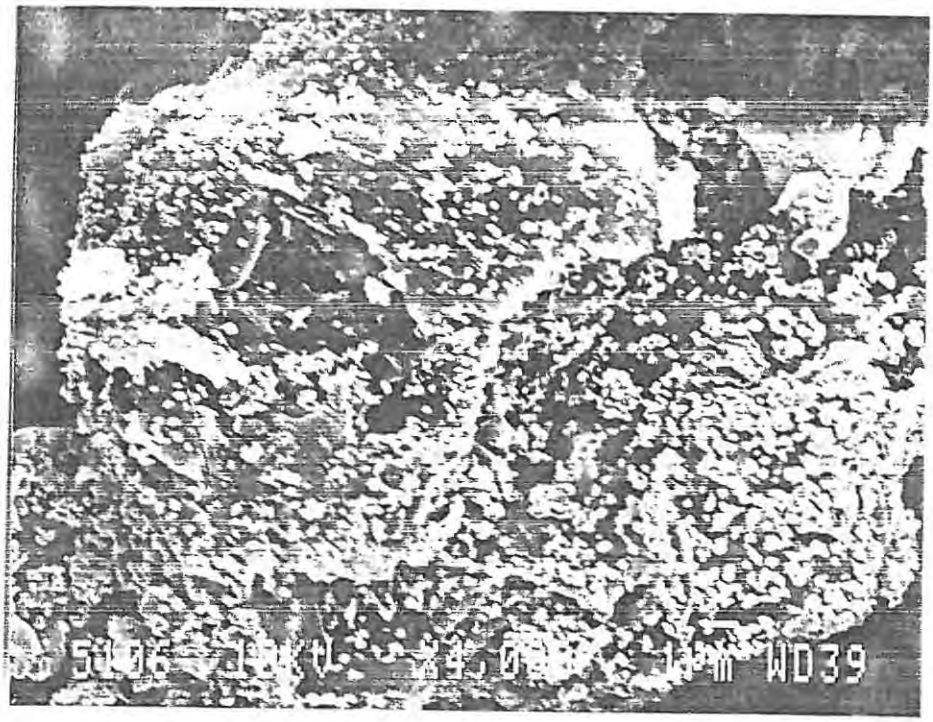

Fig 9.5b. Scanning electron micrograph of the product of a WO_3/graphite mixture (1:4 mole ratio) after reduction in hydrogen (200 mL min^{-1}) at 875 °C.

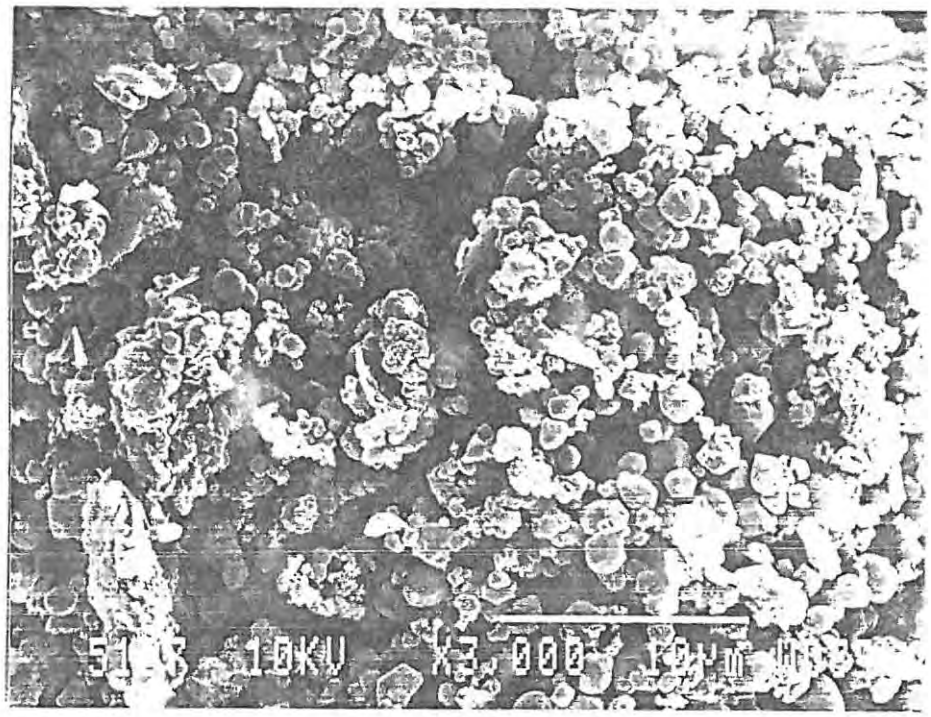

Fig. 9.5c. Scanning electron micrograph of the product of the reaction of a WO_3/graphite mixture (1:4 mole ratio) with hydrogen (200 mL min^{-1}) at 875 °C.

Chapter 10

CONCLUSIONS

The reductions of tungsten oxides with hydrogen, with carbon monoxide, and with carbon have been studied. The reactions of mixtures of tungsten trioxide and carbon with hydrogen were also investigated. The kinetics and reaction mechanisms of these reductions have been determined under the conditions investigated, and are summarised in Table 10.1.

Table 10.1. The kinetic models which best described the reactions investigated, and the activation energies calculated for the reactions.

System	Conditions	Kinetic model	E_a /kJ mol^{-1}
WO_3/CO	First stage	Zero-order	66 ± 2
	Second stage	R2	40 ± 7
		Zero-order	33 ± 8
WO_2/CO		R2	62 ± 5
WO_3/C	TG, graphite, first stage	D4	389 ± 9
	second stage	F1	438
	TG, lamp black, first stage	D4	465
	Tube furnace, graphite, first stage	D4	374 ± 2
WO_3/H_2	Mass-transfer controlled	-	-
$WO_3/C/H_2$	Mass-transfer controlled	-	-

Two main complementary experimental techniques were used in the study: thermogravimetry of small samples (less than 50 mg), and tube furnace experiments, coupled with evolved gas analysis, on larger samples (up to 2.5 g).

The reduction of tungsten trioxide with carbon

The reduction of WO_3 with carbon takes place above 900°C via the formation of CO, and involves two distinct stages. The first stage corresponds approximately to the reduction to WO_2, and is described by the Ginstling-Brounshtein (D4) rate equation, which models a process limited by diffusion in three dimensions. Activation energies of 386 ± 9 kJ mol^{-1} and 465 kJ mol^{-1} were calculated from TG experiments for the reduction with graphite and lamp black, respectively. From data obtained from tube furnace experiments, an activation energy of 374 ± 2 kJ mol^{-1} was calculated for the reduction with graphite. Lamp black was less reactive than graphite at the temperatures studied.

The second stage of the reduction is described by a first-order (F1) rate equation, and it is proposed that the reaction of CO_2 with graphite is rate-limiting towards the end of the reduction process. The activation energy for this stage was 438 kJ mol^{-1}. The importance of the CO/CO_2 ratio in the system, and its effect on the reaction rate of CO_2 with carbon, were related to the observed change in the kinetic obedience of the system.

These results differ from those of other workers, who have reported that the reduction takes place by sublimation of tungsten oxides and subsequent reduction on the carbon surface. The results which were obtained and the proposed mechanism are, however, consistent with those of the reductions of other metal oxides with carbon, which usually occur via reduction with CO.

Reduction of tungsten oxides with carbon monoxide

The reactions of WO_3 and WO_2 with CO to form WC were examined from 650 to 900°C. The mass losses at the end of these reactions with CO varied appreciably, suggesting that the reaction was incomplete at lower temperatures. Assumptions had to be made in the definition of the

extent of reaction (section 6.6.3). The reduction of WO_3 occurs in two distinct stages below 800°C. In this temperature range the first stage of reaction is zero-order and is probably related to the reduction of WO_3 to $W_{20}O_{58}$ and some $W_{18}O_{49}$. The activation energy for this stage was 66 ± 2 kJ mol^{-1}. At 800°C and above, distinct peaks were evident in the rate of mass loss curve over the initial part of the reduction, and were assigned to the stepwise formation of $W_{20}O_{58}$, $W_{18}O_{49}$, and WO_2.

The main part of the reduction took place in a single stage over the whole temperature range studied. The rate of this stage of reaction was mainly deceleratory, and was fitted best by the R2 (contracting-area) model towards the end of reaction. An activation energy of 40 ± 7 kJ mol^{-1} was calculated.

The reduction of WO_2 also occurred in a single stage, and was best described by the R2 model. An activation energy of 62 ± 5 kJ mol^{-1} was calculated. The reduction was preceded by a short induction period, possibly signifying the formation and growth of nuclei.

Differences between the kinetics of the reductions of WO_3 and WO_2 with CO, and the reduction of WO_3 with carbon, were explained in terms of different CO/CO_2 ratios in the powder layer.

The reduction of tungsten trioxide, and tungsten trioxide/ graphite mixtures, with hydrogen

The experimental arrangement was such that the kinetics of the reductions of WO_3 with hydrogen, and with carbon and hydrogen, could not be studied outside of a mass-transfer controlled regime. Regardless of whether or not carbon is present, the reduction of WO_3 with hydrogen is rapid and the H_2/H_2O ratio in the powder layer soon approaches the equilibrium ratio for the reaction taking place. The usual technique of studying the kinetics of the reaction by decreasing the temperature until mass-transfer is no longer rate-limiting could not be applied in this system owing to the substantial increase in the H_2/H_2O equilibrium ratio at lower temperatures.

The presence of graphite increased the rate of reduction of WO_3 with hydrogen above 675°C. The overall effect of graphite seems to be to decrease the amount of water vapour in the system, thus leading to an increased reaction rate. The rate of the final stage of the

reduction also appeared to increase in the presence of carbon; this effect could not be proved conclusively because the effect of a decreased proportion of WO_3 in the sample, and changes in the porosity and effective diffusivities of the WO_3/graphite mixtures, were not fully known.

Evolved gas analysis showed that significant amounts of CO_2 were evolved during the initial stages of the reduction, after which the concentration of CO_2 in the system was very low. The concentration of CO evolved from the system increased only at the end of the reduction. The amount of CO evolved at this stage of reaction increased enormously with temperature.

The morphologies of the samples of WO_3 were investigated during the course of the reduction in the different systems studied. Needles were always observed, and were assumed to result from the formation of $W_{18}O_{49}$. The strong tendency of $W_{18}O_{49}$ to be formed as needles exerts a large influence on the morphology of the sample during the rest of the reduction. This is especially true below 900°C, and in the absence of water vapour, where the mobility of the subsequent phases is too low for the shape of the needles to change drastically. Fragmentation of needles, resulting from local contraction as more dense phases are formed, is probably responsible for the small tungsten particles formed.

The growth of particles was significant in the presence of water vapour and above about 900°C. As the conditions in the system during hydrogen reduction are made drier (by increasing the flowrate) the particle sizes decreased. Thus, in the presence of water vapour, particle growth seems to occur via formation of $WO_2(OH)_2$ and the subsequent gas phase transport of tungsten.

Although the conditions in the WO_3/graphite mixtures appeared to be drier than in the absence of graphite, the tungsten particles produced in either system appeared similar. The particle size seemed to be slightly smaller when graphite was present in the sample. However, the precise effect of graphite on the particle size could not be properly ascertained without a detailed study of the mixtures.

Particle growth in the absence of water vapour presumably occurs via the formation of gaseous tungsten oxides, and appears to be significant at high temperatures. The formation of tungsten or tungsten oxide layers on graphite particles also suggests that surface migration is significant, and is enhanced by the presence of impurities.

A number of general considerations have emerged from this study. The first is that the

reduction of WO_3 with any one of the reducing agents considered here involves a number of intermediate phases, and fairly similar reaction schemes were observed for all the reducing agents. The multistage nature of the process is one of the reasons why a clear mechanistic understanding of the reduction (especially with hydrogen and CO) is still lacking. When carbon is the reducing agent, the reduction of WO_3 to WO_2 is simplified because the mass loss from the process is largely from the removal of CO. This masks the individual stages of the reduction in which CO_2 is formed.

The importance of thermodynamic considerations in the study must be emphasised. Knowledge of the reactant/product gas equilibrium ratios is vital in explaining changes in the reaction mechanism as the temperature and other conditions in the system are altered. The equilibrium ratios may also explain how the kinetics may change during the course of the reduction, as was done for the transition from a diffusion-limiting to a first-order process in the reduction of WO_3 with graphite.

The morphology of the reacting powders must also be taken into account, especially in relation to the kinetics and thermodynamics of the process. In the tungsten system, the formation of pseudomorphs plays a significant role in the process and the partial pressures of product gases will in general be higher within the pseudomorph than between pseudomorphs. The intrinsic difference between the inner and outer layers of the pseudomorphs may affect the properties such as the final sizes of particles.

The results of this research suggest further avenues of investigation. The reduction using hydrogen has still not been adequately explained, partly because the multiple reactions in the system complicate an analysis of the system, but primarily because the H_2/H_2O ratio varies across the powder layer, resulting in different reactions and perhaps different reaction mechanisms. The use of high flowrates of controlled H_2/H_2O atmospheres to reduce very small samples (across which minimal variation in the H_2/H_2O ratio would occur) is a promising approach.

Because of instrumental limitations, the simultaneous use of carbon and hydrogen as reducing agents, which was the focus of this study, was only investigated up to 975°C. The reaction between water vapour and carbon seems to be only moderately fast at 975°C, but the rate increases significantly at higher temperatures. Thus, the reduction of WO_3/carbon mixtures

with hydrogen might be investigated at higher temperatures than were used in this study. The effect of carbon on the reduction should also be studied above the critical flowrate.

From the point-of-view of possible applications, further work needs to be conducted into the properties of the final product (particularly the particle sizes) under a variety of operating conditions.

REFERENCES

1. J.A.Mullendore, in *Kirk-Othmer Encyclopedia of Chemical Technology*, 3rd ed., Vol.23, John Wiley and Sons, New York, 1983, 413ff.
2. R.Kieffer and F.Benesovsky, in *Kirk-Othmer Encyclopedia of Chemical Technology*, 3rd ed., Vol.4, John Wiley and Sons, New York, 1978, 476.
3. W.D.Schubert and E.Lassner, *Int. J. Ref. Hard Met.*, **10** (1991) 171.
4. W.D.Schubert and E.Lassner, *Int. J. Ref. Hard Met.*, **10** (1991) 133.
5. N.Asada, Y.Yamamoto, K.Shimatani, S.Honkawa and M.Miyake, *Hardmetal Ostem, Japan*, April 15-26, 1991, 5.9.1-5.9.28.
6. A.S.Petukhov, L.D.Konchakovskaya, I.V.Uvarova and L.G.Reiter, *Chem. Abstracts*, 114:10482v.
7. M.E.Brown, D.Dollimore, and A.K.Galwey, in *Comprehensive Chemical Kinetics: Reactions in the Solid State*, Vol.22, C.H.Bamford and C.F.H.Tipper (eds), Elsevier, Amsterdam, 1980.
8. P.P.Budnikov and A.M.Ginstling, *Principles of Solid State Chemistry*, Maclaren and Sons, London, 1968.
9. J.Szekely, J.W.Evans, and H.Y.Sohn, *Gas-Solid Reactions*, Academic Press, London, 1976.
10. D.A.Brosnan, M.S.Thesis, Clemson University, 1968.
11. R.E.Carter, *J. Chem. Phys.* **34** (1961) 2010.
12. Y.K.Rao, *Metall. Trans., 2 (1971) 1439.*
13. Y.K.Rao, *Chem. Engng Sci., 29 (1974) 1435.*
14. H.Y.Sohn and J.Szekeley, *Chem. Engng Sci.*, **28** (1973) 1789.
15. D.L.Kepert, *Early Transition Metals*, Academic Press, London, 1972, ch.4.
16. C.L.Rollinson, in *Comprehensive Inorganic Chemistry*, Vol.3, J.C.Bailar, H.J.Emeléus, R.Nyholm and A.F.Trotman-Dickenson (eds), Pergamon, Oxford, 1973, ch.4.
17. J.Bousquet and G.Pérachon, *Compt. Rend. Acad. Sci. Paris*, **256** (1963) 694.

18. J.Bousquet and G.Pérachon, *Compt. Rend. Acad. Sci. Paris*, **258** (1964) 934.
19. J.Bousquet and G.Pérachon, *Compt. Rend. Acad. Sci. Paris*, **258** (1964) 3869.
20. J.A.Bustnes, Du.Sichen and S.Seetharaman, *Metall. Trans.*, **24B** (1993) 475.
21. V.K.Sarin, *J. Mater. Sci.*, **10** (1975) 593.
22. W.D.Schubert, *Int. J. Ref. Hard Met.*, **9** (1990) 178.
23. T.Millner and J.Neugebauer, *Nature*, **163** (1949) 601.
24. O.Glemser and R.v.Haeseler, *Z. Anorg. Allgem. Chem.*, **316** (1962) 168.
25. T.R.Wilken, W.R.Morcom, C.A.Wert and J.B.Woodhouse, *Metall. Trans.*, **7B** (1993) 589.
26. M.S.Whittingham and P.G.Dickens, *React. Solids, Proc. Int. Symp. 7th, 1972*, (1972) 640.
27. W.R.Morcom, W.L.Worrel, H.G.Sell and H.I.Kaplan, *Metall. Trans.*, **5** (1974) 155.
28. M.G.Charlton, *Nature*, **152** (1952) 109.
29. M.G.Charlton, *Nature*, **174** (1954) 703.
30. N.E.Fouad, K.M.E.Attyia and M.I.Zaki, *Powder Technol.*, **74** (1993) 31.
31. R.Haubner, W.D.Schubert, H.Hellmer, E.Lassner and B.Lux, *Int. J. Ref. Hard Met.*, **2** (1983) 156.
32. P.Taskinen and M.H.Tikkanen, *Scand. J. Metallurgy*, **6** (1977) 223.
33. P.Taskinen, P.Hytönen and M.H.Tikkanen, *Scand. J. Metallurgy*, **6** (1977) 228.
34. Z.Zhiqiang, Q.Chungliang, W.Enxi and C.Yuhua, *Int. J. Ref. Hard Met.*, **7** (1988) 57.
35. R.Haubner, W.D.Schubert, E.Lassner, M.Schreiner and B.Lux, *Int. J. Ref. Hard Met.*, **2** (1983) 108.
36. A.K.Basu and F.R.Sale, *Trans. Instn. Min. Metall.*, **C86** (1977) 169.
37. L.G.Austin, *Ind. Eng. Chem.*, **53** (1961) 659.
38. P.Barret and L.C.Dufour, *C. R. Acad. Sci. Paris*, **258** (1964) 2337.
39. Y.Lapostolle and L.C.Dufour, *C. R. Acad. Sc. Paris*, **C270** (1970) 970.
40. J.Qvick, *React. Solids*, **4** (1987) 73.
41. B.Zeiler, W.D.Schubert and B.Lux, *Int. J. Refract Hard Met.*, **10** (1991) 83.
42. H.L.Spier, *Philips Res. Rept. Suppl.*, **3** (1962) 52.

43. B.Zeiler, W.D.Schubert and B.Lux, *Int. J. Refract Hard Met.*, **100** (1991) 91.
44. J.E.Benson, H.W.Kohn and M.Boudard, *J. Catalysis*, **5** (1966) 307.
45. G.C.Bond and J.B.P.Tripathi, *J.C.S. Faraday I*, **72** (1976) 933.
46. I.V.Uvarova, *Poroshkovaya Metallurgiya,* **213** (1980) 1-5.
47. M.I.El-Guindy and W.G.Davenport, *Metall. Trans.*, **1** (1970) 1729.
48. E.Bicknese and R.Clark, *Trans. Met. Soc. AIME*, **236** (1966) 2.
49. E.Kawasaki, J.Sanscrainte, and T.J.Walsh, *A. I. Ch. E. J.*, **8** (1962) 48.
50. A.R.Mitchell and R.H.Parker, *Min. Eng.*, **1** (1988) 53.
51. Y.Maru, Y.Kuramasu, Y.Awakura, and Y.Kondo, *Metall. Trans.*, **4** (1973) 2591.
52. V.P.Elyutin, Yu.A.Pavlov, and V.P.Polyakov, *Chem. Abstracts*, 70:13608z.
53. M.Miyake and A.Hara, *Chem. Abstracts*, 91:41466d.
54. N.V.Alekseev, A.Yu. Gurosovskii, S.N.Shorin, I.K.Tagirov, and V.Mordasov, *Chem. Abstracts*, 86:158803z.
55. A.S.Petukhov, L.D.Konchakovskaya, I.V.Uvarova, and L.G.Reiter, *Chem. Abtracts*, 114:10482v.
56. A.K.Basu and F.R.Sale, *Metall. Trans.* **9B** (1978) 603.
57. P.L.Walker, F.Rusinko, and L.G.Austin, in *Advances in Catalysis*, Vol. 11, D.D.Eley, P.W.Selwood, and P.B.Weisz (eds), Academic Press, New York, 1959.
58. A.Savitzky and M.J.E.Golay, *Anal. Chem.*, **36** (1964) 1627.
59. P.A.Gorry, *Anal. Chem.*, **62** (1990) 570.
60. P.W.Atkins, *Physical Chemistry*, 3rd ed., OUP, Oxford, 1986.
61. E.T.Turkdogan and J.V.Vinters, *Carbon*, **8** (1970) 39.
62. H.J.Borchardt and F.Daniels, *J. Am. Chem. Soc.*, **79** (1957) 41.
63. G.Gyulai and E.J.Greenhow, *Thermochim. Acta*, **6** (1973) 239.

Appendix A

SPECIFICATIONS OF THE INFRARED GAS DETECTORS

The measuring ranges of the Edinburgh Sensors infrared CO_2 and CO detectors were 0 to 1 %v/v of 1 atm, and 0 to 10% v/v of 1 atm, respectively. The accuracy of these detectors was $\pm$ 2%. Both detectors were zeroed in a stream of pure argon. The upper limit of the CO_2 detector was calibrated using a 1.113% CO_2 in argon mixture, which was supplied by Fedgas.

For computer analysis, the responses of both instruments were calibrated by introducing known volumes of CO and CO_2 into a stream of argon, and then measuring the area under the peak. These volumes were introduced by syringe through a septum which had been placed in the gas line. An average area was determined from a number of experiments, and the agreement between the measured values for the area was usually better than 2%. Because the responses of the detectors were affected by flowrates below 200 mL min^{-1}, the procedure had to be performed at flowrates of 100 and 200 mL min^{-1}. The average value for the area was expressed in units of counts mL^{-1} s^{-1} by taking the volume of the calibrant gas and the sampling interval into account.

The percentage CO and CO_2 of the exhaust gas could then be simply calculated using the formula:

$$\%X = \frac{signal\ height}{calibration\ constant * \frac{flowrate}{60}} * 100\%$$

where X is either CO or CO_2, the calibration constant is the value described above (in counts mL^{-1} s^{-1}), and the flowrate is given in mL min^{-1}.

The cumulative volume of the gas evolved over a certain time is given by:

$$V_X = \sum \left(\frac{\%X}{100\%} * sampling\ interval * \frac{flowrate}{60} \right)$$

The total mass loss for the reaction can be readily determined:

$$Mass\ Loss = \frac{44 * V_{CO_2} + 28 * V_{CO}}{10 * 8.314 * 298}$$

The mass losses calculated from the infrared detectors were within 4% of the mass losses measured from experiment, which is reasonable agreement.

Appendix B

COMPUTER PROGRAMS USED IN THE STUDY

ATOD2

```
/*************************************************************************
  Dean Venables,   Chemistry Department,   Rhodes University.

  ATOD version 1.1 - April 1993
       version 1.2 - November 1993
       version 1.3 - February 1994 (Input from two channels)
       version 1.4 - October 1994 (Input from three channels)

  ATOD is a simple program to convert analogue signals from an input
  source, such as a thermocouple or katharometer, to digital data which
  can be more easily handled.  The timing for sampling is based on
  hardware timing, which is only found on 8088 and perhaps 8086 PCs.

  Refer to the PC-26 A/D manual for further information.
 *************************************************************************/



#include  <dos.h>
#include  <ctype.h>
#include  <conio.h>
#include  <graphics.h>
#include  <math.h>
#include  <stdio.h>
#include  <stdlib.h>


#define  TRUE   1
#define  FALSE  0
#define  NUMPTS  10000
```

```
void  title_screen (void);
void  get_params (void);
void  graph_axes (void);
void  data_capture (void);
void  save_data (void);
float calc_x_max (float);


char   key, title[38];
int    data1[(NUMPTS+1)],
       data2[(NUMPTS+1)],
       data3[(NUMPTS+1)],
       num_channels,
       mark_count,
       points,
       XMAX, XMIN,
       YMAX, YMIN,
       XLEN, YLEN;
float  interval,
       markers[100],                /* If more than 100 marks are made,

                                       this program could crash! */
       x_max, x_ratio,
       x_plot_const, y_plot_const,
       y_ratio;
struct date *system_date;



   /*************************************************************************
     The main programme.
    *************************************************************************/
void  main (void)
   {
     /* Initalise A/D PPI. */
   outportb( 0x0703, 0x92 );

     /* Clear screen and display title. */
   title_screen();
   do
       {
       get_params();
       graph_axes();
```

```
        data_capture();
        save_data();
        }
    while ( key == 'Y');
    }


    /*************************************************************************
      Produces the opening screen, gives info on the program, and gets
      the date, if needed.
     *************************************************************************/
void  title_screen (void)
    {
      /* Display the title and introductory information. */
    restorecrtmode();
    clrscr();
    printf( "\n\t\t\tAnalogue-to-Digital Conversion" );
    printf( "\n\t\t\t----------------------------\n\n" );
    printf( "\t\t\t\tVersion 1.4.\n\n" );
    printf( "\t\tDean Venables, Rhodes University, 1993-4\n\n" );
    printf( "\tATOD converts an analogue voltage in the range 0 to 10 V\n" );
    printf( "\tto a digital value using the PC-26 A/D conversion board.\n" );
    printf( "\tThe data are collected as a function of time, and are\n" );
    printf( "\tdisplayed as they are collected. The data are represented\n" );
    printf( "\tby integer values, and can be stored on disk. NB: THIS\n" );
    printf( "\tPROGRAM IS ONLY LIKELY TO WORK ON PCs AND XTs!\n" );

      /* Print the date given by the system and change if necessary. */
    getdate( system_date );
    printf( "\n\tThe date is %d/%d/%d.  ",
            system_date -> da_day,
            system_date -> da_mon,
            system_date -> da_year );
    printf( "If this is not correct, please\n" );
    printf( "\tpress control-break and enter the date from DOS." );

      /* Wait for a key to be pressed. */
    printf( "\n\n\n\n\n\t\t\tPress a key to continue" );
    for  ( ; kbhit() == FALSE ; );
    getch();
    }


    /*************************************************************************
```

```
    Gets the information required for sampling the data.
    ***************************************************************/
void  get_params (void)
   {
   float  temp;

     /* Get the frequency of sampling and the maximum time to be displayed
        on the graph. */
   restorecrtmode();
   clrscr();
   printf( "\n" );
   do
      {
      printf( "\tThe sampling interval must be in the range 0.01\n" );
      printf( "\tto 10 seconds. If a sampling interval of less than\n" );
      printf( "\t0.1 seconds is chosen, the data will not be shown\n" );
      printf( "\twhile they are being collected. (However, when the\n" );
      printf( "\tdata are displayed, only every fifth datum is\n" );
      printf( "\tplotted.) The interval must also be a multiple\n" );
      printf( "\tof 0.01 seconds.\n" );
      printf( "\tWhat sampling interval would you like? " );
      scanf( "%f", &interval );
      interval += 0.005;
      interval = (int)(100*interval)/100.0;
      printf( "\n" );
      }
   while  ( interval < 0.00999  ||  interval > 10.0 );

   do
      {
      printf( "\tA maximum of %d points may be collected; with a\n",
              NUMPTS );
      printf( "\tsampling interval of %5.2f that means that the data\n",
              interval );
      printf( "\tmay be collected for a maximum of %d seconds.\n",
              (int)(NUMPTS * interval + 0.5) );
      printf( "\tHow many points do you want to sample? " );
      scanf( "%f", &temp );
      points = temp + 0.5;
      printf( "\n" );
      }
   while  ( points < 1  ||  points > NUMPTS );

     /* How many channels must be sampled? */
```

```
    printf( "\tDo you wish to sample 1, 2, or 3 channels? (1/2/3) " );
    do
        key = toupper( getch() );
    while ( key != '1' && key != '2' && key != '3' );
    printf( "%c", key );
    if ( key == '1')
        num_channels = 1;
    else
        {
        if ( key == '2' )
            num_channels = 2;
        else
            num_channels = 3;
        }

      /* Get a title for the graph. */
    printf( "\n\n\tWhat would you like to title your graph? " );

    printf( "(maximum 35 characters)\n\t" );
    title[0] = 36;
    cgets( title );
    title[0] = title[1] = ' ';
    }


    /*************************************************************************
      Draw graph axes, and label points.
     *************************************************************************/
void  graph_axes (void)
    {
    float  temp, value, increment;
    int    driver, mode, x, dec_pt, mag,
           ct, itemp1, itemp2;
    char   null_str[20], *ctemp;

      /* Set up the graphics system. */
    driver = DETECT;
    initgraph( &driver, &mode, "" );
    cleardevice();
    if ( driver == CGA )
        {
          /* Set up the correct dimensions for the CGA driver. */
        XMAX = 620;
        XMIN = 45;
```

```
    YMAX = 165;
    YMIN = 30;
    XLEN = (XMAX - XMIN);
    YLEN = (YMAX - YMIN);
    }
else
    {
      /* Otherwise assume the graphics card is Hercules. */
    XMAX = 700;
    XMIN = 60;
    YMAX = 300;
    YMIN = 40;
    XLEN = (XMAX - XMIN);
    YLEN = (YMAX - YMIN);
    }

  /* Draw the axes. */
line( XMIN, YMAX, XMAX, YMAX );
line( XMIN, YMIN, XMIN, YMAX );
line( XMIN, YMIN, XMAX, YMIN );
line( XMAX, YMIN, XMAX, YMAX );

  /* Put the title at the top of the screen. */
settextstyle( TRIPLEX_FONT, HORIZ_DIR, USER_CHAR_SIZE );
setusercharsize( 1, 1, 1, 1 );
outtextxy( (XMAX - textwidth(title)) / 2, 2, title );

  /* Put the intervals and labels on the x axis. */
strcpy( null_str, "Time / [s]" );
settextstyle( DEFAULT_FONT, HORIZ_DIR, 0 );
outtextxy( (XMAX / 2), (YMAX + 20), null_str );

strset( null_str, '\0' );
dec_pt = calc_x_max( interval * points );
x_ratio = (float)XLEN / (float)x_max;
increment = ((x_max / 5) * x_ratio);
for  ( ct = 0 ; ct <= 5 ; ct ++ )
    {
    temp = (XMIN + (int)(0.5 + ct * increment));
    line( temp, YMAX, temp, (YMAX + 4) );
    value = (x_max / 5 * ct);
    if  ( value != 0.0 )
       mag = log10((double)value);
    else
```

```
        mag = 0;
    ctemp = ecvt( (double)value, (int)(mag + 1.0),
                &itemp1, &itemp2 );
    strset( null_str, '\0' );
    if ( value < 1.0 )
        strcpy( null_str, "0\0" );
    strncpy( null_str, ctemp, itemp1 );
    if ( dec_pt > 0 )
      {
      strcat( null_str, "." );
      ctemp = ecvt( (double)(pow10(dec_pt)*(value - (int)value)), 8,
                  &itemp1, &itemp2 );
      strncat( null_str, ctemp, dec_pt );
      }
    outtextxy( temp - (textwidth(null_str) / 2), YMAX + 8, null_str );
    }

  /* Put the intervals and labels on the y axis. */
strcpy( null_str, "Voltage/[V]" );
settextstyle( DEFAULT_FONT, VERT_DIR, 0 );
outtextxy( (XMIN - 30), (YMAX / 2) - 30, null_str );

y_ratio = (float)YLEN / 10.0;
settextstyle( DEFAULT_FONT, HORIZ_DIR, 0 );
for ( ct = 0 ; ct <= 10 ; ct += 2 )
    {
    line( XMIN - 5, YMAX - (ct * y_ratio),
        XMIN, YMAX - (ct * y_ratio) );
    itoa( ct, null_str, 10 );
    outtextxy( XMIN - 10 - textwidth(null_str),
            YMAX - 3 - (ct * y_ratio), null_str );
    }

  /* Calculate the values required for plotting the data. */
x_plot_const = x_ratio * interval;
y_plot_const = y_ratio / 409.6;
}


/*************************************************************************
  Let the user start the capture process, then collect the data at the
  requested time interval and display the data on the screen. Also
  allow the user to press the "M" key to mark a time period, and store
  these marks appropriately.
```

```
   ***************************************************************/
void  data_capture (void)
   {
   unsigned char
         MSB, LSB;
   int    ct, loop2, hundredths, plot, stop_capture, plot_const,
          value, backgnd_colour, norm_colour, print_data;
   float  nextX;
   long   total1, total2, total3;

     /* Set first value to 10000 to clearly demarkate the start of the
        markers, and then set mark_count to point to the next cell in
        the array. */
   markers[0] = 10000.0;
   mark_count = 1;

     /* Wait for the user to start the data capture, then clear the
        screen, and set up the system. */
   outtextxy( (XMAX - 22*7) / 2, (YMAX / 2), "Press any key to begin" );
   outtextxy( (XMAX - 36*7) / 2, (YMAX / 2 + 15),
            "Press 'M' to mark a particular time," );
   outtextxy( (XMAX - 32*7) / 2, (YMAX / 2 + 30),
            "and 'X' to halt data collection." );
   backgnd_colour = getbkcolor();
   norm_colour = getcolor();
   setcolor( backgnd_colour );
   getch();
   outtextxy( (XMAX - 22*7) / 2, (YMAX / 2), "Press any key to begin" );
   outtextxy( (XMAX - 36*7) / 2, (YMAX / 2 + 15),
            "Press 'M' to mark a particular time," );
   outtextxy( (XMAX - 32*7) / 2, (YMAX / 2 + 30),
            "and 'X' to halt data collection." );
   setcolor( norm_colour );
   key = ' ';

   hundredths   = (interval * 100 + 0.5);
   stop_capture = FALSE;
   nextX        = XMIN;
   if  ( interval < 0.1 )
       plot = FALSE;
   else
       plot = TRUE;

     /* Plot points no sooner than every 5th second. */
```

```
plot_const = (5.0 / interval);

  /* Program counter with correct interval : 46 * 256 + 156 = 11932,
     which corresponds to an interval of 0.01 seconds. */
enable();
outportb( 0x43, 0xb6 );
outportb( 0x42, 0x9c );
outportb( 0x42, 0x2e );
LSB = (inportb(0x61) | 1) & 0xfd;
outportb( 0x61, LSB );

  /* Count off the required number of points at the correct
     time interval. */
for  ( ct = 0, print_data = plot_const ;
       (ct < points  &&  stop_capture != TRUE) ;
       ct++, print_data-- )
    {
    total1 = total2 = total3 = 0;

      /* Count off (interval*100) points. */
    for   ( loop2 = 0 ; loop2 < hundredths ; loop2++ )
       {

         /* Count off 0.01 seconds. */
       do
          LSB = inportb( 0x62 );
       while  ( (LSB & 0x20) == 0 );
       do
          LSB = inportb( 0x62 );
       while  ( (LSB & 0x20) != 0 );

         /* Read the value of channel 1, and store it. Plot the
            value to the screen. */
       outportb( 0x702, 0x02 );
       outportb( 0x702, 0x03 );

         /* Wait at least 40 micro seconds here. Count 25 times through
            a loop of about 10 instructions : at 4.77 MHz = 52 us. */
       for  ( value = 0 ; value < 25 ; value++ );

         /* Now get the value. */
       total1 += ( (inportb( 0x701 ) & 0x0f) * 256 + inportb( 0x700 ) );

         /* Read the value of channel 2, and store it. Plot the
```

```
        value to the screen. */
    if ( num_channels > 1 )
        {
        outportb( 0x702, 0x12 );
        outportb( 0x702, 0x13 );

          /* Wait at least 40 micro seconds here. Count 25 times
             through a loop of about 10 instructions :
             at 4.77 MHz = 52 us. */
        for ( value = 0 ; value < 25 ; value++ );

          /* Now get the value. */
        total2 += ( (inportb( 0x701 ) & 0x0f) * 256 +
                    inportb( 0x700 ) );
        }

      /* Read the value of channel 3, and store it. Plot the
        value to the screen. */
    if ( num_channels == 3 )
        {
        outportb( 0x702, 0x12 );
        outportb( 0x702, 0x23 );

          /* Wait at least 40 micro seconds here. Count 25 times
             through a loop of about 10 instructions :
             at 4.77 MHz = 52 us. */
        for ( value = 0 ; value < 25 ; value++ );

          /* Now get the value. */
        total3 += ( (inportb( 0x701 ) & 0x0f) * 256 +
                    inportb( 0x700 ) );
        }
    }

  /* Calculate the value of the datum. */
data1[ct] = total1 / hundredths;
if ( num_channels > 1 )
    data2[ct] = total2 / hundredths;
if ( num_channels == 3 )
    data3[ct] = total3 / hundredths;

  /* Plot the datum if allowed. */
nextX += x_plot_const;
if ( plot && print_data <= 0 )
```

```
        {
        putpixel( nextX, (int)(YMAX - (data1[ct] * y_plot_const)), 1 );
        if ( num_channels > 1 )
            putpixel( nextX, (int)(YMAX - (data2[ct] * y_plot_const)), 1 );
        if ( num_channels == 3 )
            putpixel( nextX, (int)(YMAX - (data3[ct] * y_plot_const)), 1 );
        print_data = plot_const;
        }

      /* Make a mark, if 'M' key pressed, quit if 'X' pressed. */
    while ( kbhit() != FALSE )
        {
        key = getch();
        if ( key == 'M' || key == 'm' )
            {
              /*********************************************************
                Places the x value of the point into the array, place
                a line on the screen, and return.
              *********************************************************/
              /* Only make the mark if it is not the same as the
                 previous one. */
            if ( markers[(mark_count-1)] != (ct*interval) )
                {
                markers[mark_count] = (ct*interval);
                mark_count++;
                if ( plot )
                    line ( nextX, YMIN, nextX, YMAX );
                }
            }
        else
            {
            if ( key == 'X' || key == 'x' )
                stop_capture = TRUE;
            }
        }
    }
points = ct;
restorecrtmode();
}


/*************************************************************************
  Save the data collected, followed by the markers, if any. Interpose
  the two sets of data with an easily recognizable value like "10000"
```

```
    which is outside the range of the data collected (12 bits = 4096).
    The value "10000" has already been added to the markers list in
    data_capture().
    ************************************************************************/
void  save_data (void)
   {
   int   ct, file_error;
   char  filename[25];
   FILE  *output_file;

     /* Does the user wish to save the data - make doubly sure!!!
        Get the name of the file. If there is a problem, give them the
        option of trying again. */
   clrscr();
   printf( "\n\tThe data has been collected.\n" );
   printf( "\n\tDo you wish to save the data? (Y/N) " );
   do
      key = toupper( getch() );
   while  ( key != 'N'  &&  key != 'Y' );
   printf( "%c", key );

   if  ( key == 'N' )
       {
       printf( "\n\tAre you sure? (All data will be lost!) (Y/N) " );
       do
          key = toupper( getch() );
       while  ( key != 'N'  &&  key != 'Y' );
       printf( "%c", key );
       if  ( key == 'N' )
          key = 'Y';
       else
          key = 'N';
       }

   if  ( key == 'Y' )
       {
       file_error = FALSE;
       do
          {
          printf( "\n\n\tEnter the file in which to save the data : " );
          scanf( "%s", filename );
          if ( (output_file = fopen( filename, "wt")) == NULL )
              {
              printf( "\n\n\tThere is a problem in opening the file. " );
```

```
            printf( "Would you like to try again? (Y/N) " );
            do
               key = toupper( getch() );
            while ( key != 'N' && key != 'Y' );
            printf( "%c", key );
            if ( key == 'Y' )
               file_error = TRUE;
            else
               key = 'Y';
            }
         else
               /* Unbuffered output. */
            setbuf( output_file, NULL );
         }
      while ( file_error );
      }

if ( key == 'Y' )
      {
        /* Now save the data; first the general information, then
           the actual points, and then the markers. */
      fprintf( output_file, "Analogue to Digital Conversion :\n\n" );
      fprintf( output_file, "Title : %s\n", title );
      fprintf( output_file, "Date : %d/%d/%d\n",
               system_date -> da_day,
               system_date -> da_mon,
               system_date -> da_year );
      fprintf( output_file, "Sampling interval : %.2f sec\n",
               interval );
      fprintf( output_file, "Number of points sampled : %d\n",
               points );
      fprintf( output_file, "Number of markers : %d\n\n",
               (mark_count-1) );

      for ( ct = 0 ; ct < points ; ct ++ )
         {
         if ( num_channels == 1 )
            fprintf( output_file, "%d\n", data1[ct] );
         if ( num_channels == 2 )
            fprintf( output_file, "%d %d\n", data1[ct], data2[ct] );
         if ( num_channels == 3 )
            fprintf( output_file, "%d %d %d\n", data1[ct], data2[ct],
                                                data3[ct] );
         }
```

```
        fprintf( output_file, "\n" );
        for  ( ct = 0 ; ct < mark_count ; ct++ )
            fprintf( output_file, "%f\n", markers[ct] );

        fclose( output_file );
        }
    }


    /*************************************************************************
      Calculates the value of the largest x interval marking on the
      axis.
     *************************************************************************/
float  calc_x_max (float  x)
    {
    int    mag, mag2;
    float  work;

      /* Calculate the order of magnitude required to change the real
         number x into an integer, and then work out the order of
         magnitude (mag2) of the integer number. */
    for  ( mag = 0, work = (x * pow10(mag)) ;
           (work - (int)work) > 0.001 ;
           mag++, work = (x * pow10(mag)) ) ;

      /* Now calculate the interval to be used : divide the highest number
         by the number of intervals (5), and count up to the first number
         which is a half of the order of magnitude found. */
    x *= pow10(mag+1) / 5;
    mag2 = log10((double)x);
    work = (x / (0.5 * pow10(mag2)));
    if  ( ((work - (int)work) * 100) != 0 )
        work = (int)(1.0 + work);

      /* Return x_max and the number of decimal places to be printed. */
    x_max = (5 * work * 0.5 * pow10(mag2 - mag - 1));
    if  ( (x_max / 5) == (int)(x_max / 5) )
        return 0;
    else
      {
      if  ( (x_max / 0.5) == (int)(x_max / 0.5) )
          return 1;
      else
          return 2;
```

```
    }
}
```

ALTDATA

```
/*************************************************************************
 Dean Venables, Chemistry Department, Rhodes University,  1993

   ALTDATA : May 1993,      Version 1.0
             November 1993, and
             July 1994,     Version 2.0

   ALTDATA has been designed to manipulate data from a variety of sources.  It accepts
integer input, and smoothes the data using a least squares  convolution (Savitzky-Golay)
procedure, using the number of points  specified by the user. The first derivative of the data
may also be  calculated, and the smoothed data can be reduced in size an integer  number
of times using a simple averaging routine. The raw data, reduction  factor, smoothed data, and
first derivative can all be included in or  excluded from the output file.

   References :  P.Gorry; Anal.Chem.,1990,62,570
                 A.Savitzky and M.Golay; Anal.Chem,1964,36,1627
                 Steiner et al., Anal.Chem,1972,44,1906
*************************************************************************/


#include <stdlib.h>
#include <stdio.h>
#include <conio.h>
#include <string.h>
#include <math.h>


#define  MAX    2001
#define  MAX2   8000
#define  TRUE   1
#define  FALSE  0
#define  SIZE   61


void    main (void);
void    open_files (int*);
void    filter_data (void);
void    modify_data (int);
void    derivatives (void);
void    set_params (void);
```

```
double  gram_poly (int, int, int, int);
double  gen_factor (int, int);
double  weight (int, int, int, int, int);


FILE    *input, *output;
int     out_red_factor,
        out_original,
        out_smoothed,
        out_derivative,
        max,
        smoothed[MAX2],
        deriv1[MAX2],
        data[MAX2];


   /************************************************************************ The
main program.
    ************************************************************************/ void
main(void)
   {
   int   j, red_factor;

   out_red_factor = FALSE;
   out_original   = FALSE;
   out_smoothed   = TRUE;
   out_derivative = FALSE;

   open_files( &red_factor );
   set_params();
   filter_data();
   derivatives();

   if  ( red_factor > 1)
       modify_data( red_factor );

     /* Print the data to the file. */
   if  ( out_red_factor )
       fprintf( output, "(Data reduced by a factor of %d)\n", red_factor );     for  ( j = 0; j <
max; j++ )
       {
       if  ( out_original )
           fprintf( output, " %d ", data[j] );
```

```
        if  ( out_smoothed )
            fprintf( output, " %d ", smoothed[j] );
        if  ( out_derivative )
            fprintf( output, " %d ", deriv1[j] );
        fprintf( output, "\n" );
        }

    fclose( output );
    printf( "\n\nThe data has been modified accordingly.\n" );     }


    /*************************************************************************
Open the input and output files, and find out how many times the        data will be reduced.
     *************************************************************************/ void
open_files( int *red_factor )
    {
    char    ch,
            filename[40];
    int     file;

      /* The title screen : choose the file to be read from. */     clrscr();
    printf( "\nAltdata 2.0 :" );
    printf( "\n-----------" );
    printf( "\n\nALTDATA has been designed to manipulate data from " );     printf( "a variety
of sources.\nIt accepts integer input, and " );       printf( "smoothes the data using a least
squares\nconvolution " );     printf( "(Savitzky-Golay) procedure, using the number of points\n"
);      printf( "specified by the user. The first derivative of the data " );       printf( "may also
be\ncalculated, and the smoothed data can be " );     printf( "reduced in size an integer\nnumber
of times using a " );       printf( "simple averaging routine. The raw data, reduction\n" ):
printf( "factor, smoothed data, and first derivative can all be " );       printf( "included in
or\nexcluded from the output file.\n\n" );

      /* Open the input file, and read in data. */
    printf( "\nRetrieve the graph points from which file? " );      scanf( "%s", filename );
    if  ( (input = fopen( filename, "r" )) == NULL )
        {
        printf( "\n\nCannot open the input file.\n " );
        exit(EXIT_SUCCESS);
        }
    for ( max = 0 ; (max < MAX2   &&   file != EOF) ; max++ )  file  =  fscanf( input,
"%d", &data[max] );
    max--;
    fclose( input );
```

```
    /* Open the output file. */
   printf( "\nFile in which to save the modified data? " );     scanf( "%s", filename );
   if  ( (output = fopen( filename, "w" )) == NULL )
       {
       printf( "Cannot open the output file.\n " );
       exit(EXIT_SUCCESS);
       }

    /* How many times must the data be reduced? */
   do
       {
       printf( "\nHow many times must the data be reduced? " );        printf( "(At least %d
times)  ", (int)(max/(float)(MAX)+0.5) );          scanf( "%d", red_factor );
       }
   while  ( *red_factor < (int)(max/(float)(MAX)+0.5) );
   }


   /*********************************************************************
Replaces data, which is not within 2 times the standard deviations          with the arithmetic
mean.
    *********************************************************************/ void
filter_data (void)
   {
   int     i, j, pts;
   double  arith_mean, std_dev;

   printf( "\n\nDo you wish to remove data which are not within two " );     printf( "standard
deviations of\nthe arithmetic mean? (Y/N) " );     if  ( toupper(getche()) == 'Y' )
       {
       printf( "\n\nHow many points do you wish to use for calculating " );    printf(    "the
standard deviation, for\nfiltering purposes? " );     scanf( "%d", &pts );

       for  ( i = 0 ; i < (max-pts) ; i += pts )
           {
           arith_mean = 0.0;
           std_dev = 0.0;
           for  ( j = 0; j < pts ; j++ )  arith_mean += data[i+j];        arith_mean /= pts;
           for  ( j = 0; j < pts ; j++ )
               std_dev += (data[i+j] - arith_mean)*(data[i+j] - arith_mean);              std_dev
= sqrt( std_dev / pts );
           for  ( j = 0; j < pts; j++ )
               {
               if  ( abs(data[i+j] - (int)arith_mean) > (int)(2 * std_dev) )
```

```
data[i+j] = arith_mean;
                }
            }
        }
    }


    /*****************************************************************
Take red_factor number of points from the input array, and place the average in the output
array. Be careful at the end of file.
*****************************************************************/ void
modify_data(int red_factor)
    {
    int   i, j, k,
          best, no_pts,
          index,
          total,
          total_d;


      /* Modify all the data while it is in the array. */
    for  ( i = 0 ; ((i+1)*red_factor < max) ; i++ )
        {

          /* Average red_factor number of points. */
        for  ( no_pts = total_d = total = j = 0 ;
               j < red_factor  &&  (index = (i*red_factor) + j) < max ;          j++ )
            {
            total   += smoothed[index];
            total_d += deriv1[index];
            no_pts++;
            }
        if  ( no_pts == 0 )
            {
            smoothed[i] = 0;
            deriv1[i]   = 0;
            }
        else
            {
            smoothed[i] = ( (float)total / (float)no_pts + 0.5);      deriv1[i]  = ( (float)total_d
/ (float)no_pts + 0.5);          }
        }
    max = i;
    }
```

```
   /*************************************************************************
Calculate the smoothed data, and the derivatives for this data.
*************************************************************************/ void
derivatives (void)
   {
   int     m, i, t,
           points,
           order;
   char    ch;
   double  matrix[SIZE][SIZE], temp;

     /* Get the number of points and the type of smoothing (eg. cubic,          quadratic, etc.).
*/
   printf( "\n\nEnter the number of points to be used in smoothing  " );      scanf( "%d".
&points );
   printf( "Order of smoothing (eg. quadratic = 2, cubic = 3, etc) " );    scanf( "%d", &order
);

   m = (int)((float)(points-1.0) / 2.0 + 0.5);
   for  ( i= -m ; i<=m ; i++ )
       for  ( t= -m ; t<=m ; t++ )
          matrix[t+m][i+m] = weight(i,t,m,order,0);

     /* Now smooth the data. */
   for  ( i = 0 ; i < m ; i++ )
       {
       temp = 0.0;
       for  ( t = -m; t <= m ; t++ )
          temp += matrix[i][t+m] * data[m+t];
       smoothed[i] = (temp + 0.5);
       }
   for  ( i = m ; i < max-m ; i++ )
       {
       temp = 0;
       for  ( t = -m; t <= m ; t++ )
          temp += matrix[m][t+m] * data[i+t];
       smoothed[i] = (temp + 0.5);
       }
   for  ( i = max-m ; i < max ; i++ )
       {
       temp = 0.0;
       for  ( t = -m; t <= m ; t++ )
          temp += matrix[2*m-max+1+i][t+m] * data[max-m+t-1];          smoothed[i] =
```

```
(temp + 0.5);
        }

    if ( out_derivative )
        {
          /* Now calculate the first derivative, in the same manner as the smoothing.
*/
        printf( "\n\n1st Derivative : enter the number of points " );      scanf( "%d", &points
);
        printf( "Order (eg. quadratic = 2, cubic = 3, etc) " );   scanf( "%d", &order );

        m = (int)((float)(points-1.0) / 2.0 + 0.5);
        for ( i= -m ; i<=m ; i++ )
            for ( t= -m ; t<=m ; t++ )
                matrix[t+m][i+m] = weight(i,t,m,order,1);

          /* Now find the first derivative. */
        for ( i = 0 ; i < m ; i++ )
            {
            temp = 0.0;
            for ( t = -m; t <= m ; t++ )
                temp += matrix[i][t+m] * smoothed[m+t];
            deriv1[i] = (temp + 0.5);
            }
        for ( i = m ; i < max-m ; i++ )
            {
            temp = 0.0;
            for ( t = -m; t <= m ; t++ )
                temp += matrix[m][t+m] * smoothed[i+t];
            deriv1[i] = (temp + 0.5);
            }
        for ( i = max-m ; i < max ; i++ )
            {
            temp = 0.0;
            for ( t = -m; t <= m ; t++ )
                temp += matrix[2*m-max+1+i][t+m] * smoothed[max-m+t-1];
deriv1[i] = temp;
            }
        }
    }


    /* Sets the form which the output will take. */
void  set_params (void)
```

```
{
char key;

printf( "\nThe output fill have the following form :\n" );     printf( "\n\t1) The reduction
factor will " );
if ( ! out_red_factor ) printf( "not " );
printf( "be printed." );
printf( "\n\t2) The original data will " );
if ( ! out_original ) printf( "not " );
printf( "be printed." );
printf( "\n\t1) The smoothed data will " );
if ( ! out_smoothed ) printf( "not " );
printf( "be printed." );
printf( "\n\t1) The first derivative will " );
if ( ! out_derivative ) printf( "not " );
printf( "be printed.\n\n" );

printf( "\nDo you wish to change these settings? (Y/N) " );    if ( (key = toupper(getche()))
== 'Y' )
    {
    printf( "\n\nPress 'Y' or 'N' to set the values :\n" );     printf( "\n\t1) Print the
reduction factor? (Y/N) " );          if ( (key = toupper(getche())) == 'Y' )
        out_red_factor = TRUE;
    if ( key == 'N' )
        out_red_factor = FALSE;
    printf( "\n\t2) Print the original data? (Y/N) " );
    if ( (key = toupper(getche())) == 'Y' )
        out_original = TRUE;
    if ( key == 'N' )
        out_original = FALSE;
    printf( "\n\t3) Print the smoothed data? (Y/N) " );
    if ( (key = toupper(getche())) == 'Y' )
        out_smoothed = TRUE;
    if ( key == 'N' )
        out_smoothed = FALSE;
    printf( "\n\t4) Print the first derivative? (Y/N) " );        if ( (key = toupper(getche()))
== 'Y' )
        out_derivative = TRUE;
    if ( key == 'N' )
        out_derivative = FALSE;
    }

}
```

```
/*************************************************************************
Calculates the Gram Polynomial (s=0), or its s'th derivative evaluated at i, order k, over
2m+1 points.
*************************************************************************/double
gram_poly (int i, int m, int k, int s)
{
if ( k>0 )
    {
    return    (double)( (double)(4*k-2)/(double)(k*(2*m-k+1)) *
          (i*gram_poly(i,m,k-1,s) + s*gram_poly(i,m,k-1,s-1)) -
          ((double)(k-1)*(2*m+k))/(double)(k*(2*m-k+1)) *
          gram_poly(i,m,k-2,s) );
    }
else
    {
    if ( k==0 && s==0 )
       return 1.0;
    else
       return 0.0;
    }
}


/*************************************************************************
Calculates the generalised factorial (a)(a-1)...(a-b+1).
*************************************************************************/ double
gen_factor (int a, int b)
{
int    j;
double gf;

gf = 1.0;
for ( j=(a-b+1) ; j<=a ; j++ )
    gf *= j;
return gf;
}


/*************************************************************************
Calculates the weight of the i'th data point for the t'th Least- Square point of the s'th
derivative, over 2m+1 points, order n.
*************************************************************************/ double
weight (int i, int t, int m, int n, int s)
{
```

```
    int     k;
    double  sum;

    sum = 0.0;
    for ( k=0 ; k<=n ; k++ )
        sum += (2*k+1) * (gen_factor(2*m,k) / gen_factor(2*m+k+1,k+1)) *
gram_poly(i,m,k,0) * gram_poly(t,m,k,s);
    return sum;
    }
```

Appendix C

X-RAY POWDER DIFFRACTION PATTERNS

	d (Å)	I/I_1
α-W	2.238	100
	1.582	15
	1.292	23
	1.119	8
β-W	2.52	60
	2.25	100
	2.06	80
	1.45	40
	1.40	60
	1.34	80
	1.26	60
	1.13	60
Graphite	3.35	100

	d (Å)	I/I_1
W_2C	2.60	50
	2.36	40
	2.27	100
	1.74	40
	1.49	60
	1.34	50
	1.29	40
	1.26	50
	1.25	50
WC	2.83	70
	2.51	80
	1.87	100
	1.452	60
	1.421	50
	1.293	70
	1.258	60
	1.233	70
	1.149	70

	d (Å)	I/I_1
WO_2	3.45	100
	2.828	20
	2.446	45
	2.436	55
	2.418	80
	2.393	50
	1.847	20
	1.827	20
	1.731	40
	1.724	60
	1.709	45
	1.698	50
	1.545	50
	1.537	40
	1.406	45
	1.387	20
	1.284	25
	1.222	45
	1.212	20
	1.207	25
	1.184	20

	d (Å)	I/I_1
$W_{18}O_{49}$	12.9	35
	8.27	15
	4.43	20
	3.78	100
	3.73	50
	3.63	55
	3.44	55
	3.40	40
	3.39	50
	3.17	30
	2.910	40
	2.743	35
	2.654	55
	2.620	50
	2.522	50
	2.428	30
	2.305	40
	2.218	30
	1.888	65
	1.865	25
	1.770	25
	1.728	20
	1.684	40
	1.674	35
	1.650	35
	1.630	20

	d (Å)	I/I_1
$W_{20}O_{58}$	4.28	20
	3.89	55
	3.77	100
	3.70	55
	3.64	60
	2.729	80
	2.707	45
	2.640	50
	2.620	60
	2.211	70
	1.963	35
	1.898	50
	1.884	60
	1.741	30
	1.700	20
	1.695	60
	1.680	30
	1.674	20
	1.550	65
	1.337	35
	1.282	25
	1.262	35
	1.255	30
	1.207	25
	1.141	25

	d (Å)	I/I_1
WO_3	3.835	100
	3.762	95
	3.642	100
	3.342	50
	3.109	50
	3.076	50
	2.684	75
	2.661	60
	2.617	90
	2.528	35
	2.509	40
	2.172	50
	2.149	60
	2.038	40
	2.020	30
	2.011	25
	1.991	35
	1.966	30
	1.917	50
	1.879	50
	1.820	75
	1.807	40
	1.793	50
	1.707	60
	1.687	55
	1.670	50